Investigations into the Peroxidase Activity of Ferriprotoporphyrin IX and its Complexes with Clinically Relevant Antimalarial Drugs

by
Chandre Jade Sammy

Thesis presented in partial fulfilment of the requirements for the degree of Master of Science in the Faculty of Science at Stellenbosch University

Supervisor: Dr Katherine A. de Villiers
Co-Supervisor: Dr David Kuter

March 2017

Declaration

By submitting this thesis electronically, I declare that the entirety of the work contained therein is my own, original work, that I am the sole author thereof (save to the extent explicitly otherwise stated), that reproduction and publication thereof by Stellenbosch University will not infringe any third party rights and that I have not previously in its entirety or in part submitted it for obtaining any qualification.

March 2017

Abstract

A major class of antimalarial drugs act by increasing levels of free haem, Fe(III)PPIX, within the malaria parasite. While Fe(III)PPIX is known to be toxic, the manner in which it brings about parasite death is not entirely clear. Furthermore, it is unknown as to whether the antimalarial drugs which interact with Fe(III)PPIX, modulate its toxicity. The work presented here aims to address these uncertainties. The first part of this work focusses on the interactions between clinically relevant antimalarial drugs and Fe(III)PPIX. Spectrophotometric titrations were used to investigate drug-Fe(III)PPIX complex formation under three biologically relevant environments, namely an aqueous environment (pH 7.4) representative of the malaria parasite cytosol; acetonitrile which mimics the non-aqueous interior of a lipid and the detergent SDS was used to model a lipid-water interface system, that is present at membrane surfaces. Three antimalarial drugs chloroquine (CQ), quinidine (QD) and artemisinin (Art), belonging to three distinct classes, were investigated to determine binding strength between the antimalarial drug and Fe(III)PPIX. Strong association constants for the interaction of Fe(III)PPIX with QD and CQ were determined in the aqueous (log K = 5.8 ± 0.1 and 6.5 ± 0.1), aqueous SDS system (log K = 6.2 ± 0.1 and 6.5 ± 0.1) and acetonitrile (log K = 5.92 ± 0.1 and 5.3 ± 0.2). An association constant for the interaction of Fe(III)PPIX with Art could, however, only be determined in acetonitrile (log K = 4.48 ± 0.04) owing to a weakened interaction in aqueous media. Furthermore, the first crystal structure of the complex formed between Fe(III)PPIX and the QD analogue, cinchonine, was obtained following slow evaporation from a solution of acetonitrile.

To probe the possible mechanism of toxicity of Fe(III)PPIX, its peroxidase activity was investigated using the chromogenic substrate, 2,2'-azino-bis(3-ethylbenzothiazoline-6-sulfonic acid) (ABTS). The oxidation of ABTS to $ABTS^{\cdot+}$ by Fe(III)PPIX and hydrogen peroxide (H_2O_2) was investigated in an aqueous and aqueous SDS solvent system. Radical production was found to be more stable in the aqueous SDS system, and furthermore, the rate of radical production was also found to be lower in this system compared to aqueous solution. From the available experimental data, attempts were made to determine a preliminary kinetic model for the oxidation of ABTS by Fe(III)PPIX and H_2O_2 in aqueous solution.

The modulatory effect of CQ, QD and Ar on the oxidation of ABTS by Fe(III)PPIX was monitored in both aqueous solution and aqueous SDS. Both CQ and QD were found to significantly inhibit the rate of radical production in aqueous solution by 30% and 80%, respectively. While the rate of ABTS oxidation is lower, CQ was found to extend the life of Fe(III)PPIX by reducing the rate of its degradation by H_2O_2 by 70%, while QD reduced the rate of degradative attack by 90%. Consequently, Fe(III)PPIX has reduced peroxidative activity but is present for a longer period. The same was true for QD in the aqueous SDS system, however, CQ was found to

have minimal effect on the yield of radical production compared to Fe(III)PPIX in aqueous SDS, however, the rate was still reduced. Art was found to have the opposite effect of CQ and QD and enhanced radical production by three times that of Fe(III)PPIX. This is thought to be related to the presence of the endoperoxide bridge in the structure of Art and it is proposed that the induction of oxidative stress is one of its possible mechanisms of action.

The results obtained in this study provide insight into the mechanism of drug-Fe(III)PPIX interaction. Furthermore, valuable information regarding the ABTS oxidation catalytic cycle was determined through careful consideration of the kinetic model and the assay could be used to provide insight into the mechanism of toxicity of CQ, QD and Ar.

Uittreksel

‘n Hoof klas van antimalariese dwelms tree op deur bykomende vlakte van vrye heem, Fe(III)PPIX, binne die malaria parasiet. Terwyl Fe(III)PPIX bekend is as giftig, is die manier hoe dit die dood in die parasiet bewerkstellig hoegenaamd nie duidelik nie. Die werk wat hier aangebied word, beoog om die onsekerhede aan te spreek. In die eerste deel van hierdie werkstuk word daar gefokus op die interaksie tussen kliniese relevante teen malaria dwels en Fe(III)PPIX. Spektrofotometriese titrasies was gebruik om die Fe(III)PPIX-dwelm komplekse vormasie te ondersoek onder drie biologiese relevante omgewings, naamlik ‘n waterige omgewing (pH 7.4) verteenwoordigend na die malaria parasiet sitisol; acetonitrile wat die nie-waterige interne lipied naboots en die reinigingsmiddel, SDS, was gebruik om ‘n lipied-water koppelvlak sisteem te modeliseer, wat by die membraan oppervlakte teenwoordig is. Drie teen-malariese dwelms, chlorokien (CQ), kinidien (QD) en artemisinin (Art), wat aan drie unieke klasse behoort, was ondersoek om die bindende sterkte tussen die teen-malariese dwelms en Fe(III)PPIX te bepaal. Sterk assosiasiese konstantes vir die interaksie van Fe(III)PPIX met QD en CQ was bepaal in die waterige (log K = 5.8 ± 0.1 and 6.5 ± 0.1), waterige SDS sisteem (log K = 6.2 ± 0.1 and 6.5 ± 0.1) en acetonitril (log K = 5.92 ± 0.1 and 5.3 ± 0.2). ‘n Assosiasie konstante vir die interaksie van Fe(III)PPIX met Art kon egter slegs in acetonitrile (log K = 4.48 ± 0.04) bepaal word te wyte aan ‘n verswakte interaksie in die waterige media. Verder was die eerste kristal struktuur met die komplekse vorm tussen Fe(III)PPIX en die QD analoog, cinchonine verkry deur ‘n stadige evaporasie van die acetonitrile oplossing.

Om die moontlike meganisme van toksisiteit van Fe(III)PPIX te ondersoek , was die peroksidase aktiwiteit ondersoek deur die chromogeniese substraat 2,2’-azino-bis(3-ethylbenzothiazoline-6-sulfonic acid) (ABTS) te gebruik. Die oksidasie van ABTS na $ABTS^{\cdot+}$ deur Fe(III)PPIX en waterstof peroksied (H_2O_2) was ondersoek in ‘n waterige oplossing en waterige SDS oplossing. Radikale produksie was gevind wat meer stabile was in die waterige SDS sisteem, die koers van radikale produksie was egter betekenisvol stadiger wanneer vergelyk word met die van die waterige SDS sisteem. Verder was ‘n poging tot die bepaaling van ‘n voorlopige kinetiese model vir die oksidasie van ABTS deur Fe(III)PPIX en H_2O_2 in ‘n waterige oplossing uitgevoer.

Die modulatoriese effek van CQ, QD en Ar op die oksidase van ABTS deur Fe(III)PPIX was gemonitor in beide die waterige oplossing en waterige SDS. Beide CQ en QD was gevind om radikale produksie beduidende te inhibeer by 30% en 80%, onderskeidelik. Terwyl die koers van ABTS oksidasie verlaag is, verleng CQ die lewe van Fe(III)PPIX deur die koers van sy agteruitgang deur H_2O_2 by 70% te inhibeer, terwyl QD dit by 90% geinhibeer het. Gevolglik, het Fe(III)PPIX peroxidatiewe aktiwiteite verminder, maar bly teenwoordig vir ‘n langer tydperk. Dieselfde is gevind vir QD in die waterige SDS stelsel, CQ was egter gevind dat dit ‘n minimale effek het op die opbrengs van radikale produksie vergelykend met Fe(III)PPIX in waterige SDS terwyl die koers

steeds verminder het. Dit was gevind dat Art die teenoorgestelde effek van CQ en QD en gevorderde radikale produksie drie keer meer as Fe(III)PPIX. Die gedagte is dat dit verwant is aan die teenwoordigheid van ‘n endoperoksied brug in die struktuur van Art en dit word aanbeveel dat die induksie van oksidatiewe spanning een van die moontlike meganismes van aksie is.

Die resultate wat in hierdie studie gevind is versksaf insig in die meganisme van die dwelm-Fe(III)PPIX se interaksie. Verder, was waardevolle inligting ten opsigte van die ABTS oksidasie katalitiese siklus ontdek deur sorgvuldige oorweging van die kinetiese model en die toets kon gebruik word om insig te beverkstellig in di meganisme van toksisiteit van CQ, QD en Ar.

Dedication

To my beloved parents

Abdol and Christine Sammy

Acknowledgments

First and foremost, I would like to thank my Lord and saviour for a beautiful journey of growth and discovery. Nothing would be possible without Him who holds my life in His hands.

Thank you, **Dr Katherine de Villiers** for being the most patient supervisor anyone could ask for. You have always been there to listen and encourage me to not give up. Thank you for all your help and guidance throughout my journey.

Thank you to my co-supervisor, **Dr David Kuter** for being with from beginning to end, despite the distance. Thank you for making yourself available to answer my questions and support me when I needed it. I was blessed to have you on this journey.

I would especially like to acknowledge **Dr Wilhelm Gerber** for stepping in at the last minute to save the day. Thank you for all the hard work on the kinetic aspects of my work and for helping me to get to this point. I would not have achieved this goal without you.

Thank you to **Dawie de Villiers** and **Dr Vincent Smith** for your help and patience with solving the crystal structure.

To the most loving and supportive **parents**. Thank you for being my biggest cheerleaders and for being there for me on all the late nights and long drives. Having you with me during this time has been the biggest blessing of all. I love you.

To my family, **Alaric, Linden** and **Ousie**, thank you for always showing an interest in my work and for giving me love and support throughout my journey, even though you didn't understand much of it. You are greatly valued and loved.

To my best friends, **Stephanie, Ilse** and **Mari** for putting up with me during those stressful times. I couldn't have made it through these two years without your support and understanding.

To my lab group, **Ronel Muller** and **Sharne Fitzroy**, thank you for always having an ear to listen and for the continued support throughout this journey.

Thank you to the **National Research Foundation (NRF)** for financial support throughout my postgraduate studies.

Publications and Conference Proceedings

Publications:

J. Gildenhuys, C. J. Sammy, R. Müller, V. A. Streltsov, T. le Roex, D. Kuter and K. A. de Villiers, Alkoxide coordination of iron (III) protoporphyrin IX by antimalarial quinoline methanols: a key interaction observed in the solid-state and solution, *Dalton Trans.*, 2015, **44**, 16767–16777.

Conference Proceedings:

SACI Inorganic Chemistry Conference **2015**, Rhodes University, Grahamstown, RSA

Poster Presentation: Chandre J. Sammy and Dr Katherine A. de Villiers, Investigating Haem Toxicity.

List of Abbreviations

ABTS	2,2′-azino-bis(3-ethylbenzothiazoline-6-sulfonic acid) diammonium salt
Art	artemisinin
Ar	artesunate
Cn	cinchonine
CQ	chloroquine
CQR	chloroquine-resistant strain
CQS	chloroquine-sensitive strain
DMSO	dimethyl sulfoxide
DV	digestive vacuole
EXAFS	extended X-ray adsorption fine structure
Fe(II)PPIX	iron (II) protoporphyrin IX
Fe(III)PPIX	iron (III) protoporphyrin IX
H_2O_2	hydrogen peroxide
Hb	haemoglobin
Hf	halofantrine
HO	haem oxygenase
HRP	histidine rich proteins
HySS	hyperquad simulation and speciation
MQ	mefloquine
N-AcMP8	*N*-acetylmicroperoxidase-8

NaOH	sodium hydroxide
Pf	*Plasmodium falciparum*
*Pf*CRT	*P. falciparum* CQ-resistance transporter
Pgh1	P-glycoprotein homologue 1
RBCs	red blood cells
ROS	reactive oxygen species
SCD	single crystal X-ray diffraction
SDS	sodium dodecyl sulfate
Tris	tris(hydroxymethyl)aminomethane
QD	quinidine
QN	quinine

Table of Contents

Chapter 4. The Peroxidase Activity of Fe(III)PPIX

List of Figures

Figure 1.12 The structures of monomeric porphyrin species, **(a)** urohemin I and **(b)** *N*-acetylmicroperoxidase-8 (*N*-AcMP8), used to investigate the drug complexation.[99,100,102]

Figure 1.13 Spectrophotometric titration of CQ with haem. **(a)** The spectroscopic changes in the Soret band observed when Fe(III)PPIX is titrated with CQ. **(b)** The change in absorbance of Fe(III)PPIX as a function of increasing CQ concentration indicated by the data points. The solid line shows the best fit of the 1:1 Fe(III)PPIX:CQ binding model. Reproduced with permission from reference 103.

Figure 1.14 (a) The crystal structures of Hf-Fe(III)PPIX, thermal ellipses are drawn at 50% probability. The single crystal structures of **(b)** QN-Fe(III)PPIX and **(c)** QD-Fe(III)PPIX, solvent molecules and non-relevant hydrogen atoms were removed for clarity. Atom colour coding: C, grey; H, white; Cl, yellow; F, light blue; Fe, cyan; N, dark blue and O, red. Reproduced with permission from reference 110 and 111 respectively.

Figure 1.15 The UV-visible spectra of Fe(III)PPIX in solution before (turquoise) and after (black) titration with **(a)** QD in acetonitrile and **(b)** QN in pentanol. Reproduced with permission from reference 111.

Figure 1.16 The structures previously proposed for the Fe(III)PPIX-CQ complex. **(a)** The coordination of CQ to monomeric Fe(III)PPIX,[117] **(b)** π-stacking of CQ to μ-oxo dimeric Fe(III)PPIX,[118] **(c)** μ-oxo tetramer Fe(III)PPIX adduct π-stacked with two CQ molecules,[119] **(d)** CQ molecules π-stacked between Fe(III)PPIX μ-oxo dimers[120] and **(e)** hydrogen bonded CQ to Fe(III)PPIX.[122] Reproduced with permission from reference 124.

Figure 1.17 (a) The UV-visible spectrum of the Fe(III)PPIX π-π dimer (grey dashed line) compared to that of the μ-oxo dimer (grey) and the CQ-Fe(III)PPIX complex (black). **(b)** The recently proposed structure of the Fe(III)PPIX-CQ complex. Reproduced with permission from reference 123 and 124, respectively.

Figure 1.18 The catalytic cycle of Fe(III)PPIX peroxidases redrawn based on reference 126. The porphyrin macrocyle is represented as a rectangle, and connecting lines from each of the four corners represent coordination of the metal centre via the four nitrogen atoms.

Figure 1.19 The UV-Visible spectrum of ABTS (purple). Upon oxidation, the formation of the emerald green radical cation ($ABTS^{\cdot+}$) commences which can be measured at 414, 660 and 720 nm (green), as indicated by the arrows.

Figure 3.1 Fe(III)PPIX speciation in aqueous and non-aqueous solution. The UV-visible spectrum of Fe(III)PPIX in aqueous solution (Tris buffer, 50.0 mM, pH 7.4) (**-**), acetonitrile (-) and aqueous SDS solution (**-**). The position of the charge-transfer (~600-630 nm) and Soret bands (~380-400 nm) are marked by black, green and red dotted lines for the aqueous, organic and SDS solutions respectively. Peaks positions of the Soret and charge-transfer bands are the same in purely aqueous and aqueous SDS solution and thus black and blue dotted lines overlap.

Figure 3.2 The UV-visible spectrum of Fe(III)PPIX in solution before (─) and after (─) spectrophotometric titration with QD in **(a)** aqueous solution (50 mM Tris buffer, pH 7.4), **(b)** acetonitrile and **(c)** aqueous SDS (50 mM Tris buffer, pH 7.4) solution. The spectrum of Fe(III)PPIX before titration (─) and after each subsequent addition of QD (purple to blue) can be seen in spectra **(a)**, **(b)** and **(c)**. For clarity, the enlarged spectra show the spectrum of Fe(III)PPIX in the region between 550 and 650 nm before (─) and after (─) the titration. The position of the charge-transfer band in the Fe(III)PPIX π-π dimer and QD-Fe(III)PPIX complex are marked by black and blue dotted lines, respectively. Arrows indicate the direction of spectroscopic change during titration.

Figure 3.3 The UV-visible spectra of Fe(III)PPIX in solution before (─) and after (─) addition of CQ. The conditions were **(a)** aqueous solution (50 mM Tris buffer, pH 7.4), **(b)** acetonitrile, and **(c)** aqueous SDS (50 mM Tris buffer, pH 7.4). The position of the Soret and charge-transfer band of the Fe(III)PPIX π-π dimer and that of the species after addition of CQ are marked by a black and blue dotted lines respectively and arrows indicate direction of spectroscopic change during titration.

Figure 3.4 The UV-visible spectrum of Fe(III)PPIX before (—) and after (—) titration with **(a)** artemisinin in acetonitrile and **(b)** artesunate in 1 mM aqueous SDS solution. The position of the Soret and charge-transfer band of the Fe(III)PPIX species before and after titration are marked by a black and blue dotted lines respectively. Arrows indicate direction of spectroscopic change during the titration.

Figure 3.5 Hydrogen bonds (red dashed lines) in the crystal packing of the Cn-Fe(III)PPIX complex. (i) An intramolecular hydrogen bond between the protonated quinuclidine hydrogen of Cn and the propionate group of Fe(III)PPIX and (ii) intermolecular hydrogen bond between the propionic acid group of one Fe(III)PPIX molecule and the propionate group of the neighbouring Fe(III)PPIX molecule. Non-relevant hydrogen atoms have been removed for clarity. Atom colour coding: H-white, C-grey, N-blue, O-red and Fe-cyan.

Figure 3.6 The crystal packing of Cn-Fe(III)PPIX viewed along the crystallographic *a*-axis. Hydrogen atoms are omitted for clarity. Atom colour coding: C-grey, N-blue, O-red and Fe-cyan.

Figure 4.1 The reaction between Fe(III)PPIX and H_2O_2. Spectroscopic changes for the reaction between 10.0 µM Fe(III)PPIX and 100.0 µM H_2O_2 in **(a)** aqueous and **(b)** aqueous SDS solution over a period of 30 minutes. The black line represents the spectrum of Fe(III)PPIX before the addition of H_2O_2 and the subsequent spectra at each time point are shown from purple to dark blue. Shifts in absorbance are indicated with arrows. Plots **(c)** and **(d)** show the trace at 380 nm (black circles) for the reactions in **(a)** and **(b)**, respectively, fitted with a two-phase exponential decay function (blue line).

Figure 4.2 (a) The UV-visible spectrum of ABTS (black) and the $ABTS^{\cdot+}$ (green). Beer-Lambert Law Plots for **(b)** ABTS and **(c)** $ABTS^{\cdot+}$. The extinction coefficients are 40399 ± 626 and 12807 ± 150 M^{-1} cm^{-1} respectively.

Figure 4.3 The effect of pH on the oxidation of ABTS. **(a)** The change in absorbance monitored at 660 nm over time at pH 11 (-), 9 (-), 8 (-), 7.5 (-), 7 (-) and 6.5(-) in the presence of 3.0 mM ABTS, 1.0 µM Fe(III)PPIX and 100.0 µM H_2O_2 and **(b)** the absorbance for pH 6.5 over a period of 12 hours. **(c)** The initial 150 seconds of the reaction in **(a)** plotted as a function of increasing time. **(d)** The maximum yield for the reactions described in **(a)** as a function of pH fitted with a sigmoidal function.

Figure 4.4 Effects of Fe(III)PPIX concentration on the oxidation of ABTS by H_2O_2. **(a)** ABTS radical production plotted as a function of increasing time. Experiments were carried out using 300.0 µM H_2O_2, 3.0 mM ABTS and Fe(III)PPIX concentrations of 0.3 (-), 0.6 (-), 1.0 (-) and 1.3 (-) 2.0 (-), 2.5 (-) and 4.0 (-) µM. **(b)** Maximal yield of $ABTS^{\bullet+}$ in **(a)** as a function of increasing Fe(III)PPIX concentration.

Figure 4.5 The effect of H_2O_2 on the oxidation of ABTS in aqueous solution. The conditions are 3.0 mM ABTS and **(a)** 50.0, **(b)** 100.0, **(c)** 200.0 and **(d)** 300.0 µM H_2O_2. In each set of experiments, the concentration of Fe(III)PPIX was varied as follows: 0.3 (-), 0.6 (-), 1.0 (-) and 1.3 (-) µM. **(e)** The maximum yield of $ABTS^{\cdot+}$(maximum concentration in 60 minutes) and the overall reaction rate **(f)** in the presence of 1.0 µM Fe(III)PPIX and 3.0 mM ABTS as a function of increasing H_2O_2 concentration.

Figure 4.6 The effect of ABTS concentration on the oxidation of ABTS in aqueous solution. The conditions are 100 µM H_2O_2 and **(a)** 0.8, **(b)** 1.0, **(c)** 1.5, **(d)** 2.0 and **(e)** 3.0 mM ABTS. In each set of experiments, the concentration of Fe(III)PPIX was varied as follows: 0.3 (-), 0.6 (-), 1.0 (-) and 1.3 (-) µM. The maximum yield and reaction rate in the presence of 100 µM H_2O_2 and 1.0 µM Fe(III)PPIX are plotted as a function of ABTS concentration in **(f)** and **(g)**, respectively.

Figure 4.7 The effect of ABTS concentration on the oxidation of ABTS in aqueous solution. The conditions are 1.0 µM Fe(III)PPIX in the presence of **(a)** 0.8, **(b)** 1.0, **(c)** 1.5, **(d)** 2.0 mM ABTS. In each experiment, the concentration of H_2O_2 was varied as follows: 25 (-), 50 (-), 100 (-) and 200 (-) µM. Dashed lines indicate the time at which [$ABTS^{\cdot+}$] starts to decay in the case of 200 µM H_2O_2. The maximum yield of $ABTS^{\cdot+}$ obtained in

the presence of 1.0 µM Fe(III)PPIX and **(e)** 100 µM H_2O_2 plotted as a function of increasing [ABTS] and **(f)** plotted as a function of increasing [H_2O_2] in the presence of 0.8 (black) and 2.0 mM (grey) ABTS.

Figure 4.8 The effect of ABTS concentration on the initial five minutes of ABTS oxidation in aqueous solution. The conditions are 1.0 µM Fe(III)PPIX in the presence of **(a)** 0.8, **(b)** 1.0, **(c)** 1.5 and **(d)** 2.0 mM ABTS in the presence of 25.0 (-), 50.0 (-), 100.0 (-) and 200.0 (-) µM H_2O_2. Dashed lines indicate what appears to be two different stages in the initial five minutes of the reaction.

Figure 4.9 The oxidation of ABTS in 60% (v/v) aqueous/acetonitrile. The conditions are 3.0 mM ABTS, 1.0 µM Fe(III)PPIX and 300.0 µM H_2O_2. The absorbance trace is observed to decrease in intensity which indicates poor stability of $ABTS^{\cdot+}$ in the solvent system.

Figure 4.10 Beer-Lambert Law Plots for **(a)** ABTS and **(b)** $ABTS^{\cdot+}$ in aqueous SDS. The extinction coefficients were found to be 19580 ± 121.9 and 24910 ± 834.8 M^{-1} cm^{-1}, respectively. The Beer-Lambert law plots obtained above for ABTS and $ABTS^{\cdot+}$ in aqueous solution are shown for comparison as grey, dashed lines in **(a)** and **(b)**, respectively.

Figure 4.11 Kinetics of $ABTS^{\cdot+}$ formation in the aqueous (grey) and aqueous SDS (black) system. The experiment was carried out using 1.0 µM Fe(III)PPIX, 3.0 mM ABTS and 300.0 µM H_2O_2.

Figure 4.12 Effects of Fe(III)PPIX concentration on the oxidation of ABTS by H_2O_2 in aqueous SDS solution. **(a)** ABTS radical production plotted as a function of increasing time. Experiments were carried out using 300.0 µM H_2O_2, 3.0 mM ABTS and Fe(III)PPIX concentrations of 0.3 (-), 0.6 (-), 1.0 (-) and 1.3 (-) µM. **(b)** Maximal yield of $ABTS^{\cdot+}$ in **(a)** as a function of increasing Fe(III)PPIX concentration. The trend obtained in aqueous solution is shown in grey.

Figure 4.13 The effect of varying H_2O_2 concentration on the oxidation of ABTS in aqueous SDS solution. The conditions are 3.0 mM ABTS in the presence of **(a)** 100.0, **(b)** 200.0, **(c)** 300.0 and **(d)** 400.0 µM H_2O_2 and Fe(III)PPIX concentrations of 0.3 (-), 0.6 (-), 1.0 (-) and 1.3 (-) µM. **(e)** The maximum yield (maximum concentration in 90 minutes) and overall reaction rate **(f)** obtained in the presence of 3.0 mM ABTS and 1.0 µM Fe(III)PPIX plotted as a function of increasing H_2O_2 concentration.

Figure 4.14 The effect of varying ABTS concentration on the oxidation of ABTS in aqueous SDS solution. The conditions are 100.0 µM H_2O_2 in the presence of **(a)** 1.0, **(b)** 2.0, **(c)** 3.0 and **(d)** 5.0 mM ABTS and Fe(III)PPIX concentrations of 0.3 (-), 0.6 (-), 1.0 (-) and 1.3 (-) µM. **(e)** The yield of $ABTS^{\cdot+}$ and **(f)** the overall reaction rate in the presence of 1.0 µM Fe(III)PPIX is plotted as a function of increasing ABTS concentration in.

Figure 4.15 The effect of varying ABTS concentration on the oxidation of ABTS in aqueous SDS solution. The conditions are 100.0 µM H_2O_2 in the presence of **(a)** 1.0, **(b)** 2.0, **(c)** 3.0 and **(d)** 5.0 mM ABTS and H_2O_2 concentrations of 100.0 (-), 200.0 (-), 300.0 (-) and 400.0 (-) µM. The maximum yield of $ABTS^{\cdot+}$ obtained in the presence of 1.0 µM Fe(III)PPIX and **(e)** 100.0 µM H_2O_2 plotted as a function of increasing [ABTS] and **(f)** plotted as a function of increasing [H_2O_2] in the presence of 1.0 (black) and 5.0 mM (grey) ABTS.

Figure 4.16 The effect of ABTS concentration on the initial five minutes of ABTS oxidation in aqueous solution. The conditions are 1.0 µM Fe(III)PPIX in the presence of **(a)** 1.0, **(b)** 2.0, **(c)** 3.0 and **(d)** 5.0 mM ABTS in the presence of 25.0 (-), 50.0 (-), 100.0 (-) and 200.0 (-) µM H_2O_2.

Figure 4.17 The reaction between Fe(III)PPIX and H_2O_2. The experimental data (black), fitted to a non-linear least-squares function (blue) at 340nm.

Figure 4.18 The concentration of monomeric (-), dimeric (-) and oxidized (-) Fe(III)PPIX present in aqueous solution for the reaction described in Equation 4.8 and 4.9 at a wavelength of 340nm.

Figure 5.9 The effect of H_2O_2 concentration on ABTS oxidation by the CQ-Fe(III)PPIX complex in aqueous SDS solution. The conditions are **(a)** 100.0, **(b)** 200.0, **(c)** 300.0 and **(d)** 400.0 µM H_2O_2 in the presence of 3.0 mM ABTS and 0.6 (-), 1.0 (-), 2.0 (-) and 2.5 (-) µM Fe(III)PPIX. The dotted line indicates the final yield in the absence of drug in the aqueous SDS system in the presence of 1.0 µM Fe(III)PPIX and 3.0 mM ABTS. **(e)** The maximum yield, calculated as the maximum concentration of $ABTS^{\cdot+}$ reached within the 90 minute time period, and **(f)** the overall reaction rate, is plotted as a function of H_2O_2 concentration. The conditions were 1.0 µM CQ-Fe(III)PPIX and 3.0 mM ABTS.

Figure 5.10 The effect of H_2O_2 concentration on ABTS oxidation by the QD-Fe(III)PPIX complex in aqueous SDS solution. The conditions are **(a)** 100.0, **(b)** 200.0, **(c)** 300.0 and **(d)** 400.0 µM H_2O_2 in the presence of 3.0 mM ABTS and 1.0 (-), 1.3 (-), 2.0 (-) and 2.5 (-) µM Fe(III)PPIX. **(e)** The maximum yield, calculated as the maximum concentration of $ABTS^{\cdot+}$ reached within the 90 minute time period, and **(f)** the overall reaction rate, is plotted as a function of H_2O_2 concentration. The conditions were 1.0 µM QD-Fe(III)PPIX and 3.0 mM ABTS.

Figure 5.11 $ABTS^{\bullet+}$ production in the absence and presence of antimalarial drugs in the aqueous SDS system. The conditions are 1.0 µM Fe(III)PPIX (-), CQ- (-), QD- (-) and Ar-Fe(III)PPIX (-), 3.0 mM ABTS and 300.0 µM H_2O_2.

Figure 5.12 The effect of H_2O_2 on ABTS oxidation catalysed by Ar-Fe(III)PPIX in aqueous SDS. The conditions are **(a)** 100.0, **(b)** 200.0, **(c)** 300.0 and **(d)** 400.0 µM H_2O_2 in the presence of 3.0 mM ABTS, 1.0 mM Ar and 0.3 (-), 0.6 (-), 1.0 (-) and 1.3 (-) µM Fe(III)PPIX. **(e)** The maximum yield, calculated as the maximum concentration of $ABTS^{\cdot+}$ reached within the 90 minute time period, and **(f)** the overall reaction rate is plotted as a function of H_2O_2 concentration. The conditions were 1.0 µM Fe(III)PPIX, 1.0 mM Ar and 3.0 mM ABTS.

Figure 5.13 The oxidation of ABTS by Ar-Fe(III)PPIX. An enlargement of the first five minutes of the oxidation of ABTS in the presence of Ar-Fe(III)PPIX. The conditions are **(a)** 100.0, **(b)** 200.0, **(c)** 300.0 and **(d)** 400.0 µM H_2O_2 in the presence of 3.0 mM ABTS, 1.0 mM Ar and 0.3 (-), 0.6 (-), 1.0 (-) and 1.3 (-) µM Fe(III)PPIX.

List of Tables

Chapter 1. Literature Review

1.1 Haem and Haemoproteins

Iron(II)protoporphyrin(IX), more commonly referred to as haem, is arguably one of life's most central molecules and is involved in a number of biological processes.[1] Its structure, shown in Figure 1.1, consists of four pyrrole rings coordinated to an iron atom through their nitrogen atoms. Attached to the pyrrole rings are four methyl substituents as well as two propionic acid and two vinyl groups.[1] These structural features imbue this small molecule with both hydrophobic and hydrophilic character. This amphiphilic nature allows haem to associate with hydrophobic environments, as in haemoglobin and cytochrome c enzymes, but also facilitates the formation of hydrogen bonding with amino acids, and covalent bonds with enzymes and proteins.[1] Haem is also planar and aromatic which gives rise to π-stacking capabilities. A further versatility of haem is its iron centre which is able to adopt a number of oxidation states, with +2 and +3 oxidation states being the most stable. This enables haem and haem enzymes to take part in electron transport processes as well as oxidation/reduction reactions.[1] The iron centre is also able to coordinate one or two axial ligands, to form five- and six-coordinate complexes, respectively. This key feature allows haem to be incorporated into proteins to form haemoproteins which are able to bind small molecules such as oxygen and carbon monoxide, or chelate to protein amino acids such as histidine, methionine and tyrosine. Examples of such haemoproteins include cytochrome c, the electron transport protein; myoglobin, responsible for iron storage and buffering intracellular oxygen concentrations in the human body; haem oxygenases, the producers of neuromodulators such as carbon monoxide and nitric oxide; and cytochrome p450 (Figure 1.2 (a)) which is involved in the metabolism of drugs as well as the synthesis of steroid hormones and lipids.[1,2,3,4,5] The most well-known haemoprotein is, however, haemoglobin (Hb), the structure of which can be seen in Figure 1.2 (b). Hb contains four equivalents of the haem prosthetic group which, consequently, play a key role in the functioning of this protein.[6] Haem is responsible for the oxygen-binding properties of Hb, which allows for the transport of oxygen from the lungs to all other organs in the body.

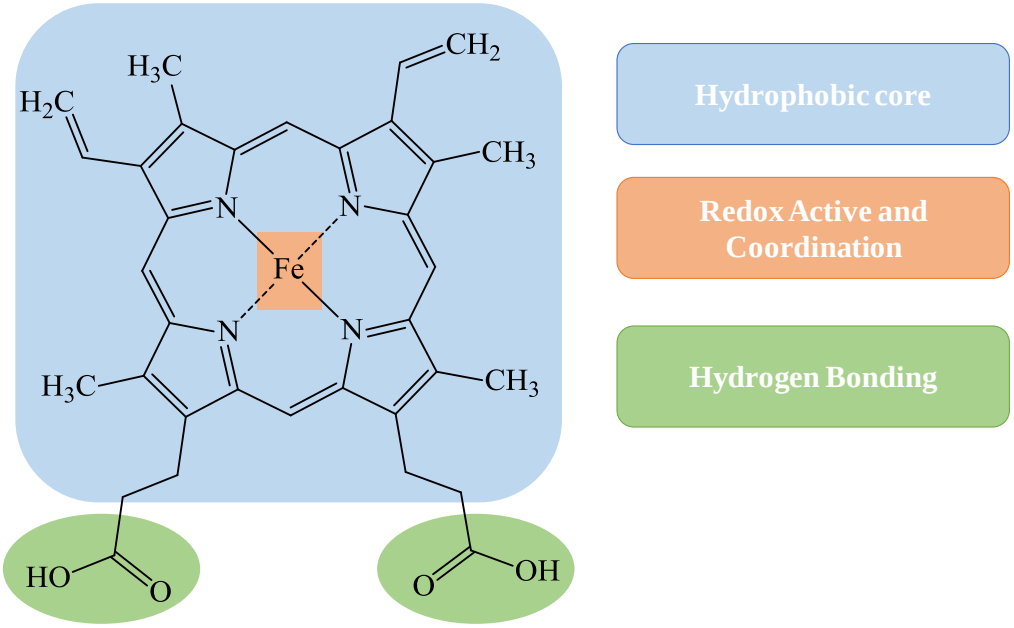

Figure 1.1 The haem prosthetic group and the diversity of its functionality. The redox active metal centre, which facilitates coordination, is shown in orange, while the green colour represents the hydrophilic periphery necessary for hydrogen bonding.

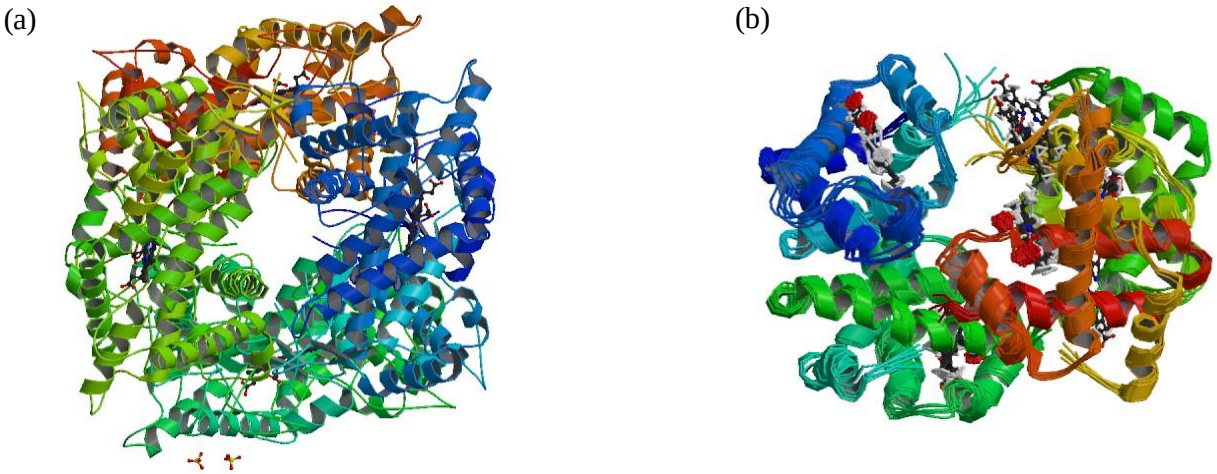

Figure 1.2 Haemoproteins found in the human body. **(a)** The structure of cytochrome p450 and **(b)** the structure of adult haemoglobin in solution obtained from the Protein Data Bank (PBD),[7] PDB ID: 2F9Q[8] and 2H35,[9] respectively.

1.2 Haem Toxicity

While the versatility and reactivity of haem is important for enzyme activity, drug detoxification and signal transduction pathways,[10] these same characteristics present toxicological problems, particularly when haem exists in the unbound or free state. The iron centre in free haem is readily oxidised, giving rise to an accumulation of Fe(III)PPIX. Indeed, in recent years the accumulation of free haem has been implicated in a number of diseases, including severe haemolysis occurring in a number of diseases including sickle cell disease and haemolytic anaemia (see Figure 1.3).[11,12] The manner in which haem exerts its toxicity is discussed in the subsequent section.

1.2.1 Sources of Toxicity

The toxic manner in which excess amounts of Fe(III)PPIX affect cells is thought to be related to its hydrophobic nature, previously discussed in Section 1.1.[13] For this reason, Fe(III)PPIX is able to easily access membranes, enhancing permeability and increasing the susceptibility to haemolysis.[11] Indeed, Fe(III)PPIX has been shown to enhance potassium loss and swelling in erythrocytes which impedes their ability to preserve crucial cation gradients and, consequently, causes haemolysis.[14] This haemolytic process is thought to occur in two phases. The first phase involves potassium loss and subsequent ATP depletion, while the second is thought to be associated with a substantial loss of haemoglobin.[14] It has further been shown that, when saturated with Fe(III)PPIX, red cell ghosts were completely disrupted and, furthermore, important interactions such as lipid-protein associations were impaired.[15]

Reactive oxygen species (ROS), derived from the redox active iron centre of Fe(III)PPIX, have been closely associated with haemolysis and related diseases. In the malaria parasite for example, the production of these ROS poses a threat to cells containing haem through oxidative stress. During this process, haem is thought to aggregate in lipid membranes and, through the production of ROS, cause lipid oxidation. During this process, unsaturated lipids, present within cell membranes, are converted to lipid radicals and, eventually, in the presence of oxygen to hydroperoxides which cause cell disruption.[11,16,17,18,19] Furthermore, the production of ROS has also been implicated in protein damage which can lead to the production of cytotoxic products.[20] In the case of membrane-bound proteins, their oxidation has been shown to occur independently of lipid peroxidation. Fe(III)PPIX mediated ROS generation has also been shown to influence gene expression in various cell systems. It has been shown to degrade DNA, converting supercoiled plasmid DNA to open circle and linear forms and, with longer incubation times, into even smaller pieces.[21] Inhibition of DNA scission in the presence of hydroxide radical scavengers has implicated these radicals in DNA damage.[11, 21]

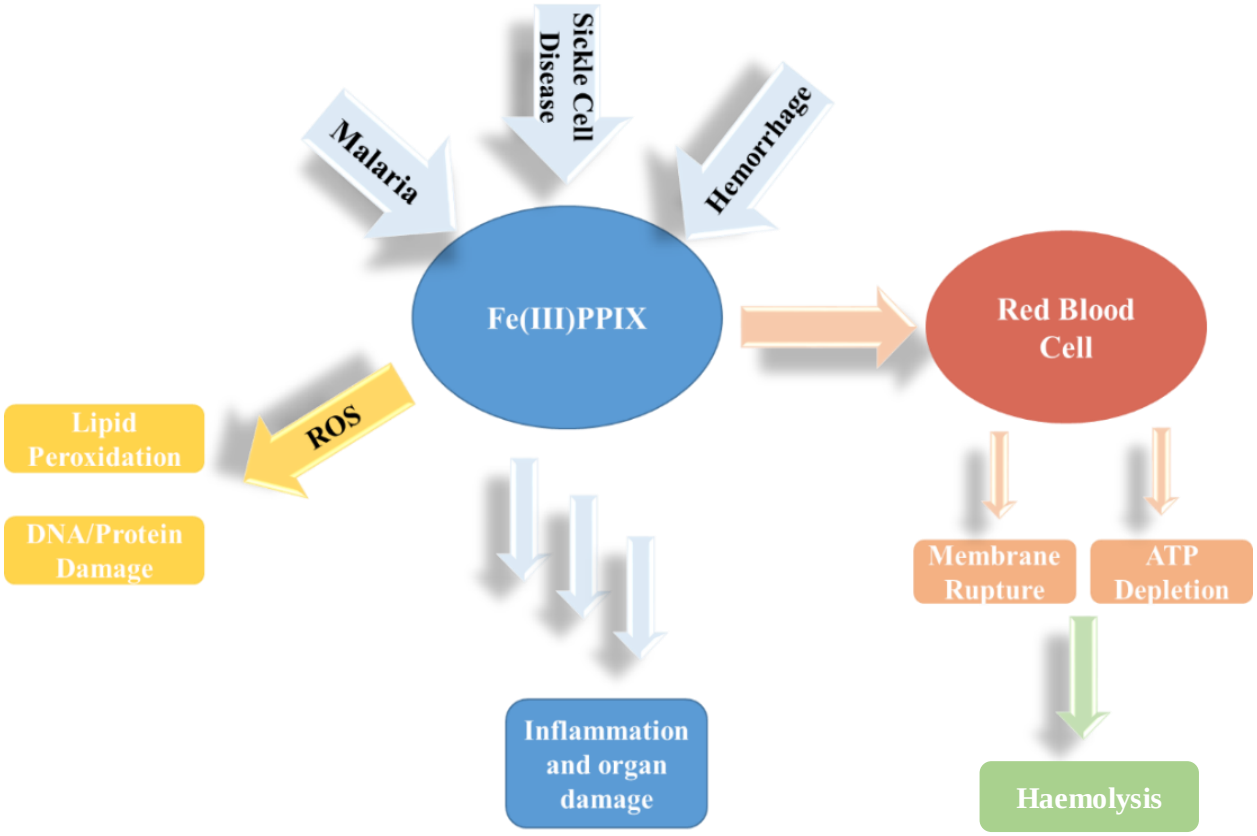

Figure 1.3 The toxic effects of Fe(III)PPIX. Redrawn from reference 11. The blue arrows at the top of the figure indicate diseases that contribute to an accumulation of Fe(III)PPIX, while the yellow, orange, green and blue arrows extending from Fe(III)PPIX indicate various toxic effects of Fe(III)PPIX.

ROS generation by Fe(III)PPIX is thought to occur via reduction of Fe(III)PPIX to Fe(II)PPIX, followed by reaction with oxygen in a manner similar to the Fenton reaction. The first step of this process (see Equation (1.1)), during which Fe(III) is reduced to Fe(II) by superoxide, proceeds in a manner similar to the Haber Weiss equation.[22] The Fenton-type reaction between hydrogen peroxide (H_2O_2) (produced via Equation 1.2), and Fe(II)PPIX follows Equation 1.3 in which hydroxide radicals and ferric iron are produced. This reaction pathway has been referred to as the "superoxide driven Fenton reaction".[22]

$$O_2^{\cdot-} + Fe^{3+} \rightarrow O_2 + Fe^{2+} \quad (1.1)$$

$$2O_2^{\cdot-} + 2H^{+} \rightarrow O_2 + H_2O_2 \quad (1.2)$$

$$H_2O_2 + Fe^{2+} \rightarrow Fe^{3+} + OH^{-} + {}^{\cdot}OH \quad (1.3)$$

Owing to this toxic threat Fe(III)PPIX poses to biological systems, humans have evolved a means to detoxify haem. This is discussed in the following section.

1.2.2 Mechanisms of Fe(III)PPIX Detoxification

Under normal conditions, protective mechanisms ensure the survival of organisms in redox active environments through Fe(III)PPIX detoxification. In humans, the haem oxygenase (HO) system plays an essential role in maintaining the levels of iron under physiological conditions.[23] The iron released during haem detoxification by HO is incorporated into ferritin (responsible for iron storage) or transferrin (responsible for iron transport).[24] In addition, it is an important antioxidant defence and has been shown to play a role in signalling pathways.[25] Currently, three HO isoforms in mammals have been identified of which HO-1 is responsible for the detoxification of Fe(III)PPIX.[26] HO isoforms have also been identified in plants and a number of other species including birds and bacteria. The mechanism of Fe(III)PPIX detoxification in humans is shown in Figure 1.4. During this process, Fe(III)PPIX is first oxidized to α-*meso*-hydroxyhaem. On deprotonation, this molecule can react with oxygen to produce verdohaem and carbon monoxide (CO). The final step of the reaction, catalysed by oxygen NADPH–cytochrome-P450-reductase, yields end products biliverdin and iron.[23] This detoxification mechanism consumes three molecules of oxygen and seven electrons.

Haem detoxification mechanisms are particularly essential for blood-sucking organisms which utilize Hb as a source of iron.[27] To cope with the large quantities of haem released during Hb catabolism, these organisms employ a series of unique detoxification mechanisms which include haem containment; degradation of Fe(III)PPIX into iron and other non-toxic intermediates; or the sequestration of haem into an inert crystalline solid.[27] The toxicity of haem and organism-specific detoxification methods can, however, be used to advantage in combating blood-feeding pathogens. Indeed, haem detoxification plays a crucial role in antimalarial chemotherapy, the details of which are discussed in the following section.

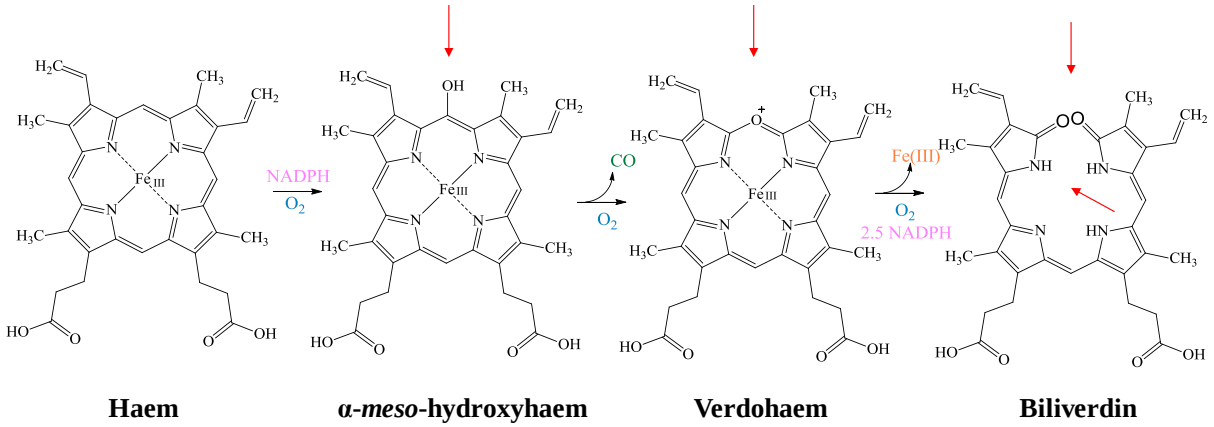

Haem **α-*meso*-hydroxyhaem** **Verdohaem** **Biliverdin**

Figure 1.4 The mechanism of Fe(III)PPIX detoxification in humans by the HO-1 enzyme. Red arrows indicate sites of enzymatic alteration. Redrawn from reference 23.

1.3 Haem Toxicity in the Malaria Parasite

1.3.1 History and Overview of Malaria

Malaria is a life-threatening parasitic disease that affects roughly 3.2 billion people throughout the world, the most vulnerable of which are children and pregnant women.[28] Since as early as 2700 BC, much debate regarding the source malaria transmission has permeated the literature.[29,30,31] It was only in the late 1800s when it was discovered that malaria can only be transmitted through the bite of a female *Anopheles* mosquito.[32] The World Health Organization estimated that, in 2015, there were 214 million reported cases of malaria of which 438 000 resulted in death.[28] While 88% of these cases occurred in Sub-Saharan Africa, roughly 40% of the world's population may be at risk of contracting malaria.[28,33] This is worrying since antimalarial drug resistance (which emerged in the 1970's) is a recurring problem leading to multi-drug resistance throughout the world. Consequently, there is a constant interest in developing new drugs to overcome resistance and eliminate malaria, however, this has been hampered by an incomplete understanding regarding the mechanism of action of known antimalarial drugs.

1.3.2 Lifecycle of the Malaria Parasite

Plasmodia are a group of parasites which cause infection through invasion of host erythrocytes.[28,33] *P. falciparum, P. malariae, P. ovale* and *P. vivax* are the four species of *Plasmodium* which cause malaria in humans.[28,29] Cases of human malaria transmitted by *P. knowlesi* have also been reported but this species more commonly infects monkeys in South-East Asia.[28] Of the five species, *P. falciparum* is the most common in Africa, while *P. vivax* is the prevailing parasite in countries outside of sub-Saharan Africa. These two species thus pose the biggest threat, with *P. falciparum* being responsible for most deaths.[28]

The life cycle of the malaria parasite is complex and involves five different stages.[33] Malaria infection commences with a bite from an infected female *Anopheles* mosquito. (Figure 1.5 (a)).[34] During this process, sporozoites are injected with the saliva of the infecting mosquito which travel through the human bloodstream until they reach the liver hepatocytes.[35] Here they proceed through a stage of asymptomatic asexual reproduction (Figure 1.5 (b)) where each sporozoite differentiates into thousands of uninucleate merozoites. The merozoites are then released into the blood stream to commence the second stage of asexual reproduction in the red blood cell (RBC) (Figure 1.5 (c)) which is referred to as the blood cycle. Merozoites undergo further development into ring, trophozoite and shizont forms before multiplying to produce a further 16-32 merozoites which proceed to invade other erythrocytes, thereby continuing this phase of the life cycle. The blood cycle occurs every 48 hours and is responsible for the characteristic symptoms associated with the disease – headaches, fever, chills and vomiting.[1] As the infection proceeds, some merozoites develop into male or female gametocytes which circulate in the blood stream until they are taken up by the female

Anopheles mosquito during its blood meal (Figure 1.5 (d)).[36] Once within the mosquito, sexual reproduction occurs (Figure 1.5 (e)) followed by maturation of the gametocytes into male and female gametes which, through fertilization, form ookinetes. The ookinete penetrates the gut wall of the mosquito to begin sporogony resulting in the formation of sporozoites which travel to the mosquito salivary glands to be injected during the next blood meal.[34,35,36] While each stage of the parasite life cycle is of importance, the blood cycle is of greatest relevance to antimalarial chemotherapies which target haem detoxification.

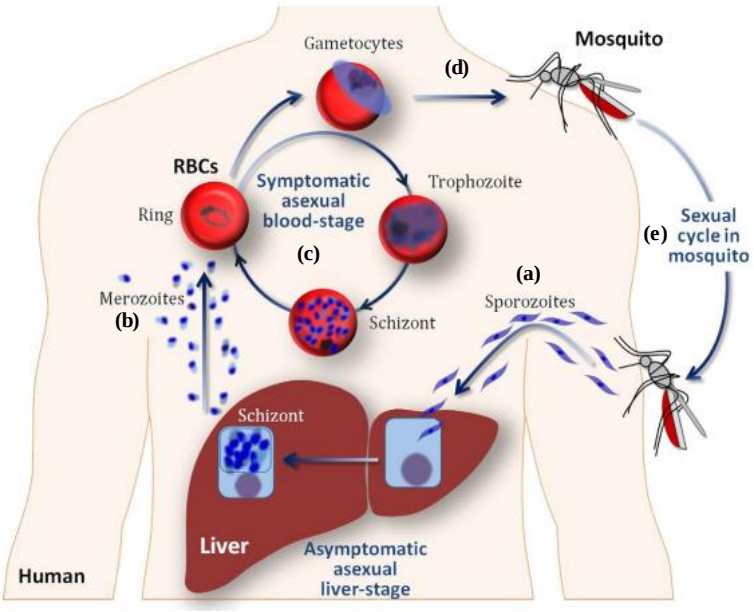

Figure 1.5 The life cycle of a malaria parasite. **(a)** A bite from the female *Anopheles* mosquito releases sporozoites which travel through the blood stream until they reach the liver **(b)** where asexual reproduction commences producing merozoites which enter RBCs to once again reproduce asexually during the blood cycle **(c)**. Some of these merozoites develop into male or female gametocytes and are released into the blood stream where they are **(d)** taken up by the mosquito during a blood meal to **(e)** undergo sexual reproduction producing sporozoites to be released during the subsequent blood meal. Reproduced from reference 35 with permission.[35]

1.3.3 The Blood Cycle

During the blood cycle, the parasite feeds on host Hb which is transported from the RBC cytoplasm into a specialized organelle in the parasite known as the digestive vacuole (DV).[37,38] While up to 65% of the Hb is digested, only 16% is used for its own protein synthesis.[39] Degradation of the remaining 49% is thought to provide space for the parasites' own growth.[38] In the DV, Hb degradation is undertaken by a number of proteolytic enzymes including aspartic proteases, three cysteine proteases as well as a zinc metalloprotease known as falsilysin.[37,40,41,42] The globin moiety of Hb is metabolized to yield amino acids, some of which are used by the parasite for growth, while the haem cofactor is released into the acidic (pH 5) aqueous milieu. Here, it is readily oxidized to Fe(III)PPIX.[38] As discussed above (see section 1.2), Fe(III)PPIX is toxic owing to its tendency to permeate membranes and generate ROS. To circumvent this toxicity, the parasite

sequesters Fe(III)PPIX in the form of an inert crystalline solid known as haemozoin or, more commonly, malaria pigment. A schematic representation of this stage of the parasite life cycle can be seen in Figure 1.6.

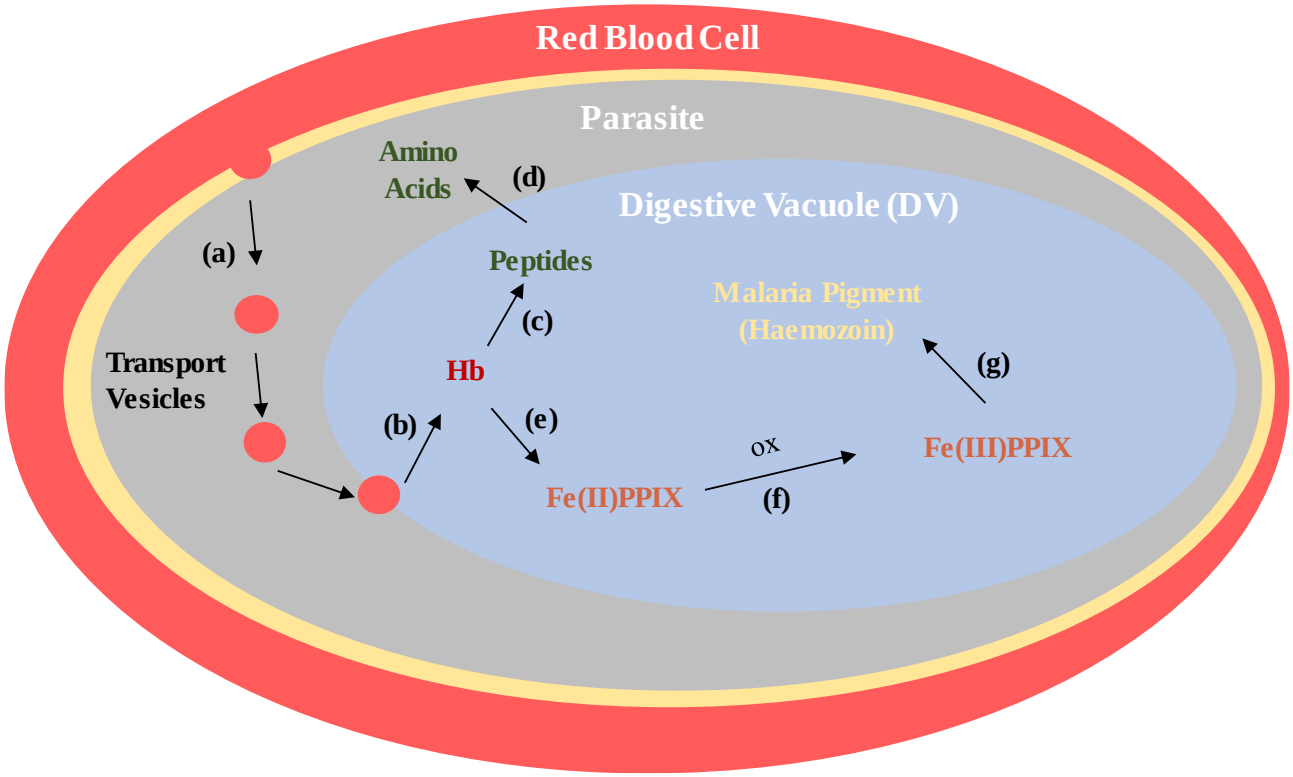

Figure 1.6 A schematic representation of the processes that occur during the blood cycle in the digestive vacuole (DV) of the malaria parasite, within the RBC of the human host. Haemoglobin (Hb) is ingested by the parasite **(a)** and transported to the DV **(b)**. Hb is digested to peptides **(c)** and further into amino acids **(d)** used for parasite growth and survival. Fe(II)PPIX is released as a side product of Hb degradation **(e)** which is immediately oxidized **(f)** to Fe(III)PPIX and poses a toxic threat to the parasite. As a result, it is sequestered **(g)** in the form of an inert crystalline solid, haemozoin (malaria pigment). Redrawn based on reference 38.

Haemozoin formation is not unique to the malaria parasite but also occurs in other blood-feeding pathogens. It has been observed in the midgut of *Rhodnius prolixus*, a vector involved in the transmission of Chagas'disease, as well as in *Schistosoma mansoni*, the causative agent of schistosomiasis in humans.[43,44] Investigating the formation of haemozoin has therefore been an essential step in understanding these diseases.

1.3.4 Haemozoin Formation

Determining the structure of haemozoin has been a controversial process, however, by means of high resolution powder X-ray diffraction, a study showed that the crystalline material consists of discrete dimers that form via coordination of the iron centre of one Fe(III)PPIX molecule to the carboxylate side chain of the

partner Fe(III)PPIX molecule and *vice versa* (see Figure 1.7).[45] The individual dimers, called μ-propionato dimers, then pack in the solid state through hydrogen bonding and π-stacking, to form haemozoin. While the structure of the haemozoin μ-propionato cyclic dimer has been conclusively proven, the mechanism of crystal growth is often incorrectly referred to as polymerisation, even today.

The mechanism of haemozoin formation has been a topic of great interest and debate. In recent years, two hypotheses for the formation of haemozoin have been proposed, namely that histidine-rich proteins (HRP) or lipids mediate its formation.[38] While previous studies have provided evidence for the presence of HRP in the parasite,[46,47] another has shown that haemozoin is still formed in parasite clones which do not contain the genes coding for HRP.[48] Consequently, the idea of lipid-mediated haemozoin formation has gained favour. Indeed, it has been shown that unsaturated lipids that contain no proteins efficiently promote β-haematin (synthetic haemozoin) formation *in vitro*.[49,50,51,52,53] Further support for lipid-mediated haemozoin formation has been reported by a number of authors who have shown haemozoin crystals either closely associated with the inner DV membrane or within neutral lipid bodies present within the DV of the parasite.[54,55] Uncertainties do however still remain regarding the exact mechanism of haemozoin formation which has hampered understanding rational design of antimalarial drugs that act by inhibiting haemozoin formation.

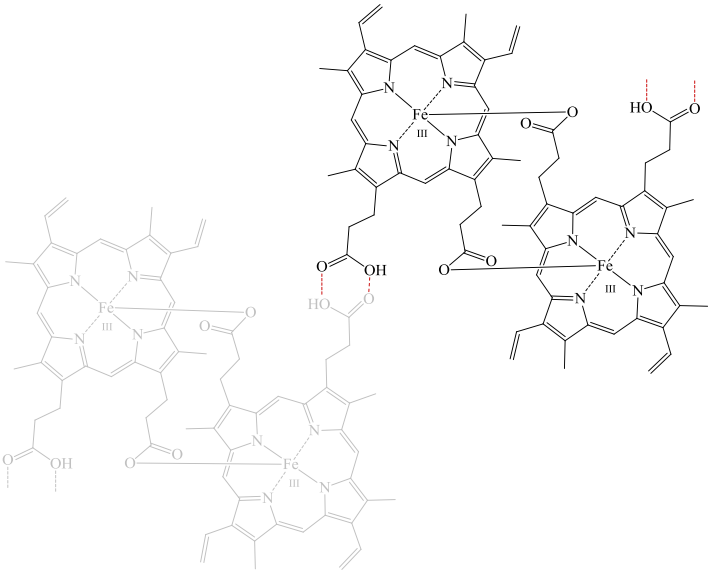

Figure 1.7 Haemozoin consists of μ-propionato cyclic dimers of Fe(III)PPIX. Two of these dimers are shown in black and grey, and the hydrogen bonding that occurs between them in the solid state is highlighted in red. Redrawn from reference 38.

1.4 Antimalarial Drugs

Quinoline antimalarial drugs are by far the most successful for the treatment of malaria. Malaria chemotherapy dates as far back as the 1600s where a powder, obtained from grinding the bark of a *Cinchona* tree was mixed with a liquid and drunk by the patient.[56] It was only in 1820, however, that the two active alkaloids quinine (QN) and cinchonine (Cn), were isolated from the bark of the *Cinchona* tree.[57,58] QN was subsequently used as the standard treatment for recurrent fevers until the 1940s, however, due to the high demand for QN, the need to develop new antimalarial drugs intensified.[57,58] The first attempts to prepare synthetic antimalarial drugs were based on the observation that methylene blue exhibited antimalarial activity.[58,59] This subsequently led to the first synthetic antimalarial drug, pamaquine in the 1920s.[58,60] Thereafter, quinacrine and, finally, chloroquine (CQ) was synthesised.[58] CQ became the mainstay drug for treatment of malaria, however, in the 1970s, the emergence of CQ resistant parasite strains increased the need for development of new antimalarial drugs. Consequently, amodiaquine was introduced as an alternative for over 40 years. Later, the development of the QN analogues mefloquine (MQ), a quinoline methanol, and halofantrine (Hf), a 9-phenanthrenemethanol, were introduced to treat CQ-resistant strains of malaria (see Figure 1.8).[58]

Following the emergence of drug resistance, arteminisin (an endoperoxide originally isolated from the Artemisia annua plant species) used in combination with other classes of antimalarial drugs has become the mainstay of treatment.[57,61] This combination therapy has greatly reduced drug resistance by introducing active ingredients targeting separate pathways. Worryingly, resistance to arteminisin has been documented and thus new antimalarial drugs are needed to combat malaria.[62] Rational design, however, has been hampered by an incomplete understanding of the mechanism of antimalarial drug action.

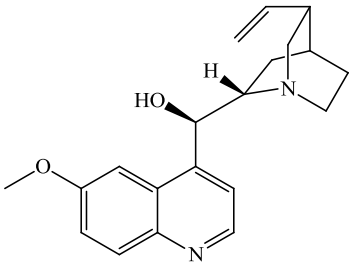

1

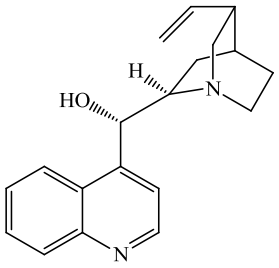

2

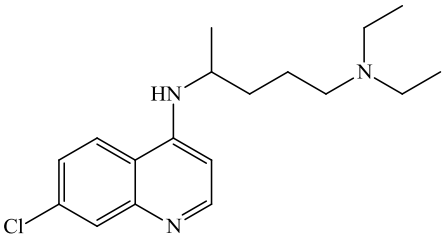

3

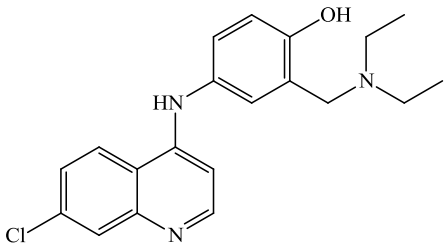

4

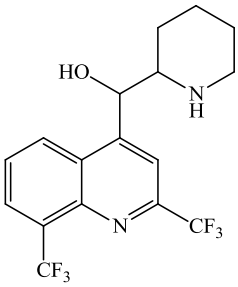

5

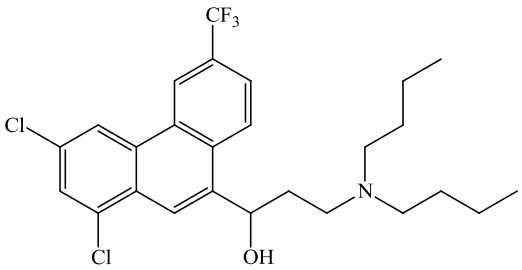

6

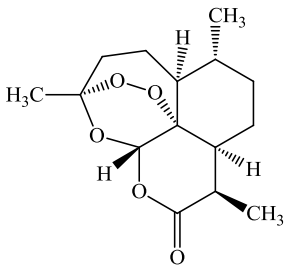

7

Figure 1.8 Molecular structures of **1**-quinine (QN), **2**-cinchonine (Cn), **3**-chloroquine (CQ), **4**-amodiaquine (AQ), **5**-mefloquine(MQ), **6**-halofantrine (Hf) and **7**-artemesinin (Art).

1.4.1 Postulated Mechanisms of Action of Clinically Relevant Antimalarial Drugs

The majority of antimalarial drugs exert their toxicity against the blood stage of the parasite life cycle, although the site of their action varies. They can be divided into five classes based on their mechanism of action, namely (i) the type I and II folate antagonists; (ii) napthoquinones; (iii) 4-aminoquinolines; (iv) quinoline methanols; and (v) endoperoxides.[63] Examples of each drug class are shown in Figure 1.9. The first class of antimalarial drug (i) targets the nucleic acid metabolism pathway. More specifically, these compounds inhibit enzymes involved in the folate pathway and, as a result, impair parasite DNA synthesis. The second class of drug (ii) is thought to target the electron transport chain of the mitochondria.[63,64] The 4-aminoquinolines and the quinoline methanols (class iii and iv) are the most commonly used antimalarials. These are thought to act on the Fe(III)PPIX detoxification pathway (see Section 1.2.2) by inhibiting haemozoin formation.[65] Some studies have also suggested that CQ may enhance oxidative stress within the parasite.[66] The final class (v) contain an endoperoxide bridge and differs greatly from the aforementioned drugs in structure. The exact mechanism of action of artemisinin has not been confirmed, however, some proposed mechanisms include protein alkylation, inhibition of calcium ATP-ase (*Pf*ATP-6), inhibition of the mitochondrial electron transport chain and accumulation in parasite lipid membranes which leave it vulnerable to a build-up of ROS.[67] The effectiveness of these antimalarial drugs have, however, been hampered by their increased tolerance in *P. falciparum*. Such mechanisms of resistance are discussed in the following section.

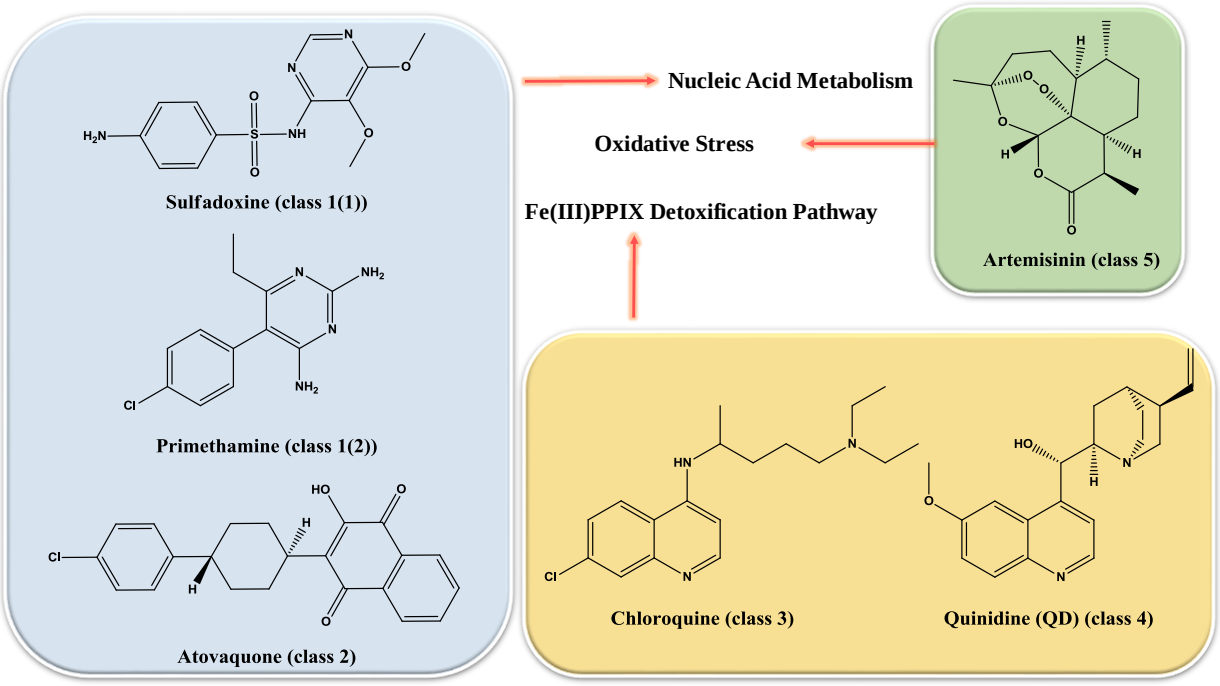

Figure 1.9 A schematic representation of the different classes of antimalarial drugs and their purported mechanisms of action or drug target in the blood stage of the malaria parasite life cycle.

1.4.2 Antimalarial Drug Resistance

The majority of studies have focused on the DV as the most likely target of antimalarial drug action and have shown that resistance arises from reduced drug accumulation in the DV rather than a change in the drug target. This was confirmed in the case of CQ by Krogstad *et al*. who found that efflux of this drug occurred at a rate 50 times faster in CQR parasite strains when compared to CQS strains.[68] It was initially suggested that increased vacuolar pH caused drug efflux by reducing the concentration of charged drug species and allowing them to diffuse out the DV. Studies have shown, however, that there is minimal variance in the pH of CQR and CQS parasites.[69,70] Several authors have implicated reduced vacuolar accumulation of CQ in resistance to this drug.[68,69]

It is now widely accepted that CQ resistance arises from mutations in the *P. falciparum* CQ resistant transporter (*Pf*CRT) protein – a transmembrane protein situated in the DV membrane.[71,72,73] While a number of mutations are necessary to confer resistance and are variable between strains, a mutation at position 76 in the amino acid sequence encoding the change from lysine to threonine (K76T) is almost always conserved.[74] This mutation is thought to facilitate CQ movement out of the DV by removing cationic charge repulsion associated with the lysine residue.[75] While beneficial for CQ resistance, variations in *Pf*CRT can greatly affect parasite fitness and impact the susceptibility of *P. falciparum* to drug treatment.[76] Indeed, CQR parasites no longer under CQ pressure will revert to CQS strains in time due to the fitness cost of this mutation. In addition to *Pf*CRT, overexpression of the *P. falciparum* multidrug resistance gene 1 (*Pf*mdr1) which is responsible for encoding the P-glycoprotein homologue 1 protein (Pgh1), has also been associated with CQ resistance, although it is thought to only modulate sensitivity towards CQ.[77] The same overexpression has been implicated in MQ, QN and Hf resistance, however, the details regarding how this affects sensitivity are not fully understood.[78]

The emergence of Art resistance has been a recent development which was first identified in regions of Cambodia. As of July 2016, Art resistance has been confirmed in Cambodia, the Lao People's Democratic Republic, Myanmar, Thailand and Viet Nam.[28] In 2014, researchers obtained information that suggested that Art resistance was related to a mutation on chromosome 13 in *P. falciparum*, namely *kelch13*.[79] Details of how this mutation affects clearance of the parasite is, however, not understood. The threat of increased resistance to all commonly used antimalarial drugs has been the drive for continued research in this area.

1.4.3 Interactions of Quinoline Antimalarial Drugs with Fe(III)PPIX

Quinoline antimalarial drugs have been shown to inhibit β-haematin formation, [47,80,81,82,] Further evidence for this mechanism of action was reported by Egan and co-workers for CQ.[83] These authors reported a dose-dependent decrease in haemozoin formed within the malaria parasite which corresponded to a decrease in parasite survival (see Figure 1.10 (a)). Moreover, a dose-dependent increase in free Fe(III)PPIX present in *P. falciparum* was also observed (see Figure 1.10 (b)) which could be closely correlated to the parasite survival inhibition dose-response curve (see Figure 1.10 (c)).[83] Furthermore, the authors provided evidence that, although Fe(III)PPIX is released in the DV of *P. falciparum*, it is subsequently redistributed to the parasite cytosol (pH 7.5).

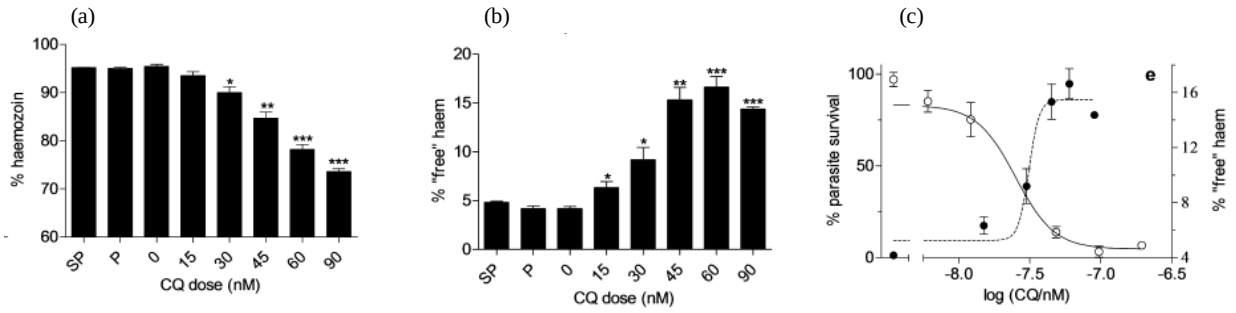

Figure 1.10 The percentage of (**a**) haemozoin formation and (**b**) free Fe(III)PPIX in *P. falciparum* as a function of increasing CQ concentration. **(c)** Percentage parasite survival (left axis) and Fe(III)PPIX (right axis) as a function of CQ concentration. Intersection occurs near the measured IC_{50} of CQ. Adapted with permission from reference 83. © 2016 ACS.

Presently, the exact mechanism of action of these antimalarial drugs is still unclear, however, two main hypotheses regarding the mechanism of haemozoin inhibition permeate literature. The first hypothesis is that haemozoin inhibition involves complex formation between free Fe(III)PPIX and the antimalarial drug in the DV of the parasite. The second proposal is that the antimalarial drugs adsorb onto the fastest growing face of haemozoin, thereby inhibiting further growth and increasing levels of toxic Fe(III)PPIX.[47,84] Drug-Fe(III)PPIX complex formation still plays an important role in this latter mechanism of action despite not being directly associated with haemzoin inhibition. Instead, these complexes likely influence the subsequent toxicity experienced by the parasite owing to the build-up of free Fe(III)PPIX in the DV where large concentrations of drug persist. Consequently, the nature of drug-Fe(III)PPIX complexes remains of considerable interest.

1.4.3.1 The Nature of Fe(III)PPIX in Solution

Initially, haem was thought to be highly aggregated in aqueous solution existing as a μ-oxo dimer.[85,86,87] This has been proved incorrect in a comprehensive study by Egan and co-workers who provided strong evidence for the formation of a Fe(III)PPIX π-π dimer in aqueous solution.[88] Reason for this discrepancy stems from high sensitivity of speciation to experimental conditions. The form of this species consists of two five coordinate Fe(III)PPIX monomers which are associated through π-π interactions between the unligated faces of the porphyrin. This species can easily be distinguished from the μ-oxo dimer by means of UV-visible spectra and magnetic susceptibility measurements.

Egan and co-workers further investigated Fe(III)PPIX speciation in aqueous solution as well as in mixed aqueous-organic solutions using a range of spectroscopic techniques. They reported that the speciation of Fe(III)PPIX is complex and highly dependent on a number of factors including the concentration, pH and nature of the solvent (see Figure 1.11).[89] The presence of monomeric Fe(III)PPIX, characterized by a sharp Soret band, was only observed at very low Fe(III)PPIX concentrations or in a solution containing a high percentage of organic solvent. The authors also confirmed that the Fe(III)PPIX π-π dimer is present in aqueous or protic solvents, regardless of the pH of the solution. On the other hand, formation of the μ-oxo dimer of Fe(III)PPIX was found to be entropically driven, but only under high pH conditions and in mixed aqueous-aprotic solvents. The reason for this is that aprotic solvents have a reduced ability to form hydrogen bonds with the axial ligand of Fe(III)PPIX. Further hydrogen bond formation is brought about by water, which consequently increases the water density around the hydroxide ligand. This entropically unfavourable process results in the release of the axial ligand and formation of the μ-oxo dimer species. Despite mounting evidence that the Fe(III)PPIX π-π dimer is the dominant species, recent authors still incorrectly report the μ-oxo dimer as the major Fe(III)PPIX species in aqueous solution.[90] Understanding the speciation of Fe(III)PPIX in solution has important implications in understanding drug-Fe(III)PPIX complex formation, which is discussed in the following section.

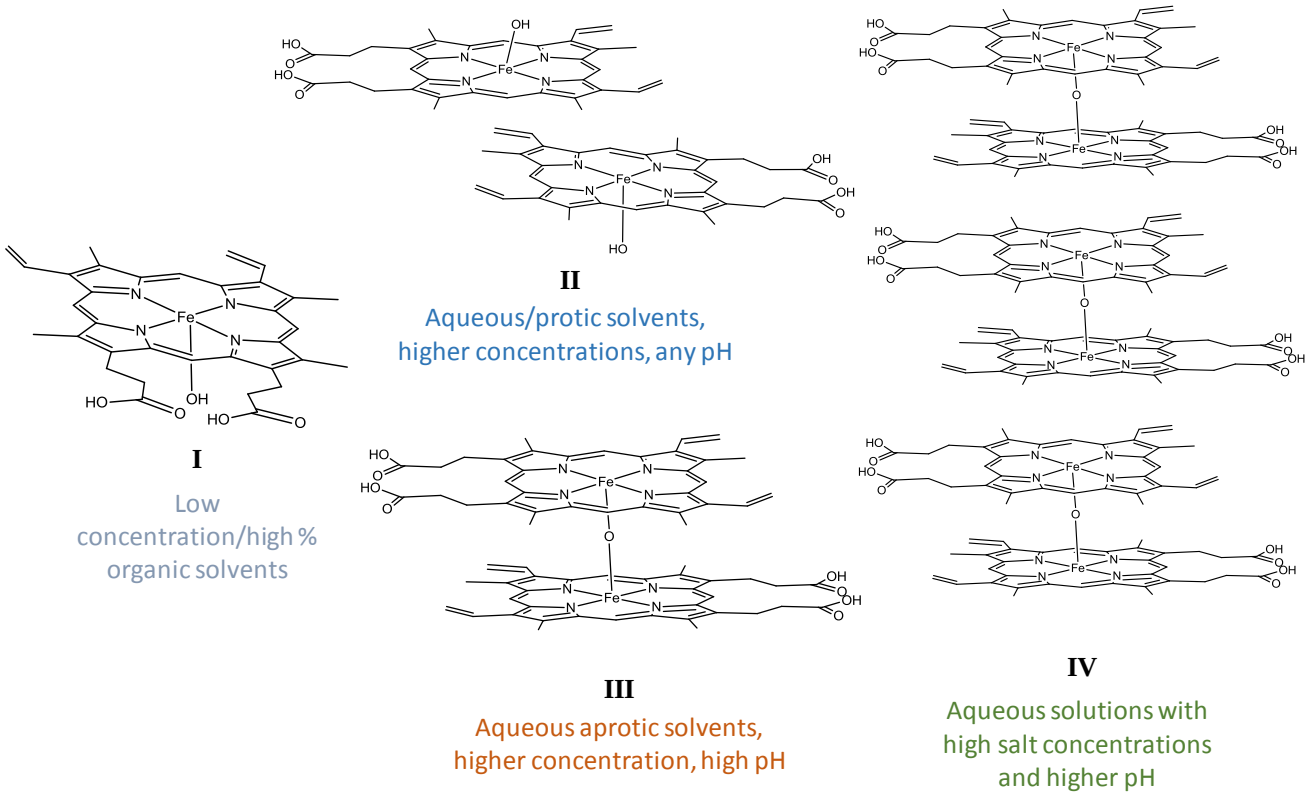

Figure 1.11 A representation of the complex speciation of Fe(III)PPIX in aqueous and mixed aqueous solutions. Redrawn from reference 89.

1.4.3.2 Drug-Haem Complex Formation

Drug-Haem Complexes in Solution

The first report of complex formation between Fe(III)PPIX and CQ was in the 1960s by Cohen *et al*.[91,92] This observation was based on changes observed in the UV-visible spectrum of Fe(III)PPIX upon titration with CQ. This study, however, served only to provide evidence that complex formation does occur, with no quantitative data reported. Later, Chou and Fitch reported the first equilibrium constants for the association of Fe(III)PPIX with CQ and a series of quinoline antimalarial drugs using equilibrium dialysis.[93] However, the difficulties noted by the authors in interpreting data and observations that aqueous Fe(III)PPIX solutions change with time, rendered these results somewhat unreliable. [94,95,96,97,98]

To circumvent such problems, quinoline association studies were conducted using iron porphyrins that exhibit a lower tendency to aggregate in aqueous solution. Constantinides and Satterlee reported association studies on the interaction between the antimalarial drugs CQ and QN with urohemin I (Figure 1.12 (a)) and uroporphyrin I, two iron porphyrins that satisfy the above critera.[99,100] Urohaemin I is a planar molecule with a five coordinate iron centre which, under the conditions of the study, remained monomeric. [99,100,101,] Another monomeric porphyrin used to study association interactions of quinoline antimalarial drugs was ferric haem-octapeptide, *N*-acetylmicroperoxidase-8 (*N*-AcMP8), see Figure 1.12 (b).[102] The results obtained between the

two individual studies show great variation and are not in agreement with the findings reported for drug-Fe(III)PPIX associations in aqueous solution (refer to Table 1.1). In fact, the binding constants determined for the association of CQ and QN with *N*-AcMP8 are lower than that of urohaemin I and Fe(III)PPIX. Egan and co-workers have postulated that the iron centre of *N*-AcMP8 is displaced towards the proximal histidine ligand and, as a result, the coordination of a second ligand to the sixth position is problematic.[102]

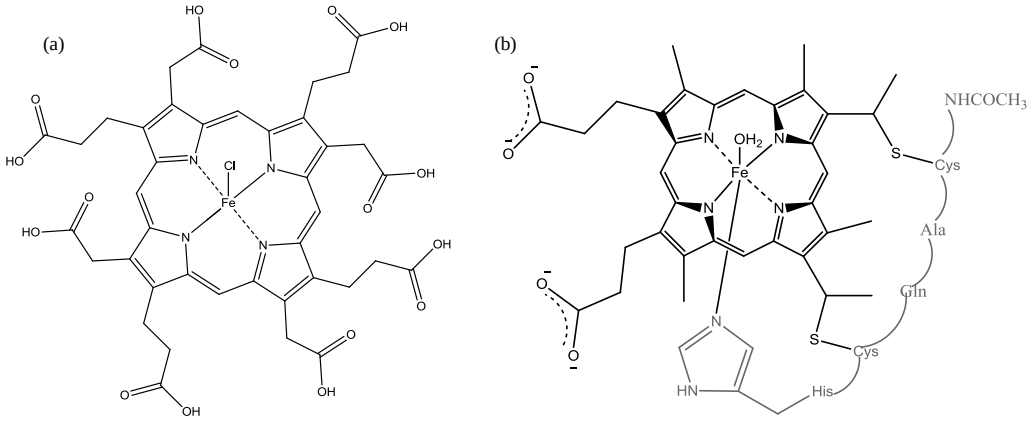

Figure 1.12 The structures of monomeric porphyrin species, **(a)** urohemin I and **(b)** *N*-acetylmicroperoxidase-8 (*N*-AcMP8), used to investigate the drug complexation.[99,100,102]

Table 1.1 Association constants for the interaction of urohemin I, *N*-AcMP8 and Fe(III)PPIX with CQ and QN.

Antimalarial Drug	Urohaemin I[†]	*N*-AcMP8[ǂ]	Fe(III)PPIX*
CQ	8.90 ± 0.02	-	5.52 ± 0.03
QN	8.60 ± 0.02	2.55 ± 0.02	4.10 ± 0.02

[†] Determined by Constantinides and Satterlee.[99,100]
[ǂ] Determined by Marques *et al*.[102]
*Determined by Egan *et al*.[103]

The inconsistency of the above results demonstrated the need to perform association studies with Fe(III)PPIX itself. Consequently, a 40% (v/v) aqueous DMSO solvent system was used to monomerise Fe(III)PPIX and investigate its interactions with quinoline antimalarial drugs (Figure 1.13).[103,104,105] The strong quenching of the Soret band of monomeric Fe(III)PPIX upon addition of drug provided an ideal method for determining association constants (Table 1.2).[92]

Binding stoichiometry and thermodynamic properties have also been determined under these conditions.[103,106,107,108,109] Many studies have been devoted to uncovering the structure of these complexes.

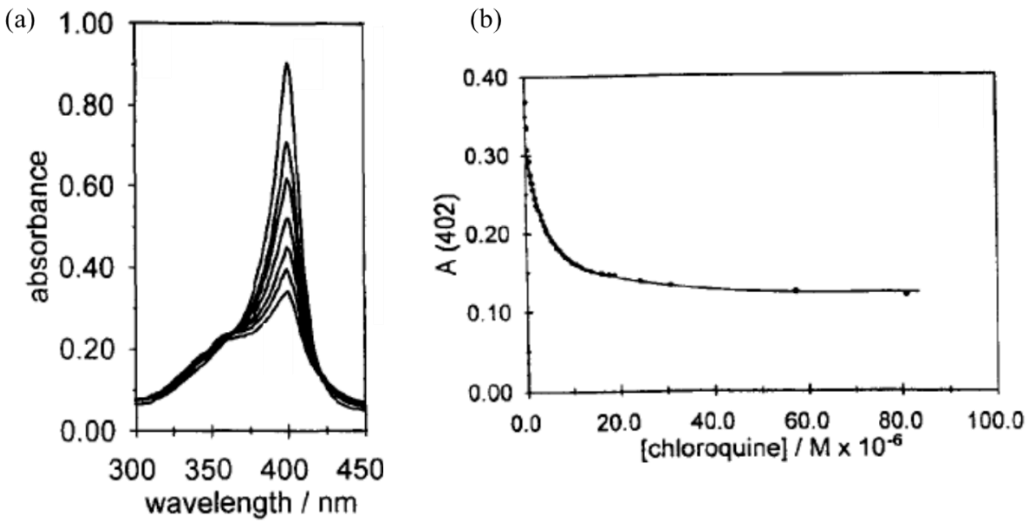

Figure 1.13 Spectrophotometric titration of CQ with Fe(III)PPIX. **(a)** The spectroscopic changes in the Soret band observed when Fe(III)PPIX is titrated with CQ. **(b)** The change in absorbance of Fe(III)PPIX as a function of increasing CQ concentration indicated by the data points. The solid line shows the best fit of the 1:1 Fe(III)PPIX:CQ binding model. Reproduced with permission from reference 103.

Table 1.2 Association constants for the interaction between Fe(III)PPIX and a series of antimalarial drugs, determined in 40% (v/v) aqueous DMSO according to a 1:1 binding model at 25 °C, pH 7.5.

Antimalarial Drug	log K
Chloroquine	5.52 ± 0.03†
Amodiaquine	5.39 ± 0.04†
Quinine	4.10 ± 0.02†
Quinidine	5.02 ± 0.03*
Mefloquine	3.90 ± 0.08†
Halofantrine	5.29 ± 0.02*

† Determined by Egan *et al.*[103]
*Determined by Egan *et al.*[106]

Quinoline Methanol Complexes with Fe(III)PPIX

Only within the last 8 years, has the structure of quinoline methanol drugs and their analogues with Fe(III)PPIX been firmly established using single crystal X-ray diffraction (SCD) and spectroscopic methods. QN, QD, MQ and Hf have been found to coordinate to Fe(III)PPIX through their deprotonated alcohol group forming a five-coordinate complex in the solid state. π-Stacking of aromatic rings with the porphyrin and hydrogen bonding between tertiary amine groups of the drug and propionate side chains of Fe(III)PPIX also feature (Figure 1.14).[110,111,112] Fe(III)PPIX-coordinated complexes have been shown to exist in non-aqueous solution using UV-visible spectroscopy and EXAFS measurements. In the former, characteristic shifts in the

charge transfer-band are indicative of coordination, while the latter has shown the distance between Fe and O (drug) to be consistent with a coordinated alkoxide (Figure 1.15).[113,114,115] These shifts were in good agreement with those previously reported as 402 and 600 nm for the QN-Fe(III)PPIX coordination complex in benzene.[116]

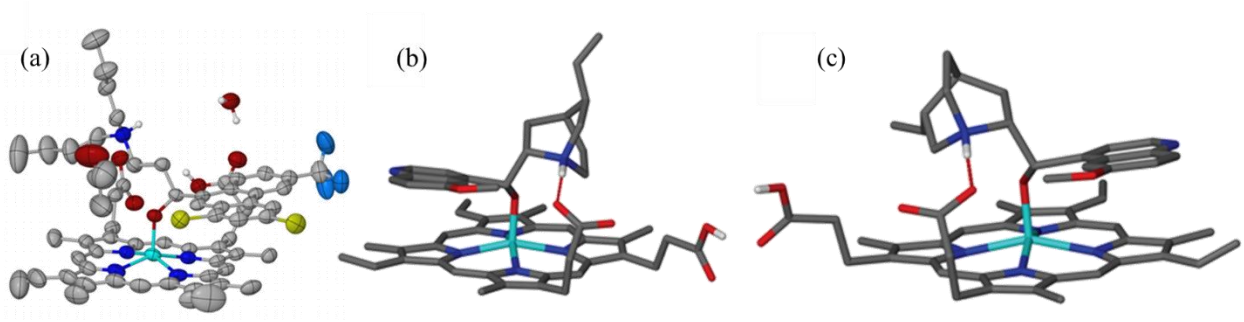

Figure 1.14 (a) The crystal structures of Hf-Fe(III)PPIX, thermal ellipses are drawn at 50% probability. The single crystal structures of **(b)** QN-Fe(III)PPIX and **(c)** QD-Fe(III)PPIX, solvent molecules and non-relevant hydrogen atoms were removed for clarity. Atom colour coding: C, grey; H, white; Cl, yellow; F, light blue; Fe, cyan; N, dark blue and O, red. Reproduced with permission from reference 110 and 111 respectively.

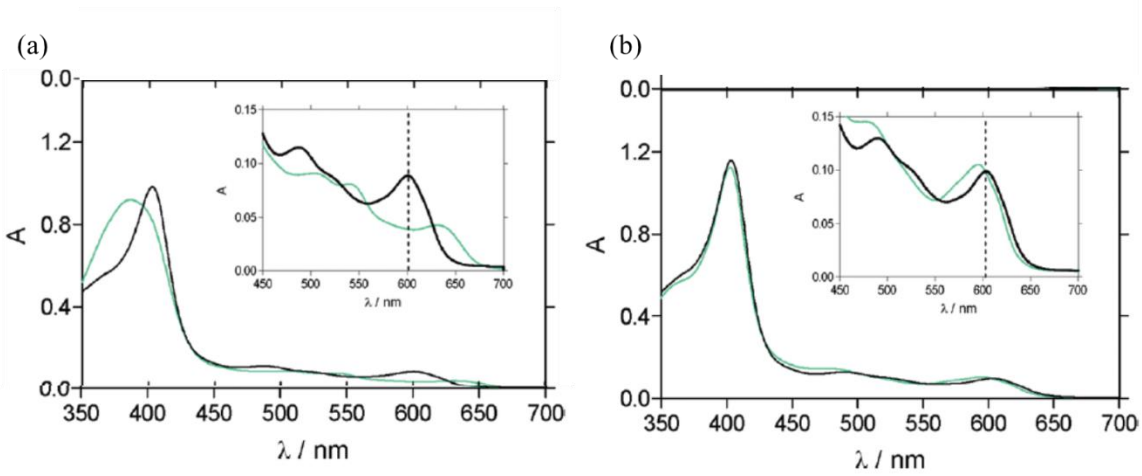

Figure 1.15 The UV-visible spectra of Fe(III)PPIX in solution before (turquoise) and after (black) titration with **(a)** QD in acetonitrile and **(b)** QN in pentanol. Reproduced with permission from reference 111.

4-Aminoquinoline Complexes with Fe(III)PPIX

While the structure of quinoline methanol complexes with Fe(III)PPIX is well established, that of the CQ-Fe(III)PPIX complex is still controversial. A number of conflicting structures have been proposed (Figure 1.16). de Dios *et al*. carried out a nuclear magnetic resonance (NMR) study which suggested a CQ-Fe(III)PPIX complex was formed in which the quinoline nitrogen atom of CQ coordinates to the iron centre of monomeric Fe(III)PPIX (Figure 1.16 (a)).[117] By contrast, Leed *et al*. used NMR inversion recovery experiments to show that, depending on the protonation state of the antimalarial drug, the distance between the iron centre of Fe(III)PPIX and drug H differs.[118] Using this observation, they proposed that CQ forms a non-covalent complex with the Fe(III)PPIX μ-oxo dimer in solution (Figure 1.16 (b)). Subsequently,

Schwedhelm *et al*. proposed that the complex instead consisted of two Fe(III)PPIX μ-oxo dimers coordinated through the propionate side chains of adjacent Fe(III)PPIX molecules and that two CQ molecules π-stacked with the outer, unligated faces of this Fe(III)PPIX tetramer adduct (Figure 1.16 (c)).[119] In 2009, a contrasted study showed that the CQ molecules act as molecular spacers and, through dispersion interactions, bind noncovalently to the unligated faces of the Fe(III)PPIX μ-oxo dimer *via* π-π interactions (Figure 1.16 (d)).[120] Earlier NMR studies performed by Moreau *et al*. had come to the same conclusion.[121] Further complication surrounding the CQ-Fe(III)PPIX complex occurred in 2014 when Acharige and Durrant proposed another binding mode in which hydrogen bonding occurs between the axial hydroxide or water ligand of a monomeric Fe(III)PPIX species and the 4-amino group of CQ as well as between the tertiary amine group of CQ and the propionate side chain of Fe(III)PPIX (Figure 1.16 (e)).[122]

A recent, thorough investigation, however, has provided convincing evidence using multiple techniques for CQ-μ-oxo dimer formation in the solid and solution state (Figure 1.17 (a))).[123] Instead of a π-stacking complex, however, the authors proposed a structure in which CQ is positioned between Fe(III)PPIX porphyrin rings and hydrogen bonds with the oxide bridge (Figure 1.17 (b)).[124] This structure was the only one that could explain the reduction in Fe-O-Fe IR stretching frequency and adequately fit solution-state EXAFS measurements of the CQ-μ-oxo complex.

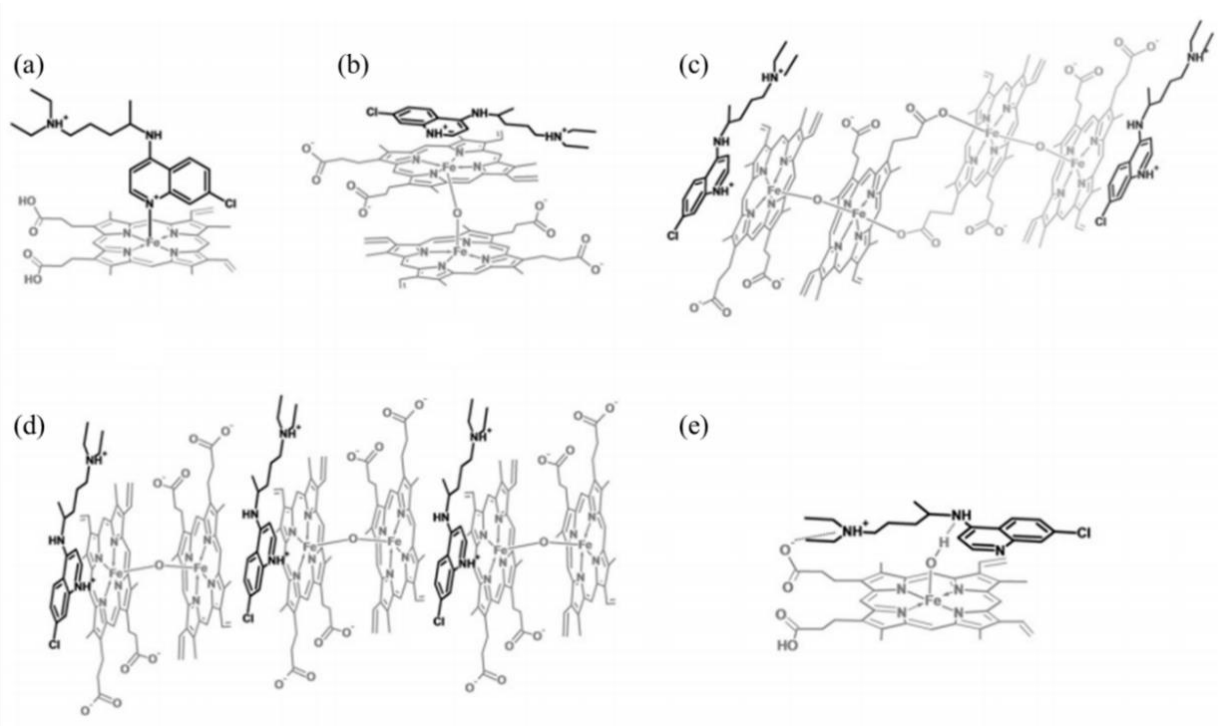

Figure 1.16 The structures previously proposed for the Fe(III)PPIX-CQ complex. **(a)** The coordination of CQ to monomeric Fe(III)PPIX,[117] **(b)** π-stacking of CQ to μ-oxo dimeric Fe(III)PPIX,[118] **(c)** μ-oxo tetramer Fe(III)PPIX adduct π-stacked with two CQ molecules,[119] **(d)** CQ molecules π-stacked between Fe(III)PPIX μ-oxo dimers[120] and **(e)** hydrogen bonded CQ to Fe(III)PPIX.[122] Reproduced with permission from reference 124.

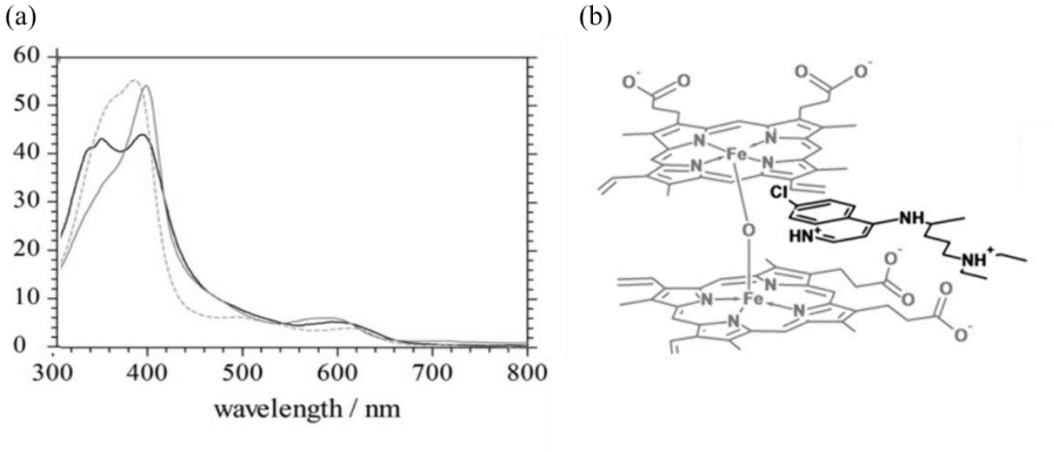

Figure 1.17 (a) The UV-visible spectrum of the Fe(III)PPIX π-π dimer (grey dashed line) compared to that of the μ-oxo dimer (grey) and the CQ-Fe(III)PPIX complex (black). **(b)** The recently proposed structure of the Fe(III)PPIX-CQ complex. Reproduced with permission from reference 123 and 124, respectively.

1.5 Toxicity of Drug-Fe(III)PPIX Complexes

Drug-Fe(III)PPIX complex formation within the parasite have been suggested to cause parasite death. Consequently, the mechanisms of how such complexes exert their toxicity is of great interest.

1.5.1 Measuring Fe(III)PPIX Toxicity

A mechanism often employed to investigate the toxicity of Fe(III)PPIX has been through the measure of peroxidase activity. Peroxidases are defined as haem enzymes which catalyse the peroxide dependent oxidation of a variety of organic and inorganic molecules.[125] While the structures of these enzymes differ substantially from one peroxidase class to another, the catalytic cycle is homologous (Figure 1.18).[126] In the first step of the cycle, H_2O_2 binds to the iron center of Fe(III)PPIX where it subsequently oxidises Fe(III)PPIX to produce an organic cation radical and releases water. This radical is known as Compound I and consists of an oxyferryl center, Fe(IV)=O, and a radical situated on the porphyrin ring. The second step involves a one electron reduction of the porphyrin radical by a substrate molecule. This produces a substrate radical and Compound II which retains the oxyferryl center but is no longer a radical itself. Finally, in what is thought to be the rate-determining step of the reaction, Compound II is once again reduced to the ferric state. During this final step, an additional substrate molecule undergoes a one electron oxidation, resulting in the production of additional substrate radicals.[127]

A useful substrate employed to monitor peroxidase reactions is, 2,2'-azinobis(3-ethylbenzothiazoline-6-sulfonate) (ABTS). This substrate meets the criteria for being specific for peroxidase, stable and non-toxic. ABTS is thought to act as a trapping agent for the iron(IV)-oxo species and, at higher pH, catabolises H_2O_2 via a catalase mechanism (refer to Equation (1.4)). Oxidation of ABTS yields a radical product that is stable and possess a unique visible absorption spectrum (see Figure 1.19). Its prominent absorption at 414, 660 and 720 nm gives it a characteristic emerald green colour, readily differentiating it from its reduced form which is yellow and absorbs around 400 nm.[128]

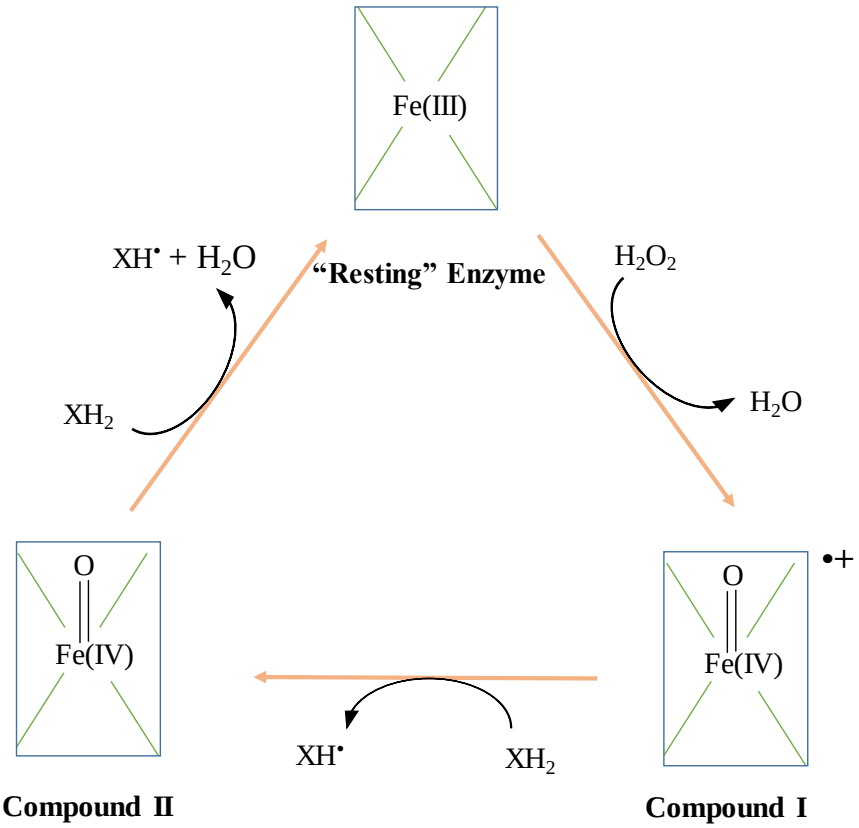

Figure 1.18 The catalytic cycle of Fe(III)PPIX peroxidases redrawn based on reference 126. The porphyrin macrocyle is represented as a rectangle, and connecting lines from each of the four corners represent coordination of the metal centre via the four nitrogen atoms.

$$2H_2O_2 \xrightarrow{\text{Catalase}} 2H_2O + O_2 \qquad (1.4)$$

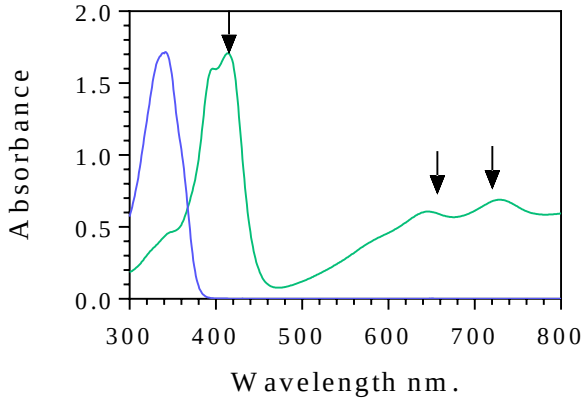

Figure 1.19 The UV-visible spectrum of ABTS (purple). Upon oxidation, the formation of the emerald green radical cation ($ABTS^{\cdot+}$) commences which can be measured at 414, 660 and 720 nm (green), as indicated by the arrows.

While ABTS has been used extensively to probe peroxidase activity of Fe(III)PPIX in a number of metalloproteins, there are few studies which have investigated the activity outside a protein environment. Unbound Fe(III)PPIX has not been used in investigations as a result of its innate nature to dimerise in solution, causing complications in the interpretation of results. Indeed, several studies on the peroxidase activity of water soluble, monomeric and non-μ-oxo dimer forming metalloporphyrins have instead been employed.[129,130,131,132,]

1.5.2 The Influence of Antimalarial Drugs on Fe(III)PPIX Toxicity

The first report that antimalarial drugs may influence Fe(III)PPIX toxicity was in 1980 by Chou and Fitch.[133] The authors alluded to complex formation which they thought enhanced the toxicity of Fe(III)PPIX through membrane damage. Later, in 1995 a study by da Costa Ferreira and co-workers reported a reduction in the peroxidase activity of Fe(III)PPIX in the presence of CQ.[134] In this study, the authors also reported a decrease in degradative attack against Fe(III)PPIX. To our knowledge, this has been the most detailed investigation into the peroxidase activity of Fe(III)PPIX and antimalarial drugs using ABTS as a reducing substrate. However, the study was performed before a clear understanding of Fe(III)PPIX solution-state behaviour was established and was not conducted under biologically relevant conditions.[134] A year later, Berman and Adams investigated the effect of Art on the peroxidase activity of Fe(III)PPIX.[135] The authors incubated the drug with Fe(III)PPIX at 30 °C, pH 7.4 for varying time periods and reported an increase in peroxidase activity, however, no details of this reaction were described. In a follow-up paper, by da Costa Ferreira and co-workers the effect of a series of antimalarial drugs, including CQ and QD, on the catalase activity of Fe(III)PPIX (Equation 1.4) was investigated.[136] They reported a substantial inhibition of the catalase activity of Fe(III)PPIX in the presence of the antimalarial drugs, resulting in a build-up of H_2O_2, detrimental to the parasite. Subsequently, Loria *et al*. reported that the antimalarial drugs CQ and quinacrine inhibited the peroxidative destruction of Fe(III)PPIX, which, consequently leads to an increase in toxic Fe(III)PPIX within the parasite, causing their death.[137] To date, however, no significant information regarding the extent of the peroxidase activity of Fe(III)PPIX and its complexes with clinically relevant antimalarial drugs have been reported under conditions relevant to the malaria parasites. This is particularly true since it is now known that the lipid environment is important for haemozoin formation. Therefore, investigating toxicity under conditions that can mimic a lipid-water interface is crucial for to understanding mechanisms of action of drugs. In light of the above findings, and to better understand the possible mechanism(s) of antimalarial drugs, a thorough investigation of their modulatory effects towards Fe(III)PPIX toxicity is required.

1.6 Aims and Objectives

1.6.1 Aims

Following a thorough review of the literature on malaria, Fe(III)PPIX toxicity and the mechanisms of action of artemisinin and the quinoline antimalarial drugs, the aim of the study was to:

> Investigate the peroxidase activity of Fe(III)PPIX under biologically relevant conditions and to compare this effect with that of Fe(III)PPIX in the presence of the clinically relevant antimalarial drugs, CQ, QD and Art.
>
> The aim is underpinned by the hypothesis that *quinoline antimalarial drugs act by inhibiting haemozoin formation, thereby increasing the concentration of Fe(III)PPIX present in the parasite which, in turn, enhances the oxidative stress on the parasite*.

1.6.2 Objectives

In order to achieve the aforementioned aim, the specific objectives of the current work were to:

1. Investigate the association of Fe(III)PPIX with CQ, QD and Art in aqueous solution.
2. Compare the strength of drug-Fe(III)PPIX association with that obtained in an environment that mimics the lipid-water interface.
3. Optimize an ABTS assay to be used as a measure of Fe(III)PPIX peroxidase activity under biologically relevant conditions.
4. Investigate the peroxidase activity of Fe(III)PPIX in an aqueous environment as well as in an environment mimicking the lipid-water interface.
5. Investigate the effect of CQ, QD and Art on the peroxidase activity of Fe(III)PPIX in both aforementioned environments.

Chapter 2. Materials, Instrumentation and General Methods

2.1 Materials

The materials used in this project were obtained commercially and were of highest purity and analytical grade. All chemicals were used without any further purification and are listed in Table 2.1.

Table 2.1 Chemicals used and their commercial source.

MATERIALS	SOURCE
Solids	
Ammonium Persulfate	Sigma-Aldrich
2,2′-Azino-bis(3-ethylbenzothiazoline-6-sulfonic acid) diammonium salt (ABTS)	Sigma-Aldrich
Haematin (porcine)	Sigma-Aldrich
Haemin (bovine)	Sigma-Aldrich
Sodium dodecyl sulfate (SDS)	Sigma-Aldrich
Sodium hydroxide pellets	Sigma-Aldrich
Tris(hydroxymethyl)aminomethane (Tris)	Sigma-Aldrich
Liquids and Solvents	
Acetone	Kimix Chemicals
Acetonitrile	Sigma-Aldrich
Dimethyl Sulfoxide (DMSO)	Sigma-Aldrich
Hydrochloric acid	Kimix Chemicals
Hydrogen Peroxide solution	Sigma-Aldrich
Nitric Acid	Kimix Chemicals
Antimalarial drugs	
Artemisinin	Sigma-Aldrich
Artesunate	Sigma-Aldrich
Chloroquine diphosphate (CQ)	Sigma-Aldrich
Cinchonine (CN)	Departmental Store
Quinidine sulfate dihydrate (QD)	Sigma-Aldrich
Quinidine (QD)	Sigma-Aldrich
Quinine hemisulfate monohydrate (QN)	Sigma-Aldrich
Quinine (QN)	Sigma-Aldrich

2.2 Instrumentation

2.2.1 Analytical Balance

An A&D HR-200 analytical balance was used to weigh off all materials.

2.2.2 Magnetic Stirrer Hot Plate

JK-MSH-Pro and Heidolph MR-2002 standard magnetic stirrer hot plates were used to stir solutions.

2.2.3 Micro Glass Syringes

Hamilton micro glass syringes (25 and 50 µL) were used for delivery of small volumes to solutions.

2.2.4 pH Meter

All pH measurements were recorded using a Mettler Toledo FE20 pH meter. The pH meter was calibrated with buffer solutions (pH 7 and pH 4) obtained from CRISON before use.

2.2.5 Single- and Multi-Channel Micro-pipettes

Gilson Pipetman single-channel (P-20, P-200, P-1000 and P-5000) and multi-channel (P8X20 and P8X200) pipettes were routinely used for delivery to solutions.

2.2.6 UV-Visible Spectrophotometer

UV-Vis spectra were recorded using a Shimadzu UV-1800 Spectrophotometer with an electronically thermo-controlled homeothermal cell holder. Cuvettes of 1 cm path length, made of Quartz from SUPRASIL, Hellma, were used in the spectrophotometer.

2.2.7 Vortex

A BOECO Vortex Mixer V1 Plus was used to mix solutions.

2.3 Computer Software

The different computer programmes and software used to analyse experimental data in this study are listed in Table 2.2.

Table 2.2 The computer programmes and software used to analyse data.

Programme	Version	Use
ChemDraw	11.0	Drawing of chemical structures
CurveFit	1.00	Fitting Titration Data
GraphPad Prism	6.0	Graphing
HypSpec	2014	Determining Association Constants
Hyperquad Simulation and Speciation (HySS)	2009	Determining Percentage Complexation
MATLAB	2010	Kinetic Analysis
Mendely	1.16.1	Referencing
Microsoft Excel	2013	Data analysis
UV Probe	2.43	Program for recording UV-Vis spectra

2.4 General Precautions and Washing of Glassware

Distilled water was used in the preparation of all water solvent solutions. All used glass- and plastic-ware were washed with soap and water followed by thorough rinsing with distilled water and finally, acetone. Fe(III)PPIX has been shown to adsorb onto glass and plastic surfaces.[88,89] Special precautions were thus required to ensure complete removal of Fe(III)PPIX from the surface of cuvettes and glassware used to store Fe(III)PPIX solutions. To do this, the glassware was thoroughly washed in 0.1 M NaOH followed by extensive rinsing with distilled water. Following this, the glassware and cuvettes were washed with 0.1 M HNO_3 and again extensively rinsed with water.

2.5 General Preparations

This section describes the preparation of solutions that were used frequently throughout this study. All materials used in the preparation of these solutions have been previously listed in Table 2.1.

2.5.1 0.10 M NaOH Stock Solution

Sodium hydroxide pellets (1.00 g, 250.0 mmol) were dissolved in distilled water to a volume of 250.0 mL in a volumetric flask.

2.5.2 1.0 M Nitric Acid Stock solution

A 1.0 M nitric acid stock solution was prepared by slowly adding 50 mL nitric acid (55 %) to 400 mL distilled water in a 500.0 mL volumetric flask. The solution was then made to volume with distilled water.

2.5.3 1.0 M Hydrochloric Acid Stock Solution

A 1.0 M hydrochloric acid stock solution was prepared by slowly adding 991 µL of 32 % hydrochloric acid solution to 5.0 mL distilled water. The solution was then made to a volume with distilled water in a 10.0 mL volumetric flask.

2.5.4 Tris Buffer Stock Solutions

A: A 130.0 mM Tris Buffer stock solution was prepared by dissolving the solid (1.57 g, 13.0 mmol) in 80 mL distilled water. The pH was adjusted to 7.5 through the addition of 1.0 M HCl in a dropwise manner. The solution was then made to volume in a 100.0 mL volumetric flask.

B: A 250.0 mM Tris Buffer stock solution was prepared by dissolving the solid (3.02 g, 25.0 mmol) in 70.0 mL distilled water. The pH was adjusted to 7.5 through the addition of 1.0 M HCl in a dropwise manner. The solution was then made to volume in a 100.0 mL volumetric flask.

Chapter 3. Speciation and Structure of Drug-Fe(III)PPIX Complexes

3.1 Introduction

The interactions between antimalarial drugs and Fe(III)PPIX have been of considerable interest in the past.[88,91,93,102,111,116] Many studies have suggested that association plays a role in antimalarial activity, with the resultant drug-Fe(III)PPIX complex responsible, in some way, for the inhibition of β-haematin formation, or itself as the cause of toxicity in the parasite.[138,139,140] Most work has been conducted in a predominantly aqueous medium, however, more recent literature suggests that a lipid environment is important for β-haematin formation.[54] Drug-Fe(III)PPIX association in such an environment has not been investigated extensively. In addition to studies performed in non-aqueous solution, solid state structures have also been determined for the complexes formed between Fe(III)PPIX and Halofantrine (Hf),[54] Quinidine (QD) and Quinine (QN),[111] however, it is not known whether the interactions observed in the solid state persist in solution.

In this work, association experiments where undertaken with three antimalarial drugs known to have differing interactions with Fe(III)PPIX. The study was conducted at 37 °C in three different media in order to mimic biological environments: i) an organic solvent (acetonitrile) was used to represent a lipid environment by means of its low dielectric constant; ii) an aqueous medium buffered at pH 7.4 was selected to represent the parasite cytosol; and iii) an aqueous solution (pH 7.4) containing the water-soluble detergent SDS provided a two-component system mimicking a lipid-water interface. In addition to these solution-state investigations, the interaction of cinchonine (Cn)-Fe(III)PPIX in the solid state could be characterised using X-ray crystallography and the first crystal structure of this complex is reported.

3.2 Experimental Methods

3.2.1 The Association of CQ, QD and Art with Fe(III)PPIX in Solution

3.2.1.1 Preparation of Solutions

SDS Stock Solution

A 10.0 mM stock solution was prepared by dissolving SDS (28.8 mg, 100.0 µmol) in distilled water to a volume of 10.0 mL in a volumetric flask.

Fe(III)PPIX Stock Solutions

A: A 1.0 mM Fe(III)PPIX stock solution was prepared by dissolving haematin (6.3 mg, 10.0 µmol) in 0.1 M NaOH to a volume of 10.0 mL in a volumetric flask.

B: A 20.0 mM Fe(III)PPIX stock solution was prepared by dissolving haematin (63.3 mg, 100.0 µmol) in 0.1 M NaOH to a volume of 5.0 mL in a volumetric flask.

C: A 1.0 mM Fe(III)PPIX stock solution was prepared by dissolving 500 µL of Fe(III)PPIX stock solution **B** in 4 mL of Tris buffer stock solution **A** (see section 2.5) and made to volume with distilled water in a 10.0 mL volumetric flask.

D: A 1.2 mM Fe(III)PPIX stock solution was prepared by dissolving haematin (7.8 mg, 12.30 µmol) in DMSO to a volume of 10.0 mL in a volumetric flask.

E: A 1.0 mM Fe(III)PPIX stock solution was prepared by dissolving 500 µL of Fe(III)PPIX stock solution **B** in 4 mL of Tris buffer stock solution **A** (see section 2.5), 1 mL SDS (10.0 mM stock solution) and made to volume with distilled water in a 10.0 mL volumetric flask.

QD Stock Solutions

A: A 2.0 mM QD stock solution was prepared by dissolving QD sulfate salt (3.2 mg, 20.0 µmol) in 4 mL of Tris buffer stock solution **A** and made to volume with distilled water in a 10.0 mL volumetric flask.

B: A 2.0 mM QD stock solution was prepared by dissolving the free base (6.5 mg, 20.0 µmol) in acetonitrile to a volume of 10.0 mL in a volumetric flask.

C: A 2.0 mM QD stock solution was prepared by dissolving QD sulfate salt (15.7 mg, 20.0 µmol) in 4 mL of Tris buffer stock solution **A**, 1 mL SDS (10.0 mM stock solution) and made to volume with distilled water in a 10.0 mL volumetric flask.

CQ Stock Solution

A: A 1.0 mM CQ stock solution was prepared by dissolving CQ diphosphate salt (5.2 mg, 10.0 µmol) in distilled water to a volume of 10.0 mL in a volumetric flask.

B: A 1.0 mM CQ stock solution was prepared by dissolving the free base (8.0 mg, 25.0 µmol) in acetonitrile to a volume of 25.0 mL in a volumetric flask. The free base form of CQ was obtained through the addition of concentrated NaOH to an aqueous solution of the commercially available salt to yield a precipitate which was centrifuged, washed with distilled water and, subsequently, recovered after drying for five days in the presence of phosphorus pentoxide.

Art/Ar Stock Solution

A: A 2.0 mM Art stock solution was prepared by dissolving artemisinin (5.7 mg, 20.0 µmol) in acetonitrile to a volume of 10.0 mL in a volumetric flask.

B: A 2.0 mM Ar stock solution was prepared by dissolving artesunate (7.7 mg, 20.0 µmol) in 4 mL of Tris buffer stock solution **A** (Section 2.5.4), 1 mL SDS (10.0 mM stock solution) and made to volume with distilled water in a 10.0 mL volumetric flask.

3.2.1.2 Experimental Procedures

General Spectrophotometric Titration Procedure

All titrations were carried out in cuvettes with 1 cm pathlength at 37 °C. Working solutions were prepared in the cuvette to a volume of 2.5 mL. To this, aliquots of drug or Fe(III)PPIX stock solutions were added using Hamilton syringes (25.0 and 50.0 µL) and the resulting spectra recorded between 300 and 800 nm after each addition. The results were analysed with HypSpec[141] using a 1:1 drug:Fe(III)PPIX binding model for QD, Art and Ar, while a 2:1 Fe(III)PPIX:drug binding model was used for CQ. All Fe(III)PPIX stock solutions were prepared daily and stored in the dark to prevent degradation. All glassware that came into contact with Fe(III)PPIX was washed according to the procedure described in section 2.4 to prevent a build-up of Fe(III)PPIX on the surface.

The Association of QD and CQ with Fe(III)PPIX in Aqueous Solution

Spectrophotometric titrations of Fe(III)PPIX with QD were carried out by adding aliquots of QD stock solution **A** to a 10 µM Fe(III)PPIX working solution (975 µL Tris buffer stock solution **A**, 25 µL of Fe(III)PPIX stock solution **A** and 1555 µL distilled water) as well as to the reference cuvette (where the volume of Fe(III)PPIX stock solution **A** was replaced with 0.1 M NaOH). Absorbance of the solution in the reference cuvette was automatically subtracted from that of the working cuvette. The final volume after titration was 2610 µL.

In the case of CQ, aliquots of Fe(III)PPIX stock solution **C** were titrated into a 20 µM CQ working solution (975 µL Tris buffer stock solution **A**, 1475 µL distilled water and 50 µL of CQ stock solution **A**) to a final volume of 2560 µL. Reasons for the altered procedure in the case of CQ are discussed in detail further on in the text. A reference cuvette was not used in this instance in order to avoid obtaining a negative absorbance reading. Instead, the spectrum of Fe(III)PPIX was taken into account when processing the data in HypSpec.

The Association of QD, CQ and Art with Fe(III)PPIX in Acetonitrile

Owing to the poor solubility of Fe(III)PPIX in pure acetonitrile, a 1:99 (v/v) DMSO/acetonitrile solvent system was used instead. Aliquots of the stock solutions of Art (**A**), CQ (**B**) or QD (**B**) were titrated into a 9.8 µM Fe(III)PPIX working solution (20 µL Fe(III)PPIX stock solution **D,** 2.48 mL acetonitrile) and reference cuvette (20 µL DMSO, 2.48 mL acetonitrile). In each case, the final volume after titration did not exceed 2700 µL.

The Association of CQ, QD and Ar with Fe(III)PPIX in Aqueous SDS

The association of Fe(III)PPIX with both QD and CQ, was investigated in the same manner as in aqueous solution with the exception that the experiment was carried out in 1 mM SDS. In the case of QD, QD stock solution **C** was titrated into the 10 µM Fe(III)PPIX working solution, while for CQ, the Fe(III)PPIX stock solution **E** was titrated into the 20 µM CQ working solution.

Owing to weaker association, spectrophotometric titrations of Fe(III)PPIX with Ar had to be conducted using a Fe(III)PPIX working solution with initial volume of 2.00 mL to allow a greater volume of Ar solution to be added. Aliquots of Ar stock solution **B** were titrated into the 8 µM Fe(III)PPIX working solution (500 µL of Tris buffer stock solution **B**, 16 µL of Fe(III)PPIX stock solution **A**, 14 µL 0.1 M NaOH, 250 µL SDS stock solution and 1220 µL distilled water) and the reference cuvette where Fe(III)PPIX was replaced with 0.1 M NaOH. The final volume after titration was 3.0 mL.

3.2.2 The Crystal Structure of the Cn-Fe(III)PPIX Complex

3.2.2.1 Experimental Method

A 3.08 mM Cn stock solution was prepared by dissolving Cn free base (9.1 mg, 30.8 µmol) in 10.0 mL acetonitrile. A 3.07 mM Fe(III)PPIX stock solution was prepared by dissolving haemin (10.0 mg, 15.3 µmol) in 500 µL DMSO. Following thorough mixing, the Fe(III)PPIX solution was made to volume with acetonitrile in a 10.0 mL volumetric flask. This mixture exists as a suspension owing to the poor solubility of Fe(III)PPIX in acetonitrile. The crystallisation medium was then prepared by adding 400 µL of this Fe(III)PPIX stock solution to 1 mL of the Cn stock solution. An additional 4 mL of acetonitrile was added to the solution after which the mixture was stirred for 30 minutes and filtered through a polytetrafluoroethylene filter disk to remove excess undissolved Fe(III)PPIX. The filtrate was recovered and stored in a glass vial which was covered with parafilm and punctured with two needle-sized holes to aid in slow evaporation of the solvent. The sample was then left to stand at room temperature for five days after which small needle-like crystals were observed on the bottom of the vial.

3.3 Results

3.3.1 The Association of QD, CQ and Art with Fe(III)PPIX in Solution

To determine the solution interaction of three clinically relevant antimalarial drugs with Fe(III)PPIX, three solvent systems were selected. The first was used to mimic the aqueous parasite cytosol and thus consisted of an aqueous medium buffered at pH 7.4. While a number of previous studies reported unreliable results conducting similar investigations in aqueous solution, this most likely has been due to a lack of understanding of the aggregation effects of Fe(III)PPIX in such a medium. This led to later studies being conducted in solvent systems not biologically relevant in order to ensure Fe(III)PPIX remained strictly monomeric. For example, Egan *et al.* previously investigated the association of Fe(III)PPIX with five clinically relevant antimalarial drugs at a pH of 7.5 and 25 °C in a 40 % aqueous DMSO solvent system.[103,106] The aggregation of Fe(III)PPIX in aqueous solution, however, is now well established.[89] In order to gain insight into the interactions that are relevant *in vivo*, it is therefore essential to carry out association studies under conditions that closely resemble the biological environment. Considering that the proposed site of action for antimalarial drugs has recently shifted from an aqueous to a lipid environment,[54] the second solvent system investigated was used to represent a non-aqueous lipid environment. Acetonitrile was selected to mimic the lipid environment owing to its low dielectric constant. Furthermore, changes in the UV-visible spectra following titration of quinoline methanol antimalarial drugs into a solution of Fe(III)PPIX have been shown to be the same in acetonitrile and 1-pentanol, which is also a model compound for a

lipid.[111] Finally, a third detergent-based solvent system was used to provide a medium containing both aqueous and lipid-like components, representing a lipid-water interface which is present at membranes, such as in the digestive vacuole of the malaria parasite where β-haematin is presumed to form.[54] The water-soluble detergent SDS was selected owing to a recent study by Wright and co-workers which showed that an aqueous SDS solution under biological conditions could facilitate β-haematin formation from Fe(III)PPIX.[142] To probe drug-Fe(III)PPIX complexation in these three solvent systems, the association of representative compounds from three different classes of antimalarial drugs with Fe(III)PPIX were investigated. These included a 4-aminoquinoline (CQ), a quinoline methanol (QD) and the endoperoxide Artemisinin (Art).

3.3.1.1 Speciation of Fe(III)PPIX in Solution

The UV-visible spectra of Fe(III)PPIX (before the addition of drug) in all three solvent systems employed in the current study show a broadened Soret band (Figure 3.1), indicative of a π-π dimer in which two Fe(III)PPIX monomers interact through π-stacking. With the exception of a general hypochromism, the addition of SDS to aqueous solution (Figure 3.1, red spectrum) produced no discernible change to the Fe(III)PPIX species in aqueous media (Figure 3.1, black spectrum). On the other hand, differences do arise in the spectra of Fe(III)PPIX recorded in aqueous solutions and acetonitrile (Figure 3.1, green spectrum), particularly in the region between 450 and 650 nm. The position of the charge transfer band in aqueous and aqueous SDS solutions at ~ 612 nm shifts in acetonitrile to ~ 628 nm. Shifts in this region are commonly related to solvent composition, pH and the characteristics of the interacting species.[103] The shift in the charge transfer band from water to acetonitrile is consistent with a change from a coordinating to a non-coordinating solvent, which may indicate different interactions at the iron centre. (Figure 3.1).[108] A notable red shift is also observed in the Soret band near 400 nm.

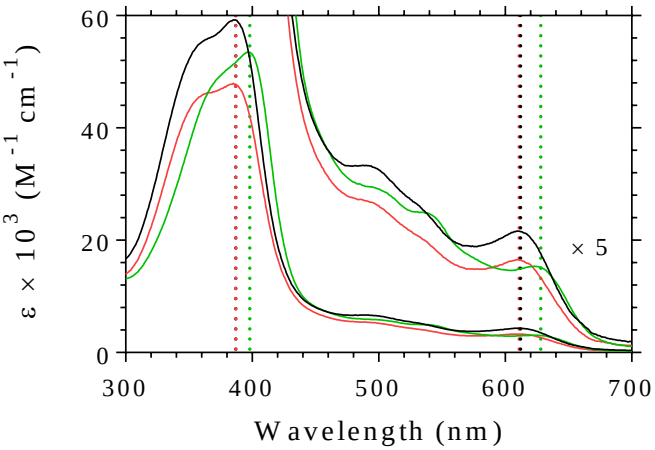

Figure 3.1 Fe(III)PPIX speciation in aqueous and non-aqueous solution. The UV-visible spectrum of Fe(III)PPIX in aqueous solution (Tris buffer, 50.0 mM, pH 7.4) (-), acetonitrile (-) and aqueous SDS solution (Tris buffer, 50.0 mM, pH 7.4) (-). The position of the charge-transfer (~600-630 nm) and Soret bands (~380-400 nm) are marked by black, green and red dotted lines for the aqueous, organic and SDS solutions respectively. Peaks positions of the Soret and charge-transfer bands are the same in purely aqueous and aqueous SDS solution and thus black and blue dotted lines overlap.

3.3.1.2 Effects of QD on the Speciation of Fe(III)PPIX in Solution

Titration of QD into an aqueous solution of Fe(III)PPIX (Figure 3.2 (a)) produced no marked difference in the charge-transfer band, however, a pronounced hypochromic effect as well as bathochromic shift of the Soret band of Fe(III)PPIX was observed. A slight, but noticeable bathochromic shift in the Q-band as well as a reduction in its intensity was also observed. Analysis of the data indicated a strong association occurred, for which the association constant (K) was quantified (on a log scale) as 5.8 ± 0.1. This compares well with the association constants previously reported for the interaction of Fe(III)PPIX with QD in acetonitrile (room temperature) (log K = 5.7 ± 0.1).[112] The titration performed in acetonitrile showed much more distinctive characteristics (Figure 3.2 (b)). The initial broad shaped Soret band resolved into a slightly sharper feature at 398 nm with a lower intensity shoulder region on the low wavelength side. A marked blue shift from ~ 628 to 600 nm could also be seen for the charge transfer band. This latter spectroscopic feature is characteristic of a coordinated QD-Fe(III)PPIX complex, the association constant for which, in this organic medium, was determined as 5.92 ± 0.09 (log scale).[111] This association constant obtained under the current conditions is larger than that which was previously described (log K = 5.7 ± 0.1). This difference can be ascribed to the increased temperature used in the current work since a titration carried out at 25 ºC revealed an association constant that is in agreement with previous work (log K = 5.82 ± 0.08) was obtained, however these three values overlap within three standard deviations of each other.[112] In the detergent system, titration of QD produced a more marked shift in the Fe(III)PPIX Soret band in comparison with both the aqueous and organic solvent systems (Figure 3.2 (c)). It is interesting to note that the intensifying and blue shifting of the charge transfer band in aqueous SDS is similar to that observed in acetonitrile. Notably, such features do not

occur in water. This observation may indicate that an element of coordination may be occurring in this solvent system, although further investigation would be required to confirm this. A somewhat stronger association constant of 6.2 ± 0.1(log scale) was determined under these conditions.

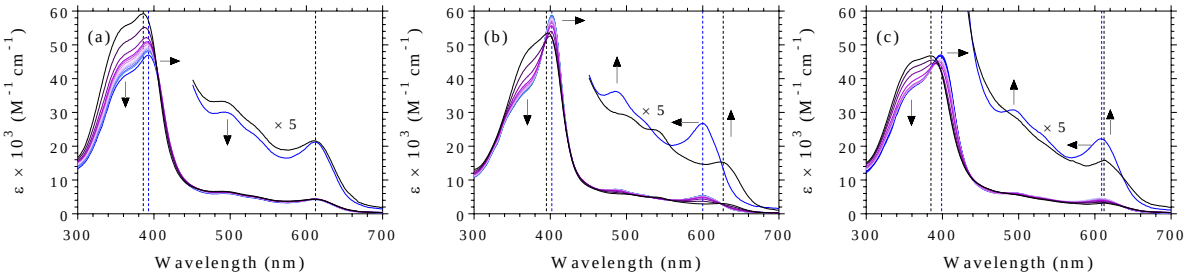

Figure 3.2 The UV-visible spectrum of Fe(III)PPIX in solution before (─) and after (─) spectrophotometric titration with QD in **(a)** aqueous solution (50 mM Tris buffer, pH 7.4), **(b)** acetonitrile and **(c)** aqueous SDS (50 mM Tris buffer, pH 7.4) solution. The spectrum of Fe(III)PPIX before titration (─) and after each subsequent addition of QD (purple to blue) can be seen in spectra **(a)**, **(b)** and **(c)**. For clarity, the enlarged spectra show the spectrum of Fe(III)PPIX in the region between 550 and 650 nm before (─) and after (─) the titration. The position of the charge-transfer band of the Fe(III)PPIX π-π dimer and QD-Fe(III)PPIX complex are marked by black and blue dotted lines, respectively. Arrows indicate the direction of spectroscopic change during titration.

3.3.1.3 Effects of CQ on the Speciation of Fe(III)PPIX in Solution

While arduous attempts were made in determining the association constants for the interaction of Fe(III)PPIX with CQ in the same manner as conducted for QD, the data from these titrations could not be successfully fit. Recently, a study suggested that complex Fe(III)PPIX speciation may occur when Fe(III)PPIX is present in excess over CQ.[123] Such conditions are present at the beginning of the titration and thus may account for the inability to fit the data. The same study suggested that association constants could instead be obtained by titrating Fe(III)PPIX into a solution containing excess CQ in order to counteract this problem. Performing titrations in this manner resulted in data that could be successfully fit and an association constant for the interaction of Fe(III)PPIX with CQ was determined (log K = 6.5 ± 0.1). While QD has been shown to coordinate to Fe(III)PPIX,[111] previous studies indicate that CQ associates with the porphyrin through π-π interactions and is unable to coordinate.[93,123] It has also been proposed that, while QD acts in a 1:1 ratio with Fe(III)PPIX, two Fe(III)PPIX equivalents are believed to associate with one molecule of CQ.[123] Findings from this study confirm this 2:1 Fe(III)PPIX:CQ stoichiometric ratio as data was unable to fit a 1:1 binding model.

The UV-visible spectrum of Fe(III)PPIX in the presence of CQ showed a reduction in absorbance of the Soret band accompanied by a broadening in the region between ~400 and 500nm. This can be seen in Figure 3.3 (a) which shows the spectrum of Fe(III)PPIX in the absence of CQ and the spectrum of the complex

determined by HypSpec.[141] In addition to this, a slight blue shift in the charge transfer band was observed. The changes in the spectrum of Fe(III)PPIX in aqueous SDS solution in the presence of CQ resemble those observed in aqueous solution (Figure 3.3 (c)). The Soret band of Fe(III)PPIX in aqueous SDS solution, however, exhibits a much sharper peak accompanied by a greater shift and increased intensity in the charge transfer band. The association constant for the interaction of Fe(III)PPIX with CQ in aqueous SDS was determined to be 6.5 ± 0.1 (log scale), identical to that determined in aqueous solution. These results are in good agreement with a previously reported study.[123] Interestingly, titrations of CQ into a solution of Fe(III)PPIX in acetonitrile did not appear to suffer from the same speciation issue as observed in aqueous solution. Association of CQ and Fe(III)PPIX in acetonitrile was found to be weaker than in water. Upon addition of CQ to Fe(III)PPIX in acetonitrile, a general hypochromic effect was observed, together with a broadening in the Soret band (Figure 3.3 (b)). A log K value of 5.3 ± 0.2 was determined for the association of Fe(III)PPIX with CQ in acetonitrile, comparable to the value reported for the association of Fe(III)PPIX with CQ in 40 % aqueous DMSO (5.52 ± 0.03).

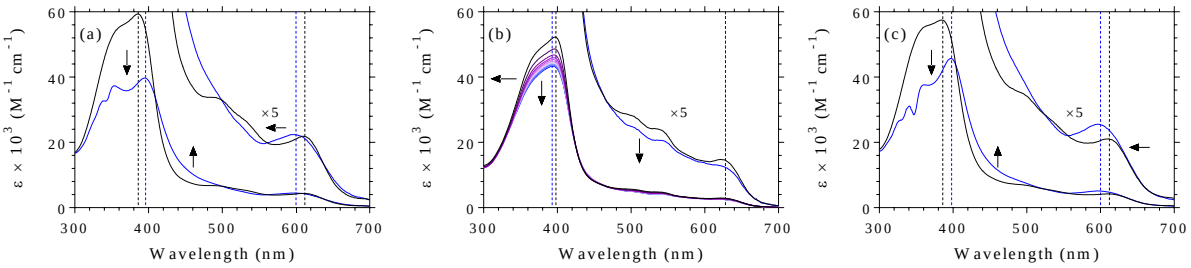

Figure 3.3 The UV-visible spectra of Fe(III)PPIX in solution before (─) and after (─) addition of CQ. The conditions were **(a)** aqueous solution (50.0 mM Tris buffer, pH 7.4), **(b)** acetonitrile, and **(c)** aqueous SDS (50.0 mM Tris buffer, pH 7.4). The position of the Soret and charge-transfer band of the Fe(III)PPIX π-π dimer and that of the species after addition of CQ are marked by black and blue dotted lines, respectively and arrows indicate direction of spectroscopic change during titration.

3.3.1.4 Effects of Art on the Speciation of Fe(III)PPIX in Solution

By contrast to the quinoline antimalarial drugs, the spectrum of Fe(III)PPIX did not undergo significant change in the presence of artemisinin. Titrations performed in acetonitrile induced no shift in the Soret band nor the charge transfer region (Figure 3.4 (a)). There was, however, a reduction in the Soret band and the association constant was calculated to be 4.48 ± 0.04 (log K). Difficulties arose with the solubility of artemisinin in water and as a result, the water soluble derivative, artesunate (the sodium hemisuccinyl ester), was used instead. Upon addition of ± 80-fold excess of artesunate over Fe(III)PPIX, no significant changes were observed in the spectrum of Fe(III)PPIX (Figure 3.4 (b)). The UV-visible spectrum of Fe(III)PPIX exhibited a general hypochromism in addition to marginal shifts in the Soret and charge transfer bands. Several attempts were made in determining the association of Fe(III)PPIX with Ar in this manner, however,

under the described conditions, presumably due to its weak binding in addition to its low solubility in water, log K values could not be determined. Attempts were made in titrating aliquots of Fe(III)PPIX into a solution of excess artesunate, however, similar complications were encountered. All the association constants obtained in this portion of work are summarised in Table 3.1. A comparison of the experimental and calculated drug-Fe(III)PPIX complex spectra are summarised in Addendum 1.

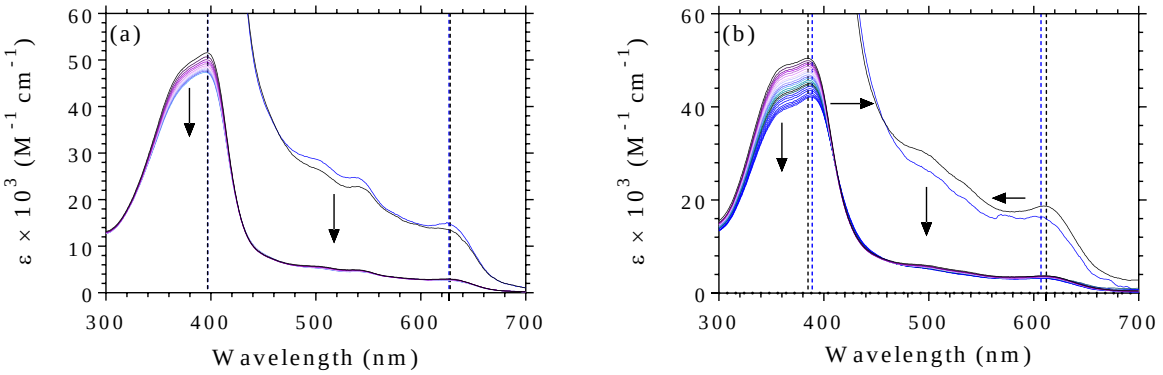

Figure 3.4 The UV-visible spectrum of Fe(III)PPIX before (─) and after (─) titration with **(a)** artemisinin in acetonitrile and **(b)** artesunate in 1 mM aqueous SDS solution. The position of the Soret and charge-transfer band of the Fe(III)PPIX species before and after titration are marked by a black and blue dotted lines respectively. Arrows indicate direction of spectroscopic change during the titration.

Table 3.1 Log K values calculated for the association of Fe(III)PPIX with QD, CQ and Art in aqueous solution, acetonitrile and 1 mM aqueous SDS solution. †

Antimalarial Drug	Binding model	Aqueous	Acetonitrile	1 mM SDS
QD	1:1	5.78 ± 0.09	5.92 ± 0.01	6.2 ± 0.1
CQ	2:1	6.5 ± 0.1	5.3 ± 0.2	6.5 ± 0.1
Art	1:1	ND‡	4.48 ± 0.04	ND‡

†Error calculated as standard error of the mean (SEM), following three experimental repeats.
‡Not determinable – weak association and insolubility prevented determination of an association constant.

3.3.2 The Crystal Structure of the Cn-Fe(III)PPIX Complex

Attempts were made to grow crystals of the CQ-Fe(III)PPIX complex in acetonitrile since that of the QD-Fe(III)PPIX complex has already been elucidated. These attempts were, however, unsuccessful. In addition to this, a QD analogue, Cn was investigated in an effort to determine if it could form a similar solid state complex as was found for the QD-Fe(III)PPIX complex. Crystals of Cn-Fe(III)PPIX were obtained

following slow evaporation of solvent from a solution of Fe(IIII)PPIX and free base Cn in acetonitrile. Following five days of evaporation at room temperature, small, needle-like crystals were observed at the bottom of the glass vial and a single crystal of dimensions 0.09 × 0.11 × 0.20 mm was selected for single crystal X-ray diffraction. Analysis revealed that Cn-Fe(III)PPIX crystallises in the orthorhombic crystal system, with space group $P2_12_12_1$.

In the asymmetric unit, coordination occurs between the alkoxide of Cn and the iron centre of Fe(III)PPIX. In addition to this there is π-stacking between quinoline ring of the drug and the Fe(III)PPIX porphyrin. Intramolecular hydrogen bonding exists between the protonated quinuclidine nitrogen atom of Cn and the propionate group of Fe(III)PPIX. Furthermore, there is intermolecular hydrogen bonding between a propionic acid group of one Fe(III)PPIX molecule and the propionate group of a neighbouring Fe(III)PPIX molecule. These features are identical to that reported for the QN- and QD-Fe(III)PPIX complexes.[111] The hydrogen bonds in the crystal structure are shown in Figure 3.5 and their geometries are reported in Table 3.2. Important crystal structure parameters are summarised in Table 3.3. The total volume of the crystal structure is 9217 Å and the crystal packing, viewed along the *a*-axis, is shown in Figure 3.6. This view shows the π-stacking between adjacent complexes.

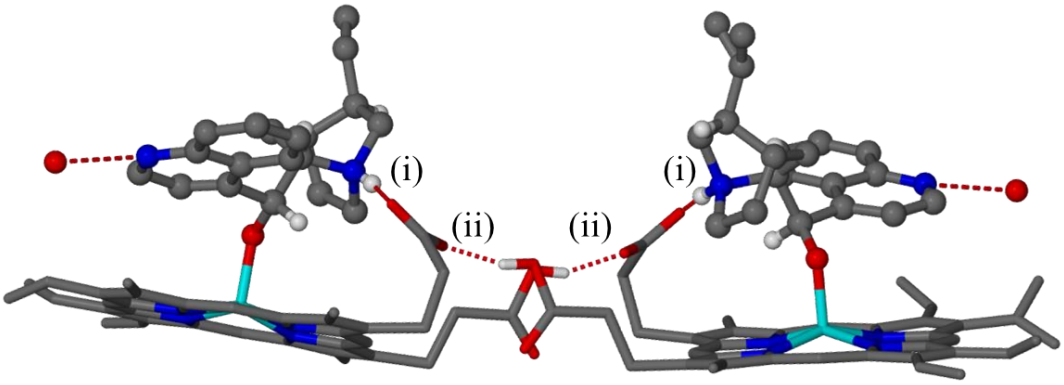

Figure 3.5 Hydrogen bonds (red dashed lines) in the crystal packing of the Cn-Fe(III)PPIX complex. (i) An intramolecular hydrogen bond between the protonated quinuclidine hydrogen of Cn and the propionate group of Fe(III)PPIX and (ii) intermolecular hydrogen bond between the propionic acid group of one Fe(III)PPIX molecule and the propionate group of the neighbouring Fe(III)PPIX molecule. Non-relevant hydrogen atoms have been removed for clarity. Atom colour coding: H-white, C-grey, N-blue, O-red and Fe-cyan.

Table 3.2 Hydrogen Bonding in the Cn-Fe(III)PPIX complex.

Bond	**D-H···A**	**D-H (Å)**	**H···A (Å)**	**D···A (Å)**	**D-H···A (°)**
i (A)	N5-H5N···O2	0.93	1.73	2.648 (8)	165
(B)	N5-H5N···O2	0.93	1.76	2.667 (8)	165
ii	O4-H4···O1	0.84	1.66	2.452(9)	156

Table 3.3 Crystal data, experimental and refinement parameters for the Cn-Fe(III)PPIX complex.

Formula	2 (C_{53} H_{49} Fe_1 N_6 O_6)
Molecular Weight	1843.66
Crystal System and Space Group	Orthorhombic, $P2_12_12_1$
Unit Cell Dimensions (Å)	a = 15.5177
	b = 23.0510
	c = 25.7674
Z	4
μ (mm^{-1})	0.386
Temperature (K)	100
R_{int}	0.226
Final R indices	R_1 = 0.0848, wR_2 = 0.2450
Goodness of Fit, S	1.03

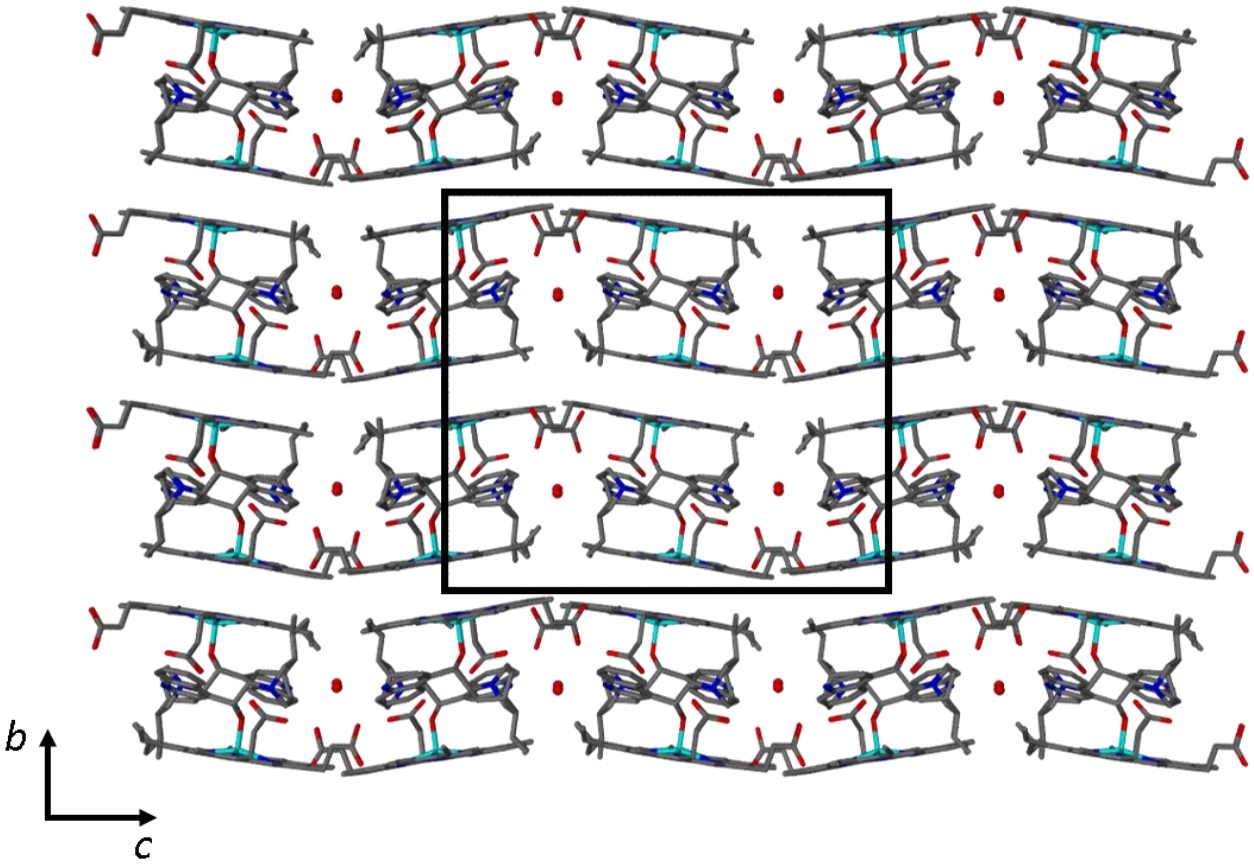

Figure 3.6 The crystal packing of Cn-Fe(III)PPIX viewed along the crystallographic *a*-axis. Hydrogen atoms are omitted for clarity. Atom colour coding: C-grey, N-blue, O-red and Fe-cyan.

3.4 Discussion

The focus of this section of work has been to spectrophotometrically determine the association constants for the interaction between Fe(III)PPIX and three clinically relevant antimalarial drugs in both aqueous and non-aqueous solvent systems. These experiments were carried out in order to determine the interactions of Fe(III)PPIX with QD, CQ and Art under biological conditions that mimic the lipid, parasite cytosol and lipid-water interface found within the malaria parasite. Association constants for the interaction of Fe(III)PPIX with QD and CQ were successfully determined in organic, aqueous and aqueous SDS solutions. Since haem precipitates under acidic conditions, the interaction between antimalarial drugs and haem cannot be investigated under conditions that mimic the DV of the malaria parasite, however, a study by Egan and co-workers has shown that haem redistributes to the cytoplasm of *P. falciparum* and therefore, the appropriate experiments were performed at pH 7.4 to mimic the parasite cytosol.[83]

A strong interaction between Fe(III)PPIX and QD was determined in acetonitrile. The UV-visible spectrum of the QD-Fe(III)PPIX coordination complex has previously been reported in benzene and later in three different organic environments.[111,116] These studies provided evidence of characteristic spectroscopic features that were used to confirm the presence of the QD-Fe(III)PPIX coordination complex in acetonitrile described in the above work. The charge transfer band of the QD-Fe(III)PPIX complex at ~603 nm, similar to that of HO-Fe(III)PPIX, provides evidence for the coordination between the metal centre of the porphyrin and the benzylic alcohol functional group of the quinoline methanol drug.[88,111] The association constant determined under these conditions is in good agreement with the value previously reported in our laboratory.[112] The spectrum obtained in aqueous solution indicates that a different complex is formed under these conditions. A weakened association between Fe(III)PPIX and QD determined in aqueous solution corresponds to the absence of the unique spectroscopic features of the QD-Fe(III)PPIX complex in the UV-visible spectrum of Fe(III)PPIX. Changes in the spectrum of Fe(III)PPIX upon titration with QD in aqueous solution correspond well with previous reports in literature.[102,103] The slight hypochromic effect on the Soret band bears resemblance to that which was previously reported for the interaction between Fe(III)PPIX and QN or CQ in 40% aqueous DMSO.[103] In the latter system, however, Fe(III)PPIX was shown to exist as a monomer and the hypochromic shift was much more pronounced. Egan has postulated that the diminished hypochromicity in purely aqueous solution stems from the dimerisation of Fe(III)PPIX, which in itself promotes a hypochromic effect.[92] A minor bathochromic shift of the Soret band was also reported in aqueous solution and in ethanol, congruent with the present study.[100,102,108] The interaction between Fe(III)PPIX and quinoline antimalarial drugs in detergent systems has not previously been reported. Interestingly, the interaction between Fe(III)PPIX and QD in the aqueous SDS system is comparable to that obtained in organic solution. The increased association constant under these conditions lends support to the recent proposal that complex formation between Fe(III)PPIX and QD is more likely to occur at a lipid-water interface and may therefore influence, or even bring about, inhibition of β-haematin formation.[54] Further support for a lipid environment as the site of antimalarial drug action was provided in the crystal structure of Cn-Fe(III)PPIX obtained

following slow evaporation from a solution of acetonitrile. The key interactions include coordination of the alkoxide group of the drug to the iron centre of Fe(III)PPIX, hydrogen bond formation between the propionate and propionic acid groups of two neighbouring Fe(III)PPIX molecules as well as intermolecular hydrogen bonding between the quinuclidine nitrogen of protonated Cn and the propionate group of Fe(III)PPIX. These key interactions are identical to those previously reported for the Hf-, QD- and QN-Fe(III)PPIX complexes.[110,111] These results lend favour to the idea that, in a lipid environment, drug-Fe(III)PPIX complexation is an important step in the hosts' defence against the parasite.

The UV-visible spectrum of Fe(III)PPIX in the presence of CQ shows a significant decrease in the Soret band in all three solvent systems, similar to what has previously been reported.[103] Egan postulated that this decrease in absorbance could either be attributed to the aggregation of Fe(III)PPIX or its association with CQ.[103] Since the UV-visible spectrum of Fe(III)PPIX in the presence of CQ differs from that of the aggregated Fe(III)PPIX species, together with the fact that the changes in the charge-transfer band bear a resemblance to those observed upon addition of QN to N-AcMP-8, it was proposed that the changes in the spectrum arise from the association with CQ and not Fe(III)PPIX aggregation.[102,103] Recently, Kuter *et al* showed that, in the presence of CQ, a CQ-μ-$[Fe(III)PPIX]_2O$ complex is formed. The formation of this complex is strong in aqueous solution and remains unchanged in the aqueous SDS system, however, a much weaker association was determined in organic solution. This finding is in agreement with what was reported by Egan *et al*. who found that the interactions of CQ with Fe(III)PPIX in 40% aqueous DMSO were weakened upon addition of acetonitrile.[103] The association constants for CQ and QD with Fe(III)PPIX presently determined in aqueous solution are greater than those obtained in 40% (v/v) aqueous DMSO. The increased strength of association in aqueous solution may suggest that hydrophobic factors are important in the formation of these complexes, particularly in the case of CQ.[103] These observations once again confirm that the nature of the solvent plays a crucial role in the strength of association constants.

Owing to weak binding and poor solubility in aqueous solution, Fe(III)PPIX-Art association constants could only be determined in acetonitrile. The interaction of Art with Fe(III)PPIX has proven to be much more complicated and showed a much weaker binding in the organic system, in comparison to both CQ and QD, with little change observed in the spectrum of Fe(III)PPIX upon addition of artesunate in the SDS system. Association constants could furthermore not be determined in aqueous solution as a result of the insolubility of artesunate. The great difference in structure of artemisinin in comparison with the quinoline antimalarial drugs has led to the idea that artemisinin possesses a different mode of action.[143] Several studies have led to the proposal that artemisinin forms a covalent adduct with Fe(III)PPIX as opposed to a coordination complex as was seen previously in the case of the quinoline methanols. [138,144,145] It has been suggested that this covalent linkage involves the generation of a free radical through the cleavage of the endoperoxide bridge of artemisinin followed by carbon alkylation of the porphyrin ring of Fe(III)PPIX.[146] The formation of this covalent bond involves minimal interaction with the iron centre and therefore shifts in the charge transfer region of the UV-visible spectrum of Fe(III)PPIX would not be expected. Contrary to this, however, Adams

and Berman performed an extensive study on the kinetics of the interaction between Fe(III)PPIX and artesunate and obtained results consistent with a three-step, time dependent, mechanism involving the coordination of oxygen to the iron centre followed by cleavage of the endoperoxide bridge and subsequent degradation of the porphyrin, however, association constants were not reported.[138] A definitive increase in absorbance at approximately 416 nm was described in their study, similar to what has previously been reported for Fe(III)PPIX-peroxo intermediates.[147,148] The equilibrium constant for the reaction between H_2O_2 and an iron(III) octa-anionic porphyrin complex at pH 8 has been previously reported as 3.29 ± 0.08 (log scale).[130] This weakened binding correlates well with the difficulties that were encountered when trying to determine the binding constants for the reaction between artesunate and Fe(III)PPIX in the detergent solution, however, the exact nature of the interaction that occurs between Fe(III)PPIX and Art is not fully resolved. It is, however, clear from the present study that Art interacts with Fe(III)PPIX in a manner that is different to that reported for the quinoline antimalarial drugs in both aqueous and organic solutions. The results also suggest that the site of action for Art is a more lipid-based environment, as the association proved to be at least measurable in organic solution.

Although the general structures of CQ and QD shows great similarity, their interaction with Fe(III)PPIX differs considerably, which in turn, suggests varying modes of action. Furthermore, the interaction of Fe(III)PPIX with CQ and QD is markedly stronger than that of Fe(III)PPIX with Art, however, the interaction of Fe(III)PPIX with QD and Art in organic solution strongly support the proposal that their site of action is in a non-aqueous, lipid-mediated environment, while the formation of the CQ-Fe(III)PPIX association complex is largely favourable in aqueous environments.

3.5 Conclusion

UV-visible spectroscopy was used to determine the association constants of three clinically relevant antimalarial drugs with Fe(III)PPIX in aqueous and non-aqueous solutions. The manner in which these antimalarial drugs interact with Fe(III)PPIX is largely reliant on the environment in which the association takes place. The strengthened interaction of QD and Art with Fe(III)PPIX in acetonitrile suggest that it is more likely that these drugs exert their toxicity in a lipid environment, while CQ may rely more greatly on hydrophobic interactions for complex formation. Furthermore, the first single crystal X-ray diffraction structure for the Cn-Fe(III)PPIX complex could be determined through evaporation from a solution of acetonitrile, an environment thought to be a lipid mimic. The chemical structure of the antimalarial drug is also important when considering the mechanism of association with Fe(III)PPIX. While QD has been shown to coordinate to the iron centre of Fe(III)PPIX in acetonitrile, in the presence of the 4-amino group of CQ, no coordination took place, but, rather, π-π interactions between the porphyrin ring and the drug have been proposed. Details of the interaction between Fe(III)PPIX and Art are not well understood, however, the present results rule out the formation of a Fe(III)PPIX-Art coordination complex, and suggest a more intricate interaction. These results supply important information relating to the complexes that may be formed *in vivo*, as well as the relative strength of the interaction under the different environments proposed for drug action. The differences in Fe(III)PPIX interaction could be expected to cause differences in toxicity of the complex. This is explored in Chapter 4.

Chapter 4. The Peroxidase Activity of Fe(III)PPIX

4.1 Introduction

Fe(III)PPIX toxicity is a topic of considerable interest as a result of its relevance to a number of diseases including atherosclerosis, hemolytic anemia, and vasculitis.[11] The mechanism of Fe(III)PPIX toxicity is thought to be related to its ability to generate superoxide radials as a by-product of Fe(II) oxidation to Fe(III) in a mechanism known as the superoxide driven Fenton reaction (see Section 1.5.1 for details).[38] Extensive studies of peroxidase, a haemoprotein enzyme which catalyses the oxidation of organic compounds by hydrogen peroxide (H_2O_2), have been carried out proving its usefulness in a number of biological assays.[129,147,149] The peroxidase reaction is of significant importance because H_2O_2 can be utilized in assays involving the oxidation of certain chromogens.[147]

The generation of reactive oxygen species (ROS), including hydroxyl radicals, is frequently used as a measure of toxicity brought about by Fe(III)PPIX. The reaction of iron (III) porphyrins with H_2O_2 has been investigated as a model for the enzyme peroxidase in a number of studies.[128,134,149] The reaction involves the oxidation of the substrate (XH) by the iron porphyrin in the presence of H_2O_2 (4.1). 2,2'-Azino-bis-(3-ethylbenzothiazoline-6-sulphonate) (ABTS) has routinely been used as a chromogenic reducing substrate for the peroxidase reaction. After oxidation of the substrate, the green $ABTS^{\cdot+}$ radical is produced (4.2), which can be monitored spectrophotometrically at 660 nm.[149]

$$2XH + H_2O_2 \xrightarrow{\text{Catalyst}} 2X + 2H_2O \qquad (4.1)$$

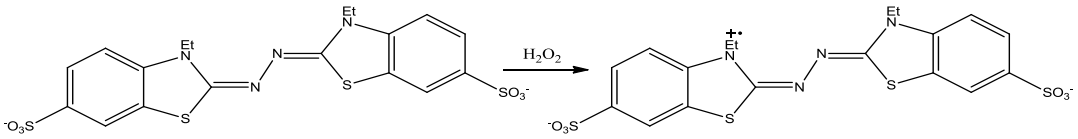

(4.2)

In order to investigate the toxicity of drug-Fe(III)PPIX complexes, the peroxidase activity of Fe(III)PPIX needs to be determined as a baseline by which to compare drug induced toxicity. In this chapter, kinetic studies of the oxidation of ABTS by Fe(III)PPIX and H_2O_2 have been carried out under biological conditions (37 °C, pH 7.5). Kinetic parameters for the oxidation of ABTS by Fe(III)PPIX in aqueous solution were determined and compared to those obtained by Ribeiro *et al.*, who have previously investigated the kinetics of ABTS oxidation by Fe(III)PPIX at 30 °C and pH 6.86.[134] These results were then used to optimize the assay in an aqueous SDS system so as to mimic the proposed environment for haemozoin formation, where it is thought that antimalarial drugs exert their toxicity.

4.2 Experimental Methods

4.2.1 The Reaction Between Fe(III)PPIX with H_2O_2

4.2.1.1 Preparation of Solutions

Fe(III)PPIX Stock Solution

A 1.0 mM Fe(III)PPIX stock solution was prepared by dissolving haematin (3.2 mg, 5.05 µmol) in 0.10 M NaOH to a volume of 5.0 mL in a volumetric flask.

H_2O_2 Stock Solution

A 1.0 mM H_2O_2 stock solution was prepared by diluting 5.0 µL of the commercial solution (30 wt. %) with distilled water to a volume of 50.0 mL in a volumetric flask.

SDS Stock Solution

A 13.0 mM SDS stock solution was prepared by dissolving the solid (37.5 mg, 130 µmol) in distilled water to a volume of 10.0 mL in a volumetric flask.

4.2.1.2 Experimental Procedure

Degradation of Fe(III)PPIX by H_2O_2 (in the absence of ABTS) was investigated spectroscopically by monitoring the decrease in absorbance of Fe(III)PPIX as a function of time. Working solutions consisted of 975 µL Tris buffer stock solution **A** (see section 2.5.4), 25 µL Fe(III)PPIX (stock solution **A**) and 1250 µL distilled water, to which 250 µL of the H_2O_2 stock solution (100.0 µM) was added to initiate Fe(III)PPIX degradation. The spectrum of Fe(III)PPIX was recorded every 60 seconds (300 to 800 nm) for a total of 30 minutes. The absorbance at 380 nm was also monitored every 10 seconds for a period of 10 minutes. The degradation of Fe(III)PPIX in an aqueous SDS solvent system (1.0 mM) was investigated in the same manner as described above. 200 µL of the SDS stock solution was introduced to the system as part of the distilled water component. All experiments were conducted in duplicate.

4.2.2 The Peroxidase Activity of Fe(III)PPIX in Aqueous Solution

4.2.2.1 Preparation of Solutions

ABTS Stock Solution

A: A 2.0 mM ABTS stock solution was prepared by dissolving ABTS (5.5 mg, 10.0 µmol) in distilled water in a 5.0 mL volumetric flask.

B: A 5.0 mM ABTS stock solution was prepared by dissolving ABTS (13.7 mg, 25.0 µmol) in distilled water in a 5.0 mL volumetric flask.

C: A 7.5 mM ABTS stock solution was prepared by dissolving ABTS (41.2 mg, 75.0 µmol) in distilled water to a volume of 10.0 mL in a volumetric flask.

Ammonium Persulfate Stock Solution

A 2.6 mM ammonium persulfate stock solution was prepared by dissolving ammonium persulfate (3.0 mg, 13.15 µmol) in distilled water to a volume of 5.0 mL in a volumetric flask.

ABTS Radical Stock Solution

A stock solution of ABTS radical with a theoretical concentration of 2.0 mM was prepared by adding 4.0 mL of ABTS stock solution **A** to 3.8 mL of the ammonium persulfate stock solution.[138] The solution was then made to a final volume of 10.0 mL in a volumetric flask with distilled water and stored at 4 °C for at least 12 hours before use.

Tris Buffer Stock Solutions

Stock solutions of Tris buffer (130.0 mM) were prepared by dissolving Tris (394.0 mg, 3.25 mmol) in 15.0 mL distilled water. The pH was adjusted to 6.5, 7.0, 8.0 and 9.0 with a 1.0 M HCl stock solution and to pH 11 with concentrated NaOH. Solutions having the required pH were then made up to 25 mL with distilled water in a volumetric flask.

Fe(III)PPIX Stock Solutions

A: A 1.0 mM Fe(III)PPIX stock solution was prepared by dissolving haematin (3.2 mg, 5.05 µmol) in 0.10 M NaOH to a volume of 5.0 mL in a volumetric flask.

B: A 0.2 mM Fe(III)PPIX stock solution was prepared by diluting 2.1 mL of Fe(III)PPIX stock solution **A** with 0.10 M NaOH to a volume of 10.0 mL in a volumetric flask.

H_2O_2 Stock Solutions

A: A 1.0 mM H_2O_2 stock solution was prepared by diluting 5.0 µL of the commercial solution (30 wt. %) with distilled water to a volume of 50.0 mL in a volumetric flask.

B: A 5.0 mM H_2O_2 stock solution was prepared by diluting 5.0 µL of the commercial solution (30 wt. %) with distilled water to a volume of 5.0 mL in a volumetric flask.

4.2.2.2 Experimental Procedure

All experiments were performed in quartz cuvettes with 1 cm pathlength at 37 °C and contained working solutions with a volume of 2.5 mL at pH 7.5 (Tris buffer, 50.7 mM), unless otherwise stated. Total composition of each component in the working solution are given in Table 4.1. When smaller volumes of a component were added, the required volume of the appropriate solvent (see above) was used to ensure the composition of each component remained constant throughout experiments. All samples were mixed thoroughly using a fine needle insert, before the absorbance was recorded at 660 nm, which corresponds to the maximum absorbance peak in the spectrum of the ABTS radical. All experiments were carried out in duplicate unless otherwise stated.

Table 4.1 Composition of components required to investigate the peroxidase activity of Fe(III)PPIX in aqueous solution (pH 7.5).

Component	Volume (µL)
Tris Buffer	975
ABTS	1245
Fe(III)PPIX	30
H_2O_2	250
Total	**2500**

Beer-Lambert Law Plot of ABTS

To obtain the Beers Law plot, separate solutions of ABTS were made up in a concentration range of 0.0-25.0 µM, using ABTS stock solution **B**, and added to a solution of distilled water and Tris Buffer (50.7 mM) in a total volume of 2.5 mL. Each solution was mixed thoroughly before the spectrum was recorded between 300 and 800 nm. The extinction coefficient was then calculated according to the Beer-Lambert law using the absorbance value at 340 nm (Equation 4.3 and 4.3a).

$$A = \varepsilon l c \tag{4.3}$$

$$\varepsilon = \frac{A}{lc} \tag{4.3a}$$

Beer-Lambert Law Plot of ABTS Radical

Individual $ABTS^{\cdot+}$ radical solutions, in the concentration range of 0.0-90.0 µM, were added to the buffer solution as above. The remaining volume was made up with distilled water and the solutions were mixed well before the absorbance spectra were recorded between 300 and 700 nm. Since the oxidation of ABTS by ammonium persulfate was not complete, the concentration of unoxidized ABTS still present could be calculated from its extinction coefficient at 340 nm (see above). The concentration of oxidized $ABTS^{\cdot+}$ radical could then be determined according to Equations 4.4 and 4.4a. The extinction coefficient for the ABTS radical was calculated as above and used in subsequent experiments to determine the yield of $ABTS^{\cdot+}$ production.

$$[\mathrm{ABTS}]_{\mathrm{Tot}} = [\mathrm{ABTS}]_{\mathrm{red}} + [\mathrm{ABTS}^{\cdot+}] \tag{4.4}$$

$$[\mathrm{ABTS}^{\cdot+}] = [\mathrm{ABTS}]_{\mathrm{Tot}} - [\mathrm{ABTS}]_{\mathrm{red}} \tag{4.4a}$$

pH Study

The effect of pH on $ABTS^{\cdot+}$ production was investigated in the presence of 3.0 mM ABTS and 1.0 µM Fe(III)PPIX. Reactions were buffered to values of 6.5, 7.0, 8.0, 9 and 11.0. The reactions were then initiated through the addition of 250 µL (100.0 µM) of H_2O stock solution **A** and the resulting absorbance measured at 660 nm over a period of 200 minutes.

Effects of Fe(III)PPIX Concentration on ABTS Radical Production

The catalytic oxidation of ABTS by H_2O_2 was investigated as a function of Fe(III)PPIX concentration. Working solutions were prepared using stock solution **B** that had final Fe(III)PPIX concentrations of 0.3, 0.6, 1.0, 1.3, 2.0, 2.5 and 4.0 µM and 3.0 mM ABTS. In each case, the reaction was initiated through the addition

of 150 µL of the 5.0 mM H_2O_2 stock solution and the resulting kinetic curve recorded at 660 nm over a period of 60 minutes at intervals of 30 seconds.

Effects of H_2O_2 Concentration on ABTS Radical Production

The catalytic oxidation of ABTS at fixed Fe(III)PPIX (1.0 µM) and ABTS (3.0 mM) concentration was investigated as a function of H_2O_2 concentrations. H_2O_2 stock solutions **A** and **B** were utilized to give concentrations of H_2O_2 in the working solution of 10.0, 50.0, 100.0, 200.0 and 500.0 µM. This experiment was subsequently repeated at Fe(III)PPIX concentrations of 0.3 µM, 0.6 µM and 1.3 µM.

Effects of ABTS Concentration on ABTS Radical Production

The oxidation of ABTS was investigated as a function of ABTS concentration, which was varied between 0.8 and 3.0 mM. This study was done in two parts. In the first part, the concentration of H_2O_2 was varied between 25.0 and 300.0 µM while the concentration of Fe(III)PPIX (1.0 µM) remained constant. In the second part, the concentration of Fe(III)PPIX was varied between 0.3 and 1.3 µM while the concentration of H_2O_2 (100.0 µM) remained constant. In total, 20 experiments were performed for each concentration of ABTS investigated, which are summarized in Table 4.2.

Table 4.2 The volumes of Fe(III)PPIX and H_2O_2 (*x* and *y*, respectively) used to determine the effect of ABTS on $ABTS^{\cdot+}$ production at 660nm.

	H_2O_2 (µM)				
Fe(III)PPIX (µM)	**25.0**	**50.0**	**100.0**	**200.0**	**300.0**
0.3	3; 62.5[a]	3; 125[a]	3; 250[a]	3; 100[b]	3; 150[b]
0.6	7.5; 62.5[a]	7.5; 125[a]	7.5; 250[a]	7.5; 100[b]	7.5; 150[b]
1.0	13; 62.5[a]	13; 125[a]	13; 250[a]	13; 100[b]	13; 150[b]
1.3	15; 62.5[a]	15; 125[a]	15; 250[a]	15; 100[b]	15; 150[b]

x = volume of Fe(III)PPIX stock solution **B**
y = volume of H_2O_2
[a] H_2O_2 stock solution **A**
[b] H_2O_2 stock solution **B**

4.2.3 The Peroxidase Activity of Fe(III)PPIX in Aqueous SDS

4.2.3.1 Preparation of Solutions

ABTS Stock Solution

A 13.0 mM ABTS stock solution was prepared by dissolving ABTS (71.3 mg, 130.0 µmol) in distilled water to a volume of 10.0 mL in a volumetric flask.

SDS Stock Solution

A 13.0 mM SDS stock solution was prepared by dissolving the solid (37.5 mg, 130 µmol) in distilled water to a volume of 10.0 mL in a volumetric flask.

4.2.3.2 Experimental Procedure

The procedure was the same as described in Section 4.2.2.2 with the exception that a 250.0 mM Tris buffer stock solution (see section 2.5.4) was used to accommodate the addition of SDS to the system. The total volume of each component can be seen in Table 4.3. All experiments were carried out in duplicate unless otherwise stated.

Table 4.3 The composition of each component required to investigate the peroxidase activity of Fe(III)PPIX in aqueous SDS solution (pH 7.5).

Component	Volume (µL)
Tris Buffer	500
ABTS	1520
SDS	200
Fe(III)PPIX	30
H_2O_2	250
Total	**2500**

4.2.4 The Kinetic Model

4.2.4.1 Preparation of Solutions

ABTS Stock Solution

A: A 2.0 mM ABTS stock solution was prepared by dissolving ABTS (5.5 mg, 10.0 µmol) in distilled water in a 5.0 mL volumetric flask.

B: A 4.0 mM ABTS stock solution was prepared by dissolving ABTS (11.0 mg, 20.0 µmol) in distilled water in a 5.0 mL volumetric flask.

Cerium (IV) sulfate ($Ce(SO_4)$) Stock Solution

A: A 2.0 mM stock solution of $Ce(SO_4)$ was prepared by dissolving the solid (6.6 mg, 20.0 µmol) in distilled water in a 10.0 mL volumetric flask.

B: A 4.0 mM stock solution of $Ce(SO_4)$ was prepared by dissolving the solid (13.2 mg, 40.0 µmol) in distilled water in a 10.0 mL volumetric flask.

4.2.4.2 Experimental Procedure

The ABTS disproportionation reaction was monitored at 520 nm for a period of 30 minutes at 12 second intervals. Using a 2:1 ABTS: $Ce(SO)_4$ ratio, the ABTS dication ($ABTS^{++}$) was formed by adding the appropriate volume of the two components to a small vial and thoroughly mixed. The dication was then added to 975 µL of the 130.0 mM Tris buffer stock solution (see Section 2.5.4) and the reaction was initiated through the addition of an equimolar amount of ABTS (Table 4.4). The concentration of $ABTS^{++}$ as well as the corresponding volumes of each component used are listed in Table 4.4.

Table 4.4 The volume of $Ce(SO_4)$ and ABTS used to obtain the required concentration of $ABTS^{++}$, together with the volume of ABTS required to initiate the formation of $ABTS^{\cdot+}$.

[$ABTS^{++}$] (mM)	**Dication**		**ABTS**
	$V_{Ce(SO_4)}$ (µL)	V_{ABTS} (µL)	V_{ABTS} (µL) [d]
0.1	250 [a]	125 [c]	62.5
0.2	500 [a]	250 [c]	125
0.4	500 [b]	250 [d]	250
0.5	626 [b]	323 [d]	313

[a] $Ce(SO_4)$ stock solution **A**
[b] $Ce(SO_4)$ stock solution **B**
[c] ABTS stock solution **A**
[d] ABTS stock solution **B**

4.3 Results

4.3.1 The Reaction Between Fe(III)PPIX and H_2O_2

High-valent iron oxo species are thought to play an important role in the oxidation of reactions such as the ABTS oxidation reaction.[130] In order to better understand the oxidation of ABTS by Fe(III)PPIX, it was important to first determine the role of Fe(III)PPIX in the reaction by investigating the rate of formation of this iron oxo species through the interaction of Fe(III)PPIX with H_2O_2. While the exact details of this interaction are unknown, it is thought that the first step in the reaction involves the association of H_2O_2 with Fe(III)PPIX to form an iron-peroxo species. Bond cleavage and subsequent degradation of Fe(III)PPIX is then thought to follow (Equation 4.5). [130,134]

$$\mathrm{Fe(III)PPIX} + \mathrm{H_2O_2} \rightleftharpoons \underbrace{\mathrm{H_2O_2 \cdots Fe(III)PPIX}}_{\textbf{iron-peroxo species}} \rightarrow \mathrm{O{=}Fe(IV)PPIX} \rightarrow \mathrm{decomposition} \qquad (4.5)$$

To probe this mechanism, the kinetics of the interaction between Fe(III)PPIX and H_2O_2 was investigated spectroscopically. These experiments were carried out in the absence of ABTS, which serves to reduce the ROS that otherwise degrade Fe(III)PPIX. Marked changes in the spectrum of Fe(III)PPIX could be seen immediately after the addition of H_2O_2 in both the aqueous (see Figure 4.1 (a)) and aqueous SDS solutions (see Figure 4.1 (b)). A decrease in the Soret band at 398 nm was observed in both solvent systems. The decrease in absorbance at 380 nm was monitored over a period of 10 minutes in aqueous (Figure 4.1 (c)) and aqueous SDS solution (Figure 4.1 (d)). The decay in both cases could be fitted with a two-phase function, which could represent the formation and subsequent decay of an iron-peroxo species. The values obtained for these rate constants are summarized in Table 4.5. This decrease in intensity was not, however, seen at longer wavelengths. Instead, the charge transfer band at 586 nm in aqueous solvent shows a slight red shift in the presence of H_2O_2 after a period of 60 minutes. The same shift is seen in the aqueous SDS solvent system but is more pronounced. While the spectrum of the degradation product is not known, it is assumed that the second function relates to the decay of the catalytic iron species.

The rate constants (calculalted using a simple two-phase decay function) determined for this time-dependent reaction are given by k_1 and k_2. It is, however, not clear from the data which reaction is governed by these rate constants but it is assumed that k_1 represents the formation of the iron-peroxo species while k_2 may represent further interaction with H_2O_2 which may lead to degradation products. The observed reaction rates for the reaction between Fe(III)PPIX and H_2O_2 indicate a faster rate for both the formation and the decay of the complex in aqueous solution (see Table 4.5). The reaction rate for the formation of the iron-peroxo species in the aqueous SDS system is approximately half of that obtained in aqueous solution.

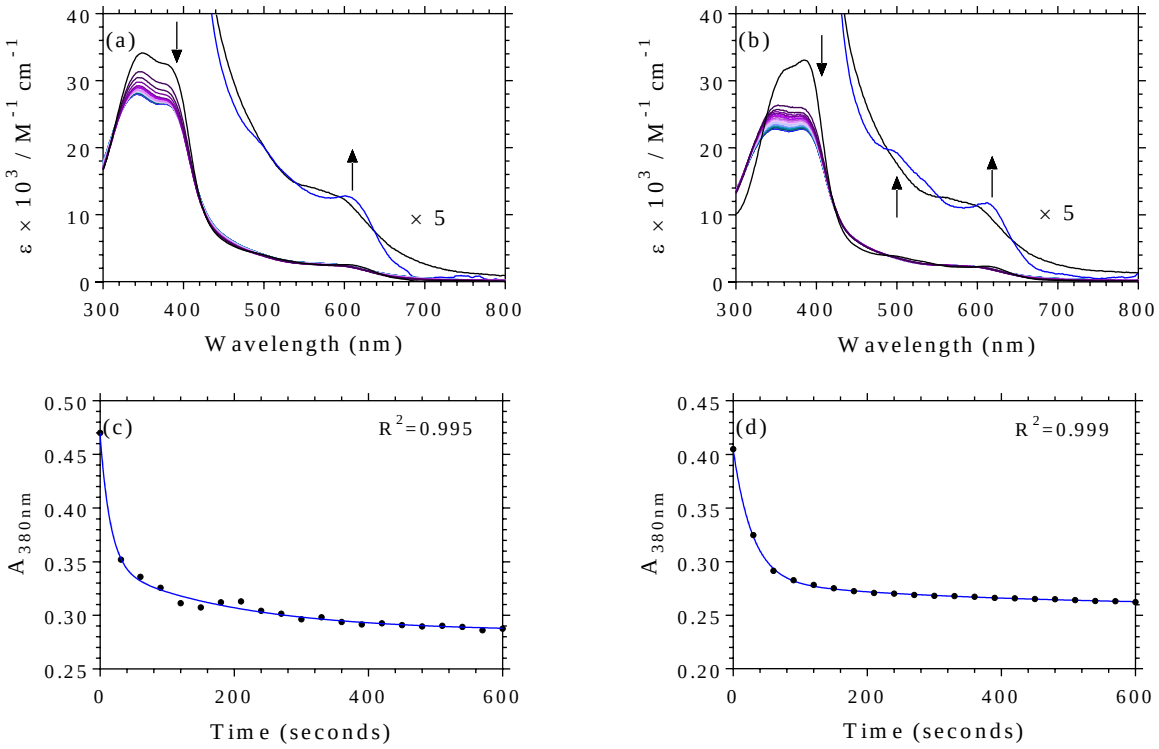

Figure 4.1 The reaction between Fe(III)PPIX and H_2O_2. Spectroscopic changes for the reaction between 10.0 µM Fe(III)PPIX and 100.0 µM H_2O_2 in **(a)** aqueous and **(b)** aqueous SDS solution over a period of 30 minutes. The black line represents the spectrum of Fe(III)PPIX before the addition of H_2O_2 and the subsequent spectra at each time point are shown from purple to dark blue. Shifts in absorbance are indicated with arrows. Plots **(c)** and **(d)** show the trace at 380 nm (black circles) for the reactions in **(a)** and **(b)**, respectively, fitted with a two-phase exponential decay function (blue line).

Table 4.5 A comparison of the observed kinetic parameters (k_{obs}) obtained for the reaction of Fe(III)PPIX with H_2O_2 in aqueous and aqueous SDS solutions.[†]

k_{obs} (× 10^{-4} s^{-1})	Aqueous)	Aqueous SDS
k_1	600 ± 100	360 ± 30
k_2	50 ± 10	26 ± 2

[†]Error calculated as standard error of the mean (SEM), following two experimental repeats.

4.3.2 The Peroxidase Activity of Fe(III)PPIX in Aqueous Solution

As mentioned above, ABTS has often been used to investigate peroxidase reactions as a result of its stability and non-carcinogenic nature.[128] The reaction is based on the one electron oxidation of ABTS to an emerald green coloured ABTS radical cation ($ABTS^{\cdot+}$), during the reduction of H_2O_2, which can be conveniently monitored at 660 nm.[128,129,134,138,147,149]

4.3.2.1 Beers Law Standard Curves

To enable determination of the concentration of the $ABTS^{\cdot+}$ radical produced, construction of a Beer-Lambert plot was required, from which the molar extinction coefficient could be extracted. The $ABTS^{\cdot+}$ radical was successfully generated by adding ammonium persulfate to ABTS, however, even after a reaction time of 12 hours, a substantial amount of unreacted ABTS was still present (see Figure 4.2 (a)). In order to accurately determine the extinction coefficient of the radical at 660 nm, a Beer-Lambert plot for the un-oxidised form of ABTS was carried out at 340 nm (Figure 4.2 (b)). The Beer-Lambert plot for the ABTS radical was then constructed by measuring the absorbance of the whole spectrum (300-800 nm). The absorbance of un-oxidised ABTS at 340 nm was then used to determine the concentration of unreacted ABTS still present in the solution which, in turn, was used to calculate the actual concentration of $ABTS^{\cdot+}$ (at 660 nm) (Equation 4.4a) present in the solution (Figure 4.2 (c)). The extinction coefficients were found to be 40399 ± 626 and 12807 ± 150 M^{-1} cm^{-1} for ABTS and $ABTS^{\cdot+}$, respectively. These values correspond well with previously reported literature values of 36000 M^{-1} cm^{-1} for ABTS and 10000-12000 M^{-1} cm^{-1} for $ABTS^{\cdot+}$.[150,134,130]

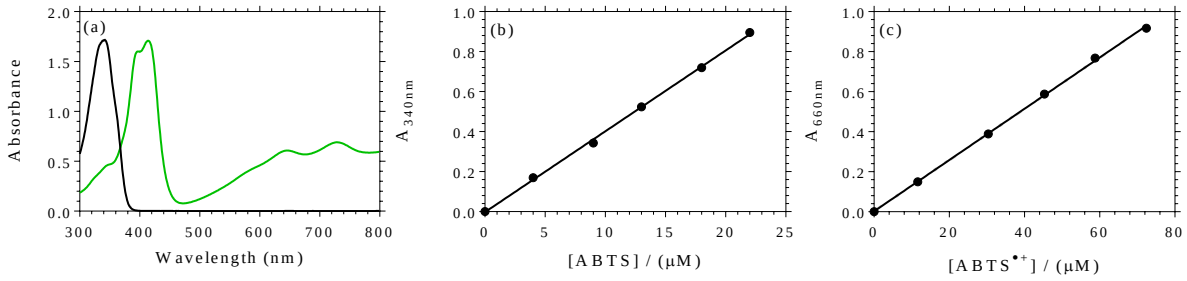

Figure 4.2 (a) The UV-Visible spectrum of ABTS (black) and the $ABTS^{\cdot+}$ (green). Beer-Lambert Law Plots for **(b)** ABTS and **(c)** $ABTS^{\cdot+}$. The extinction coefficients are 40399 ± 626 and 12807 ± 150 M^{-1} cm^{-1},respectively.

4.3.2.2 The pH dependence of the ABTS Oxidation Reaction

The aim of this study was to first optimize an ABTS assay in a system that more closely resembled the environment found within the malaria parasite. A temperature of 37 °C and a pH of 7.5 were chosen so as to better mimic the environment found within the cytoplasm of the malaria parasite and, consequently gain insight into the mechanism of Fe(III)PPIX toxicity. In 1995, Ribeiro *et al.* carried out a study on the kinetics of ABTS oxidation by Fe(III)PPIX.[134] Their study was performed at 30 °C and experiments were buffered to a pH of 6.86 using phosphate buffered saline. In order to determine whether the change in pH would affect the catalytic oxidation of ABTS, a representative kinetic reaction was conducted at varying pH values. Kinetic experiments measuring the degree of $ABTS^{\cdot+}$ production were therefore carried out in a pH range of

6.5-11. The results obtained from this study, shown in Figure 4.3, indicate that the oxidation of ABTS is sensitive to pH changes. At pH 11, the maximum yield of $ABTS^{\cdot+}$ was reached within the first 30 minutes of the reaction, however, the signal started to decay almost immediately after reaching this state, indicating that the $ABTS^{\cdot+}$ is not stable under these conditions (Figure 4.3 (a)). A similar result was obtained at pH 9. At pH 8, there was a marked increase in radical production and the product was stable for a longer period of time (60 minutes). At pH 7.5 there was a nearly two-fold increase in the yield of radical production when compared to pH 8 as well as a prolonged stability, which is maintained for periods as long as 12 hours in the case of pH 6.5 (Figure 4.3 (b)) leading to the conclusion that $ABTS^{\cdot+}$ is more stable at a lower pH. It is also evident that the overall reaction rate is affected by a change in pH. At higher pH values, the reaction reaches completion faster than at the low pH values. There is, however, little difference in the yield and rate of radical production in the pH range of 6.5-7.5, which implies that changing the pH from 6.86 (used by Ribeiro *et al.*) to 7.5 would not influence the reaction greatly. Further investigations into the initial stages of the reaction show minimal variation in the pH range of 6.5-7.5 (Figure 4.3 (c)). Furthermore, a plot of the maximum yield of $ABTS^{\cdot+}$ production (Figure 4.3 (d)) indicates a constant yield in the pH range of 6.5-7.5 and that yields only decline at pH values above 7.5. Unfortunately, further investigations could not be conducted at pH values below 6.5 owing to the poor solubility of Fe(III)PPIX under acidic conditions.[151]

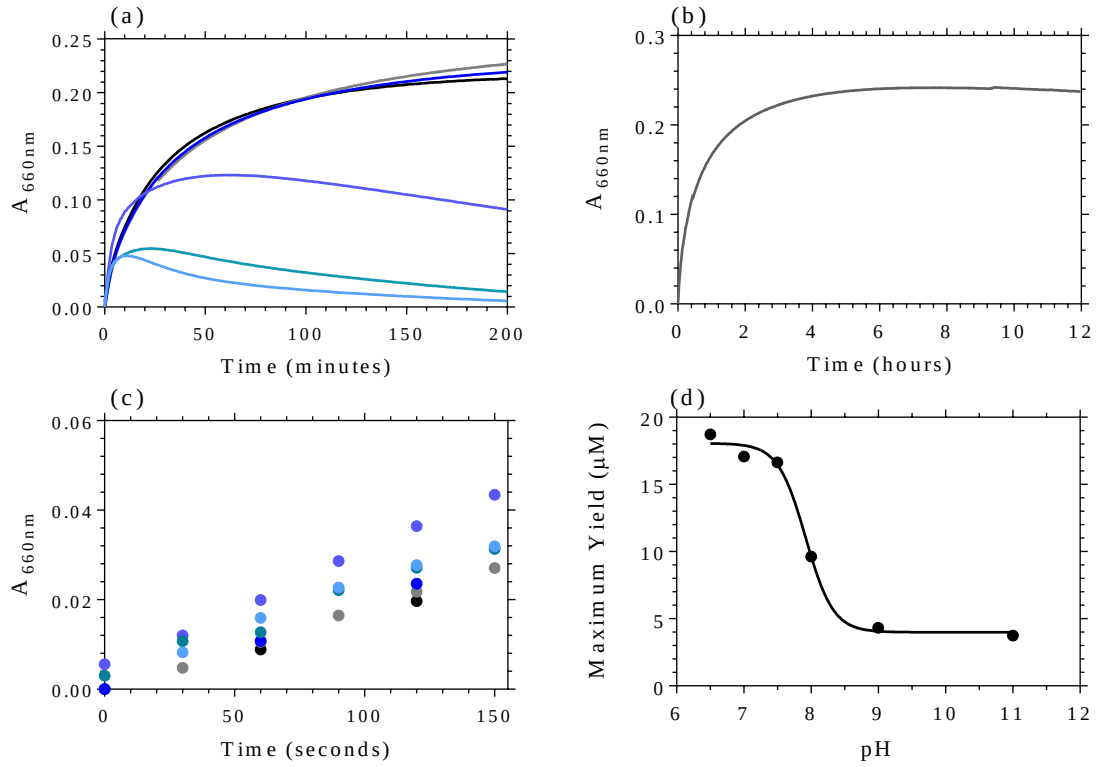

Figure 4.3 The effect of pH on the oxidation of ABTS. **(a)** The change in absorbance monitored at 660 nm over time at pH 11 (-), 9 (-), 8 (-), 7.5 (-), 7 (-) and 6.5(-) in the presence of 3.0 mM ABTS, 1.0 µM Fe(III)PPIX and 100.0 µM H_2O_2 and **(b)** the absorbance for pH 6.5 over a period of 12 hours. **(c)** The initial 150 seconds of the reaction in **(a)** plotted as a function of increasing time. **(d)** The maximum yield for the reactions described, taken as the maximum absorbance in **(a)** as a function of pH fitted with a sigmoidal function. Data points omitted for clarity.

In order to accurately investigate the kinetics of ROS generation by Fe(III)PPIX, kinetic studies of the ABTS oxidation reaction were carried out in a manner similar to those described by Ribeiro and Adams.[134,149] Accordingly, all the experiments were carried out under conditions in which a catalytic amount of Fe(III)PPIX was present and furthermore, the concentration of ABTS greatly exceeded that of both H_2O_2 and Fe(III)PPIX, ie. [ABTS] >> [H_2O_2] >> [Fe(III)PPIX]. These constraints were necessary to prevent the disproportionation of ABTS (Equation 4.6) at low ABTS concentration, as well as to reduce the catalase activity (Equation 4.7) of Fe(III)PPIX at high H_2O_2 concentrations.[130] Both of these processes are discussed in further detail below.

$$2ABTS^{\cdot+} \rightleftharpoons ABTS + ABTS^{++} \tag{4.6}$$

$$2H_2O_2 \rightarrow 2H_2O + O_2 \tag{4.7}$$

The oxidation of ABTS by Fe(III)PPIX and H_2O_2 is a three-component system, the kinetics of which are complex and not fully understood. It is unclear in the literature whether the rate of this reaction is dependent on all or some combination of these components. Therefore, in order to accurately determine the role that each component plays in the oxidation of ABTS, the concentration of each component was systematically varied and the effect on $ABTS^{\cdot+}$ formation monitored. This can then be compared to the results obtained in the presence of antimalarial drugs. The first component to be varied was Fe(III)PPIX, the details of which are discussed below.

4.3.2.3 Effects of Fe(III)PPIX Concentration on ABTS Radical Production

To determine the influence of Fe(III)PPIX on the catalytic oxidation of ABTS by H_2O_2, the kinetics of $ABTS^{\cdot+}$ radical production was monitored at a constant concentration of both H_2O_2 and ABTS, while varying Fe(III)PPIX concentration. The ability of Fe(III)PPIX to catalyse the oxidation of ABTS is evident from the experimental results. $ABTS^{\cdot+}$ formation was calculated using the extinction coefficient determined above and this concentration was plotted as a function of time (see Figure 4.4 (a)). As expected, in the absence of Fe(III)PPIX, no reaction was observed. The yield of $ABTS^{\cdot+}$ production was observed to be linearly dependent on the concentration of Fe(III)PPIX for Fe(III)PPIX concentrations up to 1.3 µM (see Figure 4.4 (b)). For this reason, only Fe(III)PPIX concentrations up to 1.3 µM were considered in subsequent experiments. This observation is of interest since catalysts are known to affect the rate of a reaction but not influence its yield which would suggest that Fe(III)PPIX does not act as a true catalyst.

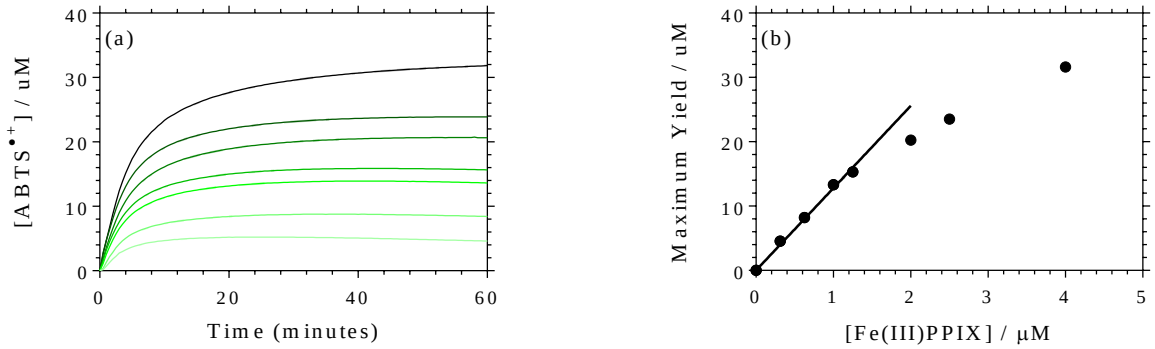

Figure 4.4 Effects of Fe(III)PPIX concentration on the oxidation of ABTS by H_2O_2. **(a)** ABTS radical production plotted as a function of increasing time. Experiments were carried out using 300.0 µM H_2O_2, 3.0 mM ABTS and Fe(III)PPIX concentrations of 0.3 (-), 0.6 (-), 1.0 (-) and 1.3 (-) 2.0 (-), 2.5 (-) and 4.0 (-) µM. **(b)** Maximal yield of $ABTS^{\bullet+}$ in **(a)** as a function of increasing Fe(III)PPIX concentration. Data points omitted for clarity.

4.3.2.4 Effects of H_2O_2 Concentration on ABTS Radical Production

As previously discussed, the oxidation of ABTS requires three components and, while Fe(III)PPIX plays an essential role in the reaction, the rate is not necessarily independent of the concentration of H_2O_2 and ABTS. Therefore, to determine if H_2O_2 concentration has an effect on the reaction kinetics, its concentration was varied in a similar manner as described for Fe(III)PPIX. The results for this study are shown in Figure 4.5. Each data set ((a)-(d)) represents a fixed concentration of H_2O_2 in which Fe(III)PPIX concentration was varied at constant ABTS concentration. Interestingly, the yield of the reaction does not appear to depend linearly on the concentration of H_2O_2 but, rather appears to become saturated at concentrations above 100.0 µM (Figure 4.5 (e)). One reason for this saturation effect could be a result of the competing catalase reaction, which occurs at high H_2O_2 concentrations. This reaction, shown in Equation 4.7, describes the disproportionation of H_2O_2 to water and oxygen, resulting in a reduction in the concentration of H_2O_2, a necessary component to bring about ABTS oxidation. From the data in Figure 4.5, it is also evident that H_2O_2 has an effect on the rate of ABTS oxidation (Figure 4.5 (f)). At higher H_2O_2 concentrations the maximum yield of $ABTS^{\cdot+}$ is reached within the first 20 minutes of the reaction, while at lower H_2O_2 concentrations, the maximum yield is not reached even after a period of 60 minutes.

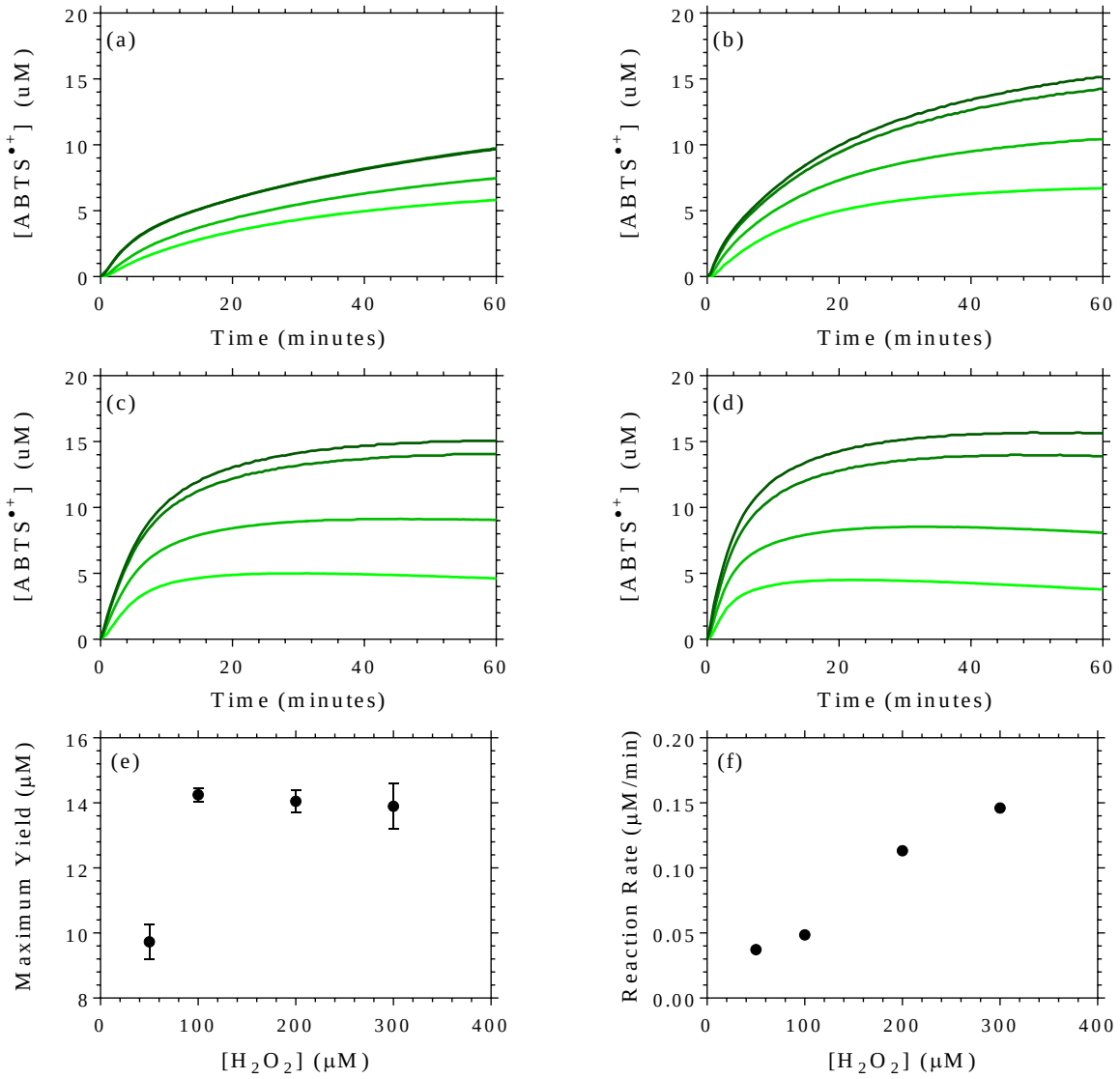

Figure 4.5 The effect of H_2O_2 on the oxidation of ABTS in aqueous solution. The conditions are 3.0 mM ABTS and **(a)** 50.0, **(b)** 100.0, **(c)** 200.0 and **(d)** 300.0 µM H_2O_2. In each set of experiments, the concentration of Fe(III)PPIX was varied as follows: 0.3 (-), 0.6 (-), 1.0 (-) and 1.3 (-) µM. **(e)** The maximum yield of $ABTS^{\cdot+}$(maximum concentration in 60 minutes) and the overall reaction rate **(f)** in the presence of 1.0 µM Fe(III)PPIX and 3.0 mM ABTS as a function of increasing H_2O_2 concentration. Data points omitted for clarity.

4.3.2.5 Effects of ABTS Concentration on ABTS Radical Production

The effect of ABTS concentration on $ABTS^{\cdot+}$ production was monitored in two stages. The first stage involved systematically varying the concentration of ABTS and Fe(III)PPIX while the concentration of H_2O_2 remained constant at 100.0 µM. The results for this experiment are shown in Figure 4.6. From the data, it is evident that there is a relationship between the yield of $ABTS^{\cdot+}$ produced and the concentration of ABTS at a given H_2O_2 concentration (Figure 4.6 (f)). Additionally, the overall reaction rate appears faster at lower ABTS concentrations (Figure 4.6 (g)).

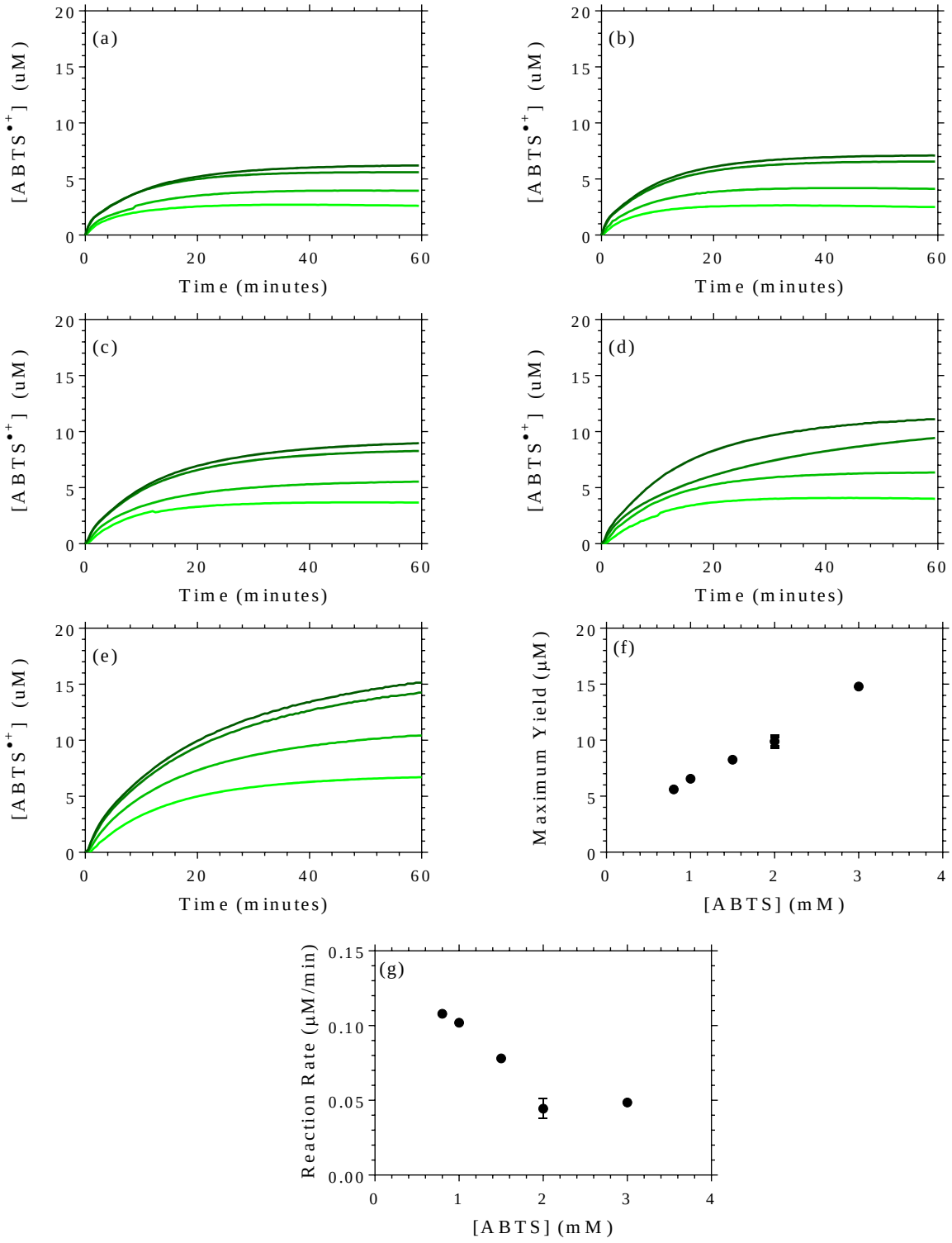

Figure 4.6 The effect of ABTS concentration on the oxidation of ABTS in aqueous solution. The conditions are 100.0 µM H_2O_2 and **(a)** 0.8, **(b)** 1.0, **(c)** 1.5, **(d)** 2.0 and **(e)** 3.0 mM ABTS. In each set of experiments, the concentration of Fe(III)PPIX was varied as follows: 0.3 (-), 0.6 (-), 1.0 (-) and 1.3 (-) µM. The maximum yield (maximum concentration in 60 minutes) and reaction rate in the presence of 100.0 µM H_2O_2 and 1.0 µM Fe(III)PPIX are plotted as a function of ABTS concentration in **(f)** and **(g)**, respectively. Data points omitted for clarity.

During the second stage of this study, the concentration of Fe(III)PPIX was fixed at 1.0 µM and the concentration of H_2O_2 was varied at differing ABTS concentrations (Figure 4.7). From the data, it is once again evident that, from lowest to highest concentration, the concentration of ABTS has a direct influence on the maximum yield of $ABTS^{\cdot+}$ produced (Figure 4.7 (e)). Contrary to what was seen for Fe(III)PPIX, for a specific ABTS concentration, $ABTS^{\cdot+}$ production does not appear to be directly dependent on H_2O_2 concentration. Rather, the maximum yield of $ABTS^{\cdot+}$ is saturated at concentrations above 50.0 µM H_2O_2 (Figure 4.7 (f)), however, there is a definite increase in the rate of the reaction when moving from lower to higher H_2O_2 concentrations.

An additional characteristic to these plots is a decay in the observed absorbance, particularly at H_2O_2 concentrations above 100.0 µM. Depending on the concentration of ABTS, the point at which the $ABTS^{\cdot+}$ concentration starts to decay varies. The decay in a particular curve is highlighted by the dotted line Interestingly, higher ABTS concentrations appear to stabilize the reaction since the decaying process only occurs after a period of 50 minutes as opposed to 20 minutes at lower ABTS concentrations. As mentioned previously, high ABTS concentrations are required to prevent $ABTS^{\cdot+}$ disproportionation.

An enlargement of the first five minutes of the experiments above are shown in Figure 4.8. These plots would indicate that the oxidation of ABTS by Fe(III)PPIX and H_2O_2 is not a simple one step process. Rather, from the graphs we speculate that there are at least two different processes occurring in the first five minutes of the reaction. The two intersecting dotted lines on the respective graphs are an attempt to indicate this visually, however further experimentation would be required to confirm their validity. The two processes may be related to the different steps in the generation of the radical. It is known from literature that one molecule of the iron porphyrin will result in the formation of two molecules of $ABTS^{\cdot+}$. The first $ABTS^{\cdot+}$ radical is thought to be formed through the reduction of $O{=}Fe(IV)por^{\cdot+}$ to O=Fe(IV)por, while the second is thought to be produced during the reduction of O=Fe(IV)por to Fe(III). The rates for these two processes need not be the same and thus could therefore account for the disjointed kinetic trace observed in the first five minutes of the reaction, however, this would require further investigation.

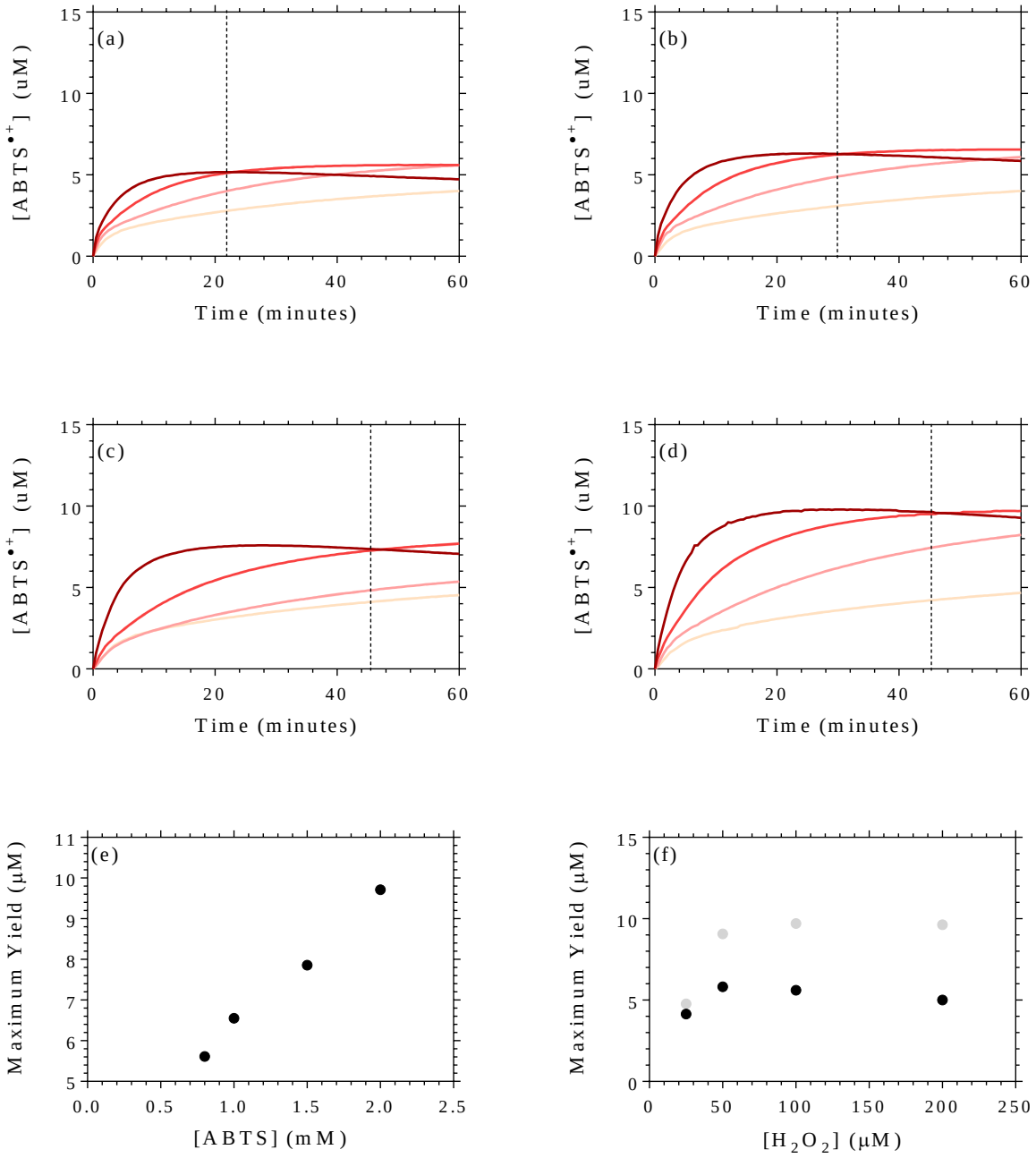

Figure 4.7 The effect of ABTS concentration on the oxidation of ABTS in aqueous solution. The conditions are 1.0 µM Fe(III)PPIX in the presence of **(a)** 0.8, **(b)** 1.0, **(c)** 1.5, **(d)** 2.0 mM ABTS. In each experiment, the concentration of H_2O_2 was varied as follows: 25.0 (-), 50.0 (-), 100.0 (-) and 200.0 (-) µM. Dashed lines indicate the time at which [$ABTS^{\cdot+}$] starts to decay in the case of 200.0 µM H_2O_2. The maximum yield of $ABTS^{\cdot+}$ obtained in the presence of 1.0 µM Fe(III)PPIX and **(e)** 100.0 µM H_2O_2 plotted as a function of increasing [ABTS] and **(f)** plotted as a function of increasing [H_2O_2] in the presence of 0.8 (black) and 2.0 mM (grey) ABTS. Data points omitted for clarity.

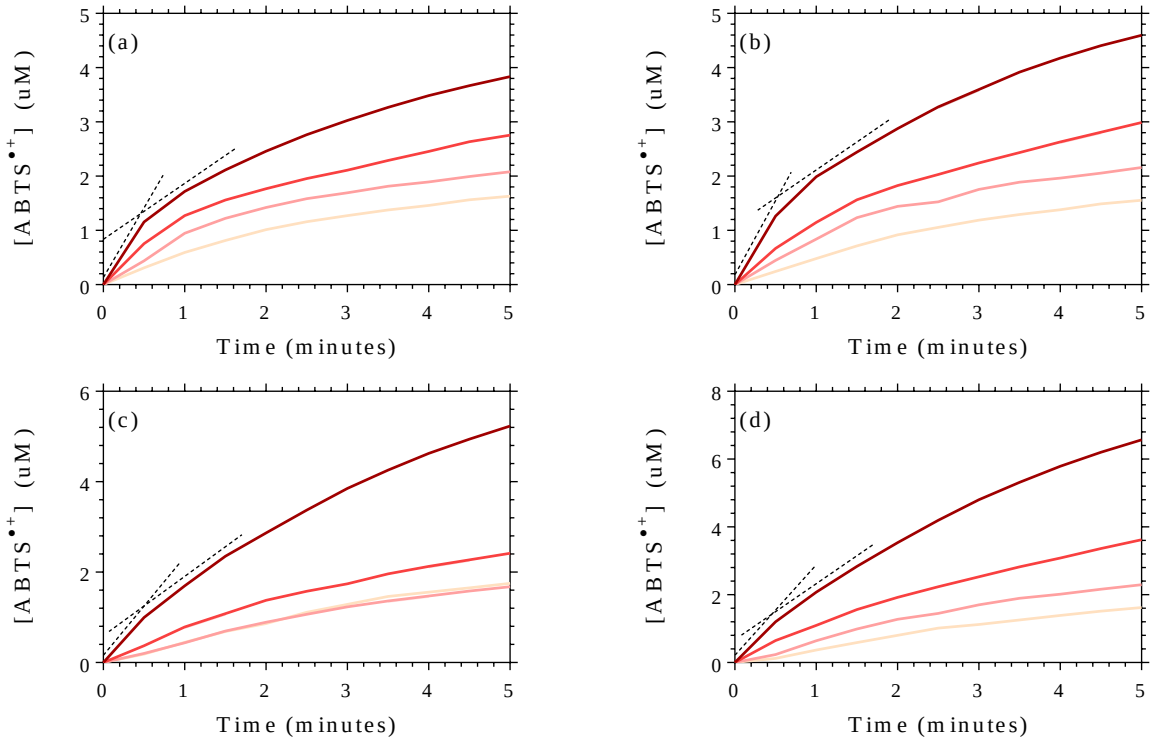

Figure 4.8 The effect of ABTS concentration on the initial five minutes of ABTS oxidation in aqueous solution. The conditions are 1.0 µM Fe(III)PPIX in the presence of **(a)** 0.8, **(b)** 1.0, **(c)** 1.5 and **(d)** 2.0 mM ABTS in the presence of 25.0 (-), 50.0 (-), 100.0 (-) and 200.0 (-) µM H_2O_2. Dashed lines drawn in the initial two minutes of the reaction indicate what appears to be two different stages in the initial five minutes of the reaction. Data points omitted for clarity.

4.3.3 The Peroxidase Activity of Fe(III)PPIX in Aqueous SDS

4.3.3.1 Beers Law Standard Curves

Recent literature has suggested that haemozoin formation most likely occurs in a non-aqueous environment.[54] Therefore, it has become obligatory to not only measure the toxicity of Fe(III)PPIX in aqueous solution, but also in lipid-like environments. Initially, acetonitrile was used to mimic this environment since it has previously been shown to facilitate drug-Fe(III)PPIX coordination,[111] however, the ABTS radical cation was found to be unstable under these conditions (see Figure 4.9).

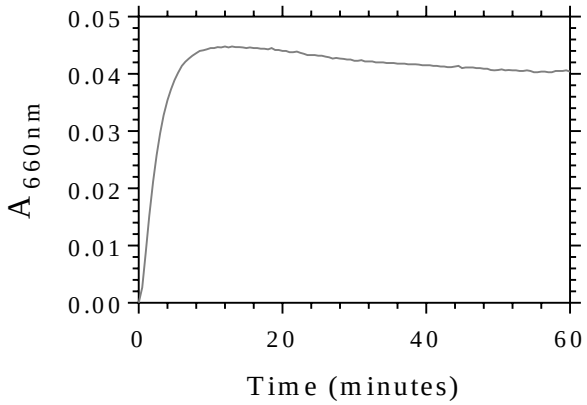

Figure 4.9 The oxidation of ABTS in 60% (v/v) aqueous/acetonitrile. The conditions are 3.0 mM ABTS, 1.0 µM Fe(III)PPIX and 300.0 µM H_2O_2. The absorbance trace is observed to decrease in intensity which indicates poor stability of $ABTS^{\cdot+}$ in the solvent system.

To accommodate this, the peroxidase activity of Fe(III)PPIX was investigated in an environment that closely resembles a lipid-water interface using the water soluble detergent SDS. A concentration of 1.0 mM SDS was employed in this study, the same as that used in Chapter 3 for the drug-Fe(III)PPIX titration study in order to ensure consistency. No previous studies of the peroxidase activity of Fe(III)PPIX under these conditions have been reported. The Beers-law plots for ABTS and $ABTS^{\cdot+}$ can be seen in Figure 4.10 (a) and (b), respectively, for which extinction coefficients of 19580 ± 122 and 24910 ± 835 M^{-1} cm^{-1} were determined. The extinction coefficient for the ABTS radical is approximately double that which was previously determined for the aqueous system, which indicates that $ABTS^{\cdot+}$ absorbs more strongly in the aqueous SDS system.

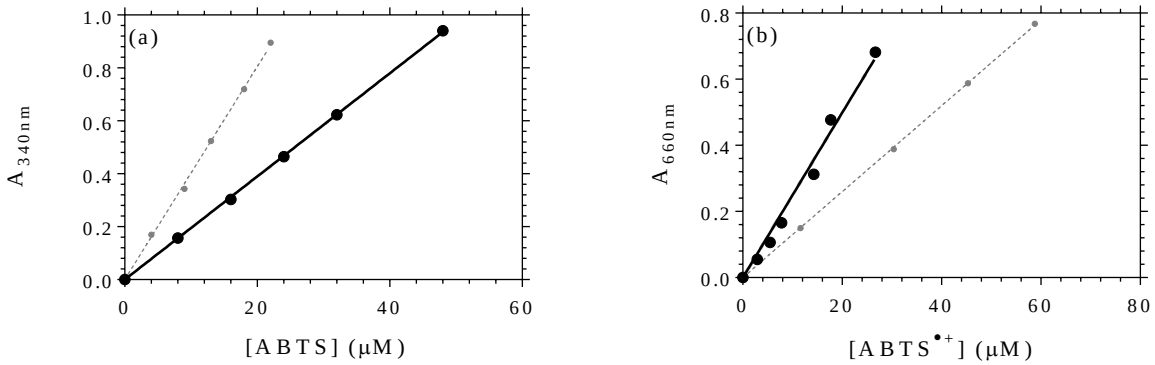

Figure 4.10 Beer-Lambert Law Plots for **(a)** ABTS and **(b)** $ABTS^{\cdot+}$ in aqueous SDS. The extinction coefficients were found to be 19580 ± 121.9 and 24910 ± 834.8 M^{-1} cm^{-1}, respectively. The Beer-Lambert law plots obtained above for ABTS and $ABTS^{\cdot+}$ in aqueous solution are shown for comparison as grey, dashed lines in **(a)** and **(b)**, respectively.

In order to compare radical production in the two systems, a kinetic study was performed under conditions of constant Fe(III)PPIX, H_2O_2 and ABTS concentrations. The results of this investigation are shown in Figure 4.11. The overall rate of the oxidation reaction appears delayed in the presence of SDS, with the reaction only reaching maximal values after a period of 100 minutes in comparison with the aqueous system, which reached completion within the first 60 minutes of the reaction time. An analysis of the reaction rates, calculated using a one-phase exponential function, for the conditions described in Figure 4.11 (Table 4.6) shows an approximate two-fold reduction when comparing the aqueous system to that of aqueous SDS. While the rate of the reaction is slower, the ABTS radical appears to be more stable under these conditions. This is based on the observation that there is no evidence of $ABTS^{\cdot+}$ decay over the described time period in the aqueous SDS system. By contrast, the signal in the aqueous system starts to decay after approximately 60 minutes.

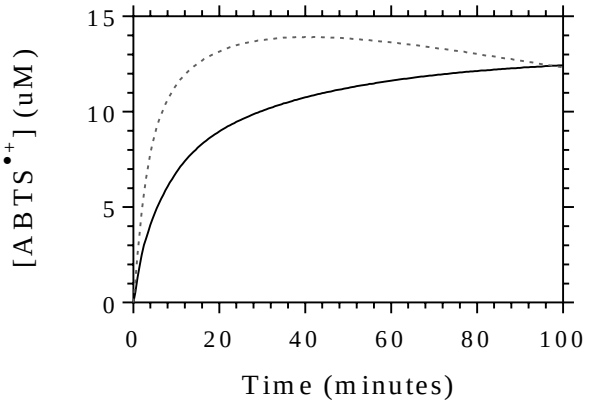

Figure 4.11 Kinetics of $ABTS^{\cdot+}$ formation in the aqueous (grey) and aqueous SDS (black) system. The experiment was carried out using 1.0 µM Fe(III)PPIX, 3.0 mM ABTS and 300.0 µM H_2O_2. Data points omitted for clarity.

Table 4.6 Summary of the reaction rate and yield obtained for the reaction described in Figure 4.11 for the oxidation of ABTS by Fe(III)PPIX in aqueous and aqueous SDS solutions. The maximum yield was taken as the maximum concentration of $ABTS^{\cdot+}$ obtained within the 100 minute period.

System	Reaction Rate (µM/s)	Maximum Yield (µM)
Aqueous	24.4 ± 0.5	13.92 ± 0.04
Aqueous SDS	11.2 ± 0.2	12.14 ± 0.04

4.3.3.2 Effects of Fe(III)PPIX on ABTS Radical Production

Kinetic studies on the oxidation of ABTS by Fe(III)PPIX in the aqueous SDS system were subsequently carried out in the same systematic manner as described above for the aqueous system. The concentration studies in the aqueous SDS system were based on the results obtained in the aqueous system. Owing to the slower rate observed in the SDS system, the experiments were conducted over a period of 90 minutes as

opposed to 60 minutes for the aqueous system and, in some cases, higher component concentrations were utilised. A kinetic study was carried out in the presence of increasing concentrations of Fe(III)PPIX in the range of 0.3-1.3 µM and constant ABTS and H_2O_2 concentrations. The results, shown in Figure 4.12 (a), reveal a similar trend as was seen in the aqueous system. In this data set, as was seen in Figure 4.4 above, there again appears to be an initial linear increase until a maximum yield is reached. An analysis of the maximum yield obtained at each individual Fe(III)PPIX concentration indicates a direct relationship for the concentration range described (Figure 4.12 (b)). At higher concentrations, a saturation effect is once more observed. This saturation occurs at lower Fe(III)PPIX concentrations in the case of aqueous SDS, however, due to the slow rate of the reaction in this environment, carrying out the reaction at lower Fe(III)PPIX concentrations was not feasible.

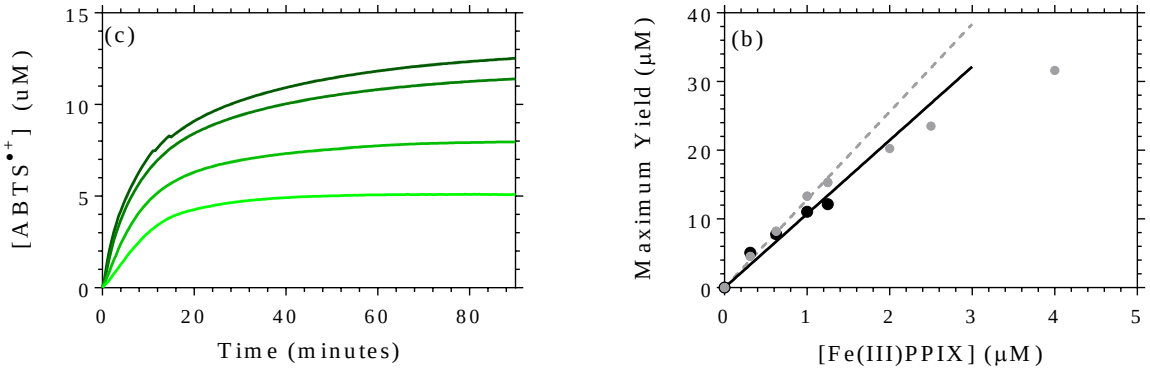

Figure 4.12 Effects of Fe(III)PPIX concentration on the oxidation of ABTS by H_2O_2 in aqueous SDS solution. **(a)** ABTS radical production plotted as a function of increasing time. Experiments were carried out using 300.0 µM H_2O_2, 3.0 mM ABTS and Fe(III)PPIX concentrations of 0.3 (-), 0.6 (-), 1.0 (-) and 1.3 (-) µM. **(b)** Maximal yield of $ABTS^{\cdot+}$ in **(a)** as a function of increasing Fe(III)PPIX concentration. The trend obtained in aqueous solution is shown in grey. Data points omitted for clarity.

4.3.3.3 Effects of H_2O_2 Concentration on ABTS Radical Production

The effect of H_2O_2 concentration on ABTS oxidation was monitored at constant ABTS and increasing Fe(III)PPIX concentrations. A H_2O_2 concentration range of 100.0-400.0 µM was used in these experiments and the results for this study are shown in Figure 4.13. These plots show a dependence of $ABTS^{\cdot+}$ production on H_2O_2 concentration, with lower yields being reached at 100.0 µM H_2O_2 when compared to 400.0 µM. This dependence, however, is not linear as the yield obtained in the presence of 300.0 µM and 400.0 µM H_2O_2 shows minimal variation and rather suggests a saturation effect at concentrations above 400.0 µM (Figure 4.13 (e)).

A comparison of these results with those obtained in aqueous solution shows minimal change in the maximum yield of $ABTS^{\cdot+}$, however, there does appear to be a substantial reduction in the overall reaction rate, particularly at lower H_2O_2 concentrations where the maximum yield is not reached within the 90-minute

recording period (Figure 4.13 (f). The aqueous SDS system also appears to enhance the stability of the radical. This is evident from Figure 4.13 (d), which shows the radical to be stable at a concentration of 400.0 µM H_2O_2, while in aqueous solution, the reaction could only be carried out at H_2O_2 concentrations below 300.0 µM. This may indicate that higher H_2O_2 concentrations are required for the catalase reaction to commence in aqueous SDS. Furthermore, in Figure 4.5 (d), a decay in the yield of $ABTS^{\cdot+}$ concentration after 30 minutes is evident for the reaction conducted at 0.3 µM Fe(III)PPIX. This is, however, not the case in the aqueous SDS system as the response was maintained for 90 minutes in each reaction described. The exact reason for the enhanced stability of the radical in aqueous SDS is not known, however, it may suggest that ROS generation is more prolonged in environments that resemble the lipid-water interface.

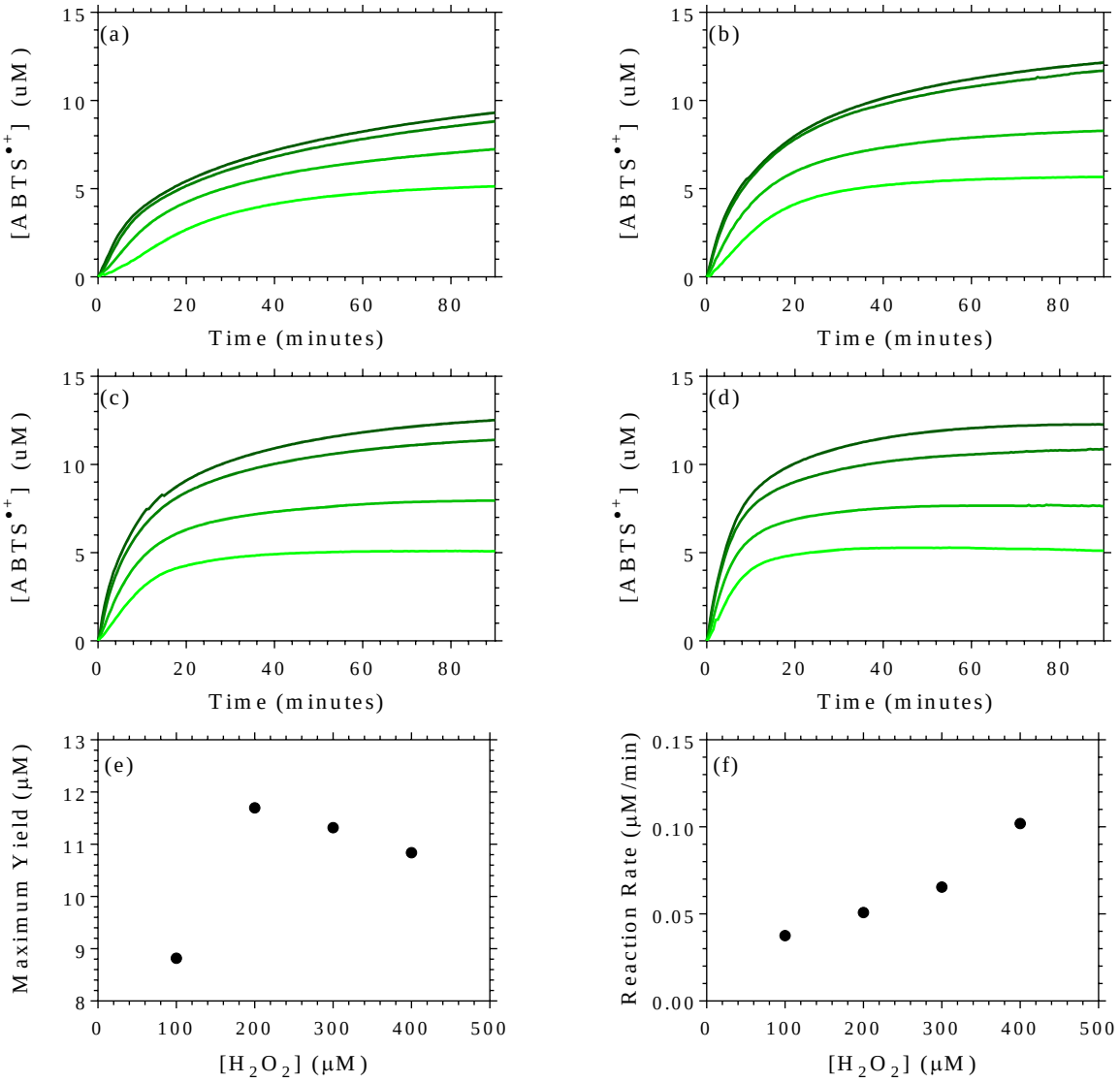

Figure 4.13 The effect of varying H_2O_2 concentration on the oxidation of ABTS in aqueous SDS solution. The conditions are 3.0 mM ABTS in the presence of **(a)** 100.0, **(b)** 200.0, **(c)** 300.0 and **(d)** 400.0 µM H_2O_2 and Fe(III)PPIX concentrations of 0.3 (-), 0.6 (-), 1.0 (-) and 1.3 (-) µM. **(e)** The maximum yield (maximum concentration in 90 minutes) and overall reaction rate **(f)** obtained in the presence of 3.0 mM ABTS and 1.0 µM Fe(III)PPIX plotted as a function of increasing H_2O_2 concentration. Data points omitted for clarity.

4.3.3.4 Effects of ABTS Concentration on ABTS Radical Production

The effect of varying ABTS concentration as a function of increasing Fe(III)PPIX concentration can be seen in Figure 4.14. It can be seen from this data that $ABTS^{\cdot+}$ production is directly related to the concentration of ABTS in each reaction up to concentrations as high as 5.0 mM (Figure 4.14 (e)). In contrast to what was observed in aqueous solution, the overall reaction rate does not appear to be affected by a change in ABTS concentration (Figure 4.5 (f)). This experiment once again provides evidence for enhanced stability in the aqueous SDS system since the radical is stable at higher ABTS concentrations.

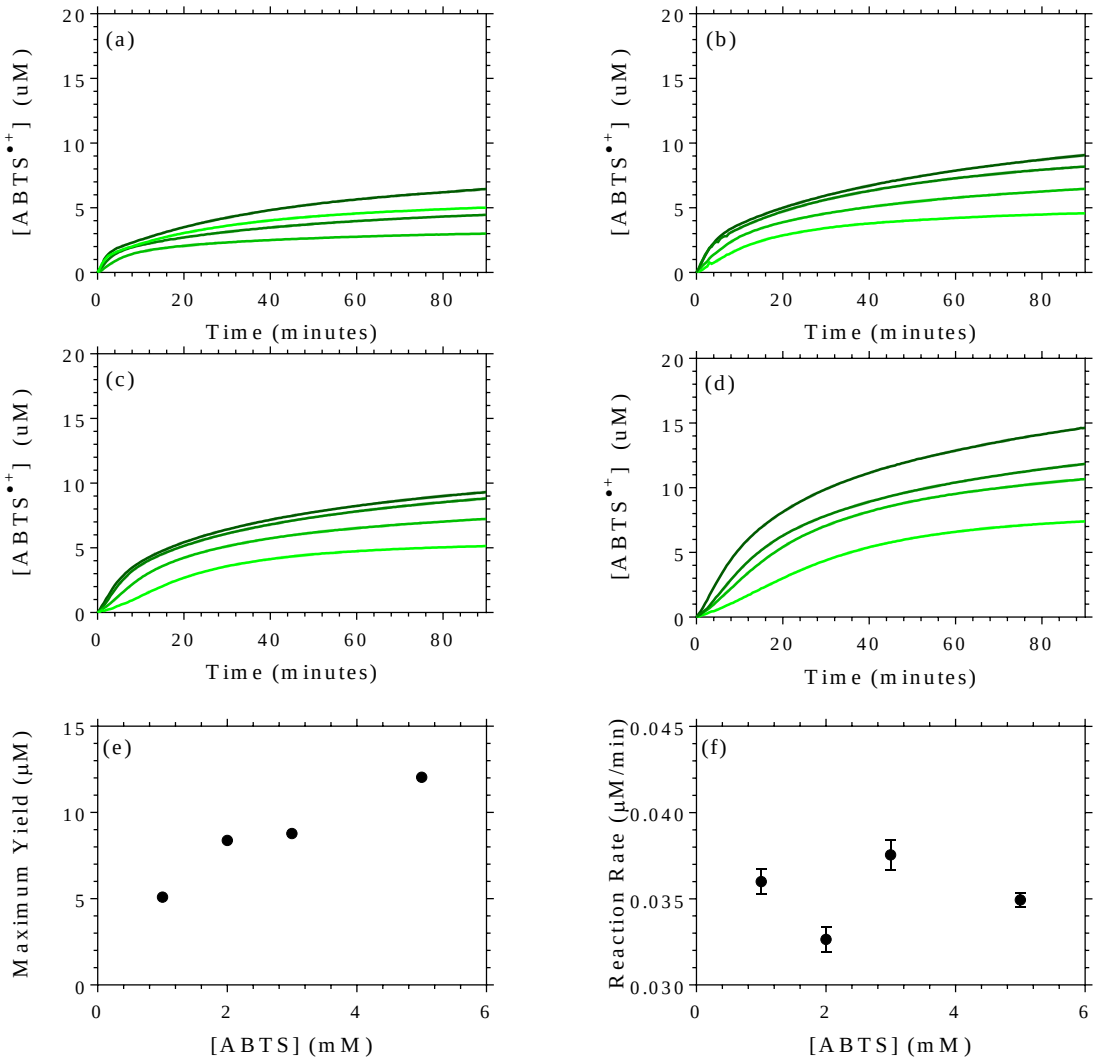

Figure 4.14 The effect of varying ABTS concentration on the oxidation of ABTS in aqueous SDS solution. The conditions are 100.0 µM H_2O_2 in the presence of **(a)** 1.0, **(b)** 2.0, **(c)** 3.0 and **(d)** 5.0 mM ABTS and Fe(III)PPIX concentrations of 0.3 (-), 0.6 (-), 1.0 (-) and 1.3 (-) µM. **(e)** The yield of $ABTS^{\cdot+}$ and **(f)** the overall reaction rate in the presence of 1.0 µM Fe(III)PPIX is plotted as a function of increasing ABTS concentration in. Data points omitted for clarity.

The data recorded during the second stage of the ABTS concentration study is shown in Figure 4.15. Here again, similar trends are observed compared to the reaction conducted in aqueous solution. As with the above

studies, minimal variation in the maximum yield of $ABTS^{\cdot+}$ production is seen when compared to aqueous solution (e). There is, however, a substantial difference in the reaction rate and the stability of the radical between the two environments. As was seen in aqueous solution, at a given ABTS and Fe(III)PPIX concentration, the maximum yield of $ABTS^{\cdot+}$ is constant in the H_2O_2 concentration range discussed, however, the rate at which this yield is achieved varies as a function of H_2O_2 concentration (f). In comparison to what was observed in aqueous solution, the signal starts to decay at a later time, providing further proof for improved stability in aqueous SDS. An enlargement of the initial five minutes of the reaction is shown in the Figure 4.16. Interestingly, in aqueous SDS solution, there is evidence of a lag phase in the initial 30 seconds of the reaction which is most evident at higher concentrations of ABTS. This is followed by an exponential phase. The lag phase was absent when the experiment was conducted in aqueous solution.

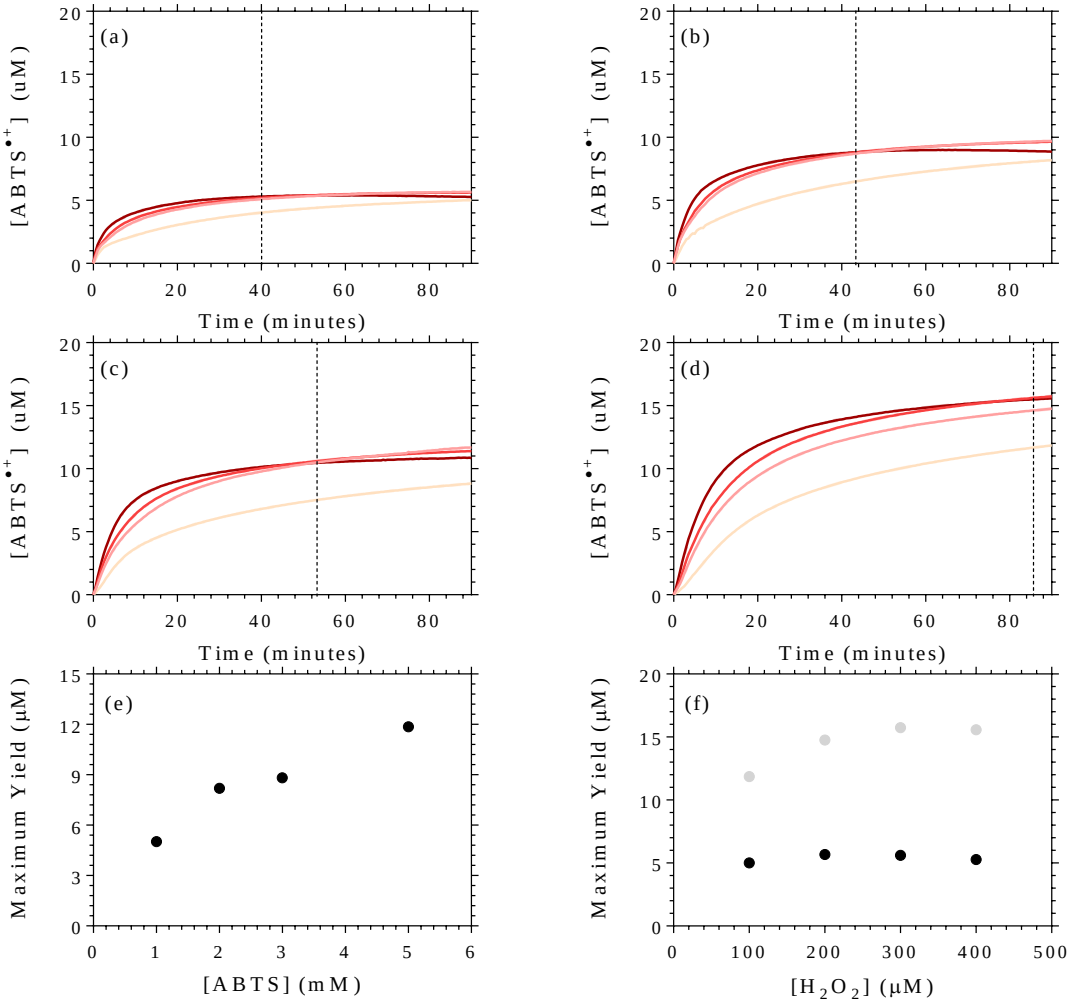

Figure 4.15 The effect of varying ABTS concentration on the oxidation of ABTS in aqueous SDS solution. The conditions are 100.0 µM H_2O_2 in the presence of **(a)** 1.0, **(b)** 2.0, **(c)** 3.0 and **(d)** 5.0 mM ABTS and H_2O_2 concentrations of 100.0 (-), 200.0 (-), 300.0 (-) and 400.0 (-) µM. The maximum yield of $ABTS^{\cdot+}$ obtained in the presence of 1.0 µM Fe(III)PPIX and **(e)** 100.0 µM H_2O_2 plotted as a function of increasing [ABTS] and **(f)** plotted as a function of increasing $[H_2O_2]$ in the presence of 1.0 (black) and 5.0 mM (grey) ABTS. Data points omitted for clarity.

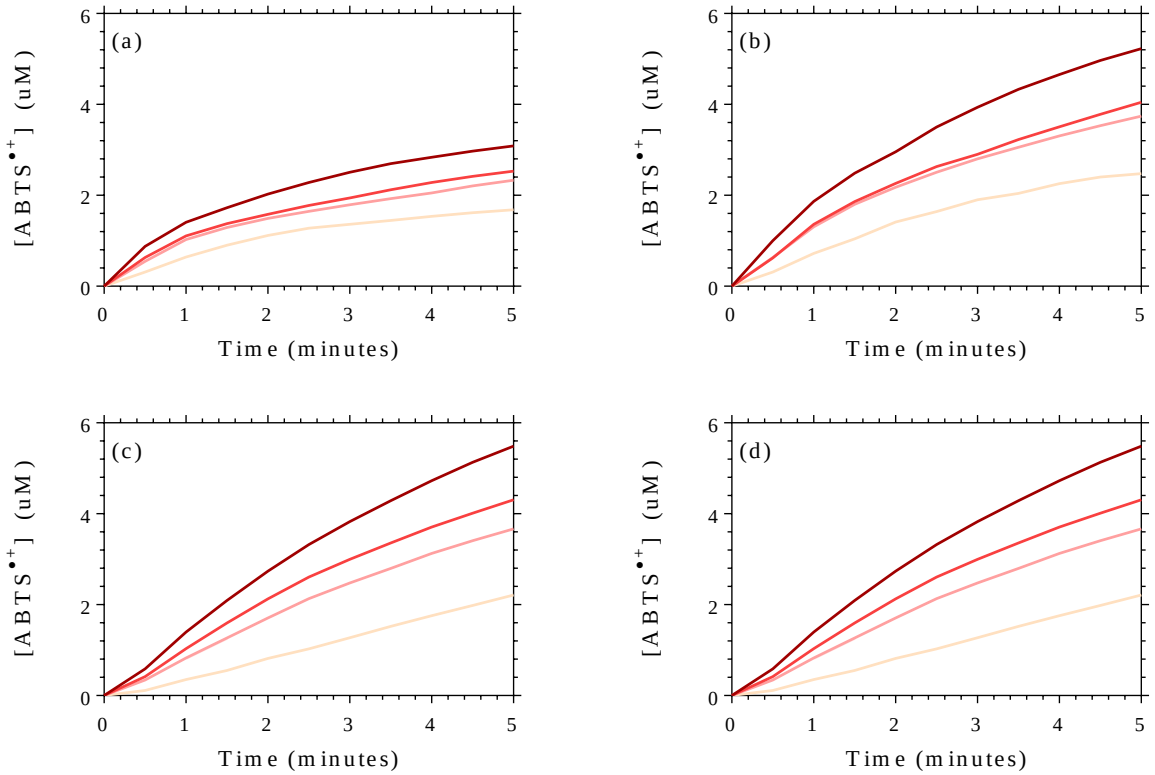

Figure 4.16 The effect of ABTS concentration on the initial five minutes of ABTS oxidation in aqueous solution. The conditions are 1.0 µM Fe(III)PPIX in the presence of **(a)** 1.0, **(b)** 2.0, **(c)** 3.0 and **(d)** 5.0 mM ABTS in the presence of 100.0 (-), 200.0 (-), 300.0 (-) and 400.0 (-) µM H_2O_2. Data points omitted for clarity.

4.3.4 The Kinetic Model

Understanding the kinetics of ABTS oxidation has been a matter of great interest in the past, however, to our knowledge, there is only one study which has investigated the kinetics of ABTS oxidation by Fe(III)PPIX.[134] In this study, the authors obtained rate constants by extrapolating the initial linear portion of the reaction, thereby determining the initial rate of the reaction. Attempts were made to determine rate constants in this manner, however, since this method disregards the data succeeding the first five minutes of the reaction, inconsistencies were obtained. It was therefore decided to determine the reaction rate in a manner that takes into account the full reaction time so as not to omit any important data. The first step in this process was thus to propose a model for ABTS oxidation by Fe(III)PPIX. The general reaction scheme for the oxidation of ABTS is shown in Scheme 4.1. This scheme has been proposed by a number of authors and is the generally accepted cycle for the oxidation of ABTS by an iron porphyrin and H_2O_2.[130,134,149] The first step of this cycle involves the reaction of Fe(III)PPIX and H_2O_2 to form an iron-peroxo species (I in Scheme 4.1), followed by the formation of the catalytically active iron species (II in Scheme 4.1). This then undergoes reduction to

form an oxo iron (IV) species (III in Scheme 4.1) while simultaneously oxidizing one molecule of ABTS. Finally, Compound III is reduced back to Fe(III)PPIX when a second molecule of ABTS is oxidised.

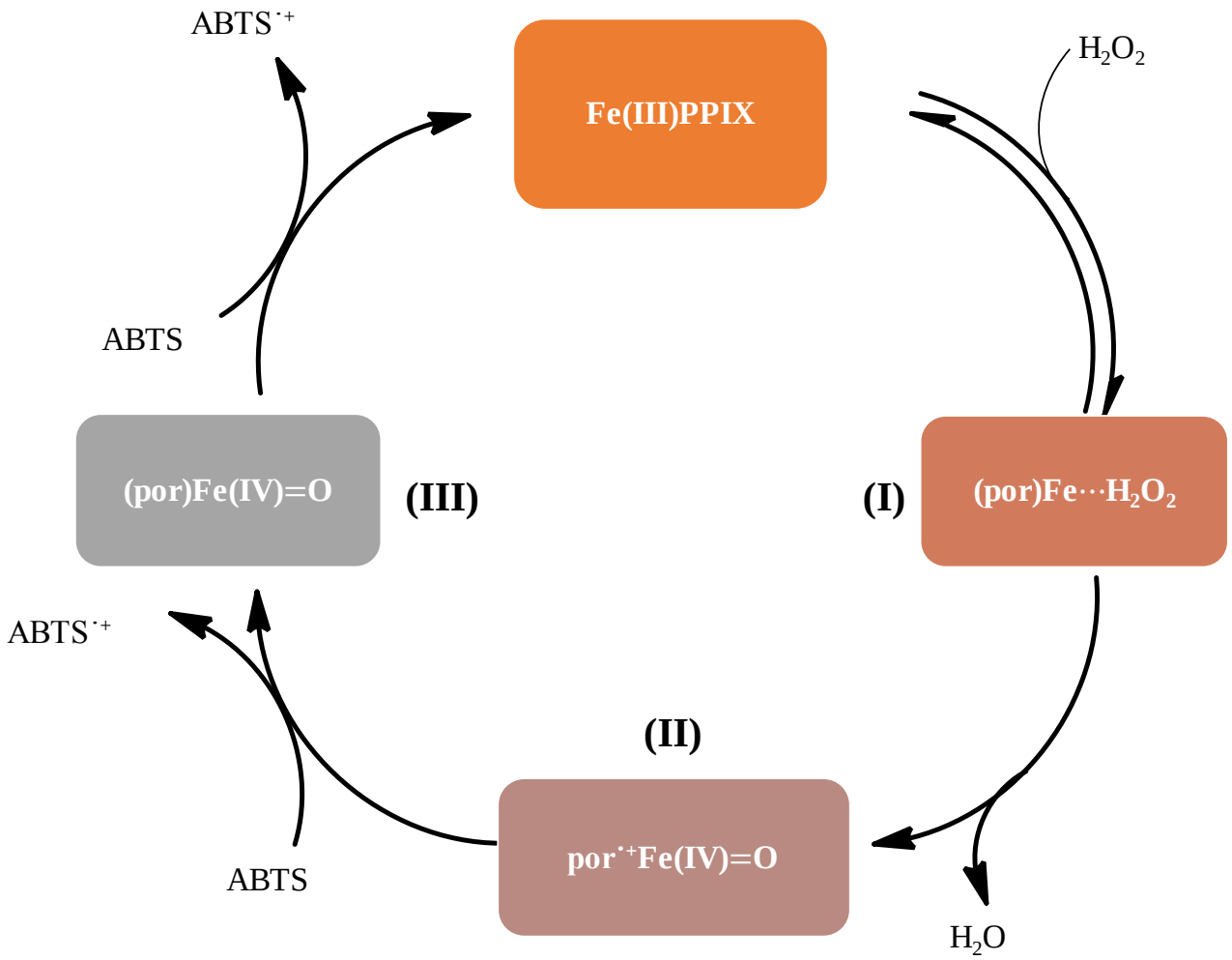

Scheme 4.1 The simplified catalytic cycle for the oxidation of ABTS in which Fe(III)PPIX reacts with H_2O_2 to form a Fe(III)PPIX-peroxo species **(I)**, which rapidly converts to the catalytically active Fe(IV) porphyrin radical cation **(II)**. Compound (**II**) can then oxidise one molecule of ABTS to produce $ABTS^{\cdot+}$ and an oxo iron (IV) porphyrin species **(III)** which in turn can oxidise a second molecule of ABTS and regenerate Fe(III)PPIX.[130,134]

The cycle of ABTS oxidation is, however, much more complex and has been proposed to consist of numerous side reactions that are not shown in Scheme 4.1. It is well known from literature, for example, that Fe(III)PPIX dimerises in solution (see Section 1.4.3.1).[89] Since it is proposed that monomeric Fe(III)PPIX ($Fe(III)PPIX_M$) is the species that takes part in the catalytic cycle, it is necessary to also know the extent of dimerisation that occurs under experimental conditions (given by k_1 and k_2 in Scheme 4.2 (a)). Furthermore, as alluded to in equation 4.4, at low ABTS concentrations, $ABTS^{\cdot+}$ disproportionates into ABTS and the ABTS dication, $ABTS^{++}$. This would result in a reduction in the yield of $ABTS^{\cdot+}$ and therefore needs to be taken into account when considering the kinetic model (see k_4 and k_5 in Scheme 4.2 (b)). Authors have also suggested that an interaction occurs between Fe(III)PPIX and ABTS to form an ABTS···Fe(III)PPIX

complex.[129,134,149] This can then proceed to react with H_2O_2 to form an ABTS···Fe(III)PPIX···H_2O_2 complex. Following the release of water, the resulting ABTS···Fe(III)PPIX radical cation can supposedly oxidise an additional molecule of ABTS (Scheme 4.2). It is unclear at this time whether these species occur as complex intermediates or transition state complexes.

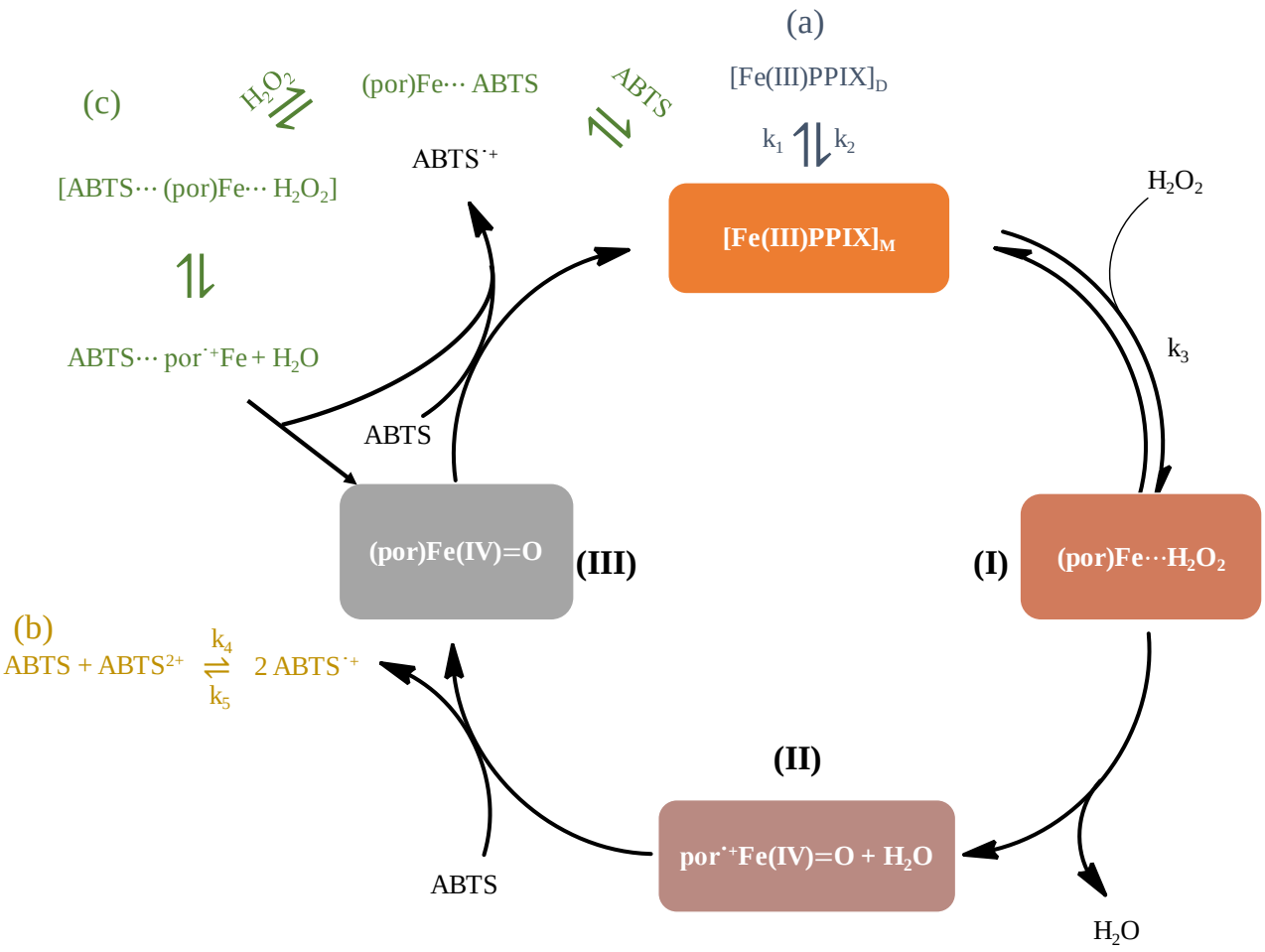

Scheme 4.2 The proposed catalytic cycle for the oxidation of ABTS. Additional reactions include **(a)** the dimerisation of monomeric Fe(III)PPIX ($Fe(III)PPIX_M$ to $Fe(III)PPIX_D$); **(b)** disproportionation of $ABTS^{\cdot+}$ to ABTS and $ABTS^{++}$ and **(c)** the suggested formation of an ABTS···Fe(III)PPIX radical cation complex following a reaction between Fe(III)PPIX, ABTS and H_2O_2.[134,149]

Since the only literature available regarding the kinetics of ABTS oxidation by Fe(III)PPIX is that of Ribeiro *et al.*,[134] it was decided to make an attempt at proposing a kinetic model and determining rate constants for this reaction in aqueous solution. Two processes described in the above schematic were investigated independently and, eventually optimised in MATLAB,[152] to obtain a preliminary catalytic cycle for the oxidation of ABTS by Fe(III)PPIX and H_2O_2 in aqueous solution. These are discussed in the subsequent sections.

4.3.4.1 The Reaction Between Fe(III)PPIX and H_2O_2 in Aqueous Solution

The reaction between Fe(III)PPIX and H_2O_2 has previously been discussed in the text as being of significant importance in the ABTS oxidation reaction. This reaction is, however, complicated by the dimerisation of Fe(III)PPIX. The reaction describing the dimerisation of Fe(III)PPIX is shown in Equation 4.8, where Fe(III)PPIX is abbreviated as Fe(III)por$_M$ for the monomeric form and Fe(III)por$_D$ for the dimeric form. The rate constants k_1 and k_2 govern forward and reverse reactions, respectively. The fitting of the model was only successful when this process was taken into account. The rate equation for the reaction between monomeric Fe(III)PPIX and H_2O_2 is shown in Equation 4.9, with rate constant k_3.

$$\mathrm{Fe(III)por_M + Fe(III)por_M \underset{k_2}{\overset{k_1}{\rightleftharpoons}} Fe(III)por_D} \tag{4.8}$$

$$\mathrm{Fe(III)por_M + H_2O_2 \xrightarrow{k_3} O{=}Fe(IV)por} \tag{4.9}$$

The reactions described in Equations 4.8 and 4.9 were then used to derive the multi-step reaction rate model according to the following objective function:

$$\sum_{t=0}^{n} (A_{exp,ti} - A_{theo,ti})^2$$

The change in concentration of each species was considered as a function of time. These are shown in equations 4.10-4.13, for Fe(III)por$_M$, Fe(III)por$_D$, H_2O_2 and O=Fe(IV)por, respectively.

$$\frac{d[\mathrm{Fe(III)por_M}]}{dt} = 2k_2\,[\mathrm{Fe(III)por_D}] - 2k_1\,[\mathrm{Fe(III)por_M}]^2 - k_3[\mathrm{Fe(III)por_M}][\mathrm{H_2O_2}] \tag{4.10}$$

$$\frac{d[\mathrm{Fe(III)por_D}]}{dt} = k_1\,[\mathrm{Fe(III)por_M}][\mathrm{Fe(III)por_M}] - k_2[\mathrm{Fe(III)por_D}] \tag{4.11}$$

$$\frac{d[\mathrm{H_2O_2}]}{dt} = -k_3[\mathrm{Fe(III)por_M}][\mathrm{H_2O_2}] \tag{4.12}$$

$$\frac{d[\mathrm{O{=}Fe(IV)por}]}{dt} = k_3[\mathrm{Fe(III)por_M}][\mathrm{H_2O_2}] \tag{4.13}$$

The multi-step reaction rate model was then optimised in Matlab using Equations 4.10-4.13 and the obtained non-linear least-squares fit is shown in Figure 4.17. From this, the extinction coefficients for each species, as well as the rate constants describing the reactions, could be determined and are listed in Table 4.7 and 4.8, respectively.

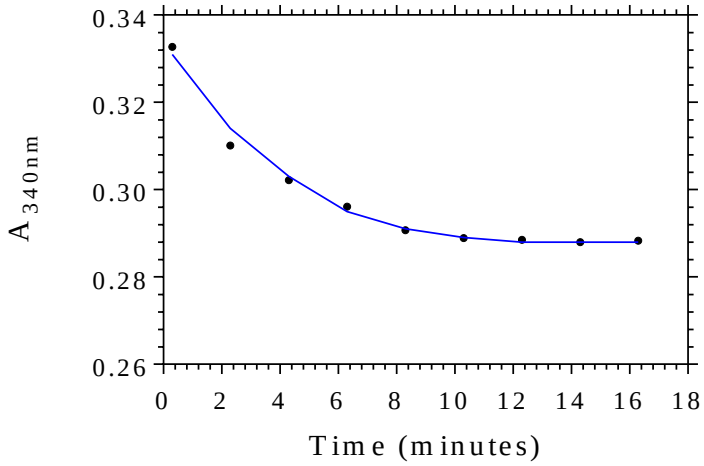

Figure 4.17 The reaction between Fe(III)PPIX and H_2O_2. The experimental data (black), fitted to a non-linear least-squares function (blue) at 340nm.

Table 4.7 Molar extinction coefficients (340 nm) determined following the optimisation of the multi-step reaction rate model for the reaction between Fe(III)PPIX and H_2O_2 using Equations 4.10-4.13.

Species	Extinction Coefficient ($M^{-1}cm^{-1}$)
$Fe(III)PPIX_M$	50491 ± 2525
$Fe(III)PPIX_D$	71253 ± 3563
H_2O_2	0 ± 0.1
$H_2O_2\cdots Fe(IV)PPIX_M$†	32008 ± 1600

†$H_2O_2\cdots$Fe(IV)PPIX is a general term that refers to an iron-peroxo species.

Table 4.8 Rate constants determined following the optimisation of the multi-step reaction rate model for the reaction between Fe(III)PPIX and H_2O_2 using Equations 4.10-4.13.

Rate Constant	k
k_1	$(6.60 \pm 0.33) \times 10^6$
k_2	1 ± 0.1
k_3	35037 ± 1752

The logarithm of the dimerisation constant (log K = 6.82, pH 7.5), where K_1 (k_1 /k_2), is in excellent agreement with that obtained by Marques and co-workers (6.82).[88] Using the calculated extinction coefficients listed in Table 4.7, the concentration of each Fe(III)PPIX species as a function of time could be determined. These results are plotted in Figure 4.18. From the data, it is evident that the dominant species at the beginning of the reaction is dimeric Fe(III)PPIX, most likely the π-π dimer.[89] When the available monomer amount is used up, more dimer monomerises, until everything is converted to the oxidised form. Furthermore, the reaction between Fe(III)PPIX and H_2O_2 is shown to be fast with saturation being reached within the first 10 minutes. This is in agreement with the conclusions reached in section 4.3.1, which showed negligible variation in the absorbance spectrum following a period of 10 minutes. It is, however, unclear as to which oxidized Fe(III)PPIX species is being formed. Additional experiments would be required to confirm whether the radical cation or just the cation Fe(IV) oxo species is formed under these conditions.

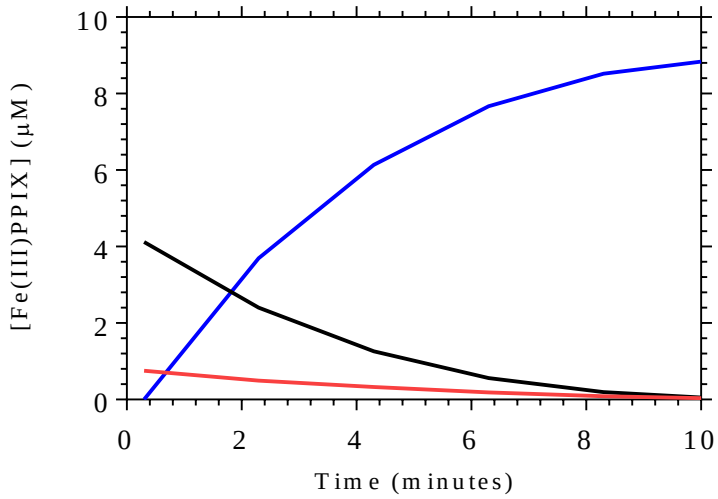

Figure 4.18 The concentration of monomeric (-), dimeric (-) and oxidized (-) Fe(III)PPIX present in aqueous solution for the reaction described in Equation 4.8 and 4.9 at a wavelength of 340nm.

4.3.4.2 The ABTS Disproportionation Reaction

The second reaction that was investigated independently was that of the disproportionation of $ABTS^{\cdot+}$. The reaction equation is shown in Equation 4.14. For experimental simplicity, the reverse of this reaction was considered (Equation 4.14a). Using the latter equation, the multi-step reaction rate model for the disproportionation of ABTS could be derived and the rate models for the individual species are shown in Equations 4.15-4.17.

$$2ABTS^{\cdot+} \underset{k_4}{\overset{k_5}{\rightleftharpoons}} ABTS + ABTS^{++} \tag{4.14}$$

$$ABTS + ABTS^{++} \underset{k_5}{\overset{k_4}{\rightleftharpoons}} 2ABTS^{\cdot+} \tag{4.14a}$$

$$\frac{d[ABTS]}{dt} = k_5\,[ABTS^{\cdot+}]^2 - k_4\,[ABTS][ABTS^{++}] \tag{4.15}$$

$$\frac{d[ABTS^{++}]}{dt} = k_5\,[ABTS^{\cdot+}]^2 - k_4\,[ABTS][ABTS^{++}] \tag{4.16}$$

$$\frac{d[ABTS^{\cdot+}]}{dt} = 2k_4\,[ABTS][ABTS^{++}] - 2k_5[ABTS^{\cdot+}]^2 \tag{4.17}$$

This experiment involved systematically varying the concentration of $ABTS^{++}$ while keeping the concentration of ABTS constant. The ABTS dication has previously been reported to have an absorbance maximum at 520 nm and therefore this wavelength was used to monitor the decay of this species to form the radical cation.[153] As expected, higher concentrations of $ABTS^{++}$ induced a higher absorbance at 520 nm, however, in each case the reaction reaches equilibrium within a period of 30 minutes.

The multi-step reaction rate model (Equations 4.14-4.17) was then optimised in Matlab to afford the extinction coefficients for $ABTS^{++}$, ABTS and $ABTS^{\cdot+}$ as well as the rate constants for the reaction and the obtained non-linear least-squares fits are shown in Figure 4.19. These are listed in Table 4.9 and 4.10, respectively. The extinction coefficient obtained for $ABTS^{++}$ is in good agreement with that obtained in a previous study (35986 vs 36000 $M^{-1}cm^{-1}$), however, it does require further optimisation in Matlab.[153] An analysis of the rate constants obtained for the reaction described in Equation 4.14 indicates that the disproportionation of $ABTS^{\cdot+}$ is approximately five times more favourable than forward reaction and therefore it is necessary to take this into account when considering the full reaction model.

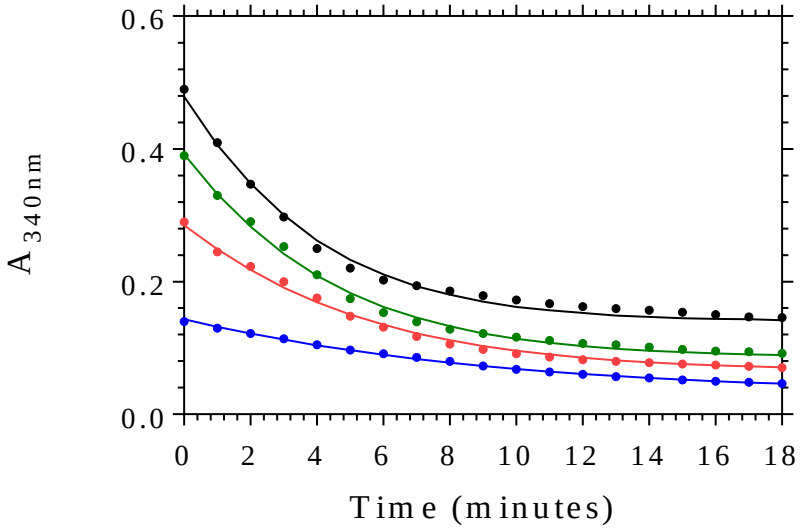

Figure 4.19 The disproportionation of $ABTS^{\cdot+}$. The experimental data (circles) fitted with a non-linear least-squares fit at 340nm for the reaction between ABTS and $ABTS^{++}$ for $ABTS^{++}$ concentrations of 0.1 (-), 0.2(-), 0.4 (-) and 0.5 (-) mM.

Table 4.9 The extinction coefficients (520 nm) calculated for $ABTS^{++}$, ABTS and $ABTS^{+}$ for the reaction shown in Equation 4.14a.

[$ABTS^{++}$] (mM)	**$ABTS^{++}$ ($M^{-1}cm^{-1}$)**	**ABTS ($M^{-1}cm^{-1}$)**	**$ABTS^{\cdot+}$ ($M^{-1}cm^{-1}$)**
0.1	36875	0	937
0.2	36646	0	1120
0.4	36163	0	1281
0.5	35158	0	1558
Average	36211	0	1224
Std. Error	762	0	263

Table 4.10 The rates of the forward and reverse reactions for the reaction shown in Equation 4.14a at each relevant $ABTS^{++}$ concentration.

[$ABTS^{++}$] (mM)	**k_4**	**k_5**
0.1	298.2	1223.1
0.2	216.7	1536.8
0.4	261.1	913
0.5	230.6	1222.9
Average	251.7	1224.0
Std. Error	36.2	254.7

4.3.4.3 Proposed Reaction Model

Following the investigation into the above two reactions, attempts were made to determine a suitable reaction model and, furthermore, a rate constant for the oxidation of ABTS by Fe(III)PPIX and H_2O_2 in aqueous solution. The first proposed model is shown in Equations 4.18-4.23. The first reaction (4.18) was that of Fe(III)PPIX monomer dimerisation. The dimerisation is an important factor when considering Fe(III)PPIX in aqueous solution. Furthermore, authors have suggested that it is the Fe(III)PPIX monomer that interacts with H_2O_2 (4.19) and not the dimer. During this reaction, the catalytically active iron(IV) porphyrin radical species is generated which reacts with ABTS (4.20) to produce one molecule of $ABTS^{\cdot+}$. During this process, it is proposed that the porphyrin cation is reduced back to Fe(IV). Once $ABTS^{\cdot+}$ has been produced, it may disproportionate into ABTS and $ABTS^{++}$ (4.21). Equation 4.22 shows the interaction between the Fe(IV) porphyrin and ABTS to generate a second molecule of ABTS and regenerate the porphyrin. As was suggested in Scheme 4.2, the oxo Fe(IV) porphyrin could further react with H_2O_2 to produce degradation products (4.23).

$$\mathrm{Fe(III)por_M + Fe(III)por_M \underset{k_2}{\overset{k_1}{\rightleftharpoons}} Fe(III)por_D} \tag{4.18}$$

$$\mathrm{Fe(III)por_M + H_2O_2 \xrightarrow{k_3} O{=}Fe(IV)por^{\cdot+} + H_2O} \tag{4.19}$$

$$\mathrm{O{=}Fe(IV)por^{\cdot+} + ABTS \xrightarrow{k_4} ABTS^{\cdot+} + Fe(IV)por} \tag{4.20}$$

$$\mathrm{2ABTS^{\cdot+} \underset{k_6}{\overset{k_5}{\rightleftharpoons}} ABTS^{++} + ABTS} \tag{4.21}$$

$$\mathrm{Fe(IV)por + ABTS \xrightarrow{k_7} ABTS^{\cdot+} + Fe(III)por_M} \quad (4.22)$$

$$\mathrm{O{=}Fe(IV)por + H_2O_2 \xrightarrow{k_8} degradative\ products} \quad (4.23)$$

The reactions described in Equations 4.18 to 4.23 were then used to derive the multi-step reaction rate model, where the change in concentration of each species is considered as a function of time. These are shown in Equations 4.24-4.32, for each component described in the above reactions. The rate constants obtained for the dimerisation of Fe(III)PPIX (Table 4.8), the reaction between Fe(III)PPIX and H_2O_2 (Table 4.8) as well as the $ABTS^{\cdot+}$ disproportionation reaction (Table 4.10) were fixed at the values listed in the relevant tables. In this manner, the reaction is simplified and therefore the program need only to optimise the rate constants for the generation of $ABTS^{\cdot+}$ (k_4, k_7) as well as that of the porphyrin degradation (k_8).

$$\begin{aligned}\mathrm{d[Fe(III)por_M]/dt} &= \mathrm{2k_2[Fe(III)por_D] - 2k_1[Fe(III)por_M]^2 - k_3[Fe(III)por_M][H_2O_2]} \\ &+ \mathrm{k_7[ABTS^{\cdot+}][Fe(III)por_M]}\end{aligned} \quad (4.24)$$

$$\begin{aligned}\mathrm{d[Fe(III)por_M]/dt} &= \mathrm{2(1)[Fe(III)por_D] - 2(6.61\times 10^6)[Fe(III)por_M]^2} \\ &- \mathrm{35000[Fe(III)por_M][H_2O_2] + k_7[ABTS^{\cdot+}][Fe(III)por_M]}\end{aligned} \quad (4.24a)$$

$$\mathrm{d[Fe(III)por_D]/dt = k_1[Fe(III)por_M]^2 - k_2[Fe(III)por_D]} \quad (4.25)$$

$$\mathrm{d[Fe(III)por_D]/dt = (6.61\times 10^6)[Fe(III)por_M]^2 - (1)[Fe(III)por_D]} \quad (4.25a)$$

$$\mathrm{d[H_2O_2]/dt = -k_3[Fe(III)por_M][H_2O_2] - k_8[O{=}Fe(IV)por][H_2O_2]} \quad (4.26)$$

$$\mathrm{d[H_2O_2]/dt = -35000[Fe(III)por_M][H_2O_2] - k_8[O{=}Fe(IV)por][H_2O_2]} \quad (4.26a)$$

$$\frac{d[O=Fe(IV)por]}{dt} = k_3[Fe(III)por_M][H_2O_2] - k_4[O=Fe(IV)por][ABTS] - k_8[O=Fe(IV)por][H_2O_2] \quad (4.27)$$

$$\frac{d[O=Fe(IV)por]}{dt} = 35000[Fe(III)por_M][H_2O_2] - k_4[O=Fe(IV)por][ABTS] - k_8[O=Fe(IV)por][H_2O_2] \quad (4.27a)$$

$$\frac{d[ABTS]}{dt} = k_5[ABTS^{\cdot+}]^2 - k_4[O=Fe(IV)por][ABTS] - k_6[ABTS^{++}][ABTS] - k_7[Fe(IV)por][ABTS] \quad (4.28)$$

$$\frac{d[ABTS]}{dt} = (1300)[ABTS^{\cdot+}]^2 - k_4[O=Fe(IV)por][ABTS] + (1300)[ABTS^{\cdot+}]^2 - (340)[ABTS^{++}][ABTS] - k_7[Fe(IV)por][ABTS] \quad (4.28a)$$

$$\frac{d[ABTS^{\cdot+}]}{dt} = k_4[O=Fe(IV)por][ABTS] - 2k_5[ABTS^{\cdot+}]^2 + 2k_6[ABTS^{++}][ABTS] + k_7[Fe(IV)por][ABTS] \quad (4.29)$$

$$\frac{d[ABTS^{\cdot+}]}{dt} = k_4[O=Fe(IV)por][ABTS] - 2(1300)[ABTS^{\cdot+}]^2 + 2(340)[ABTS^{++}][ABTS] + k_7[Fe(IV)por][ABTS] \quad (4.29a)$$

$$d[Fe(IV)por]/dt = k_4[O=Fe(IV)por][ABTS] - k_7[Fe(IV)por][ABTS] \quad (4.30)$$

$$d\frac{[ABTS^{++}]}{dt} = k_5[ABTS^{\cdot+}]^2 - k_6[ABTS^{++}][ABTS] \quad (4.31)$$

$$\mathrm{d}\frac{[\mathrm{ABTS}^{++}]}{\mathrm{dt}} = 1300[\mathrm{ABTS}^{\cdot+}]^2 - 340[\mathrm{ABTS}^{++}][\mathrm{ABTS}] \tag{4.31a}$$

$$\mathrm{d[deg]/dt} = k_8[\mathrm{O{=}Fe(IV)por}][H_2O_2] \tag{4.32}$$

This set of equations are stiff ordinary differential equations (ode) and, therefore, the MATLAB ordinary differential equation solvers could not solve the kinetic model. It was therefore attempted to model a more simplified reaction model, which is shown in Equations 4.33-4.36. In this model, only one molecule of $ABTS^{\cdot+}$ is formed before the porphyrin is regenerated. Furthermore, the additional interaction between the oxo Fe(IV) porphyrin radical species and H_2O_2 has been omitted.

$$\mathrm{Fe(III)por_M} + \mathrm{Fe(III)por_M} \underset{k_2}{\overset{k_1}{\rightleftharpoons}} \mathrm{Fe(III)por_D} \tag{4.33}$$

$$\mathrm{Fe(III)por_M} + H_2O_2 \xrightarrow{k_3} \mathrm{O{=}Fe(IV)por} \tag{4.34}$$

$$\mathrm{O{=}Fe(IV)por} + \mathrm{ABTS} \xrightarrow{k_4} \mathrm{ABTS}^{\cdot+} + \mathrm{Fe(III)por_M} \tag{4.35}$$

$$2\mathrm{ABTS}^{\cdot+} \underset{k_6}{\overset{k_5}{\rightleftharpoons}} \mathrm{ABTS}^{++} + \mathrm{ABTS} \tag{4.36}$$

The reactions described in Equations 4.33 to 4.36 were once again used to derive the multi-step reaction rate model, where the change in concentration of each species is considered as a function of time. These are shown in Equations 4.37-4.43, for each component described in the above reactions.

$$\begin{aligned}\mathrm{d[Fe(III)por_M]/dt} &= 2k_2[\mathrm{Fe(III)por_D}] - 2k_1[\mathrm{Fe(III)por_M}]^2 - k_3[\mathrm{Fe(III)por_M}][H_2O_2] \\ &+ k_4[\mathrm{ABTS}][\mathrm{O{=}Fe(IV)por}]\end{aligned} \tag{4.37}$$

$$\begin{aligned} d[Fe(III)por_M]/dt \\ = \ 2(1)[Fe(III)por_D] \ - \ 2(6.61 \times \ 10^6)[Fe(III)por_M]^2 \\ - \ 35000[Fe(III)por_M][H_2O_2] \ + \ k_4[ABTS][O = Fe(IV)por] \end{aligned} \quad (4.37a)$$

$$d[Fe(III)por_D]/dt \ = \ k_1[Fe(III)por_M]^2 \ - \ k_2[Fe(III)por_D] \quad (4.38)$$

$$d[Fe(III)por_D]/dt \ = \ (6.61 \times 10^6)[Fe(III)por_M]^2 - (1)[Fe(III)por_D] \quad (4.38a)$$

$$d[H_2O_2]/dt \ = \ - k_3[Fe(III)por_M][H_2O_2] \quad (4.39)$$

$$d[H_2O_2]/dt = \ - 35000[Fe(III)por_M][H_2O_2] \quad (4.39a)$$

$$\frac{d[O{=}Fe(IV)por]}{dt} \ = \ k_3[Fe(III)por_M][H_2O_2] - \ k_4[O{=}Fe(IV)por][ABTS] \quad (4.40)$$

$$\frac{d[O{=}Fe(IV)por]}{dt} \ = \ 35000[Fe(III)por_M][H_2O_2] \ - k_4[O{=}Fe(IV)por][ABTS] \quad (4.40a)$$

$$\frac{d[ABTS]}{dt} \ = \ k_5[ABTS^{\cdot+}]^2 - \ k_4[O{=}Fe(IV)por][ABTS] \ - \ k_6[ABTS^{++}][ABTS] \quad (4.41)$$

$$\begin{aligned} \frac{d[ABTS]}{dt} \ = \ (1300)[ABTS^{\cdot+}]^2 - \ k_4[O{=}Fe(IV)por][ABTS] \ + (1300)[ABTS^{\cdot+}]^2 \\ - (340)[ABTS^{++}][ABTS] \end{aligned} \quad (4.41a)$$

$$\frac{d[ABTS^{\cdot+}]}{dt} \ = \ k_4[O{=}Fe(IV)por][ABTS] \ - 2\,k_5[ABTS^{\cdot+}]^2 \ + \ 2k_6[ABTS^{++}][ABTS] \quad (4.42)$$

$$\frac{d[ABTS^{\cdot+}]}{dt} = k_4[O{=}Fe(IV)por][ABTS] - 2(1300)[ABTS^{\cdot+}]^2 + 2(340)[ABTS^{++}][ABTS] \quad (4.42a)$$

$$d\frac{[ABTS^{++}]}{dt} = k_5[ABTS^{\cdot+}]^2 - k_6[ABTS^{++}][ABTS] \quad (4.43)$$

$$d\frac{[ABTS^{++}]}{dt} = 1300[ABTS^{\cdot+}]^2 - 340[ABTS^{++}][ABTS] \quad (4.43a)$$

The above-mentioned reaction equations were simulated in Matlab, however, the fits were once again unsuccessful. An example of the experimental data fitted with a non-linear least squares function can be seen in Figure 4.20. Significant deviations from the proposed rate model can be seen at all points of the curve. In both data sets, the initial rate of the reaction is faster than what is proposed using the experimental model. Furthermore, at both H_2O_2 concentrations, the final yield after 60 minutes is less than what is proposed using the kinetic model. The rate constant (k_4) for the generation of $ABTS^{\cdot+}$ obtained through simulation of the kinetic model for the two data sets is listed in Table 4.11. The results show a great variation in reaction rate between the two data sets. Furthermore, the extinction coefficient for $ABTS^{\cdot+}$ is approximately four times less than what was determined experimentally.

The large discrepancies in the experimental data compared to that of the proposed kinetic model highlights the complexity of the ABTS oxidation reaction. Since both models failed to produce data consistent with that determined experimentally, it can be assumed that the proposed model is incomplete and would require more experimental work as well as computational work. This was, however, beyond the scope of this project and should therefore be considered as future work.

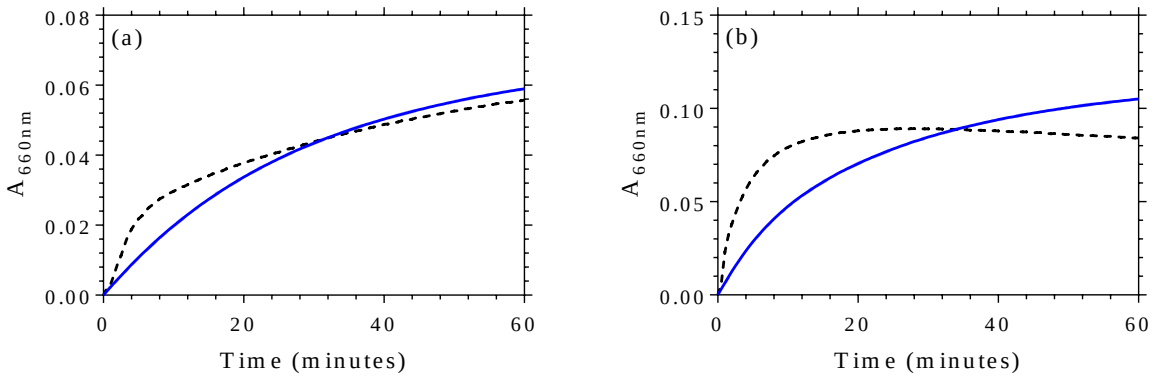

Figure 4.20 The rate model. The experimental trace (black) of absorbance as a function of time in the presence of 1.0 mM ABTS, 1 µM Fe(III)PPIX and H_2O_2 concentrations of **(a)** 25.0 and **(b)** 200.0 µM. The theoretical absorbance calculated according to the proposed rate model is shown in blue.

Table 4.11 The rate constant obtained for the oxidation of ABTS by Fe(III)PPIX and H_2O_2 (Equation 4.35) in aqueous solution together with the extinction coefficient of $ABTS^{\cdot+}$ determined, following simulation of the kinetic model.

$[H_2O_2]$ (µM)	**k_4**	**ε ($M^{-1}cm^{-1}$)**
25	2.95×10^6	3248
200	1.39×10^7	1136

4.4 Discussion

Investigations into the toxic nature of Fe(III)PPIX have proven to be vital owing to its involvement in a number of illnesses including malaria and sickle cell disease.[11] One of the mechanisms through which Fe(III)PPIX is thought to exert its toxicity is thought to be through its ability to react with H_2O_2 in a manner similar to that of a class of enzymes known as peroxidases. The main aim of this chapter was to investigate the peroxidase activity of Fe(III)PPIX in aqueous solution and subsequently compare this to the activity of Fe(III)PPIX in an environment that has a closer resemblance to one in which the Fe(III)PPIX detoxification product, haemozoin, is formed in the malaria parasite. As previously discussed in Chapter 3, the proposed site of antimalarial drug action has shifted to a non-aqueous environment, therefore, understanding the nature of Fe(III)PPIX under these conditions is an essential step in probing the mechanism of action of these antimalarial drugs. In this study, Fe(III)PPIX was found to successfully catalyse the oxidation of ABTS by H_2O_2. The mechanism by which Fe(III)PPIX catalyses this reaction, however, is not fully understood. Previous studies have proposed that the first step in the mechanism involves the association of Fe(III)PPIX with H_2O_2, although details of the structure of this intermediate species are still unknown (Equation 4.44).[128,130,134]

$$\mathrm{Fe(III)PPIX} + \mathrm{H_2O_2} \rightleftharpoons \mathrm{H_2O_2 \cdots Fe(III)PPIX} \tag{4.44}$$

Following Fe(III)PPIX association, the next step in the catalytic process is thought to involve the cleavage of a peroxide bond.[154] This process can proceed either homolytically or heterolytically and the two mechanisms can be differentiated by the end products obtained. During homolytic cleavage, hydroxide radicals and an oxo-iron(IV)-porphyrin complex are produced (Equation 4.45), while heterolytic cleavage yields water and an oxo-iron(IV)-porphyrin radical cation species (Equation 4.46). Subsequently, degradation of the iron porphyrin commences.

$$\mathrm{H_2O_2 \cdots Fe(III)PPIX} \rightarrow \mathrm{OFe(IV)(por)} + {}^{\cdot}\mathrm{OH} + \mathrm{H^+} \tag{4.45}$$

$$\mathrm{H_2O_2 \cdots Fe(III)PPIX} \rightarrow \mathrm{OFe(IV)(por^{+\cdot})} + \mathrm{H_2O} \tag{4.46}$$

A more recent paper has investigated the mechanism of the reaction between an iron(III) octa-anionic porphyrin complex and H_2O_2 using ABTS.[130] In this study, the spectrum of the porphyrin was monitored in the presence of H_2O_2 over a period of 30 seconds at 4 °C. The authors found that when the pH was less than 9, the observed decay in the Soret band could be fitted with a three-phase function. This was attributed to the three steps of the reaction, namely the formation of the iron-oxo complex, the cleavage of the iron-peroxo bond and, finally, decay of the catalytic species. Additional independent studies on the interaction between

haem octapeptide microperoxidase-8 (MP-8) have reported similar observations.[134,155,156] In the current work, the shifts in the absorbance spectrum of Fe(III)PPIX in the presence of H_2O_2 after a period of 30 minutes provided evidence of the reaction between Fe(III)PPIX and H_2O_2. In our case, however, the data were fitted with a two-phase function. The study by van Eldik and co-workers suggests that the formation of the porphyrin complex with H_2O_2 occurs within the first 30 seconds when the reaction is conducted at 4 °C.[130] For this reason, the assumption was made, that under the experimental conditions presented here, the formation of the oxo-iron complex is too fast to be monitored. Consequently, the first observed phase of the reaction is attributed to the formation and cleavage of the oxo-iron complex, while the second phase most likely represents the decay of the catalytically active oxo-iron(IV)-porphyrin radical cation species. In future work, stopped-flow kinetics may be used to further investigate this avenue, however, due to instrument failure this technique was not available at the time.

Both the oxo-iron(IV)-porphyrin complex and the oxo-iron(IV)-porphyrin radical cation species are able to react with ABTS to form the $ABTS^{\cdot+}$. A number of studies have been carried out to determine the mechanism through which this process occurs. A study by Wolfenden and Willson showed that in the presence of hydroxide radicals, the oxidation of ABTS to $ABTS^{\cdot+}$ occurs in a yield of 58 %.[154] In the presence of excess bromine, however, the hydroxide radicals will generate bromine radicals which carry out the oxidation of ABTS in a yield of 100%.[147] Ribeiro *et al.* performed an experiment on the basis of this observation in which they introduced excess bromine into their system and measured the yield of $ABTS^{\cdot+}$ production.[134] They found that there was no increase in the yield of $ABTS^{\cdot+}$ produced, implying an absence of hydroxide radicals. This led them to believe that the cleavage of the iron-peroxo species proceeds heterolytically to produce the oxo-iron(IV)-porphyrin radical cation species as opposed to hydroxide radicals. Based on this, the next steps of the reaction can be described by equations (4.47) and (4.48).

$$O = Fe(IV)(por^{+\cdot}) + H_2O \xrightarrow{ABTS} ABTS^{\cdot+} + O = Fe(IV)(por) \quad (4.47)$$

$$O = Fe(IV)(por) \xrightarrow{ABTS} ABTS^{\cdot+} + Fe(III)PPIX \quad (4.48)$$

Additional processes in the oxidation of ABTS may also occur. Adams reported a dependency consistent with the inhibition of H_2O_2 mediated degradation of the catalyst by ABTS.[149] An additional interaction in the oxidation of ABTS may, therefore, involve the formation of a complex between Fe(III)PPIX and ABTS as shown in equation (4.49). This type of reaction is not uncommon and has been reported to take place between an enzyme and an inhibitor during competitive inhibition, resulting in the formation of a non-catalytic complex (see Scheme 4.2).[157] In the current work, however, Fe(III)PPIX degradation still takes place in the presence of ABTS, coinciding with the results obtained by van Eldik and co-workers who found that the introduction of ABTS as a reducing substrate did not prevent degradation of the porphyrin by

H_2O_2.[130] A spectrophotometric titration of (MP-8) with ABTS by Adams did, however, indicate the formation of a complex between ABTS and Fe(III)PPIX, nevertheless, this was not further investigated in the current work.[149] If the formation of this catalytically inactive complex does in fact occur, the signal decay may not only be related to the degradation of Fe(III)PPIX, but, also the formation of the Fe(III)PPIX⋯ABTS complex which is not able to catalyse the oxidation reaction.

$$\mathrm{Fe(III)PPIX} + \mathrm{ABTS} \rightleftharpoons \mathrm{Fe(III)PPIX} \cdots \mathrm{ABTS} \tag{4.49}$$

A number of studies investigating the kinetics of ABTS oxidation have been reported.[130,131,132] The relative concentration of each component under investigation has been shown to be essential when investigating the kinetics of ABTS oxidation. Previous reports in literature have described a disproportionation of the $ABTS^{\cdot+}$ radical cation to afford the release of ABTS and the dication shown in equation (4.6).[129,130] This process is not favoured under acidic conditions. In more basic solutions such as those described in the above work, a high concentration of unreacted ABTS reportedly stabilizes the dication species.[130] When considering the kinetic model, this reaction was shown to favour the disproportionation of $ABTS^{\cdot+}$.

As shown in the above work, the rate of the ABTS oxidation reaction proved to be slower in the SDS solvent system. This slower rate is perhaps due to the decreased rate of H_2O_2⋯Fe(III)PPIX interaction. In Table 4.5, the rate of the formation and decay of the active catalytic species is compared in the two environments. The rate of the formation and cleavage (k_1) of the oxo-iron species is slower in the aqueous SDS system. As this is the first step of the oxidation reaction, a reason for the delay in the response is provided as the formation of the radical cannot proceed until completion of this step. The improved stability of the radical in the SDS system can also be related to the reduced rate of decay of the active iron species under these conditions. This may indicate that under conditions that mimic a lipid-water interface, Fe(III)PPIX is more stable and therefore ROS generation can be expected to be more prolonged and, consequently, more toxic.

Further evidence for the dependence of the oxidation reaction on Fe(III)PPIX can be seen in Figure 4.4 (a). From this plot, it is clear that the extent of $ABTS^{\cdot+}$ production is directly dependent on the concentration of Fe(III)PPIX present in the system and similar results were observed in the aqueous SDS system (Figure 4.12 (a)). The percentage efficiency of the ABTS oxidation reaction can be calculated according to Equation (4.50). The efficiency is a relative expression based on the reaction catalyzed by horseradish peroxidase (HRP) which proceeds with an efficiency of 200 %. This corresponds to two molecules of $ABTS^{\cdot+}$ produced per molecule of H_2O_2 metabolised as opposed to a value of 100 %, which reflects the oxidation of one molecule of ABTS.[149] The efficiency of the oxidation reaction shown in Figure 4.11 was calculated to be 4 % in both the aqueous and aqueous SDS solvent systems. The low efficiency with which Fe(III)PPIX carries out this reaction may be related to the complex speciation of Fe(III)PPIX, which varies between solvent systems. It has long been known that Fe(III)PPIX tends to aggregate in aqueous solution, [85,158] however,

conflicting ideas exist over the exact nature of the aggregate.[88] The UV-visible spectrum of Fe(III)PPIX in both aqueous and aqueous SDS solutions, investigated in Chapter 3, was identical to that of the Fe(III)PPIX $\pi - \pi$ dimer.[88,89] Furthermore, Figure 4.18 provides evidence for a higher concentration of Fe(III)PPIX dimer than monomer under the conditions described. Previous studies suggest that monomeric Fe(III)PPIX catalyses reactions with greater efficiency than aggregated forms of Fe(III)PPIX, such as the $\pi - \pi$ dimer, which appears to have a negative effect on the catalytic activity.[155] The additional interactions between the Fe(III)PPIX monomers may account for this decreased activity as the catalytically active iron centre would be less available to act as a catalyst. Adams investigated the peroxidase activity of the MP-8 under conditions where the catalyst was predominantly monomeric.[149] They obtained rate constants that were at least 100 times greater than those described for Fe(III)PPIX in this body of work. The authors also reportedly found that adherence of the initial rate of ABTS oxidation to the linear dependence weakened upon increasing concentrations of MP-8, presumably due to increased aggregation effects. The structure of MP-8, however, differs significantly from that of Fe(III)PPIX. In the former, the porphyrin is six coordinate and consists of a distal imidazole ligand which may facilitate stronger binding of H_2O_2, thereby improving the rate of ABTS oxidation.[131,132] That being said, free Fe(III)PPIX was able to successfully catalyse the production of ROS in an environment absent of protein and, although it appeared to be a weak catalyst, the extent of ROS generation may still be sufficient to pose a toxic insult to the parasite.

$$\% \text{ Efficiency} = [\text{ABTS}] \times 100 \tag{4.50}$$

Differences arose between the results obtained in the current study and those obtained in the study by Ribeiro *et al*. The marginal differences in yield and stability of $ABTS^{\cdot+}$ production described in the pH study (Figure 4.3) may account for the differences in the kinetic parameters obtained experimentally when compared to the work of Ribeiro *et al*.[134] In addition to the pH change in this system, the temperature of the reaction was increased and the buffer changed from phosphate buffered saline to Tris buffer. The effects of these aspects on ABTS radical production, however, were not investigated further as these conditions provided optimal conditions in which to measure ROS generation under conditions mimicking a biological environment. The phosphate buffer has, however, been reported to interact with Fe(III)PPIX, which would therefore compete with H_2O_2 for coordination and may introduce additional complications in the reaction.[131] In an effort to improve on the analysis undertaken by Ribeiro *et al*., attempts were made to determine a suitable kinetic model describing the oxidation of ABTS by Fe(III)PPIX and H_2O_2. Two different models were proposed, however, both models were unsuccessful in fitting the experimental data. This implies a more complex cycle which may involve the aforementioned interaction between Fe(III)PPIX and ABTS, however this was not further investigated. Future work will include modelling this reaction and incorporating it into the kinetic model to obtain better fits.

Other than the decrease in the overall rate of the oxidation reaction in the aqueous SDS solution, no significant changes were observed between the two systems. Interestingly, deviations from the linear dependency on the concentration of H_2O_2 occurred at higher concentrations in the SDS system than in aqueous solution. This may imply that higher concentrations of H_2O_2 are required for the catalase reaction to occur in this system, therefore making it a more stable environment for the ABTS oxidation reaction. This would correspond to Fe(III)PPIX being more stable under these conditions and therefore better able to catalyse the oxidation reaction. This observation may indicate that ROS generation is more prominent in lipid environments compared to aqueous solution.

4.5 Conclusion

The ABTS oxidation reaction is complex and is vulnerable to numerous side reactions that have a bearing on the degree of radical production. The above work provides evidence for the toxic nature of Fe(III)PPIX in the sense that it is able to catalyse this reaction, thereby generating reactive oxygen species in the absence of any antimalarial drug. The study revealed a two-fold reduction in reaction rate when the experiment was conducted in aqueous SDS solution. The slower rate of reaction observed in the aqueous SDS system is proposed to arise from the decreased rate of formation of the oxo-iron(IV) porphyrin complex – the primary step in the oxidation of ABTS. Despite the slower kinetics, the ABTS oxidation reaction proved to be more stable in the aqueous SDS system, thought to better mimic the environment that is relevant to haemozoin formation. Whether the enhanced stability of Fe(III)PPIX and the prolonged radical production in the aqueous SDS system can be directly related to the processes that occur at the lipid-water interface within the parasite is not confirmed, however, the current study does give insight to the species being formed in such an environment and their relative rates of formation. Further investigation of this reaction at the lipid water interface is necessary to better understand Fe(III)PPIX toxicity in this environment. For example, additional kinetic experiments need to be conducted in other detergent systems which would provide insight into whether the effects described above are conserved in lipid-like environments. While the specific rate constants were not able to be obtained from the data, the study is still able to provide information regarding the reaction between H_2O_2 and Fe(III)PPIX. The rates of formation and decay can be used as quantitative measures which can be compared to values obtained in the presence of drug. Additionally, qualitative analysis of yields of $ABTS^{\cdot+}$ produced can be used to gauge the effects of drugs on the ABTS reaction. This work, therefore, provides a suitable platform to investigate the peroxidative effects of Fe(III)PPIX in the presence of antimalarial drugs which may help understand how they contribute to death of the parasite. This is addressed in Chapter 5.

Chapter 5. The Peroxidase Activity of the complexes of Fe(III)PPIX with CQ, QD and Art

5.1 Introduction

Investigating the mechanism of antimalarial drug action has been a matter of great interest for several years.[58,63] This topic has become of increasing importance as a result of the mounting parasite resistance to commonly used antimalarial drugs, particularly towards the mainstay antimalarial drug, CQ.[159] Although these drugs are no longer sufficient to target malaria independently, an incomplete knowledge of their mechanism of action currently precludes rational design of new drugs and the possible development of vaccines. In the previous chapter, an assay used to measure the peroxidase activity of Fe(III)PPIX in an environment resembling that found in the malaria parasite was optimised. The results obtained in Chapter 4 have been used as a baseline to determine the influence antimalarial drugs (CQ, QD and Ar) have on the peroxidase activity of Fe(III)PPIX. CQ and QD are known inhibitors of haemozoin formation and cause an increase in free Fe(III)PPIX in the parasite which ultimately leads to its death.[83] This chapter, therefore, seeks to investigate the modulatory effect of drug-Fe(III)PPIX complexes on the toxicity of Fe(III)PPIX in the malaria parasite.

This chapter details the kinetics of $ABTS^{\cdot+}$ formation by the complexes of Fe(III)PPIX with CQ, QD and Ar in an aqueous environment as well as in an aqueous SDS system. The latter is thought to mimic lipid-water interfaces present in the parasite. The kinetic equations and methodology used in this chapter are based on the work detailed in Chapter 4. The results for the reaction catalysed by the CQ-Fe(III)PPIX complex are compared with those obtained by Ribeiro *et al.*,[134] while the kinetic investigations of ABTS oxidation catalysed by the complexes of Fe(III)PPIX with QD and Ar have not been reported in the literature.

5.2. Experimental Methods

5.2.1 Preparation of Solutions

5.2.1.1 The Peroxidase Activity of the CQ-Fe(III)PPIX Complex

CQ Stock Solution in Tris Buffer

A: A 76.9 µM stock solution of CQ in Tris buffer (130.0 mM) was prepared by dissolving chloroquine diphosphate salt (3.4 mg, 6.5 µmol) in Tris buffer stock solution **A** (see section 2.5.4) to a volume of 50.0 mL in a volumetric flask.

B: A 250.0 µM stock solution of CQ in Tris buffer (250.0 mM) was prepared by dissolving chloroquine diphosphate salt (6.4 mg, 12.5 µmol) in 50.0 mL Tris buffer stock solution **B** (see section 2.5.4)

5.2.1.2 The Peroxidase Activity of the QD-Fe(III)PPIX Complex

QD Stock Solution in Tris Buffer

A: A 103.0 µM stock solution of QD in Tris buffer (130.0 mM) was prepared by dissolving quinidine sulfate salt (4.0 mg, 5.2 µmol) in Tris buffer stock solution **A** (see section 2.5.4) to a volume of 50.0 mL in a volumetric flask.

B: A 150.0 µM stock solution of QD in Tris buffer (250.0 mM) was prepared by dissolving quinidine sulfate salt (5.9 mg, 7.5 µmol) in 50.0 mL Tris buffer stock solution **B** (see section 2.5.4).

5.2.1.3 The Peroxidase Activity of the Fe(III)PPIX-Ar Complex

Ar Stock Solution in Tris Buffer

A 2.6 mM stock solution of Ar in Tris buffer (250.0 mM) was prepared by dissolving artesunate (50.0 mg, 130.0 µmol) in 50.0 mL Tris buffer stock.

5.2.2 Experimental Procedure

All experiments were performed in quartz cuvettes with 1 cm path length at 37 °C. All working solutions were buffered to pH 7.5 (Tris, 50.70 mM) and had a total volume of 2.5 mL unless otherwise stated. The total volume of each component was the same as listed in Table 4.1 in the aqueous system and Table 4.3 in the aqueous SDS system. In the aqueous system, Tris buffer stock solutions **A** of CQ and QD were used while **B** stock solutions were used in the aqueous SDS system (see Table 5.1). Due to limited material, the

artesunate experiments were only carried out in SDS using the artesunate stock solution in Tris buffer. Where smaller volumes of a component were used, the remaining volume was substituted with the appropriate solvent as seen in Table 5.2 and 5.3. All samples were mixed thoroughly before the absorbance was recorded at 660 nm, which corresponds to the maximum absorbance peak in the spectrum of the ABTS radical. The studies were carried out as detailed in Section 4.2.2 and 4.3.2, with the exception that the drug-Fe(III)PPIX complex was formed before the addition of H_2O_2, and the interaction of Fe(III)PPIX with H_2O_2 was carried out according to the description in Section 4.2. All experiments were performed in duplicate unless otherwise stated.

Table 5.1 Buffer stock solutions used in the oxidation of ABTS by drug-Fe(III)PPIX complexes.

Species	Aqueous System	Aqueous SDS System
CQ-Fe(III)PPIX	A	B
QD-Fe(III)PPIX	A	B
Fe(III)PPIX-Ar	-	Ar stock solution in Tris buffer

Table 5.2 Composition of components required to investigate the peroxidase activity of Fe(III)PPIX in aqueous solution (pH 7.5). The concentration of the stock solution utilised in the experiments are shown in brackets.

Component	Volume (µL)
Tris Buffer (130.0 mM)	975
ABTS (7.5 mM)	1245
Fe(III)PPIX (0.2 mM)	30
H_2O_2 (1.0 mM/5.0 mM)	250
Total	**2500**

Table 5.3 The composition of each component required to investigate the peroxidase activity of Fe(III)PPIX in aqueous SDS solution (pH 7.5). The concentration of the stock solution utilised in the experiments are shown in brackets.

Component	Volume (µL)
Tris Buffer (250.0 mM)	500
ABTS (7.5 mM))	1520
SDS (13.0 mM)	200
Fe(III)PPIX (0.2 mM)	30
H_2O_2 (1.0 mM, 5.0 mM)	250
Total	**2500**

5.3 Results

Many ideas exist about the mechanism of action of antimalarial drugs. In particular, the mechanism of action of the quinoline antimalarial drugs CQ and QD has been a source of much debate. One proposal that is the focus of several current studies involves haemozoin inhibition through adsorption of inhibitors to the fastest growing crystal face,[47,84] while another is that the drugs complex with Fe(III)PPIX and prevent its incorporation into haemozoin in the parasite (see Section 1.4.3 for details).[80,81,84] Increased levels of free Fe(III)PPIX are a consequence of both mechanisms and it has been suggested that this causes the death of the parasite, in part because of ROS generation.[38] However, given the concentration of drugs that accumulate in the DV, drug-Fe(III)PPIX complexes may in fact be the dominant species present and thus the ability of these complexes to induce ROS could relate to the efficiency of these antimalarial drugs to kill the parasite.[160,161] The results obtained in Chapter 3, which focus on the complexes formed between Fe(III)PPIX and the antimalarial drugs CQ, QD and Ar, were used in this body of work to determine the extent of drug-Fe(III)PPIX complexation in both an aqueous and aqueous SDS environment. The peroxidase activity of Fe(III)PPIX in the presence of CQ in aqueous solution has previously been reported, although these experiments were conducted at 30 °C and pH 6.86.[134] In the current work, the peroxidase activity of the complexes of Fe(III)PPIX with CQ and QD was investigated under conditions which better mimic the cytosol of the parasite (37 °C and pH 7.5). Since Fe(III)PPIX precipitates under acidic conditions (pH < 6), investigating the peroxidase activity of Fe(III)PPIX under conditions representative of the DV (pH 4.8 – 5.2) was not possible. Nevertheless, while antimalarial drugs such as CQ have been shown to accumulate in the DV of *P. falciparum*, research has shown that in the presence of this antimalarial drug, the iron in the DV of the parasite (which is likely Fe(III)PPIX) is redistributed to the parasite cytosol.[71,83,162] Consequently, investigating Fe(III)PPIX catalysed peroxidation activity under conditions of the parasite cytosol are pertinent to understanding the mode of action of these types of antimalarial drugs. Moreover, advances in the understanding of drug-Fe(III)PPIX complexation have been made since the report by Ribeiro *et al.*,[134] which have thus necessitated the follow-up investigation of the effects of CQ on Fe(III)PPIX catalysed peroxidase activity.[111,123]

The same approach described in Chapter 4 was utilised in the current work to investigate the peroxidase activity of Fe(III)PPIX in the presence of CQ and QD. To ensure that there was complete complexation of Fe(III)PPIX by CQ and QD under the experimental conditions, association constants calculated in Chapter 3 (log K = 6.5 and 5.78 for CQ and QD, respectively) were employed. These values could be used to determine the percentage of Fe(III)PPIX complexed as a function of drug concentration (Figure 5.1) using the Hyperquad Simulation and Speciation (HySS) software package.[163] This data set indicated that concentrations of 30 and 40 µM of CQ and QD respectively would ensure 95% complexation of Fe(III)PPIX. Consequently, these drug concentrations were used in subsequent experiments.

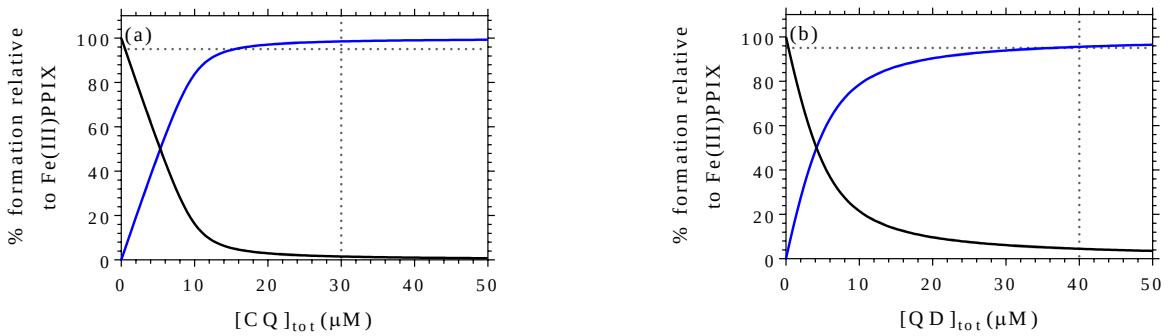

Figure 5.1 The percentage drug-Fe(III)PPIX complex formed (-) (relative to free Fe(III)PPIX (-)) in aqueous solution as a function of drug concentration for **(a)** CQ and **(b)** QD. A 2:1 Fe(III)PPIX: drug binding model was used in the case of CQ, while a 1:1 model was used for QD. Both plots were generated using a Fe(III)PPIX concentration of 10.0 μM. Dotted lines indicate the concentration of drug required to ensure 95% Fe(III)PPIX complexation.

Similarly, the concentration of drug required to ensure > 95% complexation in the aqueous SDS system was determined using the HySS software package.[163] Since the association constant for the CQ-Fe(III)PPIX complex remained unchanged in the aqueous SDS system, the data in Figure 5.1 (a) still applies, however the data obtained for QD (log K = 6.2 ± 0.1) is shown in Figure 5.2. In the case of both CQ and QD, the concentration used in all subsequent experiments performed in aqueous SDS solution was 30.0 μM. Owing to very weak binding, an association constant was not able to be determined for Ar and thus a large excess (1.0 mM) was used in an effort to provide a concentration portion of Ar-bound Fe(III)PPIX.

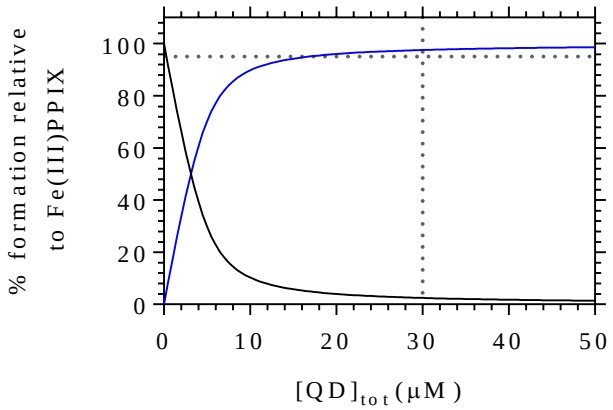

Figure 5.2 The percentage of QD-Fe(III)PPIX complex formed (-) (relative to Fe(III)PPIX (-)) in aqueous SDS solution as a function of QD concentration using a Fe(III)PPIX concentration of 10.0 μM and a 1:1 Fe(III)PPIX: QD binding model. Dotted lines indicate the concentration of drug required to ensure 95% Fe(III)PPIX complexation.

5.3.1 The Interaction Between Fe(III)PPIX and H_2O_2 in the Presence of CQ, QD and Ar

In Chapter 4, the formation of an oxo-iron(IV) porphyrin radical cation was identified as the primary step in the oxidation of ABTS. As discussed previously, this reaction has been proposed to consist of three parts; the formation of an iron-peroxo compound (I in scheme 5.1), the cleavage of this compound to form the catalytically active Fe(III)PPIX species (II in scheme 5.1) and the subsequent decay of this Fe(III)PPIX catalyst in the absence of a suitable substrate (k_{deg} in Scheme 5.1).[130]

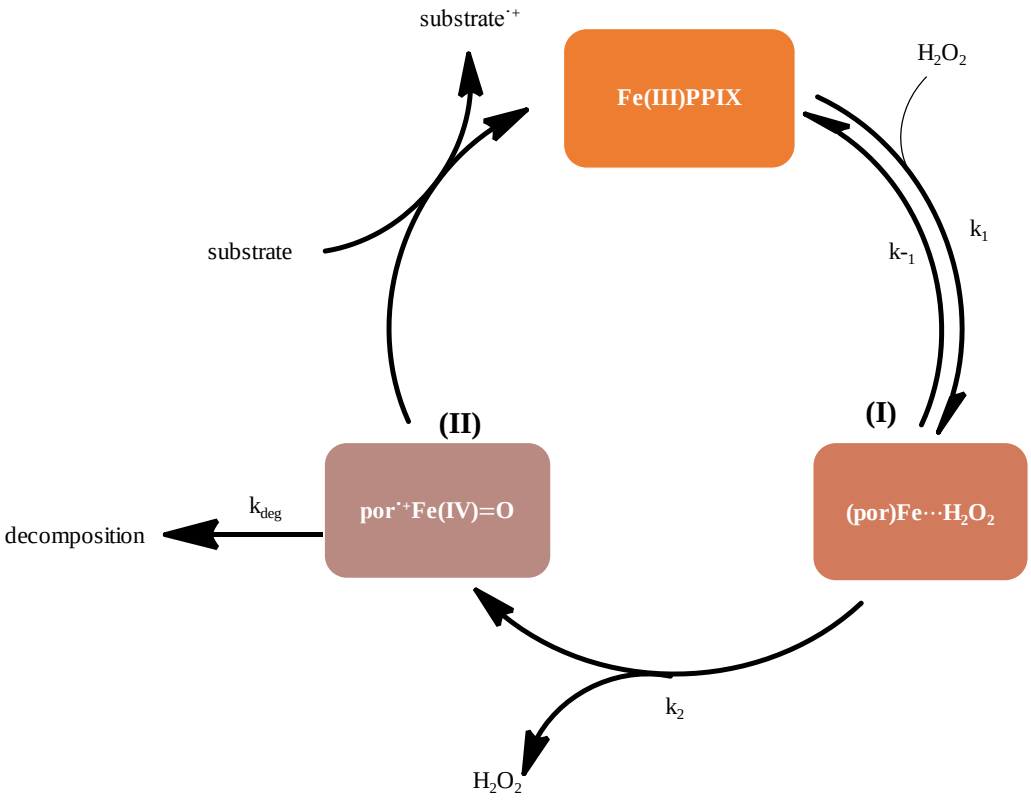

Scheme 5.1 A schematic representation of the reaction between Fe(III)PPIX and H_2O_2 which forms an iron peroxo species (I), followed by cleavage to the catalytically active porphyrin radical species (II). This species is able to oxidise substrates while simultaneously reforming the porphyrin. Alternatively, the catalytic species may undergo degradation and form decomposition products.

In Chapter 4, the peroxidase activity of Fe(III)PPIX was monitored in both the aqueous and aqueous SDS systems. It was observed that $ABTS^{\cdot+}$ was more stable in the aqueous SDS solution. This observation was related to the reduced rate of formation of the catalytically active Fe(III)PPIX species (II in scheme 5.1). The rate of formation consists of the combination of K and k_2, where $K = k_1/k_{-1}$. Similarly, the reaction between Fe(III)PPIX and H_2O_2 was investigated in the presence of antimalarial drugs in order to determine the modulatory effect that these drugs have on the formation of the catalytically active Fe(III)PPIX species (II in scheme 5.1). As discussed in Chapter 4, determining the rate constants for this reaction is an intricate task that involves the use of kinetic modelling programs. In order to obtain approximate reaction rates for comparison purposes, all the data in this section were fit with a simple exponential function. Spectra were

recorded between 300 and 800 nm for the reaction of H_2O_2 with the complexes of Fe(III)PPIX with CQ and QD in the aqueous system and are shown in Figure 5.3 (a) and (b) for CQ and QD, respectively. In both cases, the addition of H_2O_2 resulted in a hypochromic effect of the Soret band. The change in absorbance at 380 nm was then monitored over a longer period than used in Chapter 4 (60 minutes) owing to the diminished rate of this process in the presence of antimalarial drugs. When this experiment was carried out for Fe(III)PPIX in Chapter 4, the results could be fitted with a two-phase exponential decay function. The data obtained in the presence of CQ and QD could similarly be fitted using the two-phase decay function. The interaction of Fe(III)PPIX with H_2O_2 is, however, slower in the presence of QD, which suggests that this drug is better able to shield the porphyrin from further interaction with H_2O_2, thereby preventing degradation. In Chapter 3 it was observed that QD interacts with Fe(III)PPIX through coordination while CQ acts through π-stacking. This suggests that the ability of QD to coordinate to Fe(III)PPIX may serve to better shield the porphyrin from degradation.

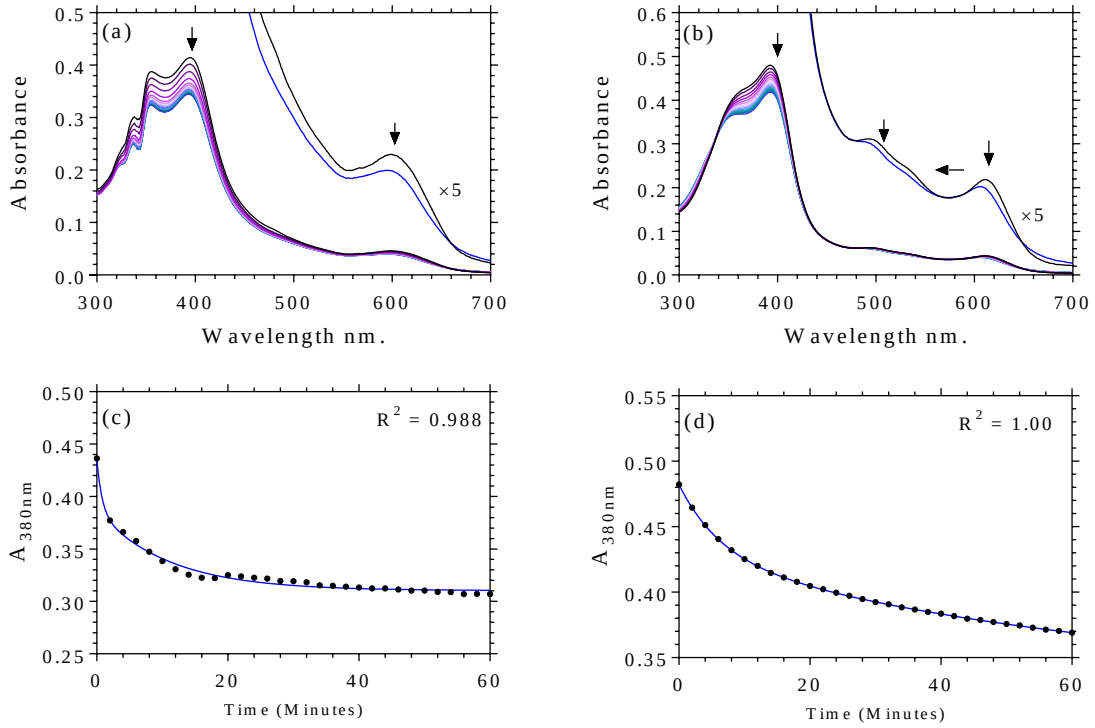

Figure 5.3 The change in the spectrum of 10.0 µM CQ-Fe(III)PPIX **(a)** and QD-Fe(III)PPIX complexes **(b)** in aqueous solution (100.0 µM H_2O_2) monitored over 60 minutes (black to blue). The region between 550 and 700 nm has been enlarged for clarity. Plots **(c)** and **(d)** show the trace of the absorbance at 380 nm (black circles) for the plots in **(a)** and **(b)** respectively, fitted with a two-phase exponential decay function (blue line).

As previously discussed, the interactions of Fe(III)PPIX with antimalarial drugs at the lipid-water interface have become a matter of great interest and therefore the effects of CQ and QD on Fe(III)PPIX stability was repeated in aqueous SDS as a comparative system, mimicking a lipid-water interface. Findings are shown in Figure 5.4. H_2O_2-induced changes in the absorbance spectra monitored over time exhibited a similar hypochromicity of the Soret band for the complexes of Fe(III)PPIX with CQ and QD as seen in the aqueous

system. The decrease in absorbance of the Soret band was also accompanied by slight shifts in the charge-transfer region of the spectrum in the case of CQ. A summary of the rate constants obtained for the reaction between Fe(III)PPIX and H_2O_2 in the presence of the antimalarial drugs CQ, QD and Ar can be seen in Table 5.4. In aqueous solution, the rate of formation of the catalytically active oxo-iron (IV) species (II in scheme 5.1) for the CQ-Fe(III)PPIX complex is approximately eight times that of the QD-Fe(III)PPIX complex (200×10^{-4} vs 26×10^{-4} s^{-1}). In aqueous SDS solution, the rate of the reaction between Fe(III)PPIX and H_2O_2 in the presence of QD shows a 6-fold increase compared to that obtained in aqueous system. The difference in rate of the reaction between Fe(III)PPIX and H_2O_2 may be related to the nature of the interaction between the drug and Fe(III)PPIX in the two systems. While the association constant for the interaction of Fe(III)PPIX with CQ remained unchanged in the two systems (see Section 3.3.1), the association constant for the QD-Fe(III)PPIX complex proved to be stronger in the aqueous SDS system. Furthermore, the spectroscopic shifts indicative of complex formation were more pronounced in the aqueous SDS system. It would therefore be expected that the stronger association and possible coordination of QD to Fe(III)PPIX in aqueous SDS solution would cause a reduction in the rate of formation of the catalytically active iron species as the QD-Fe(III)PPIX coordination bond need first be broken before formation of the catalytically active species can commence. This was, however, not the case and therefore the type of the interaction between Fe(III)PPIX and QD in aqueous solution may be related to the reduced rate of formation of the catalytically active iron species.

Owing to limited material, all reactions concerning Ar were only conducted in the aqueous SDS system. The aqueous SDS system was chosen based on the results obtained in Chapter 4 which provided evidence for increased stability of ABTS in this environment when compared to aqueous solution. The spectrum of Fe(III)PPIX in the presence of Ar showed a substantial decrease in absorbance in the first two minutes of the reaction. This observation bares resemblance to what was seen in the absence of antimalarial drugs in Chapter 4. As with CQ and QD, a hypochromic effect on the Soret band was observed and this was accompanied by a marked shift in the charge transfer band to higher energy wavelengths. All the kinetic traces were fit with a two-phase function as with Fe(III)PPIX. While the presence of Ar appears to have no influence on the rate of formation of the catalytically active iron-oxo species in aqueous SDS solution, the rate of k_2 in the presence of Ar is significantly slower (26×10^{-4} vs 6.5×10^{-4} s^{-1}). This would imply that Fe(III)PPIX is more stable in the presence of Ar since it prevents further peroxidative damage. This is a rather unexpected result as the presence of the endoperoxide bridge in Ar, an organic peroxide, would be expected to enhance the interaction of Fe(III)PPIX with H_2O_2 since it is similar to H_2O_2. The improved stability of Fe(III)PPIX may therefore be a result of the interaction that occurs between Fe(III)PPIX and Ar which, based on the findings, suggests this interaction is different to that between Fe(III)PPIX and H_2O_2. Further details of this interaction, however, could not be discerned from these measurements. It is also interesting to note that, for all cases, the rate of decay of the porphyrin is slower in the presence of antimalarial drug than without. This result provides evidence for the stability of Fe(III)PPIX in the presence of the antimalarial drug.

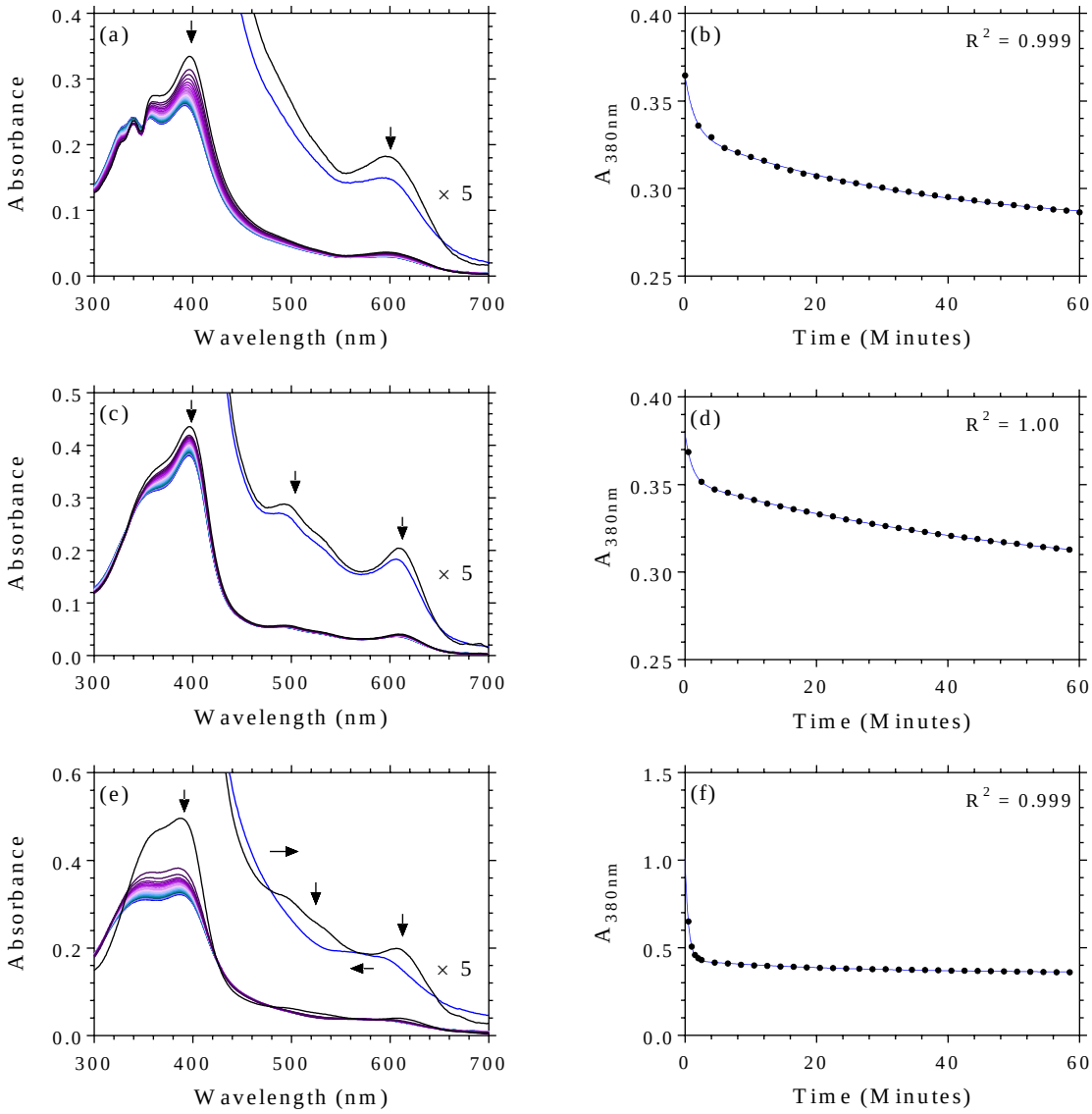

Figure 5.4 The change in the spectrum of 10.0 µM CQ-Fe(III)PPIX **(a)**, QD-Fe(III)PPIX **(c)** and Fe(III)PPIX-Ar **(e)** in the presence of 100.0 µM H_2O_2 monitored over 60 minutes (black to blue). The region between 550 and 700 nm has been enlarged for clarity. Plots **(b)**, **(d)** and **(f)** show the trace of the absorbance at 380 nm (black) of the Fe(III)PPIX drug complex shown in **(a)**, **(c)** and **(e)**, respectively. All data (black circles) were fit with a two- phase exponential decay function (blue line).

Table 5.4 Rate constants (10^{-4} s^{-1}) obtained for the reaction between the complexes of Fe(III)PPIX with CQ, QD and Ar with H_2O_2.

Species	Aqueous		Aqueous SDS	
	k_{1obs}	k_{2obs}	k_{1obs}	k_{2obs}
Fe(III)PPIX	600 ± 100	50 ± 10	360 ± 30	26 ± 2
CQ-Fe(III)PPIX	200 ± 100	15 ± 2	110 ± 10	4.9 ± 0.3
QD-Fe(III)PPIX	26.2 ± 0.3	2.46 ± 0.05	160 ± 10	3.13 ± 0.08
Fe(III)PPIX-Ar	ND‡	ND‡	310 ± 10	6.5 ± 0.3

‡Not determined due to limited material

In an effort to compare the reaction between Fe(III)PPIX and H_2O_2 in the absence and presence of antimalarial drug, a simplified reaction equation was proposed (Equation 5.1). As discussed in Chapter 4, this is a complex system and kinetic modelling programs are required to obtain numerical solutions to the rate equations. An approximate solution was therefore obtained by making the assumption that the concentration of H_2O_2, which is in vast excess over Fe(III)PPIX (100.0 vs 10.0 µM), remains somewhat constant throughout the reaction. The simplified reaction is given by Equation 5.2 where $k_1' = k_1[H_2O_2]$ The reaction rate model, which considers the change in concentration of the catalytic iron oxo species (O=Fe(IV)), for this equation can therefore be described using Equation 5.3. The integrated form of this expression is given by Equation 5.4 (See appendix 2 for derivation).[164]

$$H_2O_2 + Fe(III) \xrightarrow{k_1} O{=}Fe(IV) \xrightarrow{k_2} \text{deg. prod} \tag{5.1}$$

$$Fe(III) \xrightarrow{k_1'} O{=}Fe(IV) \xrightarrow{k_2} \text{deg. prod} \tag{5.2}$$

$$\frac{d[O{=}Fe(IV)]}{dt} = k_1[Fe(III)] - k_2[O{=}Fe(IV)] \tag{5.3}$$

$$[O{=}Fe(IV)] = \frac{k_1}{k_2 - k_1}[e^{-k_1 t} - e^{-k_2 t}][Fe(III)]_0 \tag{5.4}$$

Through substitution of the values shown in Table 5.4 for k_1 and k_2, the preliminary, approximate concentration of the catalytic iron-oxo species could be determined as a function of time, the results for which are shown in Figure 5.5. The initial concentrations of H_2O_2 and Fe(III)PPIX used in this analysis were 100.0 and 10.0 µM, respectively. The data in Figure 5.5 indicates that the reaction conducted in the absence of antimalarial drug causes a relatively fast reduction in the concentration of the active iron species in aqueous solution. In the presence of CQ, the rate at which the catalytic iron species forms and decays is

significantly reduced and even more so in the presence of QD. Similar results are seen in the aqueous SDS system (Figure 5.5 (b)). All three antimalarial drugs induced a reduction in the rate of formation and decay of the catalytic iron species, with the slowest rate observed in the presence of QD. This correlates well with the different mode of interaction between Fe(III)PPIX and QD, namely coordination, when compared to CQ which interacts through π-stacking. These preliminary results strongly suggest that, in the presence of the antimalarial drugs, the potential for oxidative attack is greater since the active iron species is present for longer periods of time.

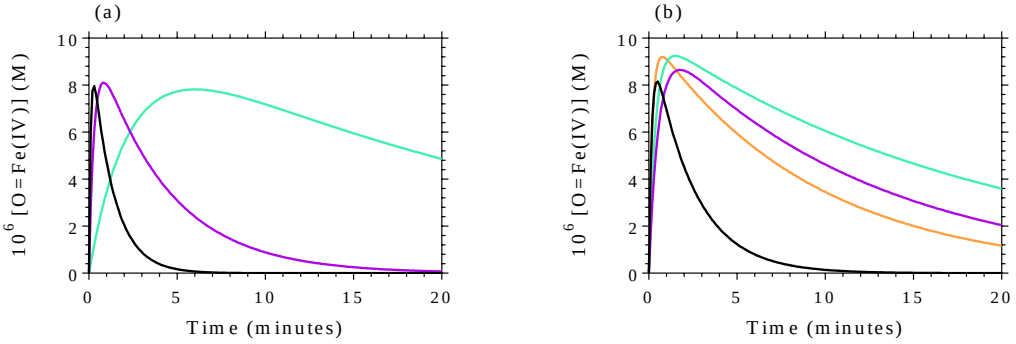

Figure 5.5 The calculated concentration of O=Fe(IV)PPIX as a function of time in **(a)** aqueous solution and **(b)** aqueous SDS solution for Fe(III)PPIX (black), CQ-Fe(III)PPIX (purple), QD-Fe(III)PPIX (turquoise) and Ar-Fe(III)PPIX (orange).

5.3.2 The Peroxidase Activity of the Complexes of Fe(III)PPIX with CQ and QD in Aqueous Solution

Previously, the peroxidase activity of Fe(III)PPIX was investigated by systematically varying the concentrations of each component (ABTS, Fe(III)PPIX and H_2O_2). In this chapter, the modulatory effect of the antimalarial drugs on ABTS oxidation was monitored by simultaneously varying the concentration of H_2O_2 and the concentration of the drug-Fe(III)PPIX complex. Since the antimalarial drugs are known to associate and (in the case of QD) coordinate to Fe(III)PPIX, the presence of these drugs in the ABTS reaction may alter the formation of the catalytically active Fe(III)PPIX species (II in scheme 5.1). For this reason, the modulatory effect of antimalarial drug concentration on ABTS oxidation was not investigated as a function of ABTS concentration as it is assumed that they have a minimal effect on this parameter.

The effect of varying H_2O_2 concentration on the kinetics of ABTS oxidation was initially monitored as a function of increasing CQ-Fe(III)PPIX concentration. The results, shown in Figure 5.6, indicate that the yield of $ABTS^{\cdot+}$ increases as a function of increasing CQ-Fe(III)PPIX concentration (which is a consequence of increasing Fe(III)PPIX concentration). A similar result was observed between the yield of $ABTS^{\cdot+}$ and the concentration of H_2O_2, however, at concentrations above 200.0 µM a saturation effect was observed (Figure 5.6 (e)). The observed rate of the reaction, calculated using a simple one-phase exponential function, is also shown to depend linearly on the concentration of H_2O_2 in Figure 5.6 (f). Furthermore, at H_2O_2 concentrations

above 200.0 µM, there is a significant reduction in the stability of $ABTS^{\cdot+}$ indicated by the decrease in concentration after a period of 30 minutes at lower CQ-Fe(III)PPIX concentrations (see Figure 5.6(d)).

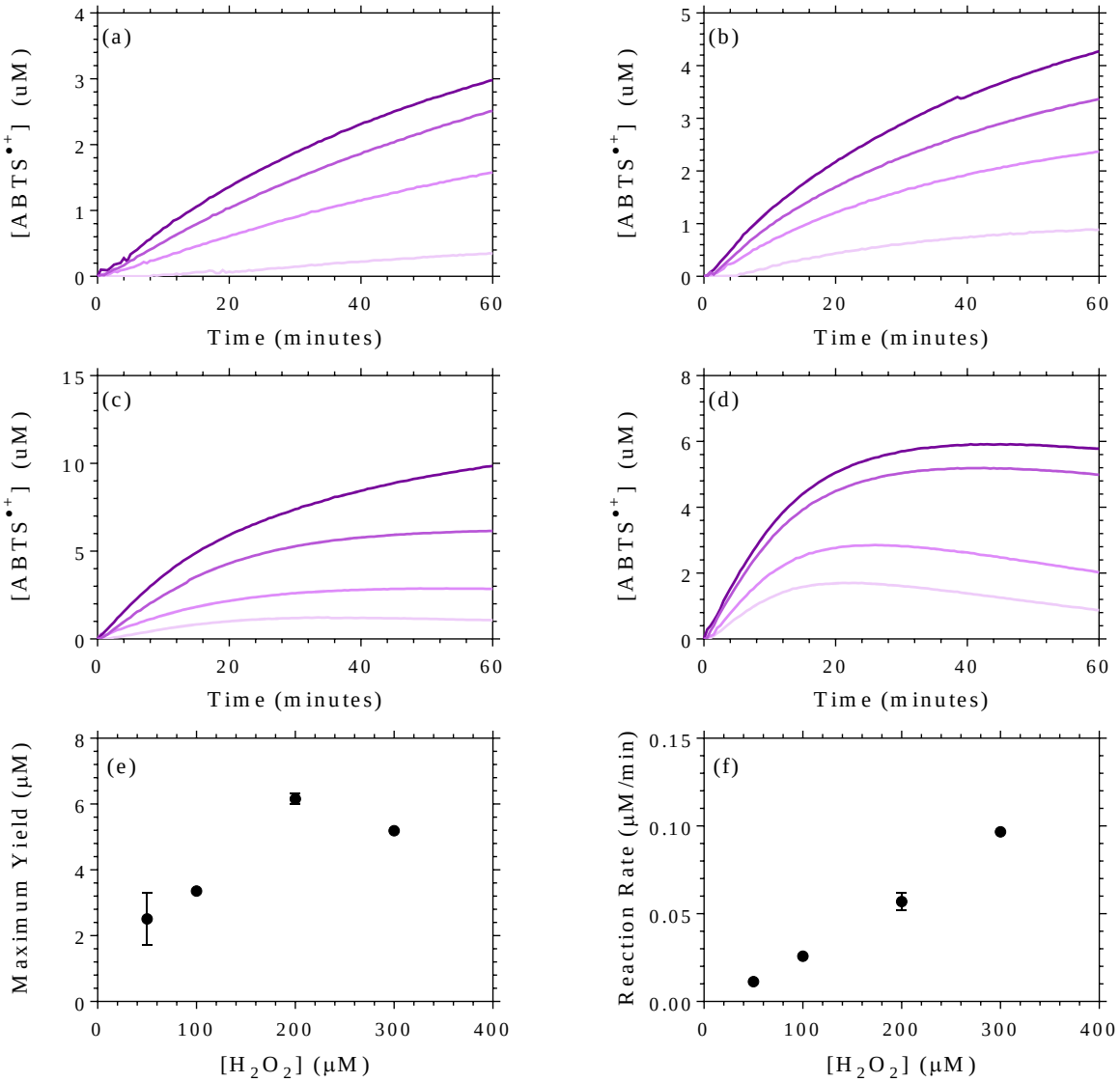

Figure 5.6 The effect of H_2O_2 concentration on ABTS oxidation by the CQ-Fe(III)PPIX complex in aqueous solution. The conditions are **(a)** 50.0, **(b)** 100.0, **(c)** 200.0 and **(d)** 300.0 µM H_2O_2 in the presence of 3.0 mM ABTS, 30.0 µM CQ and 0.3 (-), 0.6 (-), 1.0 (-) and 1.3 (-) µM Fe(III)PPIX. **(e)** The maximum yield, calculated as the maximum concentration of $ABTS^{\cdot+}$ reached within the 60 minute time period, and **(f)** the overall reaction rate, is plotted as a function of H_2O_2 concentration. The conditions were 1.0 µM CQ-Fe(III)PPIX and 3.0 mM ABTS. Data points omitted for clarity.

The same approach was followed to determine the effect of the QD-Fe(III)PPIX complex on Fe(III)PPIX-catalysed peroxidation. The results, shown in Figure 5.7, indicate that the presence of QD causes a significant reduction in the reaction rate in comparison to that obtained in its absence. A comparison of the yield as a function of H_2O_2 concentration shows no significant correlation, in contrast to what was see for CQ (Figure 5.7 (e)). Despite the reduction in reaction rate, the yield appears to be the same for both drugs.

The observed overall reduction in ABTS radical yield in the presence of CQ and QD as compared to the yield obtained in their absence is difficult to reconcile with these drugs' mechanism of toxicity (haemozoin inhibition). These results, however, are somewhat consistent with previous studies which reported a similar reduction of peroxidase activity in the presence of quinoline antimalarial drugs.[134,138] A comparison of the overall reaction rate (Figure 5.7 (f)), calculated using a simples exponential function, shows an increase in rate as a function of increasing H_2O_2 concentration with the exception of the 300.0 µM data set.

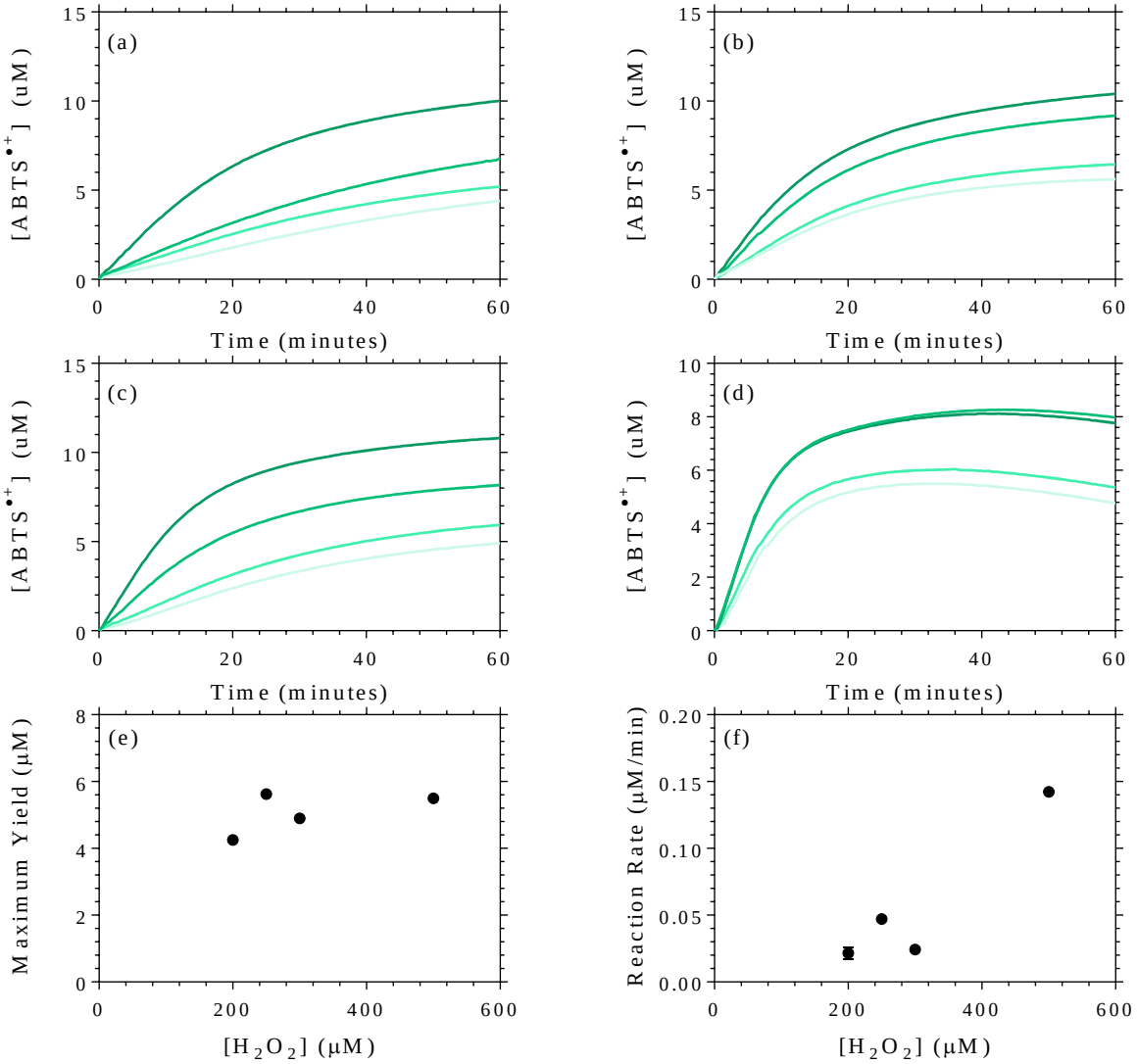

Figure 5.7 The effect of H_2O_2 concentration on ABTS oxidation by the QD-Fe(III)PPIX complex in aqueous solution. The conditions are **(a)** 200.0, **(b)** 250.0, **(c)** 300.0 and **(d)** 500.0 µM H_2O_2 in the presence of 3.0 mM ABTS, 30.0 µM QD and 1.0 (-), 1.3 (-), 2.0 (-) and 2.5 (-) µM Fe(III)PPIX. **(e)** The maximum yield, calculated as the maximum concentration of $ABTS^{\cdot+}$ reached within the 60 minute time period, and **(f)** the overall reaction rate, is plotted as a function of H_2O_2 concentration. The conditions were 1.0 µM QD-Fe(III)PPIX and 3.0 mM ABTS. Data points omitted for clarity.

A comparison of the ABTS oxidation reaction under constant ABTS, H_2O_2 and Fe(III)PPIX concentrations in the absence and presence of antimalarial drugs is shown in Figure 5.8. A 60% decrease in the yield of radical production in the presence of CQ was calculated from the experiment described in Figure 5.8. Ribeiro

et al. also reported a substantial reduction in the yield of $ABTS^{\bullet+}$ when the experiment was conducted in the presence of CQ. As discussed in Chapter 4, specific rate constants for individual steps in the complex reaction were not successfully obtained. For the sake of comparison, however, the data has been fit, at a specific set of experimental conditions, to a single-phase exponential function. This allows the deduction of an observed rate constant for the peroxidation of ABTS, k_{obs}, which provides an overall measure of efficiency that can be used to compare the effects of drugs on this reaction. These values are listed in Table 5.5. It is interesting to note that, although the yield of ABTS radical production remains unchanged for CQ- and QD-Fe(III)PPIX complexes, the overall rate of the reaction shown in Figure 5.8 is approximately four times slower for QD-Fe(III)PPIX when compared to the reaction catalysed by CQ-Fe(III)PPIX.

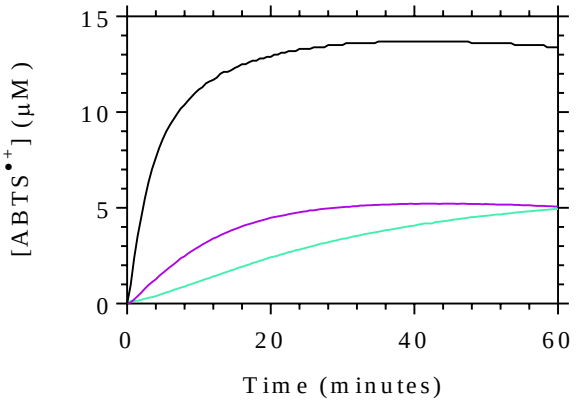

Figure 5.8 Comparative effects of CQ and QD on the kinetics of Fe(III)PPIX-catalysed ABTS oxidation in aqueous solution. $ABTS^{\cdot+}$ production as a function of time catalysed by 1.0 µM Fe(III)PPIX (-), CQ-Fe(III)PPIX (-) and QD-Fe(III)PPIX (-). ABTS and H_2O_2 concentrations were 3.0 mM and 300.0 µM, respectively. Data points omitted for clarity.

Table 5.5 A summary of the observed rate constants (k_{obs}) ($\times 10^{-4}$ µM/s), calculated using a one-phase exponential function, and maximum yield obtained for the oxidation of ABTS by Fe(III)PPIX, CQ-Fe(III)PPIX and QD-Fe(III)PPIX for the reaction described in Figure 5.8

Species	k_{obs}	Yield (µM)
Fe(III)PPIX	24.4 ± 0.5	13.54 ± 0.02
CQ-Fe(III)PPIX	16.1 ± 0.2	5.30 ± 0.02
QD-Fe(III)PPIX	4.1 ± 0.1	6.61 ± 0.08

5.3.3 The Peroxidase Activity of the Complexes of Fe(III)PPIX with CQ, QD and Ar in Aqueous SDS

Following the work carried out in the above section, the peroxidase activity of the complexes of Fe(III)PPIX with CQ, QD and Ar in aqueous SDS solution were investigated. The kinetic experiments for the oxidation of ABTS in aqueous SDS was conducted as described above for aqueous solution. This was done in order to investigate the peroxidase activity of the drug-Fe(III)PPIX complexes in an environment that resembles their proposed site of action, namely a lipid-aqueous interface. Contrary to what was observed in aqueous solution, the CQ-Fe(III)PPIX complex did not induce an inhibitory effect on the yield of $ABTS^{\cdot+}$ (Figure 5.9), although the reaction rate is slower. Interestingly, a slight lag-phase delay is observed in the aqueous SDS system at low Fe(III)PPIX concentrations which is not seen under aqueous conditions. This may be due to the competing process of CQ-Fe(III)PPIX complex formation and the formation of the iron-peroxo species which is slower in aqueous SDS. The same feature was observed when the reaction was performed in the absence of antimalarial drug, however, reasons for the decay in rate are not known. Furthermore, in comparison with what was seen for CQ in aqueous solution, the $ABTS^{\cdot+}$ radical appears more stable under the current conditions. This is evident from the elevated signal after a period of 90 minutes, as opposed to the decrease in signal that was observed in aqueous solution (Figure 5.6(d)). This instability in aqueous solution is likely the cause of the discrepancy in yield between the two solvent systems and suggests the aqueous SDS solution provides more reliable conditions with which to measure ABTS reduction. This finding highlights the importance of solvent system selection when undertaking these investigations and seems to be underappreciated in the literature. Furthermore, an analysis of the maximum yield (Figure 5.9 (e)) as well as the reaction rate (Figure 5.9 (f)), calculated according to a one-phase exponential function, indicate a linear dependence on the concentration of H_2O_2.

Contrary to CQ, the inhibition effect is still evident in the aqueous SDS solvent system when QD is present (Figure 5.10). A plot of the maximum yield as a function of H_2O_2 concentration shows a linear relationship, contrary to what was seen in aqueous solution. A comparison of the overall reaction rate using a one phase exponential association function revealed a two-fold reduction in the rate of oxidation by QD-Fe(III)PPIX when compared to CQ-Fe(III)PPIX in aqueous SDS (2×10^{-4} µM/min vs 4×10^{-4} µM/s) (see Table 5.6). A more interesting effect was, however, a lag phase observed in the first five minutes of the reaction conducted in the presence of the QD-Fe(III)PPIX complex which is not observed in the purely aqueous system. The length of the lag phase appears to be indirectly related to the concentration of both QD-Fe(III)PPIX and H_2O_2 present in the system. Since this lag phase was absent in the aforementioned experiments, it would suggest that the lag phase is related to the interaction between Fe(III)PPIX and QD in the aqueous SDS system. As discussed in Chapter 3, the QD-Fe(III)PPIX association constant in aqueous SDS (log K = 6.2 ± 0.1) was stronger than what was determined in aqueous solution (log K = 5.78 ± 0.09). As a result, the formation of the catalytically active Fe(III)PPIX peroxo species (II in scheme 5.1) is expected to be more challenging. Since this is the primary oxidant in the ABTS reaction, $ABTS^{\cdot+}$ production will not commence

until this intermediate species has been formed, resulting in a delay in the initial portion of the kinetic trace. Consequently, the reaction rate was calculated using a sigmoidal function, revealing a linear dependence on the concentration of H_2O_2 (Figure 10 (f)). CQ would have been expected to have a similar lag phase since it has the same magnitude association constant as QD. This is not so straight forward, however, since the association constants are not comparable because they represent two different binding mechanisms (2:1 and 1:1).

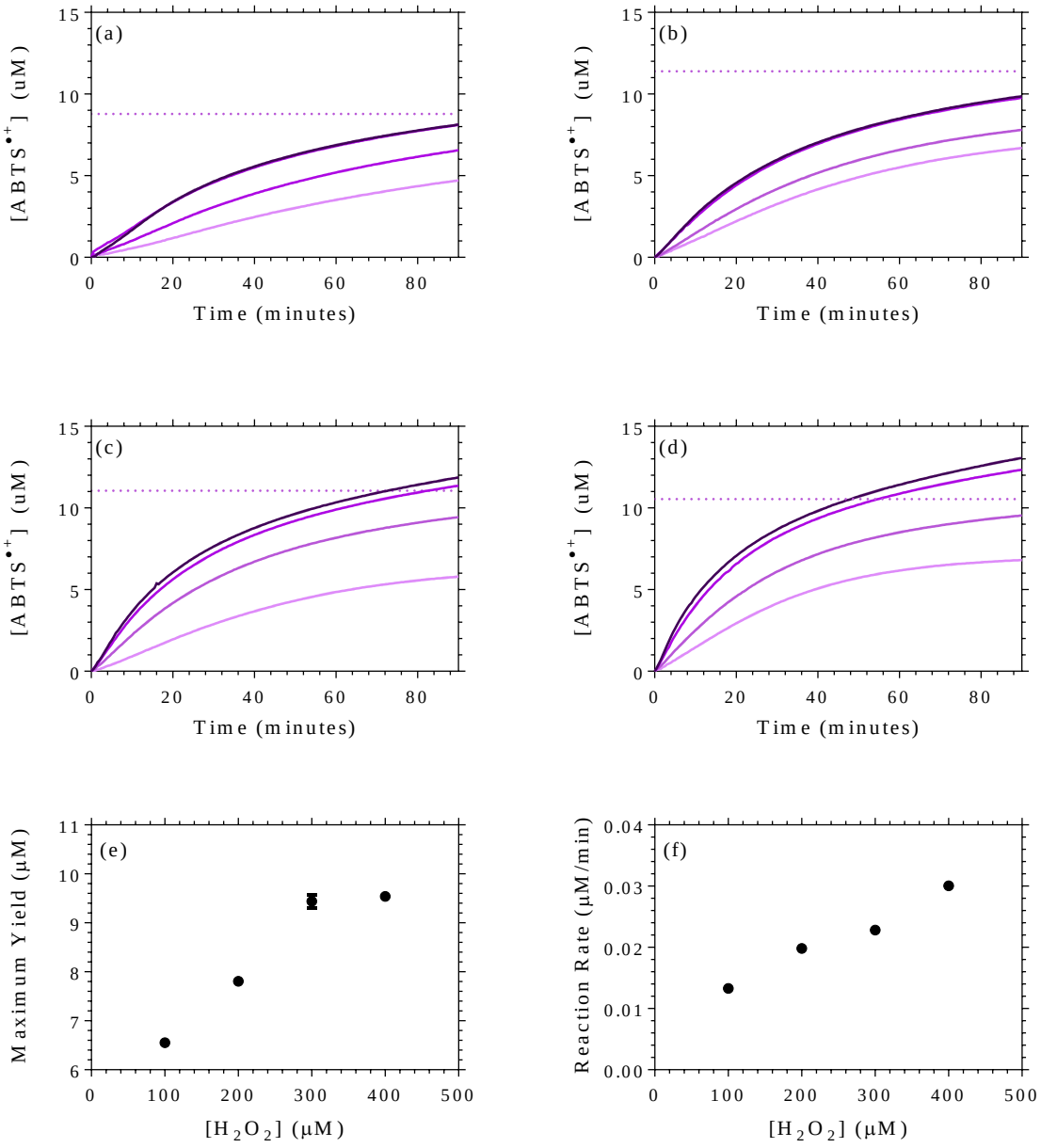

Figure 5.9 The effect of H_2O_2 concentration on ABTS oxidation by the CQ-Fe(III)PPIX complex in aqueous SDS solution. The conditions are **(a)** 100.0, **(b)** 200.0, **(c)** 300.0 and **(d)** 400.0 µM H_2O_2 in the presence of 3.0 mM ABTS and 0.6 (-), 1.0 (-), 2.0 (-) and 2.5 (-) µM Fe(III)PPIX. The dotted line indicates the final yield in the absence of drug in the aqueous SDS system in the presence of 1.0 µM Fe(III)PPIX and 3.0 mM ABTS. **(e)** The maximum yield, calculated as the maximum concentration of $ABTS^{\cdot+}$ reached within the 90 minute time period, and **(f)** the overall reaction rate, is plotted as a function of H_2O_2 concentration. The conditions were 1.0 µM CQ-Fe(III)PPIX and 3.0 mM ABTS. Data points omitted for clarity.

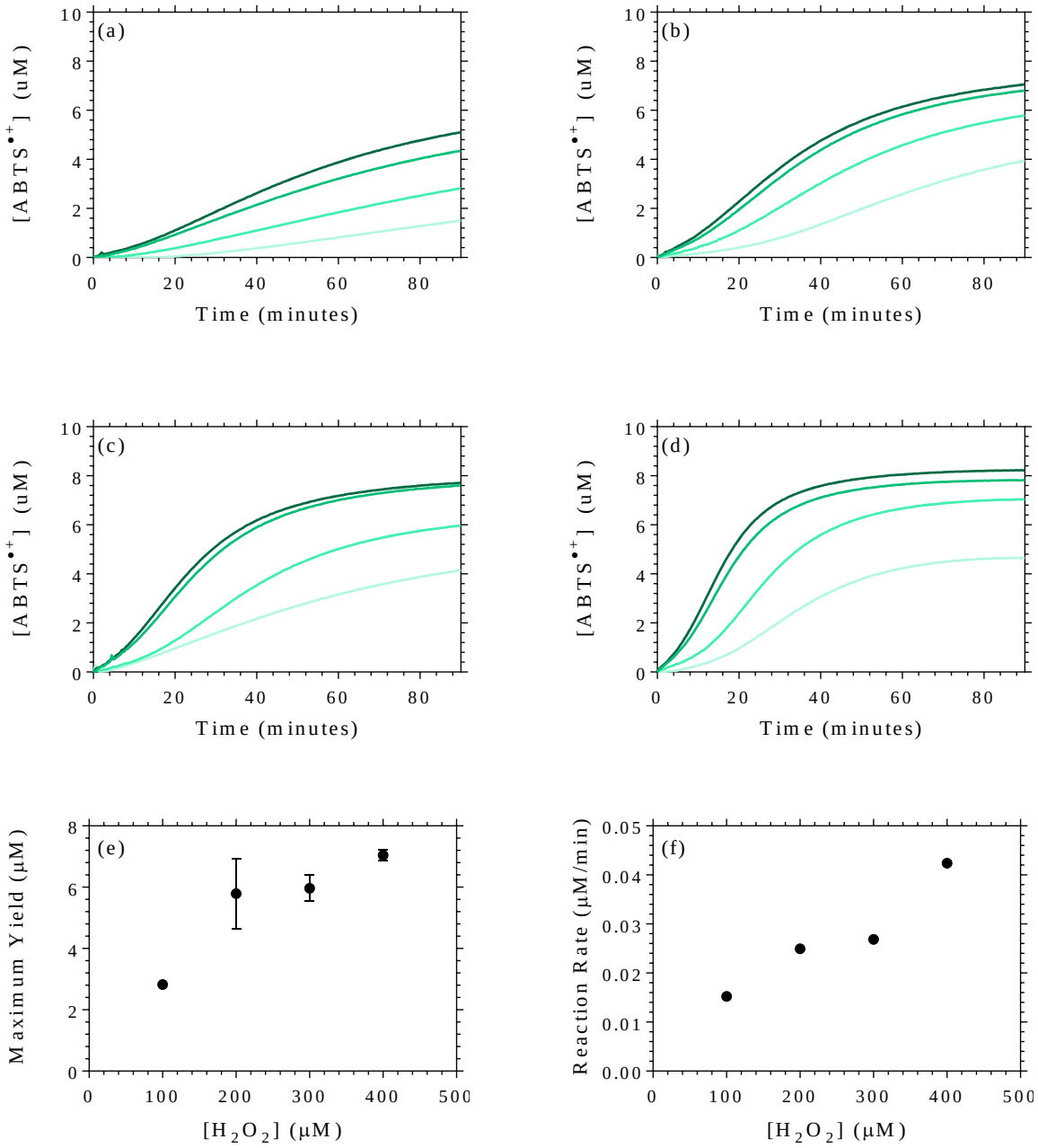

Figure 5.10 The effect of H_2O_2 concentration on ABTS oxidation by the QD-Fe(III)PPIX complex in aqueous SDS solution. The conditions are **(a)** 100.0, **(b)** 200.0, **(c)** 300.0 and **(d)** 400.0 µM H_2O_2 in the presence of 3.0 mM ABTS and 1.0 (-), 1.3 (-), 2.0 (-) and 2.5 (-) µM Fe(III)PPIX. **(e)** The maximum yield, calculated as the maximum concentration of $ABTS^{\bullet+}$ reached within the 90 minute time period, and **(f)** the overall reaction rate, is plotted as a function of H_2O_2 concentration. The conditions were 1.0 µM QD-Fe(III)PPIX and 3.0 mM ABTS. Data points omitted for clarity.

In Chapter 3, attempts were made to determine the association constants for the interaction between Fe(III)PPIX and artesunate. The association constant could, however, only be determined in acetonitrile, owing to the very weakened interaction of Ar with Fe(III)PPIX in the aqueous and aqueous SDS systems. Based on an earlier study by Adams and Berman, a concentration of 1.0 mM artesunate was utilised in all

experiments.[135] Owing to limited material, the experiments concerning artesunate were only performed once, and not in duplicate as described for the previous experiments. In addition, given the limited availability of artesunate, the kinetics of ABTS oxidation were only investigated in the aqueous SDS system. This solvent system was specifically selected based on the results obtained in Chapter 4, where improved stability of both Fe(III)PPIX and ABTS was observed under these conditions. As a consequence, the results presented below should be considered preliminary until further replicates are conducted to validate the findings.

A comparison of ABTS radical production by Fe(III)PPIX and its complexes with CQ, QD and Ar can be seen in Figure 5.11. The yield of radical production was taken as the maximum concentration of $ABTS^{\cdot+}$ produced over a period of 90 minutes. In contrast to the reaction catalysed by the complexes of Fe(III)PPIX with CQ and QD, Ar shows a marked increase in the overall rate of the reaction when compared to Fe(III)PPIX alone. In addition, the yield of the reaction in the presence of Ar is 30% greater. This result is similar to that obtained by Adams and Berman, who investigated the peroxidasic activity of Fe(III)PPIX at 30 °C and pH 7.4 in the presence of artemisinin.[135] Under these conditions they found that artemisinin enhanced the peroxidase activity of Fe(III)PPIX by the same amount as seen in the current work. The difference in the structure of the antimalarial drugs may therefore account for the differences encountered in the oxidation of ABTS on account of the presence of an endoperoxide bridge in the structure of Ar, which is absent in the quinoline antimalarial drugs. The individual data sets for the H_2O_2 concentration study in the presence of Ar (Figure 5.12) indicate a direct relationship between the yield of $ABTS^{\cdot+}$ and the concentrations of Fe(III)PPIX (up to 1.3 µM). Furthermore, a plot of the maximum yield and the overall reaction rate (Figure 5.12 (e) and (f), respectively) indicate a direct relationship to the concentration of H_2O_2. Interestingly, an enlargement of the first five minutes of the reaction reveals a lag phase similar to that described for QD in aqueous SDS solution (Figure 5.13). Whether this lag phase is related to complex formation between Fe(III)PPIX and Ar is not clear. It should also be considered that, since Ar contains and endoperoxide bridge, it itself may compete with H_2O_2 to form the oxidising species with Fe(III)PPIX.

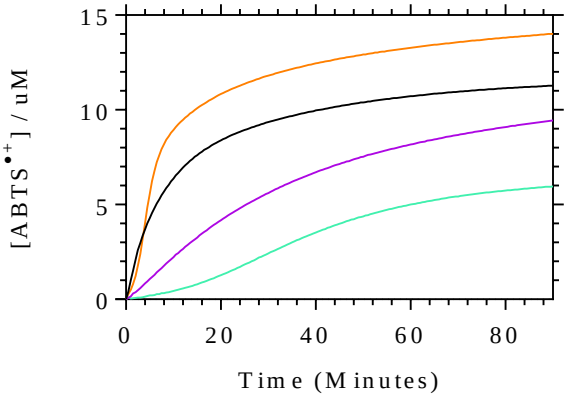

Figure 5.11 $ABTS^{\bullet+}$ production in the absence and presence of antimalarial drugs in the aqueous SDS system. The conditions are 1.0 µM Fe(III)PPIX (-), CQ- (-), QD- (-) and Ar-Fe(III)PPIX (-), 3.0 mM ABTS and 300.0 µM H_2O_2. Data points omitted for clarity.

Table 5.6 A summary of the observed rate constants (k_{obs}) (×10^{-4} µM/s), calculated using a one-phase exponential function, and yield obtained for the oxidation of ABTS by Fe(III)PPIX, CQ-Fe(III)PPIX, QD-Fe(III)PPIX and Fe(III)PPIX-Ar for the reaction described in Figure 5.10.

Species	k_{obs}	Maximum Yield (µM)
Fe(III)PPIX	11.2 ± 0.2	11.28 ± 0.04
CQ-Fe(III)PPIX	4.41 ± 0.01	9.44 ± 0.01
QD-Fe(III)PPIX	2.15 ± 0.43	5.6 ± 0.4
Ar-Fe(III)PPIX	14.9 ± 0.43	14.01 ± 0.06

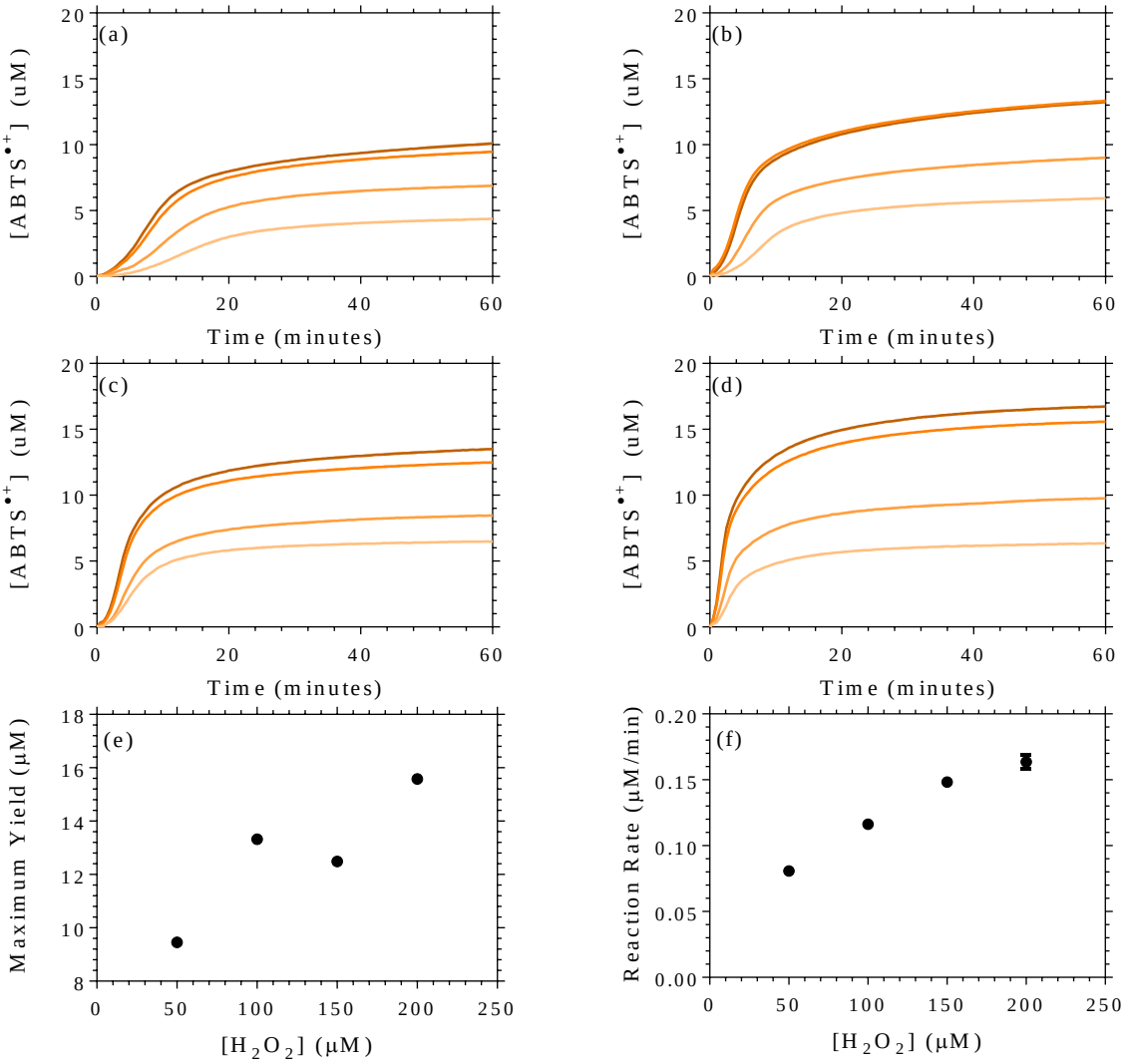

Figure 5.12 The effect of H_2O_2 on ABTS oxidation catalysed by Ar-Fe(III)PPIX in aqueous SDS. The conditions are **(a)** 100.0, **(b)** 200.0, **(c)** 300.0 and **(d)** 400.0 µM H_2O_2 in the presence of 3.0 mM ABTS, 1.0 mM Ar and 0.3 (-), 0.6 (-), 1.0 (-) and 1.3 (-) µM Fe(III)PPIX. **(e)** The maximum yield, calculated as the maximum concentration of $ABTS^{\bullet+}$ reached within the 90 minute time period, and **(f)** the overall reaction rate is plotted as a function of H_2O_2 concentration. The conditions were 1.0 µM Fe(III)PPIX, 1.0 mM Ar and 3.0 mM ABTS. Data points omitted for clarity.

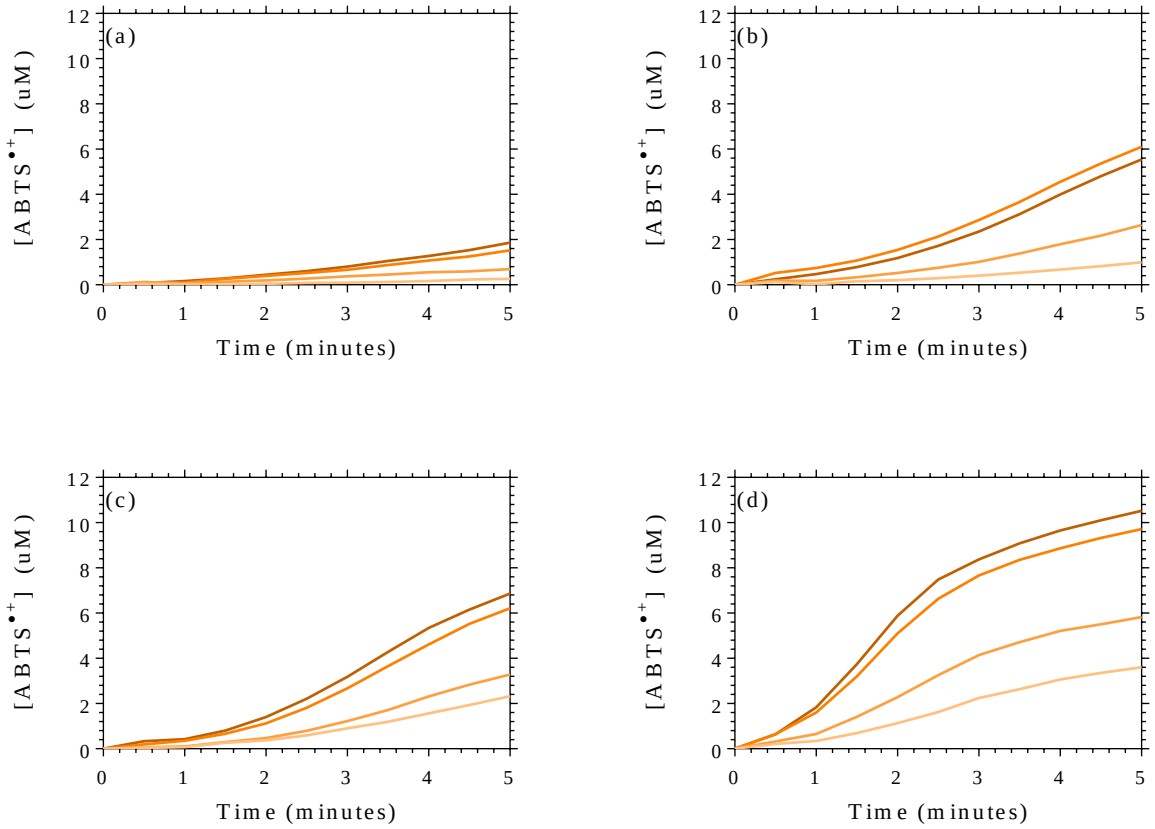

Figure 5.13 The oxidation of ABTS by Ar-Fe(III)PPIX. An enlargement of the first five minutes of the oxidation of ABTS in the presence of At-Fe(III)PPIX. The conditions are **(a)** 100.0, **(b)** 200.0, **(c)** 300.0 and **(d)** 400.0 µM H_2O_2 in the presence of 3.0 mM ABTS, 1.0 mM Ar and 0.3 (-), 0.6 (-), 1.0 (-) and 1.3 (-) µM Fe(III)PPIX. Data points omitted for clarity.

5.4 Discussion

The idea that antimalarial drugs contribute to the toxicity of Fe(III)PPIX has been in question for several years.[93] In Chapter 4, Fe(III)PPIX was shown to successfully catalyse the oxidation of ABTS. This chapter aimed to investigate whether the complexes formed between Fe(III)PPIX and the antimalarial drugs CQ, QD and Ar (previously investigated in Chapter 3) affected the peroxidase activity of Fe(III)PPIX and, in this way, better understand the mechanism of action of these well-known antimalarial drugs. Both CQ and QD have been implicated in the inhibition of haemozoin formation, increasing the amount of free Fe(III)PPIX present. The question is thus whether these antimalarial drugs enhance the toxicity brought about by Fe(III)PPIX, resulting in the overall death of the parasite. However, as discussed in Chapter 1, the mechanism of action of Ar is not fully understood.

Interestingly, in the current work there was a significant change in the kinetics of ABTS oxidation in the presence of CQ with a 30% decrease in reaction rate in aqueous solution (Figure 5.8). A similar observation was made by Ribeiro *et al.* who suggested that this decrease in efficiency arises from the additional decrease in percentage monomeric Fe(III)PPIX as a result of dimer association with CQ.[134] This proposal is indeed valid given the recent report that CQ induces the Fe(III)PPIX μ-oxo dimer in purely aqueous solution. Since this species consists of two Fe(III)PPIX monomers coordinated through an oxygen atom (Fe-O-Fe),[123] the strong interaction of the iron centre with oxide ligand may thus be the reason for the weakened catalytic activity of Fe(III)PPIX. As discussed in Chapter 4, an increase in the concentration of dimeric Fe(III)PPIX has been reported to have a negative effect on its catalytic ability. These results suggest that CQ does not enhance the peroxidase activity of Fe(III)PPIX but rather inhibits it, a phenomenon that has previously been suggested by other authors.[134,138] Riberio *et al.* suggest that although CQ appears to diminish the peroxidase activity of Fe(III)PPIX, it may play a role in protecting the catalyst from degradation.[134] The authors have proposed that CQ may shield Fe(III)PPIX from degradation through association, thereby increasing the amount of free Fe(III)PPIX available to interact with membranes and other target cells in the parasite and, in turn, increase the oxidative stress brought about by Fe(III)PPIX within the malaria parasite. The findings in the current work largely support this hypothesis where the interaction between Fe(III)PPIX and H_2O_2 was found to be significantly slower in the presence of the CQ than in its absence. Further evidence for this can be seen in Figure 5.5 which shows and extended life of the catalytically active iron species in the presence of CQ.

The reaction catalysed by the CQ-Fe(III)PPIX complex showed a 60% decrease in the reaction yield. This corresponds to approximately half the radical production obtained in the absence of drug. In Chapter 4 the mechanism of $ABTS^{\cdot+}$ production was described as the production of two molecules of $ABTS^{\cdot+}$ per molecule of H_2O_2 (see scheme 5.2). The reduction by half in the presence of CQ could be related to the absence of the second step of the reaction. This may thus suggest that the oxo-iron(IV)-porphyrin radical cation (II in scheme 5.2) is formed in the case of Fe(III)PPIX alone, while the oxo-iron (IV)-porphyrin cation

(III in scheme 5.2) and not the radical species is produced when CQ is present. The same trend was observed in the presence of QD. In addition, the rate of formation of the catalytically active complex is also markedly slower in the presence of QD in comparison to CQ. Since this is the primary step of the ABTS oxidation reaction, the generation of $ABTS^{\cdot+}$ will not commence until this species has been formed.

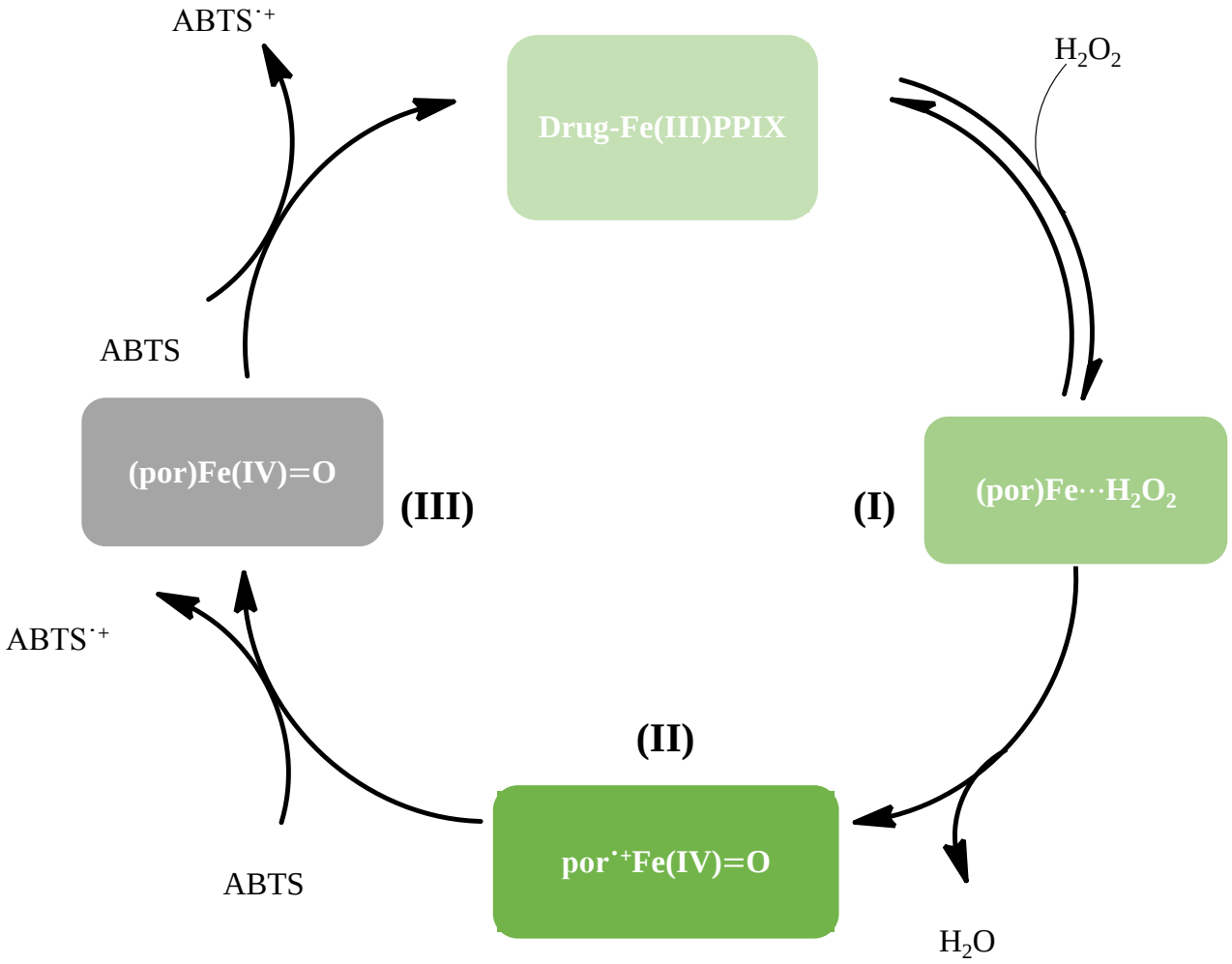

Scheme 5.2 The simplified catalytic cycle for the oxidation of ABTS in which Fe(III)PPIX reacts with H_2O_2 to form a Fe(III)PPIX-peroxo species **(I)**, which rapidly converts to the catalytically active Fe(IV) porphyrin radical cation **(II)**. Compound (**II**) can then oxidise one molecule of ABTS to produce $ABTS^{\cdot+}$ and an oxo iron (IV) porphyrin species **(III)** which in turn can oxidise a second molecule of ABTS and regenerate Fe(III)PPIX.[134] Antimalarial drugs interacting with Fe(III)PPIX may cause a disruption in this process.

The influence of the antimalarial drugs, CQ and QD on the peroxidase activity of Fe(III)PPIX in a lipid-like environment has not previously been reported. Interestingly, when the peroxidase activity of the complexes of Fe(III)PPIX with CQ and QD was investigated in 1.0 mM SDS, differences arose in the kinetics of ABTS oxidation. Similar to the work done in Chapter 4, the overall reaction rate of ABTS oxidation, was slower in the aqueous SDS system than in aqueous solution for the reaction catalysed by the CQ- and QD-Fe(III)PPIX complexes. Interestingly, when the reaction was catalysed by the QD-Fe(III)PPIX complex, the first 10

minutes of the reaction appeared to consist of a lag phase, absent in the oxidation of ABTS catalysed by Fe(III)PIX and its complex with CQ. A closer analysis of the association constants obtained in Chapter 3 shows a slight increase in the strength of association between Fe(III)PPIX and QD in the aqueous SDS system (6.2 ± 0.1) when compared to the aqueous system (5.78 ± 0.09). The association constant for the interaction of Fe(III)PPIX with CQ is not considerably different to that of QD in the aqueous SDS solution and, therefore, it would suggest that the lag phase observed in the presence of QD is related to the type of interaction that occurs between Fe(III)PPIX and these two classes of antimalarial drugs. This, in turn, will have an influence on the rate of formation of the catalytically active Fe(III)PPIX species and, consequently, formation of $ABTS^{\cdot+}$. One of the more interesting observations in the aqueous SDS system, however, was the yield of $ABTS^{\cdot+}$ produced in the presence of the drugs CQ and QD. In aqueous solution, the ABTS oxidation reaction catalysed by the complexes of Fe(III)PPIX with CQ and QD showed a reduction of approximately 60% in the yield of $ABTS^{\cdot+}$ production when compared to the reaction catalysed by Fe(III)PPIX. In the aqueous SDS system, however, the yield of $ABTS^{\bullet+}$ production was relatively unchanged in the presence of CQ. These results may provide evidence for enhanced radical production by the CQ-Fe(III)PPIX complex in an environment mimicking the lipid-water interface. Alternatively, these results may indicate that, while the Fe(IV) cation radical may not be formed in aqueous solution, SDS may facilitate the formation of the Fe(IV) cation radical in the case of CQ. In Chapter 4 it was found that Fe(III)PPIX is more stable in the aqueous SDS system and, as a result, radical production is prolonged under these conditions. This could provide reasons for the improvement in ROS generation for the reaction catalysed by the CQ-Fe(III)PPIX complex in the aqueous SDS system.

Studies have proposed that the mechanism of action of the antimalarial drug CQ involves the accumulation of the complex formed between Fe(III)PPIX and CQ, which results in an increase in oxidative stress and subsequent death of the parasite.[83,165] In contrast to this, however, several authors have reported a reduction in the oxidative stress of the parasite in the presence of CQ, in agreement with the work described in this chapter. Monti *et al*. discussed the potential for CQ to contribute to the oxidative stress of the parasite.[166] Their argument was based on experiments in which they found that the activity of CQ was independent of the degree of oxygen tension in the parasite culture, which contradicts the proposal that CQ acts through oxidative stress.[167] In addition to this, they found that CQ reduced, rather than enhanced β-haematin-induced lipid peroxidation, in agreement with the findings in current work.[167] Similar to what has been described in the current work as well as by Ribeiro *et al*, the inhibition of the peroxidative degradation of Fe(III)PPIX has been attributed to the mechanism of action of chloroquine in a separate study.[137] As CQ has been the mainstay antimalarial drug for several years, the focus of these studies have been on the effect that this drug has on the toxicity of Fe(III)PPIX. Investigations into the peroxidase activity of Fe(III)PPIX in the presence of QD and related antimalarial drugs has not been reported. In a study by Adams, QN was reported to have similar inhibitory effects on the peroxidase activity as was described, although the details of this were not included in the publication.[138] Both CQ and QD have been shown to inhibit the peroxidase activity of Fe(III)PPIX, however, as discussed, the drugs may act by inducing a proliferation in the amount of

Fe(III)PPIX molecules present in the cell which, due to the toxic nature of Fe(III)PPIX discussed in Chapter 4, could result in parasite death. This has recently been shown to play a vital role in determining the cytotoxic effect of antimalarial drugs.[168] In a follow up study by Ribeiro *et al.*, the influence of quinoline antimalarial drugs on the catalase activity of Fe(III)PPIX was investigated.[136] The catalase reaction, previously discussed in Chapter 4, describes the disproportionation of H_2O_2 to oxygen and water. The authors found that both CQ and QD substantially inhibited the catalase activity of Fe(III)PPIX which, consequently, inhibits the antioxidant activity by increasing the concentration of H_2O_2 in the cell, and is detrimental to the parasite. This, together with the apparent ability of these drugs to shield Fe(III)PPIX from degradation, provides alternative interpretations for their antimalarial activity.

The association studies involving the species formed between Fe(III)PPIX and artesunate in aqueous SDS solution could not be determined under the conditions described in Chapter 3. For this reason, the concentration of artesunate required to ensure association with Fe(III)PPIX could not be accurately determined. In the current work, it was decided to use a concentration of 1.0 mM artesunate in all experiments, based on conditions previously described in a study by Adams and Berman.[135] When the oxidation of ABTS was carried out under these conditions, the rate of the oxidation reaction showed a marked increase in the presence of artesunate when compared to the reaction catalysed by the quinoline antimalarial drugs as well as Fe(III)PPIX with a five-fold increase in toxicity. This result differs completely from those obtained for the quinoline antimalarial drugs CQ and QD and hints to a different mechanism of action of this drug or, in addition, a different interaction with Fe(III)PPIX. The different mechanism of action was also alluded to in Chapter 3, where the association constant for the interaction between Fe(III)PPIX and artesunate could not be determined in the manner described for CQ and QD. The study by Adams and Berman reported similar results, with a three-fold increase in the yield of radical production in the presence of artemisinin.[135] The change in the mechanism of action is thought to be related to the structural difference of Art in comparison with the quinoline antimalarial drugs. More specifically, the mechanism of action of artemesinin has been closely related to the endoperoxide bridge present in its structure.[169] As this work has shown, peroxides are able to take part in several reactions involved in the generation of ROS, thereby resulting in the death of the parasite. The question of how the endoperoxide bridge breaks to form ROS has been a matter of great interest. The possible formation of an artemisinin-Fe(III)PPIX adduct through alkylation has already been discussed in Chapter 3. Another alternative is that Art forms a complex with Fe(III)PPIX by interacting with the iron centre, similar to the reaction between Fe(III)PPIX and H_2O_2. A study by Adams investigated the kinetics of the formation of a complex between Fe(III)PPIX and artesunate in a 25% aqueous DMSO solvent system, where Fe(III)PPIX is known to exist in a monomeric form.[138] They reported distinct spectroscopic changes including a decrease in absorbance at 399 nm together with an increase in absorbance at 424 nm. In the current work, the interaction between Fe(III)PPIX and H_2O_2 in the presence of Ar shows similar changes in the spectrum as was seen in Chapter 4 for the reaction in the absence of artesunate. The rate of formation of the purported Fe(III)PPIX-peroxo species under the conditions described was also unchanged in the presence of artesunate. In addition, the rate of decomposition

of the catalytic species is slower in the presence of Ar, which indicates that radical production is more prolonged in the presence of artesunate. Consequently, in similarity to the quinoline antimalarial drugs, the presence of Ar may too increase the amount of free Fe(III)PPIX present within the parasite, thereby posing a toxic threat to the parasite.

Overall, these results provide evidence for improved stability of the Fe(III)PPIX in the aqueous SDS system. In addition to this, ROS generation catalysed by the complexes of Fe(III)PPIX with CQ and QD proved to be more pronounced in an environment that mimics the lipid-water interface in comparison to that in aqueous solution. This contributes to the proposal that the antimalarial drugs exert their toxicity in a lipid-like environment, however, the exact mechanism of action is still not confirmed. The significant reduction of Fe(III)PPIX decay in the presence of CQ and QD lend favour to the idea that these drugs increase the amount of free Fe(III)PPIX in the parasite and provide an improved stability under oxidative conditions. Ar appears to also provide greater stability to Fe(III)PPIX, however, by contrast to CQ and QD, is able to increase radical production leading to a more toxic effect. Whether the enhanced ROS generation results from the covalent adduct formed between Fe(III)PPIX and Ar or an interaction between Ar and the iron centre cannot be confirmed, however, it is most likely that one aspect of the mechanism of action of Ar is brought about by the generation of ROS within the parasite which, subsequently, leads to parasite death. The often contradictory results reported in the literature may arise from the variability with respect to reaction conditions. Indeed, the current work has shown differences in findings obtained in the aqueous and aqueous SDS solvent systems. Furthermore, many authors have conducted experiments using buffers that are incompatible with ABTS. [128,134] These observations highlight that thorough consideration of experimental conditions of the ABTS system must be undertaken when performing such investigations.

5.5 Conclusion

The antimalarial drugs CQ, QD and Ar were investigated for their influence on the peroxidase activity of Fe(III)PPIX in aqueous solution as well as in a lipid mimic. The environment in which the experiment was conducted was found to greatly affect the degree of ROS generation. It is also important to note that while the aqueous SDS system is a mimic for the environment at the lipid-water interface, these results are not sufficient to determine the exact nature of ROS generation within the malaria parasite. However, preliminary results would indicate that, while QD and CQ were shown to inhibit the peroxidase activity of Fe(III)PPIX in aqueous solution, when the reaction was carried out in the aqueous SDS system, the yield of radical production proved to be unaffected in the presence of CQ. These results together with the improved stability of Fe(III)PPIX under these conditions lend favour to the proposal that the site of action of quinoline antimalarial drugs is at the lipid-water interface within the parasite. The mechanism of action of CQ and QD was, therefore, not found to be a result of enhancing the peroxidase activity of Fe(III)PPIX, however, it was determined that they act by shielding Fe(III)PPIX from peroxidative degradation, thereby increasing the build-up of toxic Fe(III)PPIX within the parasite. The mechanism of action of Ar was, however, found to involve its ability to enhance the peroxidase activity of Fe(III)PPIX by approximately three times that produced by Fe(III)PPIX. The results determined in this body of work provide interesting information with regard to the mechanism of action of three clinically relevant antimalarial drugs which differ in structure. To further our knowledge of antimalarial drug action, the study needs to be expanded to include related antimalarial drugs and, from this, determine a trend in the effect of these drugs on the peroxidase activity of Fe(III)PPIX.

Chapter 6. Overall Conclusion and Future Work

6.1 Overall Conclusion

The work presented in this dissertation was underpinned by the hypothesis that quinoline antimalarial drugs act by inhibiting haemozoin formation, thereby increasing the concentration of Fe(III)PPIX present in the parasite which, in turn, enhances the oxidative stress on the parasite. Consequently, the main aim of the project was to investigate the peroxidase activity of Fe(III)PPIX under biologically relevant conditions and to compare this effect with that of Fe(III)PPIX in the presence of the clinically relevant antimalarial drugs, CQ, QD and Art. The aim was approached by first investigating the interaction between Fe(III)PPIX and the antimalarial drugs, CQ, QD and Art. Experiments were conducted using spectrophotometric titrations in three different biologically relevant environments, namely an aqueous solution (pH 7.4) which was used to mimic the environment found within the parasite cytosol; an organic environment comprised of acetonitrile representing the non-aqueous lipid; and finally, the detergent SDS was used to mimic the lipid-water interface which is the proposed site of β-haematin formation. The results obtained provided evidence for coordination between Fe(III)PPIX and QD in acetonitrile but not in the aqueous or aqueous SDS environments. Coordination did not occur between CQ and Fe(III)PPIX but, rather, π-stacking between the drug and the Fe(III)PPIX μ-oxo dimer is suggested. Nevertheless, the association between Fe(III)PPIX and QD and CQ was strong in both aqueous and aqueous SDS environments. In contrast, the association constant between Fe(III)PPIX and Art was much weaker and could only be quantified in acetonitrile.

The peroxidase activity of Fe(III)PPIX which is a standard measure for Fe(III)PPIX toxicity was next investigated in order to establish whether antimalarial drugs enhance this effect. This was investigated using the chromogenic substrate ABTS and an assay optimised to investigate the peroxidase activity of Fe(III)PPIIX. This work confirmed Fe(III)PPIX to be toxic owing to its ability to oxidise ABTS in the absence of any antimalarial drugs. The oxidation of ABTS by H_2O_2 and catalysed by Fe(III)PPIX was investigated by systematically varying the concentration of each component in the system. The results obtained in this study were then used to optimise the assay in the aqueous SDS system. The reaction was found to be 50% slower in the aqueous SDS system than in the aqueous system, however, the delay in the rate was accompanied by an increase in the stability of $ABTS^{\cdot+}$ and was therefore determined to be the more suitable environment in which to measure ABTS oxidation. This decrease in rate could be accounted for by the reduced rate of the reaction between Fe(III)PPIX and H_2O_2, proposed as the primary step in ABTS oxidation. Whether this enhanced stability can be directly related to the ROS generation at the lipid-water interface is not known and would require further investigation. Attempts were made to develop a kinetic

model describing the full oxidation of ABTS by Fe(III)PPIX and H_2O_2 in aqueous solution, however, the complexity of the reaction prevented a successful fitting of a model to the data.

The study on the oxidation of ABTS by Fe(III)PPIX was subsequently used as a baseline to measure the modulatory effects of the antimalarial drugs CQ, QD and Ar on the peroxidase activity of Fe(III)PPIX. In aqueous solution, CQ was shown to reduce the reaction rate by 30% and the yield by 60% while QD was found to inhibit the yield by 80%. An analysis of the rate of the reaction between Fe(III)PPIX and H_2O_2 in the presence of the antimalarial drugs revealed a reduction in rate compared to Fe(III)PPX in the absence of drug. This may suggest that the antimalarial drugs shield Fe(III)PPIX from peroxidative attack and, in this way, increase the concentration of free Fe(III)PPIX present within the parasite which ultimately leads to parasite death. Support for this hypothesis was found when the concentration of the catalytically active iron species was found to be elevated for longer periods in the presence of both CQ and QD when compared to Fe(III)PPIX.

A similar result was obtained in aqueous SDS. Although CQ still inhibited the rate of $ABTS^{\cdot+}$ radical formation, the yield remained unchanged when compared to the reaction catalysed by Fe(III)PPIX in the absence of antimalarial drug. This data further suggests the enhanced stability of $ABTS^{\cdot+}$ in this environment. Interestingly, QD exhibited a lag phase during the initial stage of the reaction, absent in the reaction conducted in the presence of CQ and in the absence of drug. This could be related to the nature of the drug-Fe(III)PPX interaction in the case of QD (coordination) compared to CQ (π-stacking). Contrary to both CQ and QD, however, Ar was found to increase both the rate and the yield of $ABTS^{\cdot+}$ formation in aqueous SDS. This could be related to the structure of this antimalarial drug which contains an endoperoxide bridge, similar in structure to H_2O_2. The mode of action of Ar therefore differs from that of CQ and QD in that it enhances the peroxidase activity of Fe(III)PPIX, thereby increasing the oxidative stress on the parasite, leading to its ultimate death.

Overall, this research project provides some insight into the mechanism of toxicity of Fe(III)PPIX together with its complexes formed with CQ, QD and Art. Important information regarding the manner in which Fe(III)PPIX and H_2O_2 oxidise ABTS in aqueous solution was gleaned. Further investigations into the side reactions would allow the development of a full kinetic model. This work presents an additional avenue that should be considered in future drug design. These drugs do not only inhibit β-haematin formation, but also increase Fe(III)PPIX toxicity. This additional factor is likely to have an effect on the efficacy of drugs. These findings therefore suggest that optimization of the effects of drug-Fe(III)PPIX complex toxicity also be considered when designing new compounds with the potential for antimalarial activity. The findings here serve as a preliminary indication of this, but further in depth studies regarding the mechanism of toxicity is warranted.

6.2 Future Work

The work in Chapter 3 focusses on investigating the interaction between Fe(III)PPIX and the antimalarial drugs, CQ, QD and Art. Information regarding the strength of association between Fe(III)PPIX and these antimalarial drugs was gleaned from this study, however, the following future studies are suggested:

1. To investigate the interaction between Fe(III)PPIX and Art using additional spectroscopic techniques such as NMR and IR spectroscopy.
2. To investigate a broader range of antimalarial drugs, particularly in the aqueous SDS system, to determine the effect on the strength of association in an environment mimicking the site of β-haematin formation.

While the work in Chapter 4 provides insight into the mechanism of ABTS oxidation by Fe(III)PPIX and H_2O_2 in an aqueous and aqueous SDS environment, the following future studies are proposed to further our understanding:

3. To investigate the suggested interaction between Fe(III)PPIX and ABTS in order to simulate it and obtain an accurate kinetic model for the oxidation of ABTS by Fe(III)PPIX and H_2O_2.
4. To investigate the oxidation of ABTS using lipids and phospholipids in order to determine the effect that this has on the oxidation of ABTS.

The oxidation of ABTS by Fe(III)PPIX and H_2O_2 was used as a baseline to measure the modulatory effect of the antimalarial drugs CQ, QD and Art on the peroxidase activity of Fe(III)PPIX in Chapter 5. This study provided insight into the mechanism of toxicity of these antimalarial drugs, however, the following future studies are proposed to further our understanding:

5. To investigate the ABTS oxidation reaction in the presence of Art in an aqueous environment, mimicking that of the parasite cytosol.
6. To model the kinetic data obtained in this study and, therefore, determine what effect the antimalarial drugs have on the proposed kinetic model for the oxidation of ABTS.
7. To investigate a broader range of antimalarial drugs so as to determine whether a trend exists amongst antimalarial drugs belonging to the same class.

Appendix 1

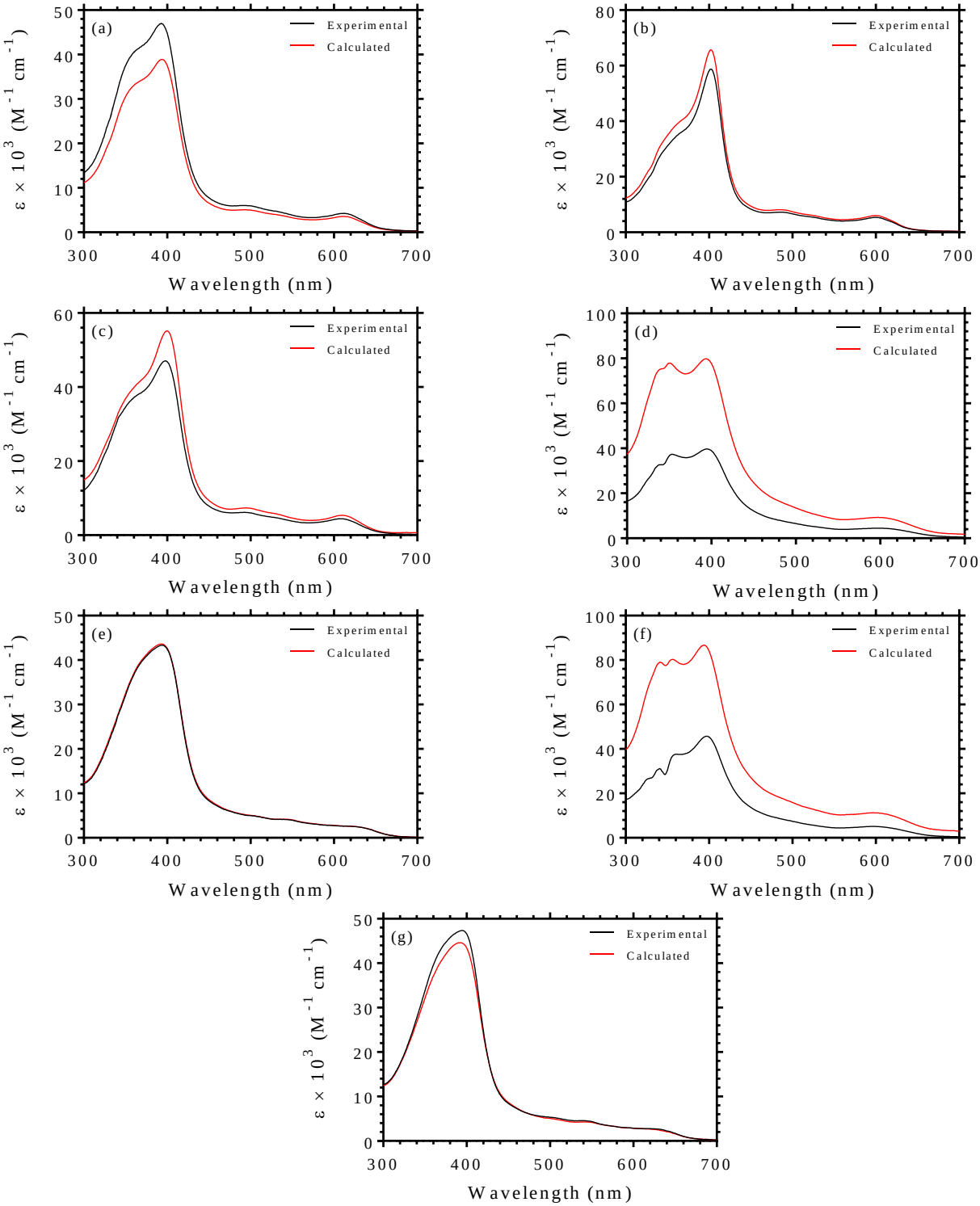

Figure 1. The calculated (black) and experimental spectra obtained for the association of Fe(III)PPIX with QD in (a) aqueous, (b) acetonitrile, (c) aqueous SDS, CQ in (d) aqueous, (e) acetonitrile, (f) aqueous SDS and Art in (f) acetonitrile.

Appendix 2

Derivation of equation 5.4.[164]

Considering the reaction:

$$A \xrightarrow{k_1} B \xrightarrow{k_2} C$$

The reaction rates can therefore be described as follows:

$$\frac{d[A]}{dt} = -k_1[A]$$

$$\frac{d[B]}{dt} = k_1[A] - k_2[B]$$

$$\frac{d[C]}{dt} = k_2[B]$$

Since at the beginning of the experiment only A is present, it follows that:

$$\int_{A_0}^{A} \frac{d[A]}{[A]} = -\int_0^t k_1 dt$$

And

$$\ln[A] = \ln[A_0] - k_1 t$$

Alternatively, the reaction can be written as:

$$[A] = [A_0]e^{-k_1 t}$$

Substitution into equation 3 gives the following expression:

$$\frac{d[B]}{dt} + k_2[B] = k_1[A_0]e^{-k_1 t}$$

Where this first order differential has the solution:

$$[B] = \frac{[A_0]k_1}{(k_2 - k_1)} e^{-k_1 t} - e^{-k_2 t}$$

Chapter 7. References

1. J.-J. Chen, R. N. V. S. Suragani, H. Ding, B. D. Sumer, J. Gao, F. Gao, L. Zhang, Y. Li, R. Sessoms, D. P. Huynh, A. Arvey, C. Leslie, T. Chernova and A. G. Smith, *Heme Biology: The Secret Life of Heme in Regulating Diverse Biological Processes.*, World Scientific, 2011.
2. K. Li, Y. Li, J. M. Shelton, J. A Richardson, E. Spencer, Z. J. Chen, X. Wang and R. S. Williams, *Cell*, 2000, **101**, 389–399.
3. M. D. Maines, *Annu. Rev. Pharmacol. Toxicol*, 1997, **37**, 517–54.
4. I. G. Denisov, T. M. Makris, S. G. Sligar and I. Schlichting, *Chem. Rev.*, 2005, **105**, 2253–2277.
5. G. A. Ordway and D. J. Garry, *J. Exp. Biol.*, 2004, **207**, 3441–3446.
6. S. Ramakrishnan, K. G. Prasannan and R. Rajan., *Textbook of Medical Biochemistry*, Orient Longman, Madras, 3rd edn., 1990.
7. F. C. Bernstein, T. F. Koetzle, G. J. B. Williams, E. F. Meyer, M. D. Brice, J. R. Rodgers, O. Kennard, T. Shimanouchi and M. Tasumi, *Arch. Biochem. Biophys.*, 1978, **185**, 584–591.
8. P. Rowland, F. E. Blaney, M. G. Smyth, J. J. Jones, V. R. Leydon, A. K. Oxbrow, C. J. Lewis, M. G. Tennant, S. Modi, D. S. Eggleston, R. J. Chenery and A. M. Bridges, *J. Biol. Chem.*, 2006, **281**, 7614–7622.
9. Y. Xu, Y. Zheng, J.-S. Fan and D. Yang, *Nat. Methods*, 2006, **3**, 931–937.
10. P. Ponka, *Am. J. Med. Sci.*, 1999, **318**, 241–256.
11. S. Kumar and U. Bandyopadhyay, *Toxicol. Lett.*, 2005, **157**, 175–188.
12. M. A. Arruda, A. G. Rossi, M. S. de Freitas, C. Barja-Fidalgo and A. V Graça-Souza, *J Immunol*, 2004, **173**, 2023–2030.
13. G. Balla, G. M. Vercellotti, U. Muller-Eberhard, J. Eaton and H. S. Jacob, *Lab. Invest.*, 1991, **64**, 648–655.
14. A. C. Chou and C. D. Fitch, *J. Clin. Invest.*, 1981, **68**, 672–677.
15. I. Kirschner-Zilber, E. Rabizadeh and N. Shaklai, *Biochim. Biophys. Acta*, 1982, **690**, 20– 30.
16. J. M. Gutteridge and A. Smith, *Biochem. J.*, 1988, **256**, 861–865.
17. T. H. Schmitt, W. A. Frezzatti and S. Schreier, *Arch. Biochem. Biophys.*, 1993, 307, 96–103.

18. M. Beppu, M. Nagoya and K. Kikugawa, *Chem. Pharm. Bull. (Tokyo).*, 1986, **34**, 5063.

19. S. H. Vincent, R. W. Grady, N. Shaklai, J. M. Snider and U. Muller-Eberhard, *Arch. Biochem. Biophys.*, 1988, **265**, 539–550.

20. V. Jeney, J. Balla, A. Yachie, Z. Varga, G. M. Vercellotti, J. W. Eaton and G. Balla, *Blood*, 2002, **100**, 879–887.

21. R. L. Aft and G. C. Mueller, *J. Biol. Chem.*, 1983, **258**, 12069–12072.

22. G. Minotti and S. D. Aust, *Chem. Phys. Lipids.*, 1987, **44**, 191–208.

23. P. R. Ortiz De Montellano, *Curr. Opin. Chem. Biol.*, 2000, **4**, 221–227.

24. V. F. Fairbanks, in *Manual of Clinical Hematology*, Lippincott Williams & Wilkins, Philadelphia, 3rd edn., 2002.

25. P. R. Ortiz de Montellano and A. Wilks, *Adv. Inorg. Chem.*, 2000, **51**, 359–407.

26. S. Shibahara, R. Müller, H. Taguchi and T. Yoshida, *Proc. Natl. Acad. Sci.*, 1985, **82**, 7865–7869.

27. L. Kořený, M. Oborník and J. Lukeš, *PLoS Pathog.*, 2013, **9**, e100308.

28. WHO 2016

29. F. E. Cox, *Parasit. Vectors*, 2010, **3**, 5.

30. P. Manson-Bahr, *Proc. R. Soc. Med.*, 1961, **54**, 91–100.

31. A. F. A. King, *Pop Sci*, 1883, **23**, 644–658.

32. B. Grassi, A. Bignami and G. Bastianelli., *Ulteriori ricerche sul ciclo dei parassiti malarici umani nel corpo del zanzarone.*, R. Accademia dei Lincei, 1898.

33. R. Tuteja, *FEBS J.*, 2007, **274**, 4670–4679.

34. D. J. Wyler, *Clin. Infect. Dis.*, 2016, **16**, 449–456.

35. J. M. Bautista, P. Marín-García, A. Diez, I. G. Azcárate and A. Puyet, *J. Proteomics*, 2014, **97**, 107–125.

36. A. F. Cowman and B. S. Crabb, *Cell*, 2006, **124**, 755–766.

37. N. T. Huy, Y. Shima, A. Maeda, T. T. Men, K. Hirayama, A. Hirase, A. Miyazawa and K. Kamei, *PLoS One*, 2013, **8**.

38. T. J. Egan, *Mol. Biochem. Parasitol.*, 2008, **157**, 127–136.

39. M. Krugliak, J. Zhang and H. Ginsburg, *Mol. Biochem. Parasitol.*, 2002, **119**, 249–256.

40. P. J. Rosenthal, J. H. McKerrow, M. Aikawa, H. Nagasawa and J. H. Leech, *J. Clin. Invest.*, 1988, **82**, 1560–1566.

41. R. Banerjee, J. Liu, W. Beatty, L. Pelosof, M. Klemba and D. E. Goldberg, *Proc. Natl. Acad. Sci. U. S. A.*, 2002, **99**, 990–995.

42. K. K. Eggleson, K. L. Duffin and D. E. Goldberg, *J. Biol. Chem.*, 1999, **274**, 32411–32417.

43. M. F. Oliveira, J. R. Silva, M. Dansa-Petretski, W. de Souza, U. Lins, C. M. Braga, H. Masuda and P. L. Oliveira, *Nature*, 1999, **400**, 517–518.

44. M. F. Oliveira, J. C. P. D'Avila, C. R. Torres, P. L. Oliveira, F. D. Rumjanek and W. De Souza, *Mol. Biochem. Parasitol.*, 2000, **111**, 217–221.

45. S. Pagola, P. W. Stephens, D. S. Bohle, a D. Kosar and S. K. Madsen, *Nature*, 2000, **404**, 307–310.

46. M. Chugh, V. Sundararaman, S. Kumar, V. S. Reddy and W. A. Siddiqui, *Proc. Natl. Acad. Sci.*, 2013, **110**, 1–6.

47. D. J. Sullivan, I. Y. Gluzman and D. E. Goldberg, *Science*, 1996, **271**, 219–222.

48. G. S. Noland, N. Briones and D. J. Sullivan, *Mol. Biochem. Parasitol.*, 2003, **130**, 91–99.

49. K. Bendrat, B. J. Berger and A. Cerami, *Nature*, 1995, **378**, 138–139.

50. C. D. Fitch, G-z. Cai, Y. F. Chen and J. D. Shoemaker, *Biochim. Biophys. Acta.*, 1999, **1454**, 31–37.

51. C. D. Fitch, G-z. Cai and J. D. Shoemaker, *Biochim. Biophys. Acta.*, 2000, **1535**, 45–49.

52. A. N. Hoang, K. K. Ncokazi, K. A. de Villiers, D. W. Wright and T. J. Egan, *Dalton Trans.*, 2010, **39**, 1235–44.

53. M. A. Ambele and T. J. Egan, *Malar. J.*, 2012, **11**, 337.

54. J. M. Pisciotta, I. Coppens, A. K. Tripathi, P. F. Scholl, J. Shuman, S. Bajad, V. Shulaev and D. J. Sullivan, 2007, **204**, 197–204.

55. S. Kapishnikov, A. Weiner, E. Shimoni, P. Guttmann, G. Schneider, N. Dahan-Pasternak, R. Dzikowski, L. Leiserowitz and M. Elbaum, *Proc. Natl. Acad. Sci.*, 2012, **109**, 11188–11193.

56. J. Achan, A. O. Talisuna, A. Erhart, A. Yeka, J. K. Tibenderana, F. N. Baliraine, P. J. Rosenthal and U. D'Alessandro, *Malaria. J.*, 2011, **10**, 144.

57. S. R. Meshnick and M. J. Dobson, *The History of Antimalarial Drugs*, Humana Press Inc., Totowa, NJ, 6th edn., 2001.

58. M. Foley, *Pharmacol. Ther.*, 1998, **79**, 55–87.

59. K. Krafts, E. Hempelmann and A. Skórska-Stania, *Parasitol. Res.*, 2012, **111**, 1–6.

60. P. F. Russell, *Man's Mystery of Malaria*, Oxford University Press, London, 1955.

61. D. L. Klayman, *Science*, 1985, **228**, 1049–1055.

62. S. R. Meshnick, *Int. J. Parasitol.*, 2002, **32**, 1655–1660.

63. P. Olliaro, *Pharmacol. Ther.*, 2001, **89**, 207–219.

64. P. L. Olliaro and Y. Yuthavong, *Pharmacol. Ther.*, 1999, **81**, 91–110.

65. J. Ziegler, R. Linck and D. W. Wright, *Stud. Nat. Prod. Chem.*, 2001, **25**, 327–366.

66. Y. Sugioka, M. Suzuki, K. Sugioka and M. Nakano, *FEBS Lett.*, 1987, **223**, 251–254.

67. P. M. O'Neill, V. E. Barton and S. A. Ward, *Molecules*, 2010, **15**, 1705–1721.

68. D. J. Krogstad, I. Y. Gluzman, D. E. Kyle, A. M. J. Oduola, S. K. Martin, W. K. Milhous, P. H. Schlesinger and P. H. Schlesinger, *Science*, 1987, **238**, 1283–1285.

69. A. Yayon, Z. I. Cabantchik and H. Ginsburg, *EMBO J.*, 1984, **3**, 2695–2700.

70. R. Hayward, K. J. Saliba and K. Kirk, *J. Cell Sci.*, 2006, **119**, 1016–1025.

71. T. J. Egan and D. Kuter, *Future Microbiol.*, 2013, **8**, 475–489.

72. R. L. Summers, M. N. Nash and R. E. Martin, *Cell. Mol. Life Sci.*, 2012, **69**, 1967–1995.

73. D. A. Fidock, T. Nomura, A. K. Talley, R. A. Cooper, S. M. Dzekunov, M. T. Ferdig, L. M. Ursos, A. B. Sidhu, B. Naudé, K. W. Deitsch, X. Z. Su, J. C. Wootton, P. D. Roepe and T. E. Wellems, *Mol. Cell*, 2000, **6**, 861–71.

74. A. Ecker, A. M. Lehane, J. Clain and D. A. Fidock, *Trends Parasitol.*, 2012, **28**, 504–514.

75. C. P. Sanchez, W. D. Stein and M. Lanzer, *Trends Parasitol.*, 2007, **23**, 332–339.

76. I. Petersen, S. J. Gabryszewski, G. L. Johnston, S. K. Dhingra, A. Ecker, R. E. Lewis, M. J. de Almeida, J. Straimer, P. P. Henrich, E. Palatulan, D. J. Johnson, O. Coburn-Flynn, C. Sanchez, A. M. Lehane, M. Lanzer and D. A. Fidock, *Mol. Microbiol.*, 2015, **97**, 381–395.

77. M. B. Reed, K. J. Saliba, S. R. Caruana, K. Kirk and a F. Cowman, *Nature*, 2000, **403**, 906–909.

78. A. F. Cowman, D. Galatis and J. K. Thompson, *Proc. Natl. Acad. Sci. U. S. A.*, 1994, **91**, 1143–7.

79. E. A. Ashley, M. Dhorda, R. M. Fairhurst, C. Amaratunga, P. Lim, S. Suon, S. Sreng *et al.*, *N. Engl. J. Med.*, 2014, **371**, 411–423.

80. T. J. Egan, D. C. Ross and P. A. Adams, *FEBS Lett.*, 1994, **352**, 54–57.

81. A. Dorn, S. R. Vippagunta, H. Matile, C. Jaquet, J. L. Vennerstrom and R. G. Ridley, *Biochem. Pharmacol.*, 1998, **55**, 727–736.

82. A. F. Slater, W. J. Swiggard, B. R. Orton, W. D. Flitter, D. E. Goldberg, A. Cerami and G. B. Henderson, *Proc. Natl. Acad. Sci. U. S. A.*, 1991, **88**, 325–329.

83. J. M. Combrinck, T. E. Mabotha, K. K. Ncokazi, M. A. Ambele, D. Taylor, P. J. Smith, H. C. Hoppe and T. J. Egan, *ACS Chem Biol*, 2013, **8**, 133–137.

84. R. Buller, M. L. Peterson, Ö. Almarsson and L. Leiserowitz, *Cryst. Growth Des.*, 2002, **2**, 553–562.

85. S. B. Brown, T. C. Dean and P. Jones, *Biochem. journal*, 1970, **117**, 733–739.

86. S. Brown, P. Jones and I. Lantzke, *Nature*, 1969, **223**, 960–961.

87. D. H. O'Keeffe, C. H. Barlow, G. A. Smythe, W. H. Fuchsman, T. H. Moss, H. R. Lilienthal and W. S. Caughey, *Bioinorg. Chem.*, 1975, **5**, 125–147.

88. K. A. de Villiers, C. H. Kaschula, T. J. Egan and H. M. Marques, *J. Biol. Inorg. Chem.*, 2007, **12**, 101–117.

89. C. Asher, K. A. de Villiers and T. J. Egan, *Inorg. Chem.*, 2009, **48**, 7994–8003.

90. A. P. Gorka, A. de Dios and P. D. Roepe, *J. Med. Chem.*, 2013, **56**, 5231–5246.

91. S. N. Cohen, K. O. Phifer and K. L. Yielding, *Nature*, 1964, **202**, 805–806.

92. T. J. Egan, *J. Inorg. Biochem.*, 2006, **100**, 916–926.

93. A C. Chou, R. Chevli and C. D. Fitch, *Biochemistry*, 1980, **19**, 1543–1549.

94. W. Graf, K. Pommerening and W. Scheler, *Acta Biol. Med. Ger.*, 1971, **26**, 895–909.

95. J. Shack and W. Clark, *J. Biol. Chem.*, 1947, **171**, 143–187.

96. G. Blauer and B. Zvilichovsky, *Arch. Biochem. Biophys.*, 1968, **127**, 749–755.

97. V. Srinivas and C. M. Rao, *Biochem. Int*, 1990, **21**, 849–855.

98. K. Kuželová, M. Mrhalová and Z. Hrkal, *Biochim. Biophys. Acta*, 1997, **1336**, 497–501.

99. I. Constantinidis and J. D. Satterlee, *J. Am. Chem. Soc.*, 1988, **110**, 927–932.

100. I. Constantinidis and J. D. Satterlee, *J. Am. Chem. Soc.*, 1988, **110**, 4391–4395.

101. J. D. Satterlee and J. A. Shelnuttlb, *J. Phys. Chem.*, 1984, **88**, 5487–5492.

102. H. M. Marques, K. Voster and T. J. Egan, *J. Inorg. Biochem.*, 1996, **64**, 7–23.

103. T. J. Egan, W. W. Mavuso, D. C. Ross and H. M. Marques, *J. Inorg. Biochem.*, 1997, **68**, 137–145.

104. G. S. Collier, J. M. Pratt, C. R. De Wet and C. F. Tshabalala, *Biochem. J.*, 1979, **179**, 281–289.

105. I. R. Lantzke and D. W. Watts, *J. Am. Chem. Soc.*, 1967, **89**, 815–821.

106. T. J. Egan, E. Hempelmann and W. W. Mavuso, *J. Inorg. Biochem.*, 1999, **73**, 101–107.

107. C. H. Kaschula, T. J. Egan, R. Hunter, N. Basilico, S. Parapini, D. Taramelli, E. Pasini and D. Monti, *J. Med. Chem.*, 2002, **45**, 3531–3539.

108. T. J. Egan and K. K. Ncokazi, *J. Inorg. Biochem.*, 2004, **98**, 144–152.

109. T. J. Egan, R. Hunter, C. H. Kaschula, H. M. Marques, A. Misplon and J. Walden, *J. Med. Chem.*, 2000, **43**, 283–291.

110. K. A. de Villiers, H. M. Marques and T. J. Egan, *J. Inorg. Biochem.*, 2008, **102**, 1660–1667.

111. K. A. de Villiers, J. Gildenhuys and T. Le Roex, *ACS Chem. Biol.*, 2012, **7**, 666–671.

112. J. Gildenhuys, C. J. Sammy, R. Müller, V. A. Streltsov, T. le Roex, D. Kuter and K. A. de Villiers, *Dalton Trans.*, 2015, **44**, 16767–16777.

113. J. L. Hoard, M. J. Hamor and W. S. Caughey, *J. Am. Chem. Soc.*, 1965, **87**, 2312–2319.

114. C. Lecomte, D. L. Chadwick, P. Coppens and E. D. Stevens, *Inorg. Chem.*, 1983, **22**, 2982–2992.

115. M. R. Johnson, W. K. Seok, W. Ma, C. Slebodnick, K. M. Wilcoxen and J. A. Ibers, *J. Org. Chem.*, 1996, **61**, 3298–3303.

116. D. C. Warhurst, *Biochem. Pharmacol.*, 1981, **30**, 3323–3327.

117. A. C. de Dios, R. Tycko, L. M. B. Ursos and P. D. Roepe, *J. Phys. Chem. A*, 2003, **107**, 5821–5825.

118. A. Leed, K. DuBay, L. M. B. Ursos, D. Sears, A. C. De Dios and P. D. Roepe, *Biochemistry*, 2002, **41**, 10245–10255.

119. K. F. Schwedhelm, M. Horstmann, J. H. Faber, Y. Reichert, M. Buchner, G. Bringmann and C. Faber, *Open Spectros. J.*, 2008, **2**, 10–18.

120. G. T. Webster, D. McNaughton and B. R. Wood, *J. Phys. Chem. B*, 2009, **113**, 6910–6916.

121. S. Moreau, B. Perly, C. Chachaty and C. Deleuze, *Biochim. Biophys. Acta*, 1985, **840**, 107–116.

122. A. M. D. Acharige and M. C. Durrant, *Transit. Met. Chem.*, 2014, **39**, 721–726.

123. D. Kuter, S. J. Benjamin and T. J. Egan, *J. Inorg. Biochem.*, 2014, **133**, 40–49.

124. D. Kuter, V. Streltsov, N. Davydova, G. A. Venter, K. J. Naidoo and T. J. Egan, *J. Inorg. Biochem.*, 2016, **154**, 114–125.

125. T. L. Poulos and R. E. Fenna, *Metal Ions in Biological Systems-Peroxidases: structure, function, and engineering*, Marcel Dekker Inc., 1994.

126. G. Battistuzzi, M. Bellei, C. A. Bortolotti and M. Sola, *Arch. Biochem. Biophys.*, 2010, **500**, 21–36.

127. H. B. Dunford, *Heme Peroxidases*, John Wiley, Chichester, 1999.

128. J. M. McCoy-Messer and R. C. Bateman Jr, *Biotechniques*, 1993, **15**, 270–273.

129. R. E. Childs and W. G. Bardsley, *Biochem. J.*, 1975, **145**, 93–103.

130. A. Brausam, S. Eigler, N. Jux and R. Van Eldik, *Inorg. Chem.*, 2009, **48**, 7667–7678.

131. M. F. Zipplies, W. A. Lee and T. C. Bruice, *J. Am. Chem. Soc.*, 1986, **108**, 4433–4445.

132. T. C. Bruice, M. F. Zipplies and W. A. Lee, *Biochemistry*, 1986, **83**, 4646–4649.

133. A. C. Chou and C. D. Fitch, *J. Clin. Invest.*, 1980, **66**, 856–858.

134. M. C. de Almeida Ribeiro, O. Augusto and A. M. da Costa Ferreira, *J. Chem. Soc. Dalt. Trans.*, 1995, **23**, 3759–3766.

135. P. Adams and P. Berman, *Free Radic. Biol. Med.*, 1997, **22**, 1283–1288.

136. M. C. de Almeida Ribeiro, O. Augusto and A. M. da Costa Ferreira, *J. Inorg. Biochem.*, 1997, **65**, 15–23.

137. P. Loria, S. Miller, M. Foley and L. Tilley, *Biochem. J.*, 1999, **339**, 363–370.

138. P. A. Adams and P. A. Berman, *J. Pharm. Pharmacol*., 1996, **48**, 183–187.

139. T. J. Egan, *J. Inorg. Biochem*., 2002, **91**, 19–26.

140. D. J. Sullivan, *Int. J. Parasitol*., 2002, **32**, 1645–1653.

141. Gans, A. Sabatini and A. Vacca, *Talanta*, 1996, **43**, 1739-1753.

142. R. D. Sandlin, K. Y. Fong, R. Stiebler, C. P. Gulka, J. E. Nesbitt, M. P. Oliveira, M. F. Oliveira and D. W. Wright, *Cryst. Growth Des*., 2016, 16, 2542–2551.

143. S. R. Meshnick, Int. J. Parasitol., 2002, 32, 1655–1660.

144. C. Loup, J. Lelièvre, F. Benoit-Vical and B. Meunier, Antimicrob. Agents Chemother., 2007, **51**, 3768–3770.

145. Y. Hong, Y. Yang and S. R. Meshnick, Mol. Biochem. Parasitol., 1994, **63**, 121–128.

146. A. Robert and B. Meunier, J. Am. Chem. Soc., 1997, **119**, 5968–5969.

147. H. K. Baek and H. E. Van Wart, Biochemistry, 1989, **28**, 5714–5719.

148. J. E. Erman, J. L. B. Vitello, M. A. Miller, A. Shaw, K. A. Brown and J. Kraut, Biochemistry, 1993, 32, 9798–9806.

149. P. Adams, *J. Chem. Soc. Perkin Trans. 2*, 1990, **8**, 1407–1414.

150. S. L. Scott, W. J. Chen, A. Bakac and J. H. Espenson, *J. Phys. Chem.*, 1993, **97**, 6710–6714.

151. T. J. Egan, *J. Inorg. Biochem.*, 2008, **102**, 1288–1299.

152. MATLAB 7.10.0, The MathWorks *Inc*., *Natick, Massachusetts, United States* (2010).

153. B. Branchi, C. Galli and P. Gentili, *Org. Biomol. Chem.*, 2005, **3**, 2604–2614.

154. B. S. Wolfenden and R. L. Willson, *J. Chem. Soc. Perkin Trans. 2*, 1982, 7, 805–812.

155. P. Jones, D. Mantle and I. Wilson, *J. Chem. Soc. Dalton Trans.*, 1983, 1, 161–64.

156. D. A. Baldwin, H. M. Marques and J. M. Pratt, *J. Inorg. Biochem.*, 1987, **30**, 203–217.

157. I. H. Segel, Enzyme Kinetics, Wiley, New York, 957th edn., 1975.

158. S. B. Brown, H. Hatzikonstantinou and D. G. Herries, *Int. J. Biochem*., 1980, 12, 701–707.

159. U. D'Alessandro and H. Buttiens, *Trop. Med. Int. Heal.*, 2001, **6**, 845–8.

160. D. J. Sullivan, I. Y. Gluzman, D. G. Russell and D. E. Goldberg, *Proc. Natl. Acad. Sci. U. S. A.*, 1996, **93**, 11865–11870.

161. F. Dubar, S. Bohic, C. Slomianny, J.-C. Morin, P. Thomas, Y. Kalamou, Hadidjatou Guérardel, P. Cloetens, J. Khalife and C. Biot, *Chem. Commun.*, **48**, 910–912.

162. J. M. Combrinck, J. Egan, G. R. Hearne, H. M. Marques, S. Ntenteni, B. T. Sewell, P. J. Smith, D. Taylor, D. A. van Schalkwyk, J. C. Walden and T. J. Egan, *Biochem J.*, 2002, **365**, 343–347.

163. L. Alderighi, P. Gans, A. Ienco, D. Peters, A. Sabatini and A. Vacca, *Coord. Chem. Rev.*, 1999, **184**, 311–318.

164. F. Wilkinson, *Chemical Kinetics and Reaction Mechanisms*, Van Nostrand Reinhold, New York, N.Y., 1980.

165. T. J. Egan, *Mini Rev. Med. Chem.*, 2001, 113–123.
166. D. Monti, N. Basilico, S. Parapini, E. Pasini, P. Olliaro and D. Taramelli, *FEBS Lett.*, 2002, **522**, 3–5.
167. F. Omodeo-Salè, D. Monti, P. Olliaro and D. Taramelli, *Biochem. Pharmacol.*, 2001, **61**, 999–1009.
168. K. J. Wicht, J. M. Combrinck, P. J. Smith, R. Hunter and T. J. Egan, *J. Med. Chem.*, 2016, **59**, 6512–6530.
169. A. Brossi, B. Venugopalan, L. Dominguez Gerpe, H. J. C. Yeh, J. L. Flippen-Anderson, P. Buchs, X. D. Luo, W. Milhous and W. Peters, *J. Med. Chem.*, 1988, **31**, 645–650.